NEW SENSOR APPLICATIONS OF POLY(PHENYLENE ETHYNYLENE)S

by

JORDAN HOWARD WOSNICK

B.Sc. (Hons. First Class), Chemistry
McGill University, 1998

Submitted to the Department of Chemistry
in Partial Fulfillment of the Requirements for the Degree of

DOCTOR OF PHILOSOPHY

at the

MASSACHUSETTS INSTITUTE OF TECHNOLOGY

September, 2004

Signature of Author: _____
Department of Chemistry
June 21, 2004

Certified by: _____
Timothy M. Swager
Thesis Supervisor

Accepted by: _____
Robert W. Field
Chairman, Departmental Committee on Graduate Studies

This doctoral thesis has been examined by a Committee of the Department of Chemistry as follows:

Professor Daniel S. Kemp: _____
Chairman

Professor Timothy M. Swager: _____
Thesis Advisor

Professor Alice Y. Ting: _____

Dedicated to Caroline,
for her love, support, and patience.

New sensor applications of poly(phenylene ethynylene)s

by

Jordan Howard Wosnick

Submitted to the Department of Chemistry on June 21, 2004
in Partial Fulfillment of the Requirements for the degree of
Doctor of Philosophy in Chemistry

ABSTRACT

The principle of energy migration in conjugated polymers has been shown to have broad applicability to the design of sensors capable of detecting a variety of analytes. The infinitely customizable nature of these materials makes them powerful building blocks for a new generation of fluorescent sensors that exploit intricate chemical and photophysical effects to maximize sensitivity and selectivity. This dissertation discusses three new sensor applications of poly(phenylene ethynylene)s (PPEs) that make use of their chemical and photophysical properties to elicit fluorescence changes in response to analytes.

A series of water-soluble carboxylate-functionalized PPEs has been prepared in which the carboxylate groups are attached to the polymer backbone by means of oligoethylene glycol spacers. The fluorescence properties of these polymers are strongly dependent on ionic strength and surfactant concentration, and the polymers can be activated and coupled to amine-containing biomolecules in solution. This technique has been used to generate a quenched polymer-peptide system that functions as a 'turn-on' fluorescence sensor for trypsin.

Highly fluorescent PPE films on glass slides and silica microspheres have been prepared by electrostatic layer-by-layer assembly of a polyanionic PPE. These films are capable of efficiently transferring energy to dye-labeled polycations adsorbed to the film surface. Suspensions of PPE-coated microspheres have been used for the detection of quenchers in aqueous solution and show up to 200-fold sensitivity enhancements *versus* similar dissolved polymers.

A series of calix[4]arene-functionalized PPEs have been synthesized and used for the detection of the Ba^{2+} and *N*-methylquinolinium ions in solution. Fluorescence quenching by these analytes was shown to be assisted by specific host-guest interactions involving the calix[4]arene macrocycles.

Thesis Supervisor: Timothy M. Swager
Title: Professor of Chemistry

Contents

List of Abbreviations

1,2-alt	the 1,2-alternate conformation of calix[4]arenes
1,3-alt	the 1,3-alternate conformation of calix[4]arenes
cone	the cone conformation of calix[4]arenes
DIPA	*N,N*-diisopropylamine
DIPC	*N,N'*-diisopropylcarbodiimide
DMF	*N,N*-dimethylformamide
DNP	2,4-dinitrophenyl
EDAC	*N*-ethyl-*N'*-(3-(1-dimethylamino)propyl)carbodiimide HCl
LB	Langmuir-Blodgett
LBL	layer-by-layer deposition
MES	2-(*N*-morpholino)ethanesulfonic acid
MMP	matrix metalloprotease
MV^{2+}	methylviologen
NHS	*N*-hydroxysuccinimide
NMP	*N*-methylpyrrolidinone
paco	the partial cone conformation of calix[4]arenes
PAH	poly(allylamine) (hydrochloride)
PBS	phosphate-buffered saline
PDAC	poly(diallyldimethylammonium chloride)
PPE	poly(phenylene ethynylene)
ppm	parts per million
PPV	poly(phenylene vinylene)
PSS	poly(styrenesulfonate)
QY	fluorescence quantum yield
TBS	Tris-buffered saline
THF	tetrahydrofuran
TNT	2,4,6-trinitrotoluene
Tris	tris(hydroxymethyl)aminomethane

Chapter 1

Sensor applications of conjugated polymers — a primer

Partially adapted from:

Swager, T. M.; Wosnick, J. H. *MRS Bull.* **2002,** 446.

An introduction to conjugated polymer sensors

Once merely an intellectual curiosity, electronically conjugated polymers have become one of the most promising types of new materials. Their study has attracted researchers from a wide variety of fields and spans the range from purely application-focused investigations to basic research into their structure and properties. The attraction of conjugated polymers in modern materials chemistry and engineering is a direct consequence of a particularly unique property: they are organic structures that can have the properties of metals or semiconductors. This feature leads to a natural tendency to see conjugated polymers as infinitely customizable replacements for inorganic materials in electronics applications. However, some of the more unusual properties of conjugated polymers open up a far wider range of potential applications that go far beyond what is possible with inorganic materials. The Swager group has had a long-standing interest in using conjugated polymers as amplifying elements for the creation of chemical sensors that push the limits of conventional sensor technology.[1] This chapter describes the general principles behind the sensor applications of conjugated polymers, with a particular emphasis on poly(phenylene ethynylene)s (PPEs) — the conjugated polymer of choice for fluorescent sensing — and on the evolution of sensor design in the Swager group.[2]

Exciton generation and migration

The overlapping π-orbital structure of conjugated polymers means that their electronic properties are dominated by orbital 'bands' akin to those found in inorganic semiconductors. Semiconductors such as silicon and germanium are made less resistive by 'doping' them with electron-deficient (boron) or electron-excessive (phosphorus) atoms that introduce free charge carriers ('holes' or electrons, respectively) into the system, and many conjugated polymers

behave similarly: in this subset of conjugated polymers, commonly known as *conducting* polymers, conductivity is induced through chemical or electrochemical redox events that supply the needed charge carriers. For conducting polymers, charge mobility is a collective property of the entire polymer chain and is partly governed by the structure of the polymer itself. Defects in the polymer structure — whether present naturally or deliberately introduced by manipulating molecular structure and conformation — can have a strong effect on the electronic properties of the polymer. This phenomenon has formed the basis for a variety of conducting polymer-based chemical sensors that signal the presence of the analyte of interest by changes in oxidation potential or conductivity.[2]

The fact that a small number of defects can affect a collective property like conductivity forms the basis for a versatile amplification mechanism.[3] Key demonstrations in the Swager group have shown that this concept — the 'molecular wire' approach — can also be applied to fluorescent, semiconductive conjugated polymers in which absorption of a photon generates an excited-state electron-hole pair known as an exciton. In this case, migration of the exciton along the polymer backbone fulfills the role played by the charge carrier in an electrically conducting polymer.[4] Excitons are known to follow downhill energy gradients when possible, and this phenomenon is exploited in applications such as electroluminescent displays, where pure colors are be produced by allowing excitons to become 'trapped' at deliberately introduced low-energy sites (usually red-emissive fluorophores) after migrating through the display material (usually a green-emissive fluorophore). Because migration of excitons *from* these low-energy trapping sites is energetically unfavorable, their electronic properties dominate those of the bulk material even at very low concentrations. In the same way, trapping sites introduced into a conjugated polymer can serve as energy sinks that effectively 'harvest' all of the excitons generated in the polymer.

Because these trapping sites need only be very dilute for their effects to dominate the properties of the polymer, this type of energy harvesting constitutes an amplification mechanism that magnifies the observable effects of the traps.

The opportunity to apply exciton migration in conjugated polymers to the amplification of sensory signals is provided by analytes that can serve as traps or that generate trapping sites. In the mid-1990s, former Swager group graduate student Qin Zhou prepared a π-conjugated poly(phenylene ethynylene) (PPE) bearing cyclophane groups (Figure 1.1).[5] It was previously known that cyclophanes are efficient receptors for the guest *N,N'*-dimethyl-4,4'-bipyridinium, also known as methylviologen (MV^{2+}), an excellent electron acceptor and fluorescence quencher. MV^{2+} was found to quench the fluorescence of these PPEs 40-60 times better than it quenches a small-molecule model compound containing the same receptor. Fluorescence lifetime measurements (see below) confirmed that MV^{2+} is bound in the cyclophane moieties of these polymers, and it was concluded that the observed sensitivity arises from the additive nature of the poly-receptor / ligand interaction.

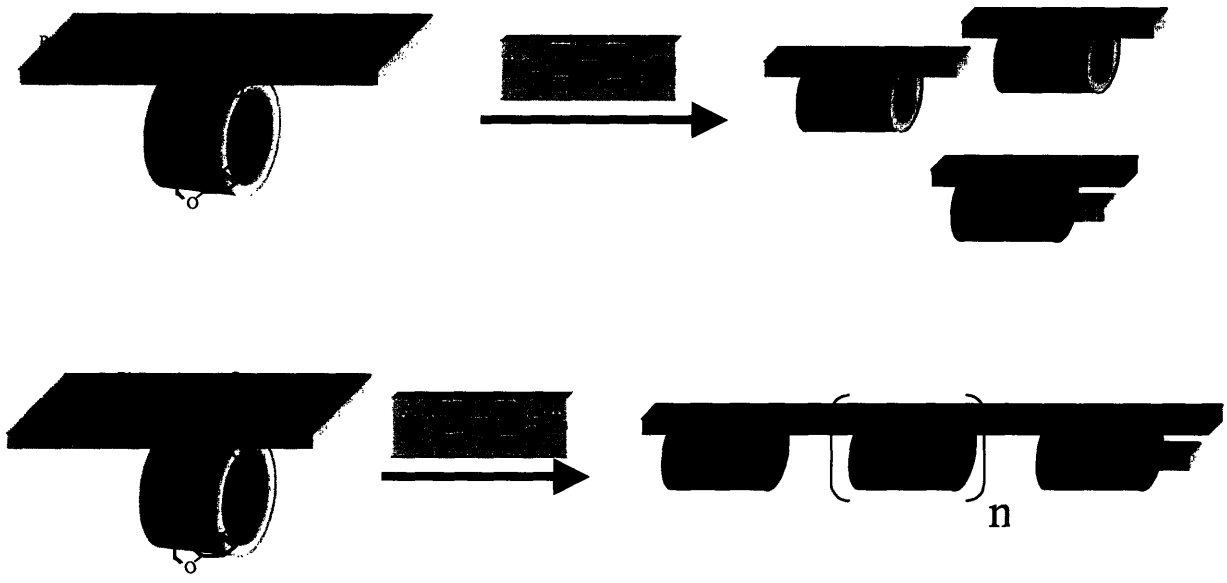

Figure 1.1. The initial demonstration of amplified fluorescence sensing in a conjugated polymer. When isolated fluorescent receptors are used (top), the reduction in fluorescence signal on analyte binding reflects the quenching effects of the analyte on a single unit. When the receptors are part of a conjugated polymer, only a single receptor unit need be occupied to observe a collective system response.

The mechanism of sensory signal amplification by conjugated polymers can be illustrated using a band diagram of the kind used to describe semiconductor behavior (Figure 1.2). The extended valence and conduction bands of the conjugated polymer — somewhat analogous to the bonding and anti-bonding molecular orbitals of a small molecule — are separated in energy by a characteristic bandgap E_g. On absorption of a photon, an exciton is generated and begins to migrate along the polymer backbone. In the absence of an external quencher, the exciton remains intact for a characteristic fluorescence lifetime τ and then recombines, causing the emission of a photon (fluorescence) or the dissipation of the excitation energy as heat. However, when a suitable electron-accepting analyte is present, electron transfer from the polymer to the analyte

occurs and the exciton recombines non-radiatively (Figure 1.2a). The net effect of the presence of the analyte is to quench the fluorescence of the entire polymer chain, making the system a 'turn-off' sensor for this analyte. In the case of non-quenching analytes, ligand binding introduces a local minimum in the polymer bandgap in which excitons can be trapped (Figure 1.2b). Selective recombination of excitons from this low-energy well results in a new emission that is red-shifted relative to the intrinsic fluorescence of the polymer, making this process a type of 'turn-on' sensory mechanism.

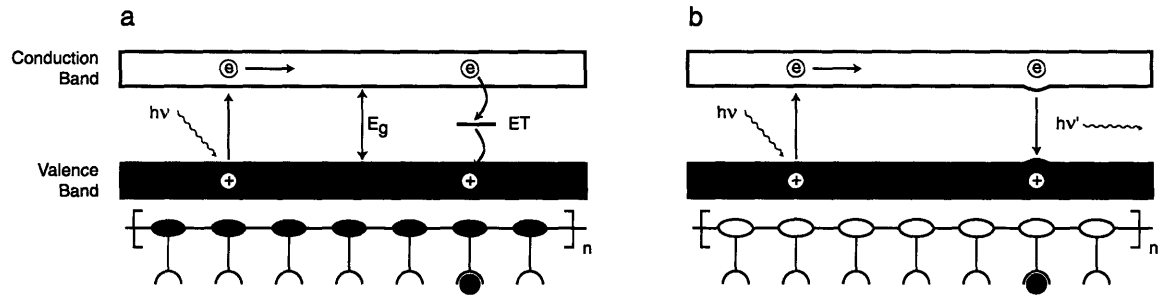

Figure 1.2. Schematic representation of exciton migration in a conjugated polymer and how it produces amplification. (a) Turn-off sensor: an exciton migrates along the polymer backbone until it encounters an electron-accepting analyte that facilitates non-radiative recombination, leading to fluorescence quenching. (b) Turn-on sensor: binding of an analyte causes a local change in the polymer bandgap, creating an energy well that the exciton becomes trapped in. Recombination of excitons from this well results in a new red-shifted emission.

PPEs: the conjugated polymer of choice for sensory applications

Optimal signal amplification in conjugated polymers requires that excitons have as much mobility as possible in order to maximize the chances of encountering an analyte before radiative recombination occurs. For this reason, any structural features present in a conjugated polymer that impede exciton mobility will also reduce the amplification advantage these materials provide. This consideration has led to the adoption of the poly(phenylene ethynylene) (PPE) family as the conjugated polymer of choice in the Swager group (Scheme 1.1). PPEs are easily

synthesized from aromatic diiodides and diacetylenes by a Sonogashira polymerization reaction, and their bandgaps can be tailored by modifying the substituents on the aromaitc rings. PPEs behave as linear rigid rods over short distance scales, and the cylindrical symmetry of the triple bond allows these polymers to maintain electronic conjugation even when the aromatic rings are twisted relative to one another. In contrast, the closely related poly(phenylene vinylene)s (PPVs), which are also highly fluorescent, have much more conformational flexibility and thus a wider range of π-orbital energies. The conformational freedom of PPVs causes interruptions in electronic conjugation, meaning that individual polymer chains can often be thought of as collections of isolated fluorophores of various conjugation lengths rather than a single large fluorophore. Excitons pass between these segments by Förster energy transfer (FRET), which is facilitated in this case by good spectral overlap between the 'donor' and 'acceptor' segments.[6] The dispersion in energy levels ensures that low-energy segments in PPVs can act as internal trapping sites that reduce exciton mobility. These intrinsic traps compete with the analyte-induced trapping processes and necessarily decrease the degree of amplification possible in PPVs.

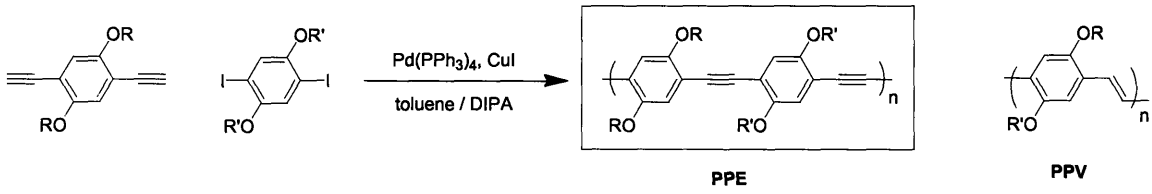

Scheme 1.1. Synthesis and structure of a generic poly(phenylene ethynylene) (PPE) and structure of a generic poly(phenylene vinylene) (PPV). Although standard *para*-dialkoxy substituents are shown, many others are possible.

Relative to PPVs, the symmetry of PPEs leads to a more extended conjugated structure and a much narrower range of π-orbital energy levels. As a consequence, PPEs have sharper

spectral features and the polymer in this case behaves as a true 'molecular wire' with no endogenous local energy minima to compete with those introduced by analytes of interest. The result is a relatively 'smooth' energy surface along which excitons travel primarily by direct orbital coupling (Dexter energy transfer).[7]

Dimensionality effects in conjugated polymer sensors

Conceptually, the use of conjugated polymers to provide increased sensitivity in sensory schemes can be seen as amplification by increased dimensionality: rather than being confined to a single receptor site which may or may not be bound to an analyte, the exciton is free to migrate along a one-dimensional extended electronic structure consisting of multiple receptors wired in series. Occupancy of any one of these receptors by an analyte gives rise to an observable signal. Given this model, it would seem that increasing the molecular weight of the conjugated polymer should improve the amplification it affords by means of the additive effects of additional receptor units. However, Qin Zhou's work on amplified quenching of PPEs with MV^{2+} revealed an intrinsic limit on the degree of amplification possible in a one-dimensional system. She found that increasing the polymer molecular weight gave rise to larger amplification up to a size equivalent to 140 phenylene-ethynylene repeat units, and that further extensions in molecular weight beyond the 140-unit limit did not significantly add to the sensitvity of the system. This result was attributed to the 'random walk' nature of the exciton as it migrates along the polymer backbone — with the relatively flat energy surface provided by the PPE, the exciton is likely to revisit the same empty receptor units several times during the lifetime of the excited state.

The Swager group has devoted a considerable amount of effort into finding ways to maximize the efficiency of exciton migration and overcome the 140-unit amplification limit.

These studies, discussed in the following sections, have focused on expanding the dimensionality of exciton migration in conjugated polymers by optimizing exciton transport along polymer chains, between polymer chains in a monolayer, along energy gradients in multi-layer structures and by extending polymer lifetimes.

Controlling polymer aggregation in PPEs

The extension of exciton migration to more than one dimension must necessarily take into consideration the photophysics of polymer interactions.[8] It has long been known that PPE aggregation caused by π-stacking in neighboring polymer chains has deleterious effects on the fluoresence quantum yield (QY) of these materials. Addressing this self-quenching while taking advantage of exciton migration in two and three dimensions required a system in which the contrasting needs of inter-polymer exciton migration and the prevention of polymer aggregation are balanced. Toward this end, former Swager group postdoc Jye-Shane Yang prepared a polymer in which rigid pentiptycene groups are embedded into the PPE backbone (Figure 1.3). The pentiptycene units act as rigid spacers that prevent polymer aggregation when the polymer is cast as a thin film and reliably ensure a high QY. In what is arguably the most famous demonstration of the potential of conjugated polymer sensors, films of this polymer were found to be highly sensitive to fluorescence quenching by trinitrotoluene (TNT), a common explosive used in land mines.[9] The free volume defined by the pentiptycene group also provides voids large enough for small molecules such as TNT to diffuse into, further enhancing the sensitivity of this system. This polymer forms the basis for the most sensitive devices yet created for the detection of land mines: these instruments are capable of providing a fluorescence response to

the very low vapor pressure of TNT above a buried land mine. The femtogram sensitivity of these devices rivals the low detection limits provided by trained mine-sniffing dogs.[10]

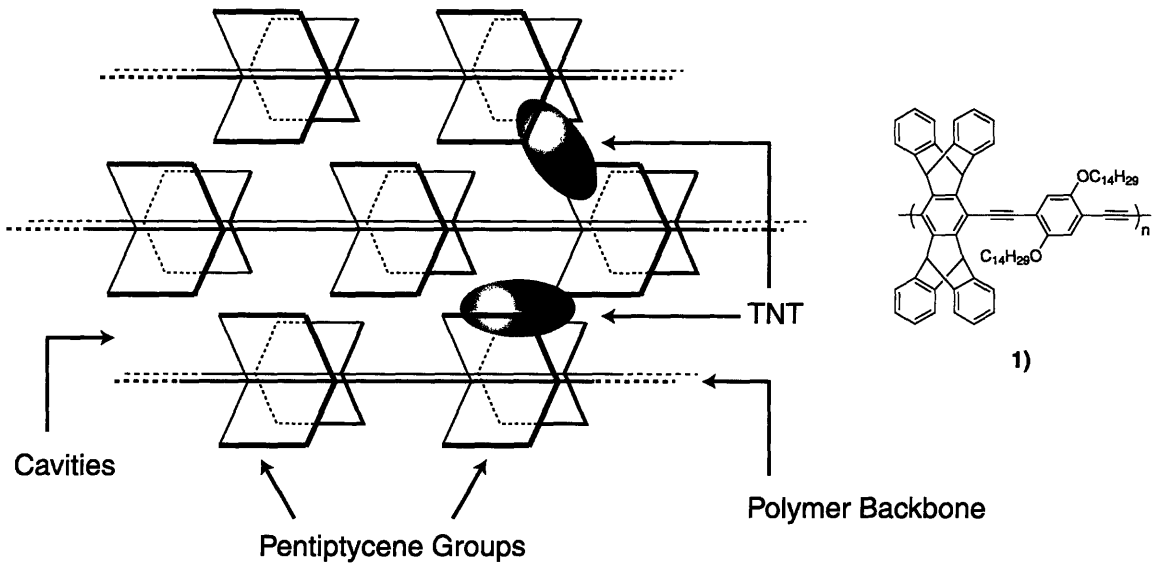

Figure 1.3. A pentiptycene-containing polymer which maintains a high fluorescence quantum yield even when cast into a thin film. The rigid nature of the pentiptycene units prevents deleterious π-stacking effects and provides galleries for the binding of the explosive TNT, which effectively quenches the fluorescence of this polymer.

An alternative approach to dealing with the effects of polymer aggregation is to capitalize on them in the design of sensors. Former Swager group graduate student Jinsang Kim prepared a PPE bearing 15-crown-5 units close to the polymer backbone (Scheme 1.2).[11] While this crown ether unit interacts with many different alkali metal cations, it is known to form 2:1 complexes with the K^+ ion. Addition of K^+ to a solution of this polymer *induces* polymer aggregation and results in a decrease in the fluorescence of the solution. The Na^+ and Li^+ ions, which form 1:1 complexes with the crown ether ring, do not induce aggregation and the polymer fluorescence remains constant in the presence of these ions. This system thus functions as a selective 'turn-off' sensor for K^+.

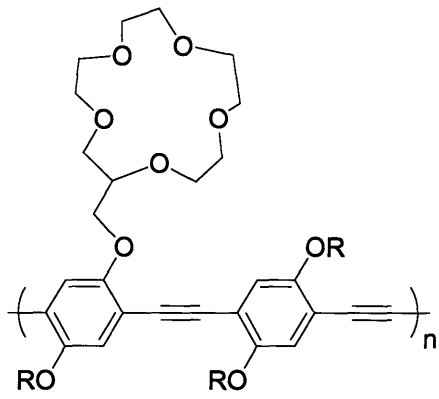

Scheme 1.2. The fluorescence of this crown ether-bearing polymer is attenuated in the presence of K^+ due to the formation of 2:1 crown ether-ion complexes that promote polymer aggregation.

A detailed understanding of how polymers interact in thin films is crucial to optimizing exciton migration in multi-dimensional conjugated polymer structures. While the polymers described above were designed to either prevent or exploit aggregation effects, careful investigations into the effect of higher dimensionality on exciton mobility required organized assemblies of polymers in controlled orientations. This goal was accomplished by Jinsang through the extensive use of Langmuir-Blodgett (LB) techniques. In LB processing, external pressure is used to form aligned monolayers of polymers at the air-water interface. These monolayers can be systematically transferred to solid substrates to create films of any desired thickness or orientation. The degree of control afforded by the LB technique allowed the study of inter-polymer interactions and energy migration within a polymer monolayer and between layers in a multi-layer structure. Jinsang and former Swager group postdoc Igor Levitsky found that the use of aligned LB films provided a clear sensory advantage over isolated polymer chains in solution in turn-off and turn-on assays.[12,13] By creating trapping sites on the surface of aligned PPE multi-layer films, it was shown that energy transfer through the three-dimensional structure to the traps was facilitated by increasing the number of underlying layers, up to a limit of about

16 layers.[14] At this thickness, the rate of exciton migration through the multi-layer film is comparable to the lifetime of the exciton. Although exciton migration is clearly enhanced relative to polymers in solution, the quenching sensitivity of the multi-layer structures suffers from the inability of the exciton to 'find' the traps.

To overcome this limitation, a system was devised to direct excitons along a well-defined energy gradient in a manner analogous to the photosynthetic systems of light-harvesting organisms. A multilayer film consisting of three PPEs of different bandgaps was prepared (Figure 1.4) in which the polymer bandgap sequentially decreases from one component to the next.[15] Direct excitation of the polymer with the largest bandgap (most blue-shifted absorption and emission) was found to result in efficient energy transfer to a monolayer of the polymer with the smallest bandgap, even when the total number of polymer layers in the system exceeded 16. The use of the layered 'vectorial' energy transfer structure was shown to be superior to films consisting of simple mixtures of polymers of different bandgaps and constitutes a promising strategy for harnessing exciton migration for analytical purposes.

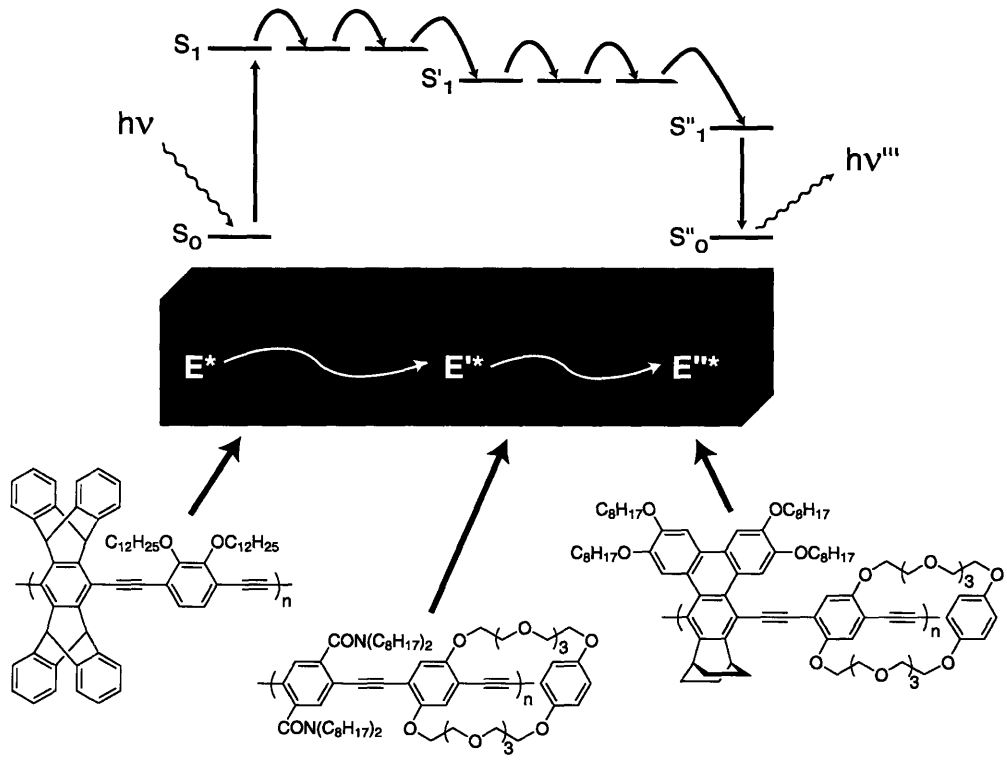

Figure 1.4. A three-layer striated film of PPEs, designed to transport energy from the highest-bandgap (most blue-shifted) polymer to the lowest-bandgap (most red-shifted) polymer. The excitons follow the downhill energy surface provided by the steadily decreasing bandgaps. Emission from this system arises predominantly from the most red-shifted polymer.

As demonstrated above, maximizing the effiency of exciton migration in conjugated polymers represents a means to improving the sensitivity of conjugated polymer-based sensors. An alternative approach to improving the sensitivity of PPE-based sensors is to augment the number of potential receptor sites that can be sampled by the migrating exciton by extending the fluorescence lifetime of the polymer. Former Swager group graduate student Aimee Rose and visiting scientist Shigehiro Yamaguchi prepared PPEs in which polycyclic aromatic structures are integrated into the polymer backbone.[7,16] These aromatic units were chosen based on their known long fluorescence lifetimes, a characteristic that is preserved when they are integrated into polymers. As shown in Scheme 1.3, PPEs with integrated dibenzochrysene and triphenylene

units have significantly longer fluorescence lifetimes than a standard *para*-dialkoxy PPE. This property makes these materials useful for the generation of stimulated emission as well as basic studies into the mechanism of exciton migration in PPEs.

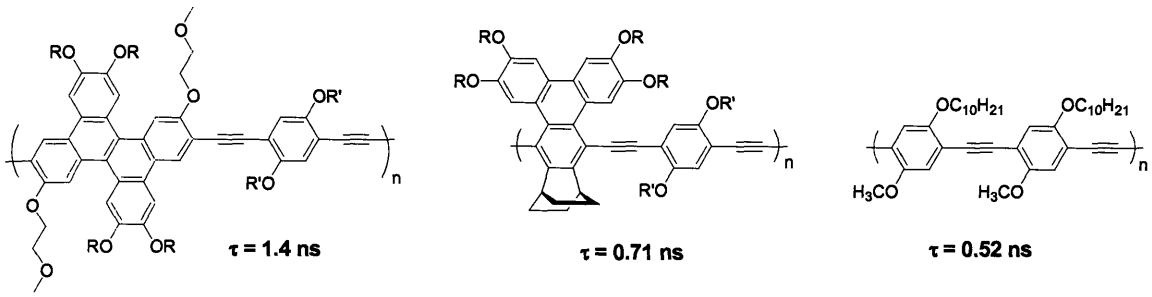

Scheme 1.3. PPEs containing integrated dibenzochrysene (left) and triphenylene (middle) units have significantly longer fluorescene lifetimes than standard *para*-dialkoxy PPEs (right).

Energy transfer to dyes as an amplification mechanism

The harnessing of exciton migration and energy transfer in conjugated polymers to achieve specific analytical goals has been of long-standing interest in the Swager group. Schemes in which light-harvesting conjugated polymers are used to amplify the fluorescence signals of small-molecule fluorophores are of particular interest in this regard due to the ubiquity of fluorescence techniques in biochemistry. In this context, the role of the polymer can be seen as that of the donor in a classical Förster energy transfer (FRET) scheme, with the red-shifted small-molecule fluorophore acting as an energy acceptor. The first practical demonstration of this effect in the Swager group was made by former postdoc Tyler McQuade, who used layer-by-layer assembly (see Chapter 3) to deposit pH-sensitive fluorescein dyes on the surface of a PPE thin film.[17] At alkaline pH values the fluorescein units are strong absorbers and highly fluorescent, and excitation of the polymer results in strong emission from the fluorescein acceptors as a result of efficient FRET between these two species. In acidic environments

fluorescein is rendered colorless and non-fluorescent, and the elimination of the FRET pathway leads to emission solely from the PPE itself (Figure 1.5). In this case, light-harvesting by the polymer led to an amplification factor of approximately one order of magnitude relative to direct excitation of the fluorescein groups. This system thus constitutes a PPE-amplified fluorescent pH sensor in which energy transfer is modulated by the fluorescence properties of the acceptor.

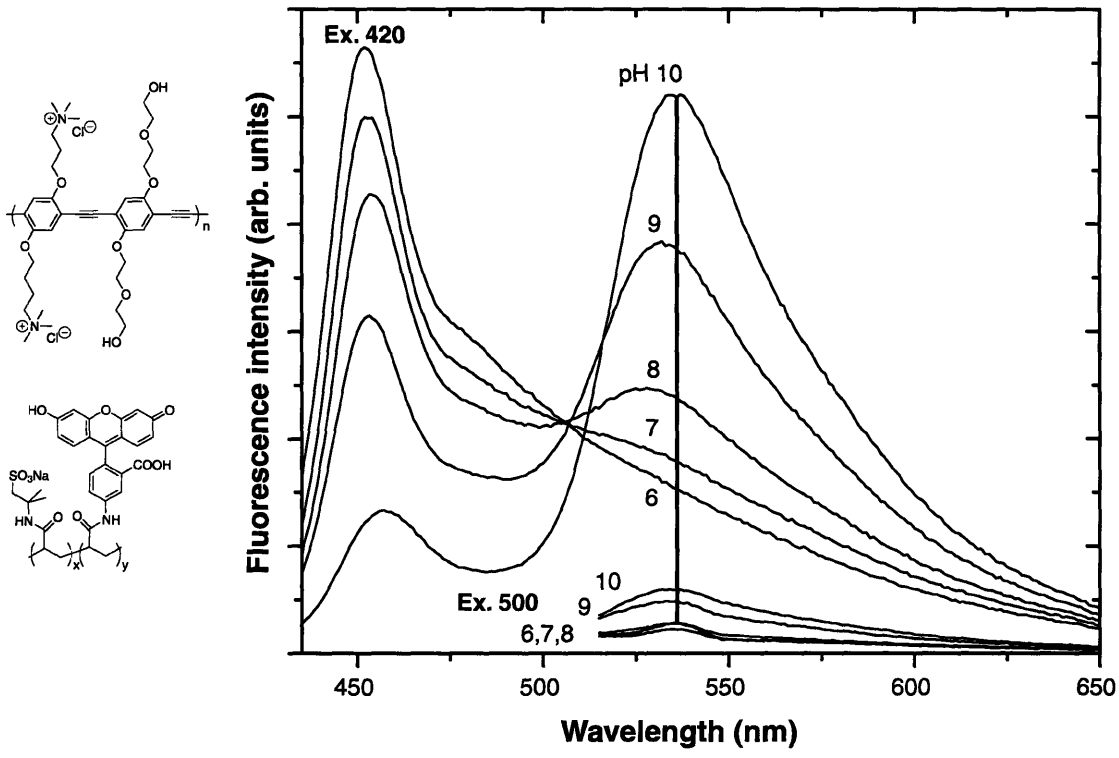

Figure 1.5. A bilayer film is assembled electrostatically from the two polymers shown at left. The emsision of the system is pH-dependent: in alkaline environments, excitation of the PPE at 420 nm results in efficient energy transfer to the fluoresceinamine dyes, which fluoresce at 535 nm. In acidic environments, the fluoresceinamine moieties are no longer efficient FRET acceptors and the polymer emission (460 nm) predominates. Direct excitation of the system at the absorbance maximum of the fluoresceinamine groups produces a much weaker signal in all cases, indicating that emission at high pH is amplified by the polymer.

Former Swager group graduate student Kenichi Kuroda used an alternative approach to create a polymer-amplified sensory platform. In this application, a PPE was end-capped with thermally responsive poly(*N*-isopropylacrylamide) (polyNIPA) blocks, which cause the polymer

to precipitate at high temperatures. When this block co-polymer was mixed with a rhodamine-labeled polyNIPA derivative in aqueous solution, no FRET was seen. However, co-precipitation caused by heating the mixture gave rise to efficient energy transfer from the PPE donor to the rhodamine acceptor.[18] This result suggests that it is possible to combine the advantages of a homogeneous solution assay with precipitation-induced sensitivity enhancement, an innovation that holds great promise for the design of highly refined polymer-amplified biosensors.

Tools of the trade: assessing sensory response in fluorescence studies

Many of the sensor applications discussed in this dissertation rely on polymer fluorescence quenching by an analyte of interest as the basis of the sensory response. Quantitative analysis of the efficiency of fluorescence quenching for a given fluorophore-analyte pair is generally carried out by means of the Stern-Volmer equation:[19]

$$F_0/F = 1 + K_{SV}[Q]$$

where F_0 is the initial fluorescence of the fluorophore, F is its fluorescence in the presence of the quencher, [Q] is the concentration of the quencher, and K_{SV} is the Stern-Volmer quenching constant. Experimentally, K_{SV} values can be determined from the slope of a plot of F_0/F *versus* [Q] over a range of quencher concentrations. The magnitude of K_{SV} thus provides a measure of the efficiency of the quencher toward the particular fluorophore in use and is dependent on solvent, temperature, and other environmental factors.

When discussing quenching effects in fluorescent conjugated polymers (or any other fluorescent material), it is helpful to distinguish between the two major mechanisms through which quenching can take place. In *dynamic* quenching, collision of a fluorophore in an excited state with a quenching analyte results in a non-radiative relaxation event. The efficiency of

quenching in this case is dependent on the frequency of successful collision events. From this, it follows that fluorophores with longer fluorescence lifetimes will show larger fluorescence reductions at a given quencher concentration due to an increase in the probability of successful collision events. For dynamic quenching the Stern-Volmer constant K_{SV} can be expressed as the product $k_q\tau$, where k_q is the bimolecular quenching rate constant and τ is the fluorescence lifetime of the fluorophore.

In *static* quenching, the fluorophore forms a non-fluorescent ground-state complex with the quencher, and the observed K_{SV} value is equivalent to the quencher-fluorophore association constant (K_{SV} has the units of M^{-1}). Because both static and dynamic processes can give linear Stern-Volmer plots, it is sometimes difficult to distinguish between the two without further information. However, exceptionally large K_{SV} values are usually indicative of static quenching processes: substituion of these values into the dynamic quenching equation $K_{SV} = k_q\tau$ yields nonsensically large values of k_q (faster than the rate of diffusion) and thus indicates that collisional quenching is impossible within the lifetime of the fluorophore. The most reliable way to discriminate between static and dynamic quenching processes is by recording changes in the fluorescence lifetime in response to increases in quencher concentration. For pure dynamic quenching, quencher-fluorophore collisions increase under these conditions and the fluorescence lifetimes become shorter. For pure static quenching, pre-formed quencher-fluorophore complexes do not contribute to the observed fluorescence at all and the overall lifetime of the system remains independent of the quencher concentration. The use of lifetime-based studies thus provides an important tool in elucidating fluorophore-quencher interactions.

Conclusions

The principle of energy migration in conjugated polymers has been shown to have broad applicability to the design of sensors capable of detecting a variety of analytes. The infinitely customizable nature of these materials makes them powerful building blocks for a new generation of fluorescent sensors that exploit intricate chemical and photophysical effects to maximize sensitivity and selectivity. The remainder of this dissertation discusses three systems based on poly(phenylene ethynylene)s that take advantage of their properties to create new analytical tools. As our understanding of the fundamental science of these materials progresses, future innovations will be limited only by our imaginations.

References

(1) Several recent 'perspective' articles have described the Swager group's approach to the use of conjugated polymers in chemical sensors. For example, see (a) Swager, T. M.; Wosnick, J. H. *MRS Bull.* **2002,** 446. (b) Wosnick, J. H.; Swager, T. M. *Curr. Opin. Chem. Biol.* **2000,** *4,* 715. (c) Kuroda, K.; Swager, T. M. *Macromol. Symp.* **2003,** *201,* 127.

(2) The reader is referred to two reviews on the sensor applications of conjugated polymers for a complete picture of how these materials are used. (a) McQuade, D. T.; Pullen, A. E.; Swager, T. M. *Chem. Rev.* **2000,** *100,* 2537. (b) Zheng, J.; Swager, T. M. Book chapter in press.

(3) Swager, T. M. *Acc. Chem. Res.* **1998,** *31,* 201.

(4) Swager, T. M.; Gil, C. J.; Wrighton, M. S. *J. Phys. Chem.* **1995,** *99,* 4886.

(5) (a) Zhou, Q.; Swager, T. M. *J. Am. Chem. Soc.* **1995,** *117,* 7017. (b) Zhou, Q.; Swager, T. M. *J. Am. Chem. Soc.* **1995,** *117,* 12593.

(6) Nguyen, T.-Q.; Wu, J.; Doan, V.; Schwartz, B. J.; Tolbert, S. H. *Science* **2000,** *288,* 652.

(7) Rose, A.; Lugmair, C. G.; Swager, T. M. *J. Am. Chem. Soc.* **2001,** *123,* 11298.

(8) Kim, J.; Swager, T. M. *Nature* **2001,** *411,* 1030.

(9) (a) Yang, J.-S.; Swager, T. M. *J. Am. Chem. Soc.* **1998,** *120,* 5321. (b) Yang, J.-S.; Swager, T. M. *J. Am. Chem. Soc.* **1998,** *120,* 11864.

(10) Cumming, J. C.; Aker, C.; Fisher, M.; Fox, M.; La Grone, M. J.; Reust, D.; Rockley, M. G.; Swager, T. M.; Towers, E.; Williams, V. *IEEE Trans. Geosci. Remote Sens.* **2001,** *39,* 1119.

(11) Kim, J.; McQuade, D. T.; McHugh, S. K.; Swager, T. M. *Angew. Chem. Intl. Ed. Engl.* **2000,** *39,* 3868.

(12) (a) Levitsky, I. A.; Kim, J.; Swager, T. M. *Macromolecules* **2001,** *34,* 2315. (b) Kim, J.; Levitsky, I. A.; McQuade, D. T.; Swager, T. M. *J. Am. Chem. Soc.* **2002,** *124,* 7710.

(13) McQuade, D. T.; Kim, J.; Swager, T. M. *J. Am. Chem. Soc.* **2000,** *122,* 5885.

(14) Levitsky, I. A.; Kim, J.; Swager, T. M. *J. Am. Chem. Soc.* **1999,** *121,* 1466.

(15) Kim, J.; McQuade, D. T.; Rose, A.; Zhu, Z.; Swager, T. M. *J. Am. Chem. Soc.* **2001,** *123,* 11488.

(16) Yamaguchi, S.; Swager, T. M. *J. Am. Chem. Soc.* **2001,** *123,* 12087.

(17) McQuade, D. T.; Hegedus, A. H.; Swager, T. M. *J. Am. Chem. Soc.* **2000,** *122,* 12389.

(18) Kuroda, K.; Swager, T. M. *Macromolecules* **2004,** *37,* 716.

(19) For a discussion of the derivation of the Stern-Volmer equation and related quenching effects, see Lakowicz, J. R.; *Principles of fluorescence spectroscopy;* Kluwer Academic: New York, 1999.

Chapter 2

Carboxylate-functionalized water-soluble PPEs for bioconjugation and protease detection

Introduction

Fluorescence-based techniques are widely used in all aspects of biochemistry. The large number of parameters that play a role in fluorescence — such as luminescence quantum yields, polarization, fluorescence lifetimes, quenching effects, and energy transfer — make it an information-rich technique that can be adapted to the investigation of a wide variety of phenomena.[1] The choice of fluorophore used in biochemical experiments has historically been governed by the range of naturally occuring fluorescent biomolecules (such as tryptophan and the green fluorescent protein) and synthetic small-molecule fluorophores (such as the fluorescein and rhodamine families). While considerable effort has been made in addressing the shortcomings of some of these fluorophores, such as solvent-dependent quantum yield and instability, there is clearly room for innovation in fluorophore design.

An obvious category of potential fluorophore for biochemical sensory applications is conjugated polymers, and the application of these materials to the detection of biochemical events has seen a surge in interest in last several years. This phenomenon can be traced to recent efforts to overcome a major limitation of conventional conjugated polymer materials — their insolubility in water. Conjugated polymers are inherently hydrophobic due to their extended aromatic backbones, and modifications are required to render them soluble in aqueous environments. Most solutions to this problem have centered on the addition of charged side-chains to the conjugated polymer backbone, leading to polyelectrolyte conjugated polymers that have been used in a number of sensory strategies.[2] Many biosensor schemes based on conjugated polymers — in particular the work of the Heeger, Whitten and Schanze groups — have made use of the interactions between polyanionic conjugated polymers and cationic fluorescence

quenchers to produce a sensory response. One of the quenchers in common use by these groups is the herbicide *N,N'*-dimethyl-4,4'-bipyridinium, also known as methylviologen (MV^{2+} — see Chapter 1). This electron-poor dication is a strong quencher of the fluorescence of conjugated polymers, and its potency is maximized when an anionic conjugated polymer is used. For example, Whitten and co-workers found that methylviologen quenches a sulfonate-substituted poly(phenylene vinylene) (PPV) with a Stern-Volmer constant of around 10^7.[3] These authors attributed this very large quenching effect to both efficient electron transfer to MV^{2+} and non-specific polymer aggregation induced by the presence of the dication, and used a biotinylated MV^{2+} derivative to create a system in which the fluorescence of the polyanionic PPV is restored on addition of avidin. Another approach was taken by Schanze, Lakowicz and co-workers, who developed viologen-boronic acids in which the quenching ability of the MV^{2+} core is reduced by complexation with the vicinal diol units of monosaccharides.[4] These sugar-sensitive quenchers were used together with a PPE bearing sulfonate sidechains to create a sensor for fructose, glucose and galactose.

The detection of DNA hybridization is of major importance in genomic analysis and has also been the target of several conjugated polymer-based assays. The groups of Leclerc[5] and Nilsson[6] have exploited changes in the photophysical properties of cationic polythiophenes on complexation to anionic DNA to create highly sensitive DNA sensors. Bazan and Heeger have used the interaction of cationic polyfluorene derivatives with polyanionic nucleic acids to control energy transfer between the conjugated polymer and fluorophore-labeled target DNA.[7] Whitten *et al.* have used the biotinylation-mediated co-localization of conjugated polymers, quencher-labeled probe DNA and peptide-nucleic acid scaffolds on microparticles to create assays capable of detecting single-nucleotide mismatches.[8]

A unifying feature of most of the research described above is the use of simple, unmodified conjugated polyelectrolytes as amplification elements. These systems are usually based on conjugated polymers in which charged groups are either integrated into the polymer backbone or are attached to it by means of short alkyl spacer groups. Because the dominant mechanism of signal transduction involves the manipulation of electrostatic effects — which are ubiquitous in biochemistry — these sensor designs necessarily suffer from the possibility of reductions in sensitivity or fidelity through non-specific polymer-analyte interactions. Previous research by former Swager group graduate student Kenichi Kuroda has sought to overcome these limitations using non-ionic water-soluble polymers with dendritic sidechains.[9]

The approach to the integration of conjugated polymers into biosensor schemes presented in this chapter has focused on the role of small-molecule dyes in biochemistry and the need to create conjugated-polymer systems that can be chemically manipulated in ways similar to these dyes. This focus necessarily draws on the basic chemistry used to label biomolecules with fluorophores and on the entire field of bioconjugation.[10] Among the many schemes used for the preparation of bioconjugates, one of the most popular involves the attachment of biomolecule amine groups — such as those found on the side chains of lysine residues in proteins — to dyes bearing amine-reactive functional groups such as isothiocyanates or activated esters. The variety of amine-reactive dye derivatives available from commercial suppliers such as Sigma and Molecular Probes is a testament to the popularity of this class of bioconjugation reaction. In particular, activated ester derivatives (such as succinimide and pentafluorophenyl esters) are available for a wide variety of small-molecule fluorophores and represent a popular compromise between the sometimes-conflicting requirements of high activity toward amine groups, long-term storage stability, and robustness of the biomolecule-label linkage. With these concerns in mind,

we envisioned a conjugated polymer system containing activated ester groups that could be integrated into existing bioconjugation schemes (Figure 2.1).

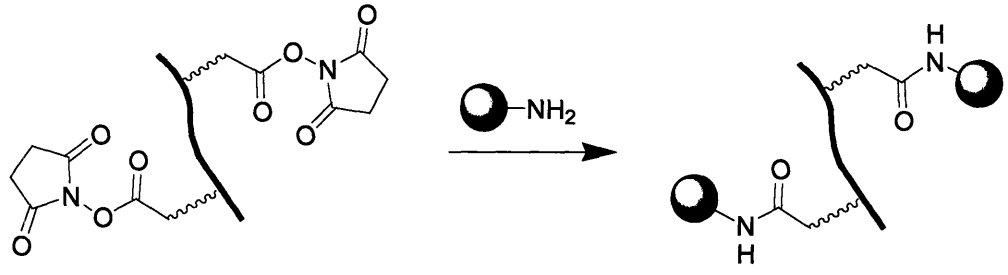

Figure 2.1. Schematic representation of a conjugated polymer functionalized with activated succinimide esters and used for attachment of a biomolecule through a pendant amine group.

The development of conjugated polymer systems capable of post-polymerization functionalization opens up a wide range of potential sensor applications for these materials. In particular, they can provide an entry into polymer sensor schemes where the recognition elements cannot be directly integrated into the monomer design for synthetic or scale reasons: in these cases, the solvent- or reagent-sensitive recognition element can be installed post-polymerization through the use of activated ester derivatives. Several applications of this post-polymerization functionalization principle are described in this chapter, but our efforts have been focused on a single model biosensory system that best illustrates the potential applications of these polymers.

The design inspiration for this model system came from previous observations surrounding the use of PPE thin films as sensors for the explosive TNT (see Chapter 1). In these studies, the penetration of TNT molecules into the polymer film and the strong association of TNT with the polymer backbone were found to be key factors in ensuring optimal fluorescence quenching and thus a strong sensory response. We conceived of a related system in which

quencher *removal* from a conjugated polymer forms the basis of a 'turn-on' response. Such a scheme requires a suitable quencher-polymer pair, joined by a tether that can be cleaved or removed by a recognition or enzymatic event (Figure 2.2).

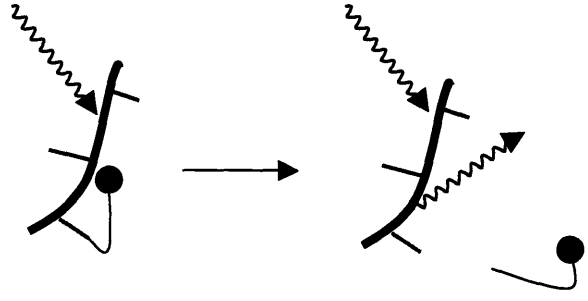

Figure 2.2. Schematic representation of a conjugated-polymer turn-on sensor based on quencher removal. Covalent attachment of a quencher (dark circle) to the polymer backbone causes the polymer to stay in a non-fluorescent ('off') state. On cleavage of the quencher-polymer tether, the quencher is removed and fluorescence is turned 'on'.

An obvious choice of tether in a scheme such as Figure 2.2 is an oligopeptide chain susceptible to degradation by a protease. The system would then signal the presence of this protease by the generation of new fluorescence.[11] Enzymatic cleavage of the tether would add a second gain mechanism — supplied by ability of a single enzyme molecule to hydrolyze multiple oligopeptide tethers — to the amplification inherent in the amplified quenching of PPEs by nitroaromatics. From a bioanalytical perspective, a protease assay based on quencher removal from a conjugated polymer can be seen as a polymer-amplified variant of internally-quenched fluorogenic probes based on small-molecule donor-acceptor pairs (Figure 2.3).[1] With careful optimization of quencher efficiency and loading, the combination of the non-linear effects of enzymatic catalysis and amplified quenching could result in an assay scheme of unparalleled sensitivity.

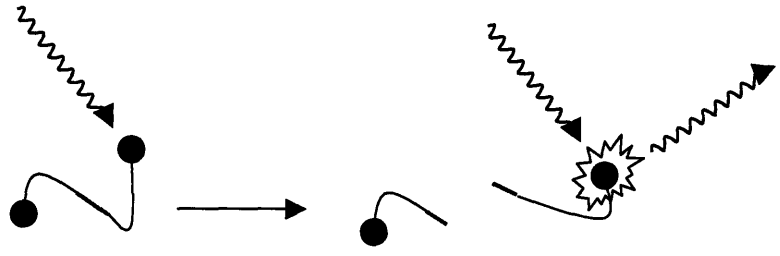

Figure 2.3. Schematic representation of the mechanism of action of conventional small molecule-based fluorogenic probes. A dye pair (dark circles) consisting of a normally fluorescent donor and non-fluorescent acceptor are joined by an enzyme-cleavable tether that maintains the system in an internally quenched 'off' state. On cleavage of the tether, donor-acceptor energy transfer is interrupted and the fluorescence of the donor is turned 'on'.

In this chapter we describe the design and synthesis of a series of carboxylate-functionalized PPEs that can be converted into activated esters and used in post-polymerization bioconjugation schemes. These PPEs have been used together with a fluorescence-quenching oligopeptide to prepare a PPE-peptide substrate that forms the basis for a fluorogenic turn-on assay for proteases after the principle illustrated in Figure 2.2. The photophysical properties of these PPEs in aqueous solution and in the presence of quenchers and surfactants has been investigated and used to provide a model that reveals the role of electrostatic and hydrophobic interactions in the behavior of the PPE-peptide assay system.

Results and Discussion

Synthesis of carboxylate-functionalized PPEs

A number of potential designs were explored for the preparation of PPEs containing carboxylic acid-bearing sidechains suitable for conversion into activated esters. The requirements of our proposed applications dictated that the polymers be water-soluble, and we wished to maximize the flexibility of the system by choosing a modular linker unit to join the

carboxylic acid moieties to the polymer backbone. The monomer 2,5-bis(carboxymethyl)-1,4-diiodobenzene was known from previous research carried out in the Swager group, but potential steric problems arising from the close proximity of the carboxylate group to the eventual location of the polymer backbone decreases its utility for bioconjugation. We chose to prepare a set of monomers (Scheme 2.1) based on extension of the sidechain of this dicarboxylic acid with ester derivatives of commercially available ω-aminoalkanoic acids. Hydrolysis of the resulting methyl esters **(2)** produced carboxylic acid monomers **1**. Compounds **1** and **2** were only sparingly soluble in common organic solvents, which made synthesis and purification difficult. The relatively low water solubility of **2** also suggested that these monomers would not be sufficiently hydrophilic for use in the preparation of water-soluble PPEs.

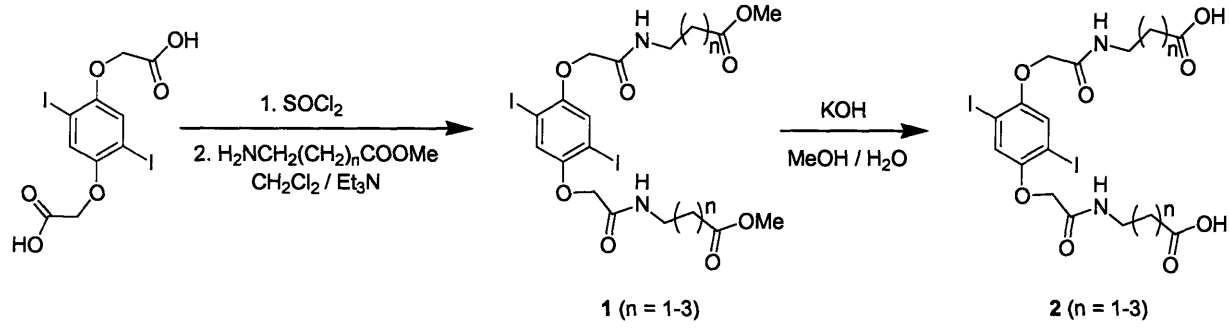

Scheme 2.1. Synthesis of extended-chain methyl ester monomers **1** and carboxylic acids **2.**

The synthetic and solubility problems encountered with amide-based sidechains suggested that a sidechain of greater overall hydrophilicity would be required to obtain fully water-soluble polymers. In addition, we envisioned that the steric needs of large biomolecules would be best served by a system in which the carboxylic acid unit was positioned farther from the polymer backbone than the commerically available amines used in Scheme 2.1 would allow. Accordingly, we chose to make use of the well-known water solubility and easy availability of oligoethylene

glycols to construct a set of two monomers, **9** and **10,** containing carboxylic acid groups separated from the monomer core by glycol spacers (Scheme 2.2).

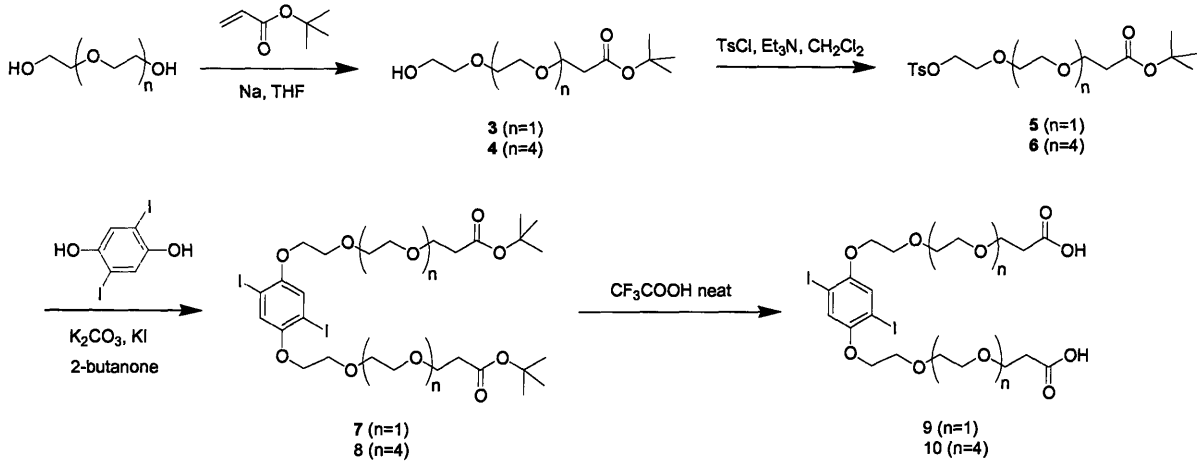

Scheme 2.2. Synthesis of carboxylate monomers **9** and **10**.

The initial functionalization of diethylene glycol and pentaethylene glycol, which were selected to provide a choice of two very different backbone-carboxylate spacings in the completed polymer, was carried out based on a literature precedent.[12] Michael addition of a large excess of the deprotonated glycol to *tert*-butyl acrylate provided a mixture of the mono-addition product and unreacted glycol which could be easily separated owing to the high water solubility of the unreacted starting material. Conversion of the remaining free alcohol group of the glycol to the tosylate followed by a Williamson etherification with 2,5-diiodohydroquinone provided the *tert*-butyl-protected acid monomers **7** and **8** as clear oils. While these compounds are highly soluble in organic solvents and would therefore be easy to incorporate into a polymer synthesis reaction, we chose to remove the *tert*-butyl groups at the monomer stage to avoid synthetic incompatibilities between common de-*tert*-butylation reagents and the electrophile-sensitive PPE backbone. Simple dissolution of **7** and **8** in neat trifluoroacetic acid provided acid monomers **9** and **10** as white solids. Both **9** and **10** have high solubility in common organic solvents.

While monomers **9** and **10** could conceivably be converted into succinimide esters before polymerization, we chose to delay the activation of the carboxylic acid groups until after polymerization because of concerns about the stability of the succinimide esters to the polymerization conditions. In this context, monomers **9** and **10** were co-polymerized with diacetylene co-monomers containing di- and triethylene glycol methyl ether sidechains to provide polymers **11, 12** and **13.** Morpholine was used as the polymerization medium in these reactions, simultaneously serving as both an excellent solvent for the growing polymer chain and as the amine base needed for the Sonogashira coupling reaction (Scheme 2.3). In addition, the use of this solvent facilitated the purification of the water-soluble product polymers: the reaction mixtures were typically purified by pouring the morpholine solution into water and dialyzing the resulting solution against several changes of distilled water in 10,000-MWCO dialysis tubing. Solid samples of **11, 12** and **13** could be recovered by lyophilization of the resulting aqueous solutions.

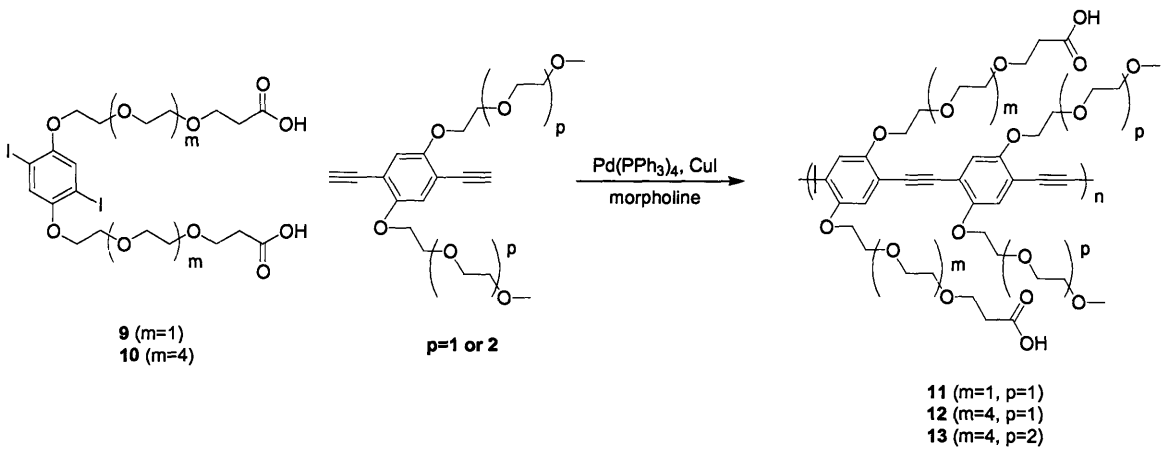

Scheme 2.3. Synthesis of carboxylate PPEs **11, 12** and **13** from monomers **9** and **10** and oligoethylene glycol-substituted diacetylene co-monomers.

While all three polymers could be re-dissolved in DMF, water and aqueous buffer solutions, the ease of re-dissolution generally followed the order **11** < **12** < **13,** suggesting that a greater total number of glycol units per polymer repeat unit increases the solubility of the polymer.

Photophysical properties of carboxylate-functionalized PPEs

The absorbance and fluorescence spectra of polymer **12** were measured in DMF (Figure 2.4) and aqueous solution (Figure 2.5).

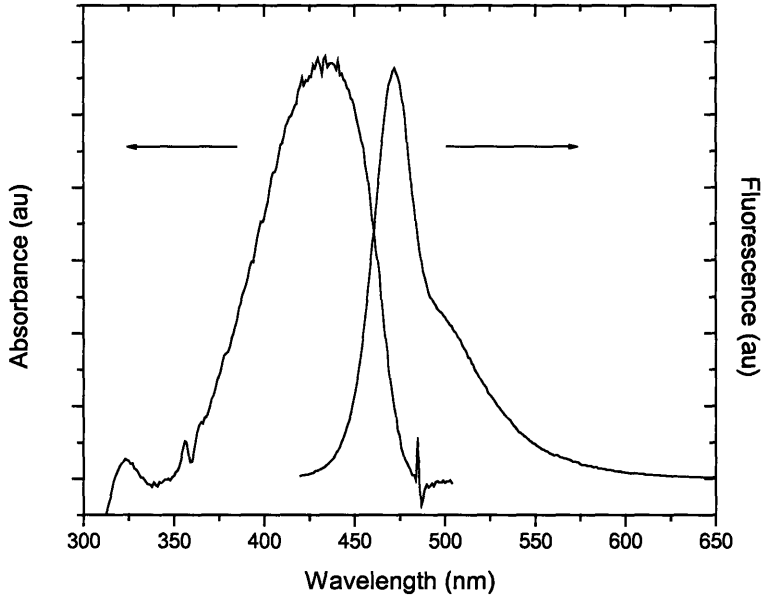

Figure 2.4. Absorbance (left) and fluorescence (right) spectra of **12** in DMF solution.

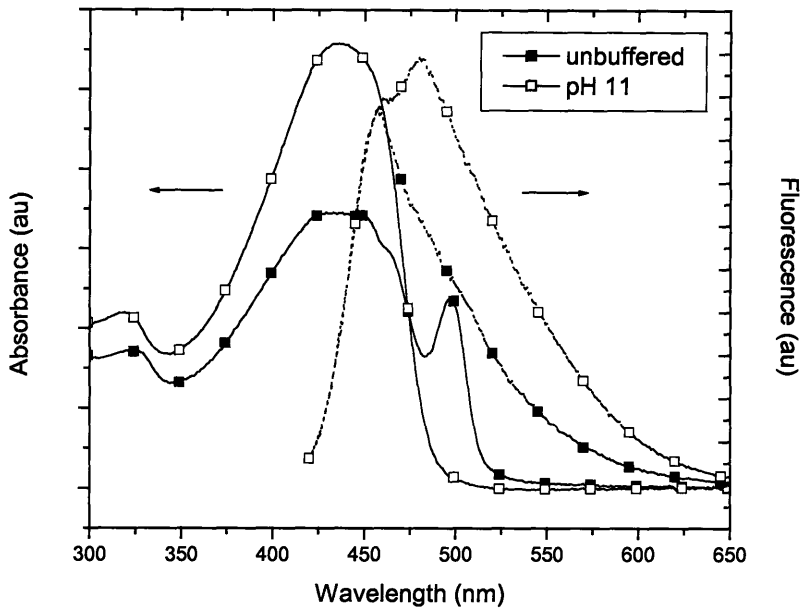

Figure 2.5. Absorbance (left, solid lines) and fluorescence (right, dotted lines) spectra of **12** in unbuffered water (pH ~ 6) and in a solution adjusted to pH 11. The concentration of polymer is identical in both cases.

In DMF, polymer **12** shows absorbance and fluorescence features typical of non-aggregated PPEs dissolved in 'good' solvents, including a single absorbance feature centered around 430 nm and an emission profile with a maximum at 470 nm. However, the spectra of **12** in aqueous solution (Figure 2.5) are highly distorted and pH-dependent. In addition to the typical 430 nm absorbance feature characteristic of PPEs, the absorbance spectrum of **12** in unbuffered water (pH ~ 6) displays a sharp peak at 500 nm indicative of aggregation caused by polymer π-stacking. The fluorescence of **12** under these conditions is somewhat blue-shifted relative to typical PPE fluorescence spectra in 'good' solvents. In NaOH solution at pH 11, the spectral features of **12** change remarkably: the sharp 500 nm absorbance feature disappears completely, and the emission spectrum shows an additional broad, red-shifted feature.

The absorbance features of **12** would seem to suggest that this polymer undergoes a pH-sensitive aggregation process wherein a well-defined polymer aggregate dominates at low pH.

Rendering the polymer solution alkaline increases the negative charge on the carboxylate-functionalized PPE, augmenting the water solubility of individual polymer chains and discouraging inter-chain interactions. A similar mechanism has been proposed by Schanze and co-workers to explain the pH- and solvent-dependent spectroscopic features of phosphonate- and sulfonate-substituted PPEs.[13]

Although the minimization of polymer aggregation effects would seem to be necessary to achieve the greatest possible sensitivity in assay schemes based on these PPEs, the need for stable, near-neutral buffered solutions precludes the use of a highly alkaline environment to control aggregation in these applications. Instead, we screened a number of commercially available non-ionic surfactants for their ability to increase the fluorescence quantum yield (QY) of PPEs in neutral and buffered solutions. Triton X-100 (Scheme 2.4) was found to be remarkably effective in this regard: the addition of about 0.5 wt% of this surfactant to a solution of **13** in water increased the QY of the polymer from 0.11 to 0.20. The same effect was observed in a solution of **13** in a pH 7.5 Tris-buffered saline (TBS) solution, although its overall magnitude was not as strong (Figure 2.6). This difference can be attributed to the larger inherent hydrophobic forces in solutions of high ionic strength.

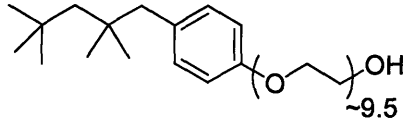

Scheme 2.4. Structure of the non-ionic surfactant Triton X-100.

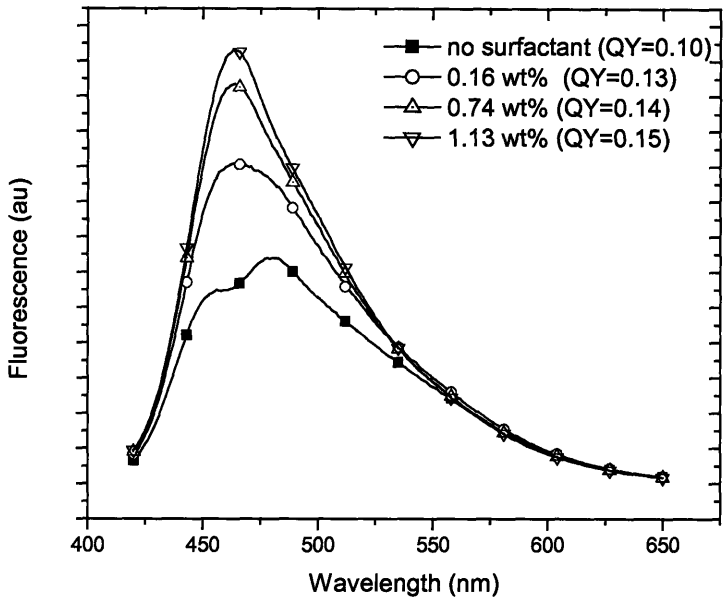

Figure 2.6. Fluorescence enhancement of polymer **13** in Tris-buffered saline (TBS; 50 mM Tris pH 7.5, 150 mM NaCl, 5 mM $CaCl_2$) on addition of Triton X-100, with approximate quantum yields. The concentration of polymer is identical in each of the scans.

The data in Figure 2.6 clearly show that 30-50% increases in QY are possible with the addition of small concentrations of Triton X-100. Concomitant with the fluorescence intensity increases is a gradual change in the shape of the fluorescence spectra. In the absence of surfactant, the spectrum of **13** in TBS resembles that of **12** in water at pH 11 — a dual-peak structure with a red-shifted emission maximum around 480 nm. Addition of surfactant causes the red-shifted emission band to disappear, with the result that the fluorescence profile of **13** in the presence of 1.13 wt% Triton X-100 begins to resemble the spectrum observed in the 'good' solvent DMF (Figure 2.4).

The results of the pH and surfactant experiments suggest that in aqueous solution the polymer exists in equilibrium between an aggregated, π-stacked form of relatively low QY and a highly solubilized form of higher QY in which inter-chain interactions are minimized. To

determine if these two forms can be identified photophysically, the fluorescence lifetime of polymer **13** was measured in DMF and three different buffers, both with and without added surfactant (Table 2.1).

Table 2.1. Fluorescence lifetimes of **13** in aqueous buffer solutions and in DMF. Numbers in brackets indicated the relative amplitudes of the component lifetimes. Polymer solutions were excited at 405 nm and fluorescence recorded at 470 nm using RF phase modulation (see Experimental section).

Surfactant / Buffer	pH 5.0 (acetate)	pH 7.3 (PBS)	pH 8.5 (borate)	DMF
no surfactant	0.64 ns (0.82) 3.81 ns (0.18)	0.64 ns (0.82) 4.05 ns (0.18)	0.67 ns (0.93) 3.97 ns (0.07)	0.77 ns
0.1 wt% Triton X-100	0.77 ns (0.97) 3.90 ns (0.03)	0.70 ns (0.87) 3.24 ns (0.13)	0.75 ns (0.98) 3.71 ns (0.02)	-
0.2 wt% Triton X-100	-	0.73 ns (0.92) 4.24 ns (0.08)	-	-

The fluorescence lifetime of **13** in DMF solution was 0.77 ns, a value typical for PPEs in 'good' solvents. In the case of aqueous solutions, we found that the fluorescence decay was bi-exponential, indicating the presence of two distinct fluorescent species in solution or two distinct radiative decay pathways.[1] The components of the fluorescence decay correspond to a dominant short-lived species of τ = 0.6-0.7 ns — similar to the lifetime of the polymer in DMF — together with minor contributions from a longer-lived 3-4 ns component. As Table 2.1 indicates, the relative populations of the two species are strongly affected by the addition of surfactant, which was found to greatly increase the amplitude of the short-lifetime component at the expense of the longer-lived species. Alkaline buffer environments also generally favored increased contributions from the short-lifetime component. In general, the data indicate that the same conditions that promote large quantum yields and sharp emission spectra (organic solvents, alkaline pH values or surfactant in aqueous solutions) also result in an increase in the relative contribution of the short-lived species. These observations are consistent with a model in which

the polymer chains are aggregated in neutral to acidic solutions and well-solvated in organic solvents, when the solution is rendered alkaline, or when surfactant is added. In this case the short-lived component of the fluorescence lifetime represents the radiative lifetime of the non-aggregated polymer and is increased in amplitude when the relative proportion of polymer chains in this state is increased. Similarly, the long-lived fluorescence decay can be assigned to polymer aggregates that are broken up at conditions of high pH and surfactant concentration and are completely absent in DMF solutions. These aggregates are expected to form through strong hydrophobic and π-stacking interactions between polymer chains, and their long fluorescence lifetime is the signature of a weakly allowed transition from the lowest excited state of the aggregate to the ground state.[13] In phosphate-buffered saline (PBS) solutions of **13** the high ionic strength of the medium encourages greater aggregation through hydrophobic interactions, requiring higher concentrations of surfactant to break up aggregates compared to buffer solutions lacking added salts.

Quencher selection and quenching efficiency

An assay substrate of the type illustrated in Figure 2.2 derives its sensitivity from both the quantum yield of the polymer fluorophore and the degree of quenching in the initial non-fluorescent form. The success of quencher-removal protease detection is therefore critically dependent on the optimization of the 'off' state to give the lowest possible background fluorescence. Simple fluorogenic protease substrates like the one depicted in Figure 2.3 generally use small-molecule fluorophore-quencher pairs such as the MCA-DNP and EDANS-DABCYL systems (Scheme 2.5). In these systems quenching occurs via Förster energy transfer and is

maximized by the good spectral overlap between the donor fluorescence and acceptor absorbance within each pair.

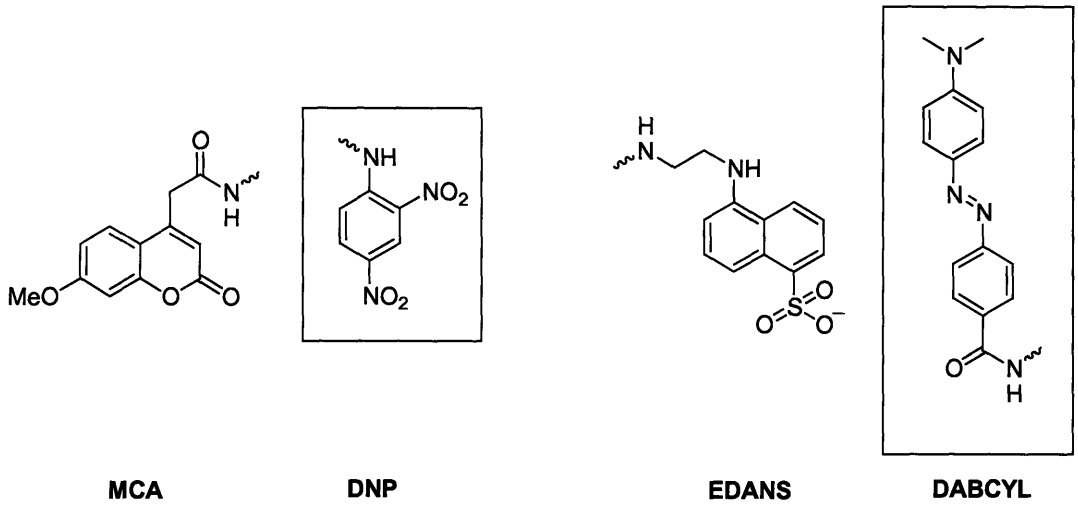

Scheme 2.5. Two common fluorophore-quencher pairs used in commercial fluorogenic probes for proteases. Quencher structures are enclosed in boxes. MCA = 7-methoxycoumarin-4-acetyl; DNP = 2,4-dinitrophenylamino; EDANS = 2-(1-sulfonatonaphthyl-5-amino)ethylamino; DABCYL = 4-(4-dimethylaminophenylazo)benzoyl.

We chose to investigate the DNP quencher unit based on the known sensitivity of PPEs to quenching by nitroaromatics. In addition, we hoped to capitalize on the commercial availablity of dinitrophenyl-substituted lysine (LysDNP) and related derivatives suitable for use in solid-phase peptide synthesis. To determine the suitability of the DNP chromophore as a PPE fluorescence quencher, an analysis of the Stern-Volmer quenching constants for LysDNP with polymer **13** was carried out in unbuffered aqueous solution and in pH 7.5 TBS, both with and without surfactant (Figure 2.7).

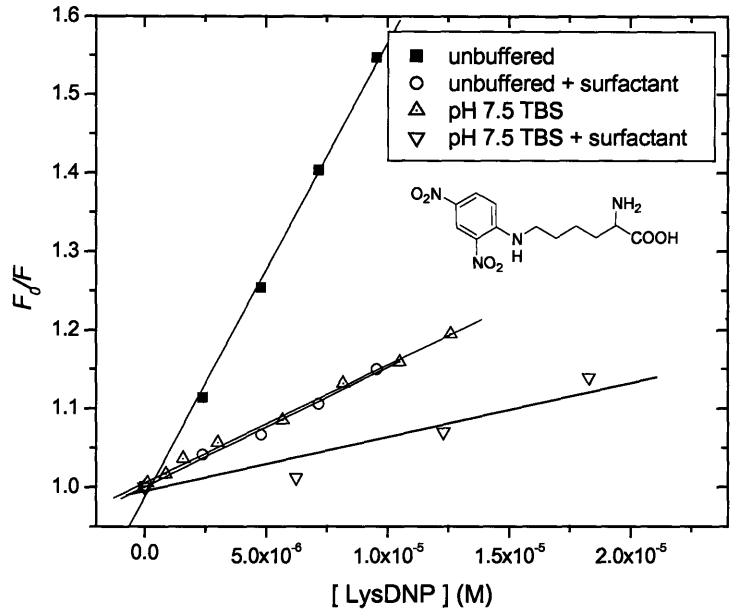

Figure 2.7. Stern-Volmer quenching F_0/F of polymer **13** by LysDNP (structure shown) as a function of concentration in solutions of varying composition.

Quenching of **13** was found to be highly efficient in neutral, unbuffered water, showing a Stern-Volmer quenching constant K_{SV} of 5.8×10^4 M^{-1}. The presence of Triton X-100 at low concentration reduced this value by a factor of four to 1.4×10^4 M^{-1}, similar to the K_{SV} determined in Tris-buffered saline (1.5×10^4 M^{-1}). Addition of surfactant to the Tris-buffered saline solution reduced K_{SV} still further to 1.0×10^4 M^{-1}. The large magnitude of K_{SV} in all of these cases strongly implies that static binding of LysDNP is responsible for the observed quenching (see Chapter 1), and in this context the differences in K_{SV} observed under various solvent and surfactant conditions can be understood in terms of variations in the effective association constant of LysDNP and **13**. Here the addition of surfactant and the use of a controlled near-neutral pH reduces hydrophobically driven interactions between LysDNP and **13**, suggesting that the pH, ionic strength and surfactant concentration of the assay medium is important in determining the

background fluorescence of a quencher-linked substrate such as the one illustrated in Figure 2.2. These parameters will thus directly affect the 'on' / 'off' signal contrast achievable in such a system.

Covalent bioconjugation with carboxylate PPEs

The experiments described above clearly indicate that the DNP chromophore is a potent quencher of the fluorescence of carboxylate polymers such as **13** in aqueous solution. However, the mechanism of the quencher-removal assay illustrated in Figure 2.2 requires that there be a fundamental contrast between the 'off' (tethered) and 'on' (cleaved) states of the polymer substrate when the absolute quencher concentration is kept constant. A demonstration of this contrast effect must verify that DNP groups covalently tethered to the polymer sidechain are significantly more effective at quenching the polymer fluorescence than the equivalent concentration of DNP groups in solution. The difference in quenching efficiency revealed by such an experiment is a direct determinant of the signal gain possible in a quencher-removal protease assay.

The experiment designed to determine this 'on' / 'off' contrast also provided the opportunity to test the utility of carboxylate PPEs **11, 12** and **13** in bioconjugation schemes. We prepared **15** (Scheme 2.6) for use as a biomolecule 'mimic' — an amine-containing substance, suitable for covalent attachment to an activated-ester PPE, which would allow the coupling reaction to be followed in the fluorimeter.

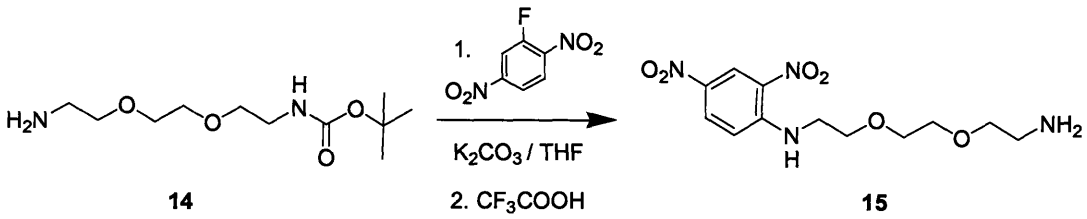

Scheme 2.6. Synthesis of the hydrophilic biomolecule 'mimic' **15**.

To establish the baseline quenching ability of **15** relative to *unactivated* carboxylate PPEs, we continuously monitored the fluorescence of a stirring solution of **12** in borate buffer as 15-nmol aliquots of **15** were added (Figure 2.8). As expected, **15** served as an effective quencher of the unactivated polymer **12**, producing significant fluorescence quenching at low concentrations.

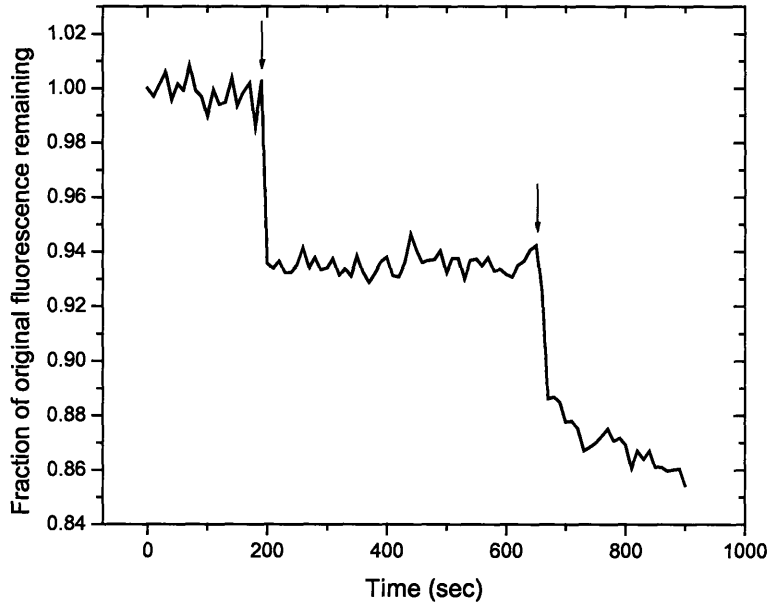

Figure 2.8. Fluorescence of a solution of **12** in borate buffer (pH 8.5) in response to addition of aliquots of **15** (arrows). Each addition corresponds to a concentration increase of approximately 5 μM in **15**. The fluorescence at 470 nm (λ_{ex} 405 nm) was recorded every 10 s.

Following standard methods for the activation of carboxylate-containing small molecules, a solution of **12** in DMF was treated with excess *N*-hydroxysuccinimide (NHS) and

diisopropylcarbodiimide (DIPC). After a short activation period, the activation solution was diluted into borate buffer and treated with a single aliquot of **15**. The fluorescence of the activated polymer solution was followed after addition of the quencher (Figure 2.9).

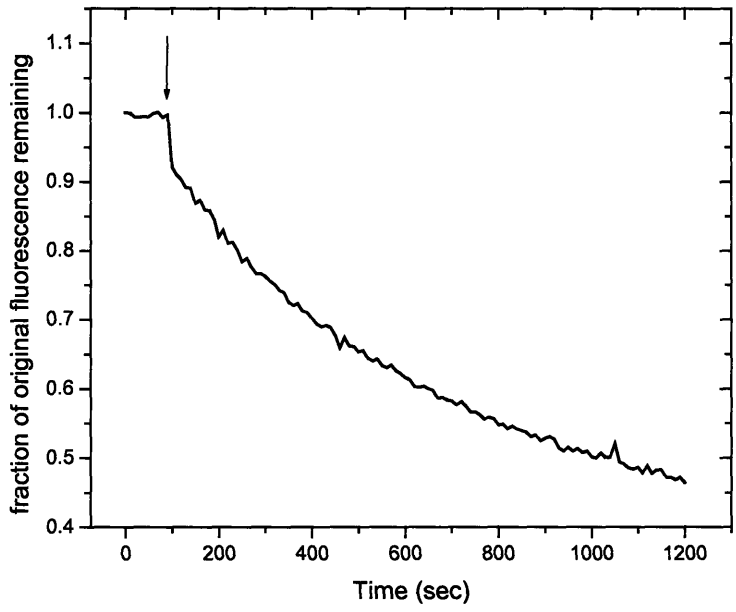

Figure 2.9. Fluorescence of a solution of **12,** previously activated with excess NHS and DIPC in DMF for 10 minutes, after dilution into borate buffer (pH 8.5) and addition of **15** at 5 μM (arrow).

Whereas the presence of 5 μM of **15** reduces the fluorescence of unactivated polymer **12** to about 93% of its initial value (Figure 2.7), the same concentration of **15** added to *activated* **12** results in a time-dependent reduction to about 50% of its initial fluorescence after 15 minutes (Figure 2.9). The exponential decay of Figure 2.9 is consistent with a mechanism in which the fluorescence-quenching amine-containing **15** is covalently 'captured' by the activated-ester form of **12** as an amide. It is important to note that the absolute quencher concentration remains the same throughout each experiment: differences in fluorescence intensity at any given time can be accounted for by the distribution of quencher in the solution (either free or covalently bound to

the polymer). In this case the covalent tether leads to a high 'effective concentration' of **15** around the polymer and more significant quenching, even though K_{SV} does not change. In related experiments, we found that extending the activation time resulted in faster fluorescence decay on addition of **15**, consistent with a more complete conversion of the carboxylate groups of **12** to activated esters.

To confirm that amide bond formation between the activated ester form of **12** and quencher **15** is in fact responsible for the time-dependent reduction in fluorescence seen in Figure 2.9, we attempted to disrupt the quencher-capture reaction through the addition of a large excess of hydroxylamine (Figure 2.10). Hydroxylamine is a powerful nucleophile that is used in bioconjugation schemes to quickly consume excess activated ester.

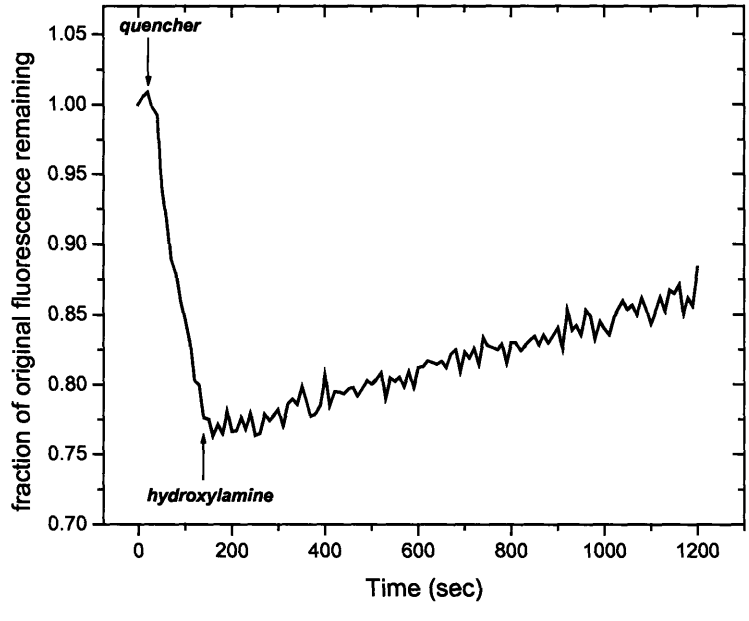

Figure 2.10. Fluorescence of a solution of **12**, previously activated with excess NHS and DIPC in DMF for 90 minutes, after dilution into borate buffer (pH 8.5), addition of a 15-nmol aliquot of **15** (first arrow) followed by excess hydroxylamine (second arrow).

The addition of hydroxylamine completely halted the fluorescence decay caused by the previous addition of **15,** showing that it effectively competes for the activated ester groups present on the polymer sidechains. The slow increase in the fluorescence of the polymer solution after hydroxylamine addition suggests that the activation process itself has a deleterious effect on polymer fluorescence and that destruction of the activated ester groups or excess NHS or DIPC improves the fluorescence properties of the system. In this case the addition of hydroxylamine turns 'on' polymer fluorescence by destroying excess activation reagent or disrupting polymer cross-links.

Protease target selection and linker design

The enzymatic specificity of the quencher-removal protease assay illustrated in Figure 2.2 arises entirely from the oligopeptide tether used to link the quenching unit to the polymer backbone. As a first demonstration of the utility of our proposed protease detection scheme, we turned to the matrix metalloprotease (MMP) family. The MMPs are zinc proteases that are involved in normal biological processes and are also strongly associated with tumor angiogenesis and metastasis.[14] While a wide variety of conventional fluorogenic substrates are available for these enzymes, their important role in the progression of cancer has inspired the development of a number of unusual fluorogenic probes. For example, the group of Weissleder has invested considerable effort in the design of MMP substrates for *in vivo* imaging. These substrates consist of near-infrared fluorophores tethered to a soluble polylysine backbone by oligopeptide linkers susceptible to hydrolysis by MMPs, and are ordinarily non-fluorescent due to self-quenching of the dyes.[15] On enzymatic cleavage of the linkers, free fluorophore is released and the system becomes fluorescent. These systems were used to image tumors and to quantify MMP inhibition

in live mice. In conceptually related work, Matrisian and co-workers very recently reported a dendrimer-based internally quenched substrate for MMPs based on fluorescein-labeled oligopeptides covalently attached to a PAMAM dendrimer.[16]

The specific target of our proposed quencher-removal protease assay was matrix metalloprotease 13 (MMP-13), a human collagenase first isolated and characterized in the mid-1990s.[17] MMP-13 has been associated with both arthritis and breast carcinomas and is thus of direct medical interest. While the natural substrate of MMP-13 is collagen, a highly active non-natural substrate sequence ($k_{cat}/K_m \sim 10^6$) has been identified, making this enzyme-substrate pair attractive for our application.[18] This substrate sequence, GPLGMRGL, is hydrolyzed by the enzyme at the G-M bond and contains the PXGX motif (where X is a hydrophobic amino acid) used in earlier fluorogenic substrates for proteases.[19] We also recognized that the presence of a single Arg residue in the middle of this sequence would render it susceptible to cleavage at the R-G bond by the common digestive enzyme trypsin. A modified version of this sequence, AcHN-LysDNP-GPLGMRGLGGGGK **(16)**, was synthesized using standard solid-phase techniques in conjunction with Dr. Charlene Mello and Jennifer Burzycki of the US Army Natick Soldier Center. Our modifications were designed to provide both a source of the DNP quencher (LysDNP) and a free amine handle (C-terminal Lys residue) for covalent attachment of **16** to activated-ester derivatives of carboxylate PPEs **11-13.** The N-terminal acetyl group was introduced manually onto the bead-bound peptide to ensure that the conjugation reaction would proceed solely through the C-terminal Lys residue.

Preparation and evaluation of polymer-peptide substrates

After HPLC purification and characterization, the fluorescence-quenching peptide **16** was covalently tethered to polymer **12** using a variation on the technique described above. To ensure the fidelity of the coupling reaction, we made use of the fact that carbodiimide activation of carboxylate groups is efficient in mildly acidic solutions and very slow in alkaline solutions.[10] A DMF solution of polymer **12** was treated with excess 1-ethyl-3-(3-(1-dimethylamino)propyl)carbodiimide hydrochloride (EDAC, a water-soluble carbodiimide) and NHS, added as solutions in pH 5.5 MES buffer. After approximately one hour, a solution of **16** in pH 8.5 borate buffer was added. The use of an alkaline environment in this step was critical to both stop the activation reaction and facilitate amide bond formation between **16** and activated **12**. A parallel reaction using the previously described biomolecule 'mimic' **15** was carried out to provide a non-peptidic control substrate (Scheme 2.7).

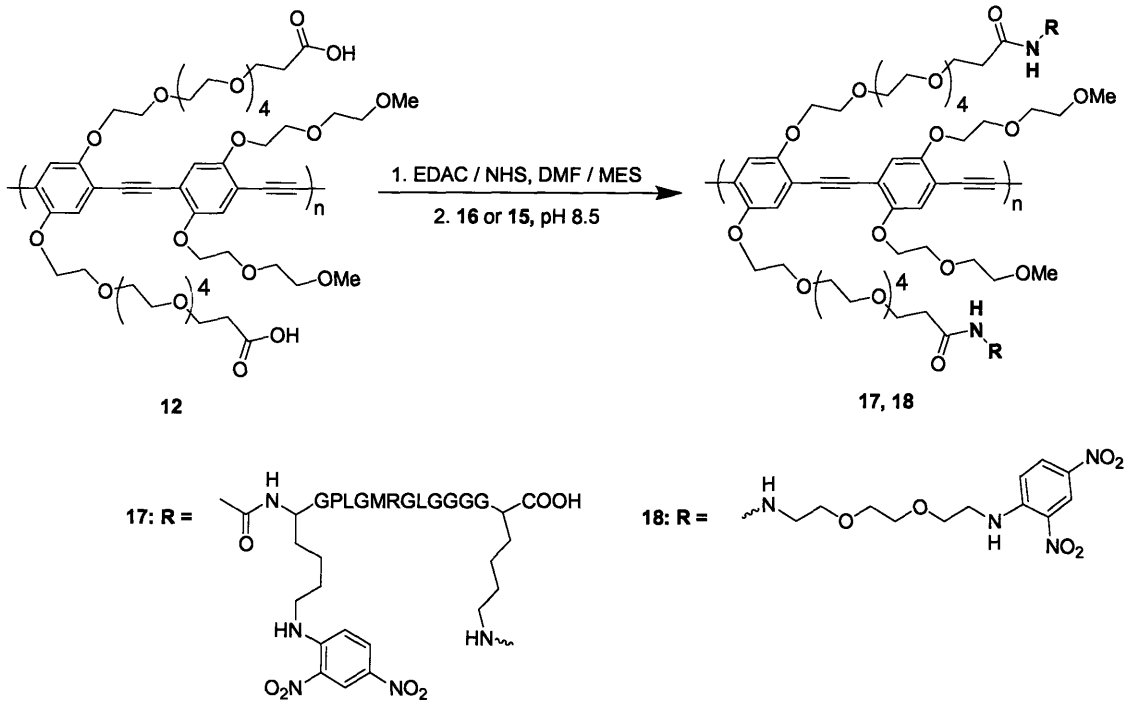

Scheme 2.7. Synthesis of polymer-peptide substrate **17** and mimic **18.**

Polymer-peptide **17** and mimic **18** were purified by dialysis against frequent changes of water to remove unreacted starting material and coupling by-products. Both substrates were non-fluorescent, and the absorbance spectrum of **17** in Tris-buffered saline clearly showed contributions from the absorbance of both the PPE backbone (centered at 435 nm) and the pendant DNP chromophores (centered at 360 nm) (Figure 2.11).

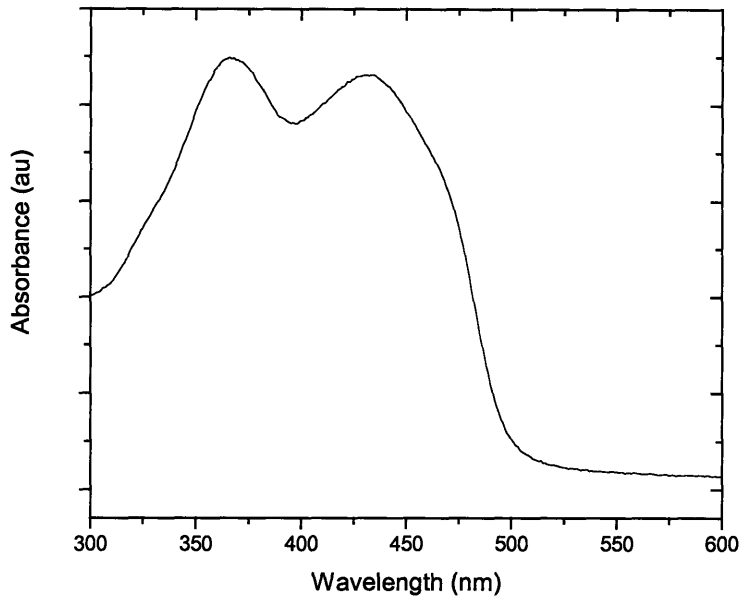

Figure 2.11. Absorbance spectrum of a solution of **17** in TBS.

We made use of the relative contributions of the DNP chromophore and the absorbance of the PPE backbone to determine the ratio of DNP to polymer repeat units in **17.** The extinction coefficients of **13** and LysDNP were evaluated independently at 360 and 435 nm (Table 2.2). By solving for the observed absorbances of **17** at these wavelengths (Figure 2.11), its peptide loading was determined to be 1.7 peptides per polymer repeat unit.

Table 2.2. Extinction coefficients of **13** (representative of polymer **12**) and LysDNP (representative of peptide **16**) determined in pH 7.5 TBS. All values are reported in units of M^{-1} cm^{-1}. Polymer values are reported on a repeat-unit basis.

Wavelength / Species	Polymer 13	LysDNP
360 nm	11,500	17,400
435 nm	30,400	5,800

Trypsin-catalyzed fluorescence turn-on

The response of substrate **17** to trypsin-catalyzed peptide cleavage was followed by monitoring the fluorescence of a dilute solution (1.1 μM) in TBS after addition of a small quantity of trypsin (3 μg/ml) (Figure 2.12). The fluorescence of **17** is rapidly and strongly enhanced under these conditions.

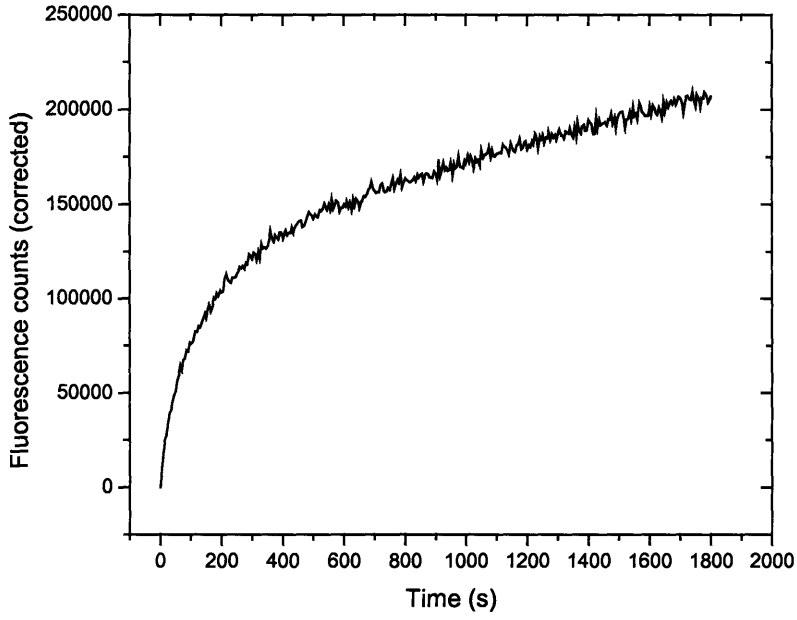

Figure 2.12. Fluorescence response of **17** (1.1 μM) to treatment with trypsin at 3 μg/ml.

The observed response in this case is characterized by a rapid initial generation of fluorescence followed by a slower, linear evolution of fluorescence with time. Comparison of the absorbance and fluorescence spectra of **17** before and after digestion with trypsin reveal an approximately tenfold increase in fluorescence intensity after 30 minutes. The absorbance spectrum of **17** is changed slightly after trypsin digestion, especially around 360 nm, suggesting that the dipole strength of the DNP chromophore is sensitive to complexation to the polymer backbone.

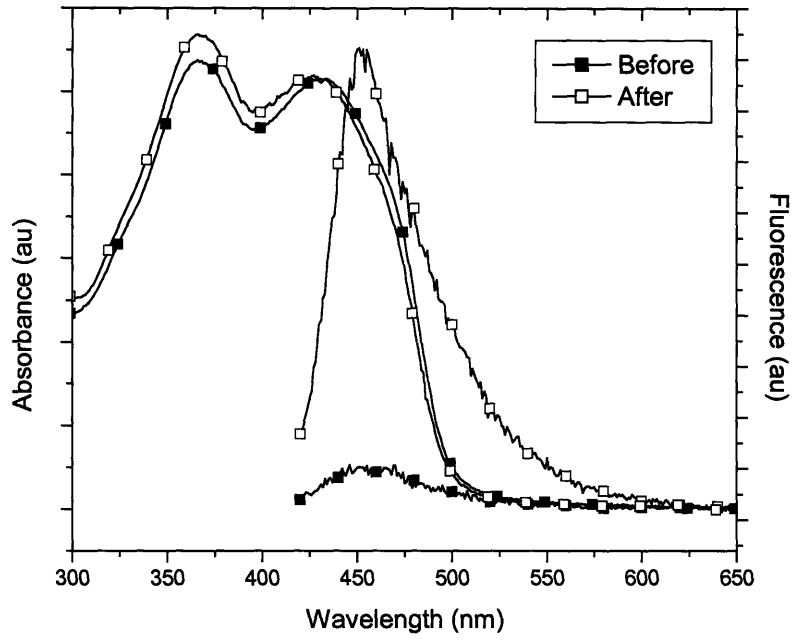

Figure 2.13. Absorbance (left) and fluorescence (right) spectra of **17** (1.1 μM) before and after digestion with trypsin (3 μg/ml).

To verify that the fluorescence turn-on in this system is due to the enzymatic action of trypsin and not a non-specific binding effect, a set of parallel experiments was conducted using the trypsin inhibitor benzamidine hydrochloride and the non-peptidic substrate **18** (Figure 2.14). The presence of a large excess of inhibitor and the use of the non-peptidic substrate **18** reduces rate of fluorescence turn-on to undetectable levels. Unsurprisingly, the inhibitor alone is also unable to trigger a fluorescence increase in **17**.

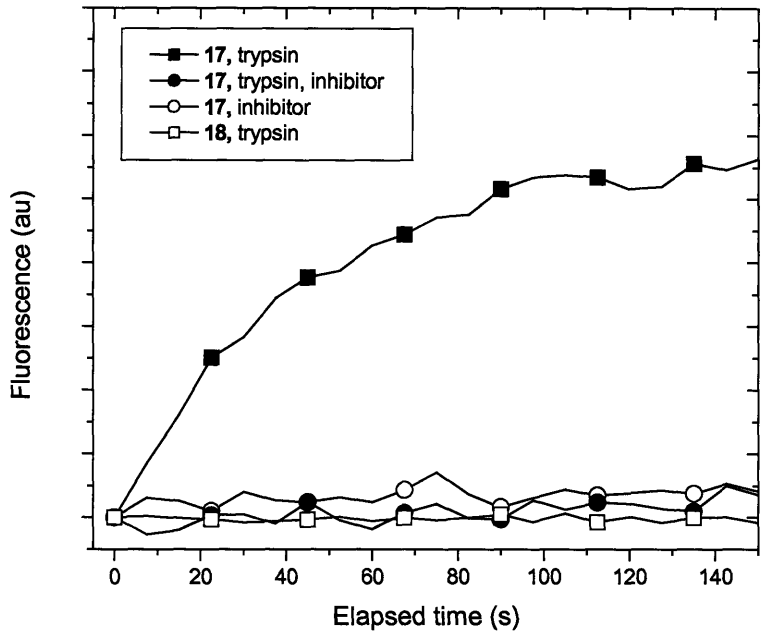

Figure 2.14. Fluorescence turn-on of **17** (0.26 μM) with trypsin (1 μg/ml), in the presence of excess benzamidine hydrochloride inhibitor (0.4 mg/ml), with inhibitor alone, and the parallel fluorescence response of **18**.

Trypsin-induced fluorescence enhancement in a small-molecule mimic of 17

Compound **20,** a small-molecule mimic of **17,** was prepared and subjected to digestion by trypsin in an attempt to quantify the enhancement provided by exciton migration in the polymer-peptide substrate (Scheme 2.8). Though the quencher-polymer linker in **20** is shorter than the one used for **17** — a feature which should encourage quenching in the 'off' state and promote large enhancements in fluorescence on quencher removal — hydrolysis of **20** by trypsin in TBS causes only a threefold enhancement in fluorescence intensity (Figure 2.15), several times smaller than the tenfold increase observed for **17.** This result demonstrates the advantages of amplified quenching of PPEs in sensor design.

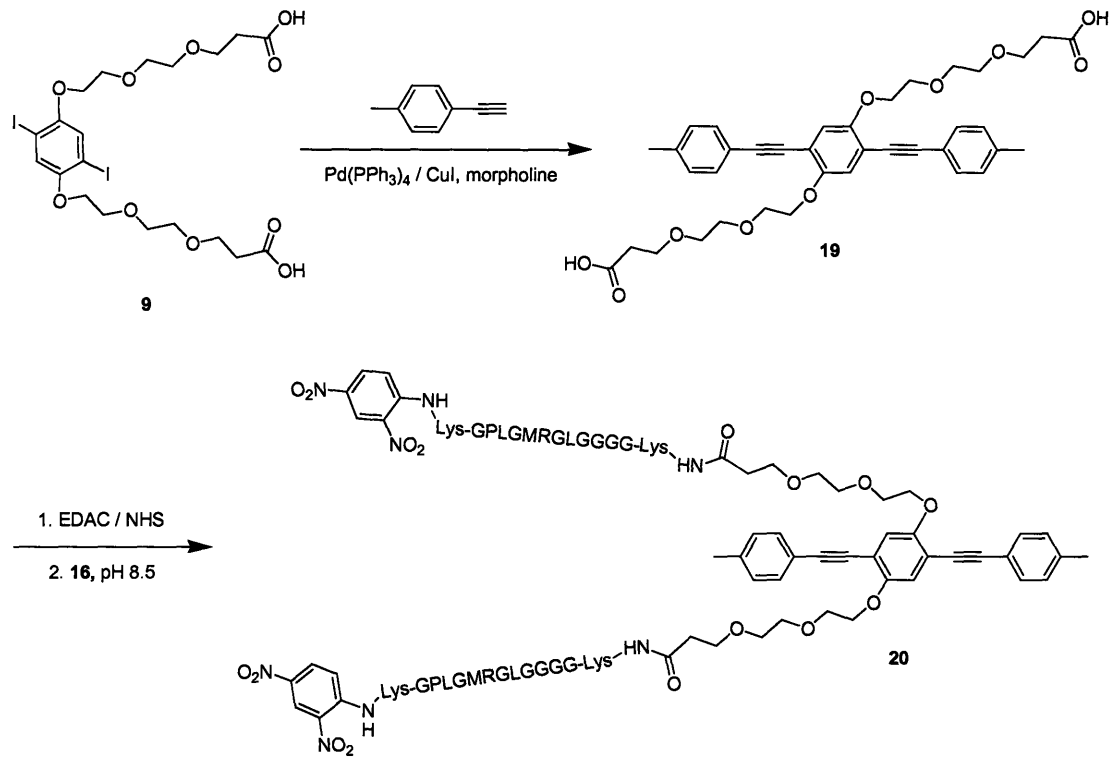

Scheme 2.8. Synthesis of the PPE mimic **19** and peptide-polymer small-molecule mimic **20.**

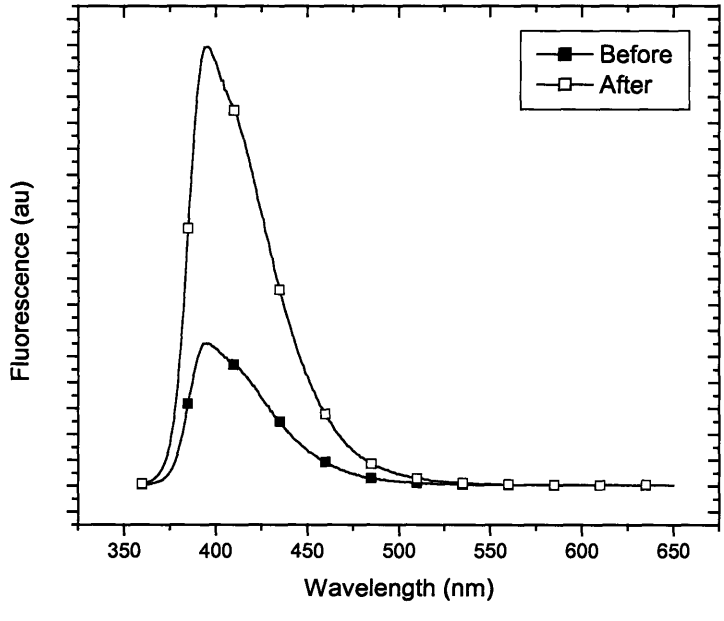

Figure 2.15. Fluorescence spectra of **20** in pH 7.5 Tris-buffered saline before and after digestion by trypsin.

Ionic strength effects on fluorescence enhancement

The linear response of conventional fluorogenic probes for proteases make them useful for the quantitative determination of enzyme activity. Although a polymer-peptide system operating on the basis of quencher removal shares some design similarities with these small-molecule fluorogenic probes, the possibility of amplified quenching effects and the spatially constrained nature of the multiple oligopeptide tethers in **17** are likely to introduce significant non-linear effects that would complicate any effort to collect absolute kinetic data from this system. Despite these limitations, we wished to determine if the fluorescence effects of ionic strength and surfactant concentration described earlier play a significant role in the fluorescence turn-on of substrates such as **17.** To this end, we prepared a modified polymer-peptide substrate **17′** in which the peptide loading is reduced to 0.25 peptide chains per repeat unit (*versus* 1.7 for **17**). On digestion by trypsin, the degree of fluorescence enhancement in this substrate was found to be 6.6-fold in Tris-buffered saline (Figure 2.16), 4.4-fold in the same solvent containing 0.16 wt% Triton X-100 (Figure 2.17), and 11.5-fold in Tris buffer without added salts (Figure 2.18). These interesting results show that even low peptide loading levels such as those found in **17′** are sufficient to provide 'on' / 'off' contrast of a magnitude similar to that seen in the highly quenched substrate **17.** This effect can be seen as a manifestation of the amplifying effects of exciton migration in PPEs — relatively few tethered peptides are required to cause efficient quenching of the fluorescence of the polymer.

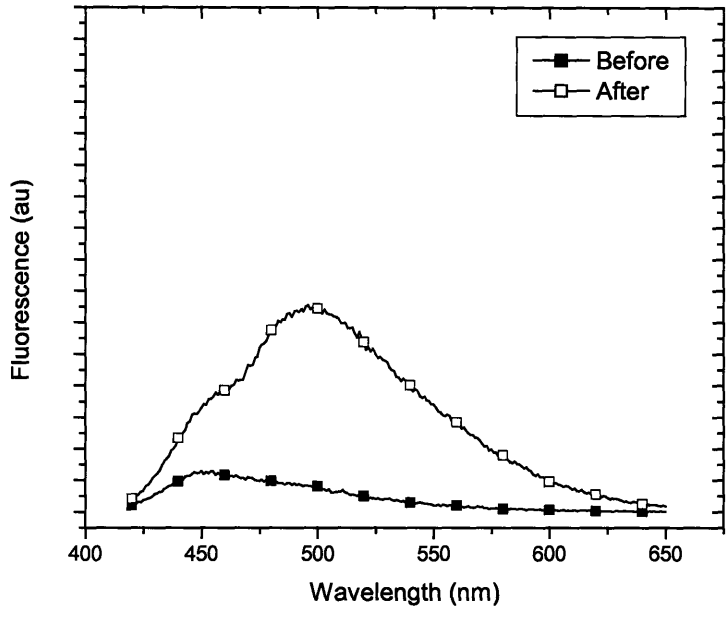

Figure 2.16. Fluorescence spectra of **17'** in pH 7.5 Tris-buffered saline before and after digestion by trypsin. The fluorescence scales of Figures 2.16- 2.18 are identical and data were collected from solutions equal in concentration.

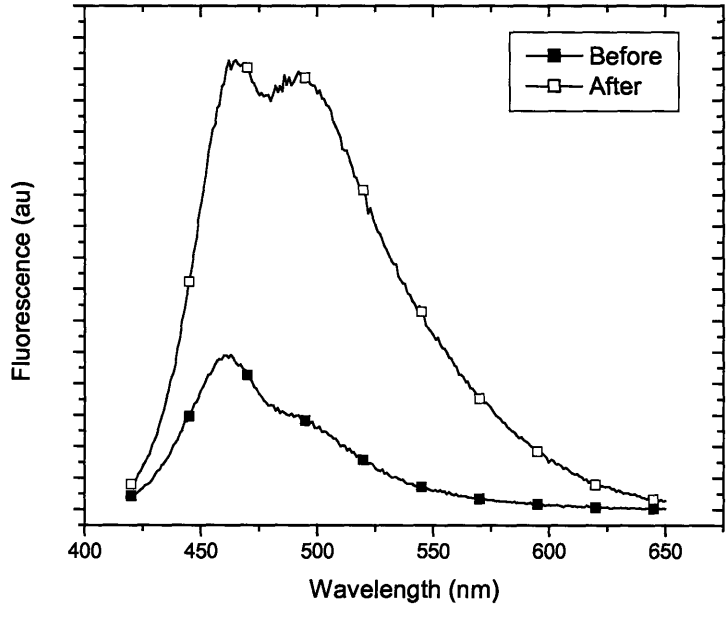

Figure 2.17. Fluorescence spectra of **17'** in pH 7.5 Tris-buffered saline containing 0.16 wt% Triton X-100 before and after digestion by trypsin.

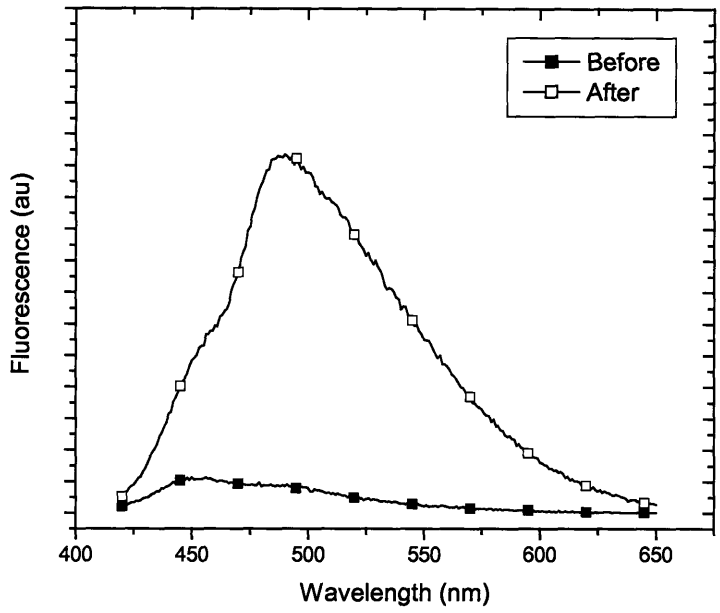

Figure 2.18. Fluorescence spectra of **17′** in pH 7.5 Tris buffer before and after digestion by trypsin.

Examination of the data presented in Figures 2.16, 2.17 and 2.18 reveals several interesting phenomena. In general, the absolute fluorescence intensity of **17′** in TBS containing 0.16 wt% Triton X-100 (Figure 2.17) is higher both before and after trypsin digestion than the corresponding measured intensities in the absence of surfactant. While a surfactant-mediated increase in the relative QY of the polymer is expected in the absence of any external quencher, the fact that surfactant alone is able to increase the fluorescence of the tethered 'off' form of **17′** is remarkable. Furthermore, while the initial fluorescence intensities of **17′** in Tris buffer and Tris-buffered saline are comparable, the use of the latter limits the final fluorescence output of the system considerably. It is also interesting that in all three cases the final fluorescence spectrum contains a dominant red-shifted band that is largely absent in intact **17′**. This suggests

that the presence of the intact polymer chain of **17′** may play a role in preventing polymer aggregation.

We subjected samples of **17′** to digestion by trypsin at very low concentrations (50 ng/ml) to determine how the reaction medium affects the relationship between peptide hydrolysis and fluorescence generation. Fluorescence enhancement in this system was followed as a function of time (Figure 2.19) and correlated to the actual rate of quencher release, measured by assaying the free peptide fragment AcHN-LysDNP-GPLGMR by HPLC (Figure 2.20).

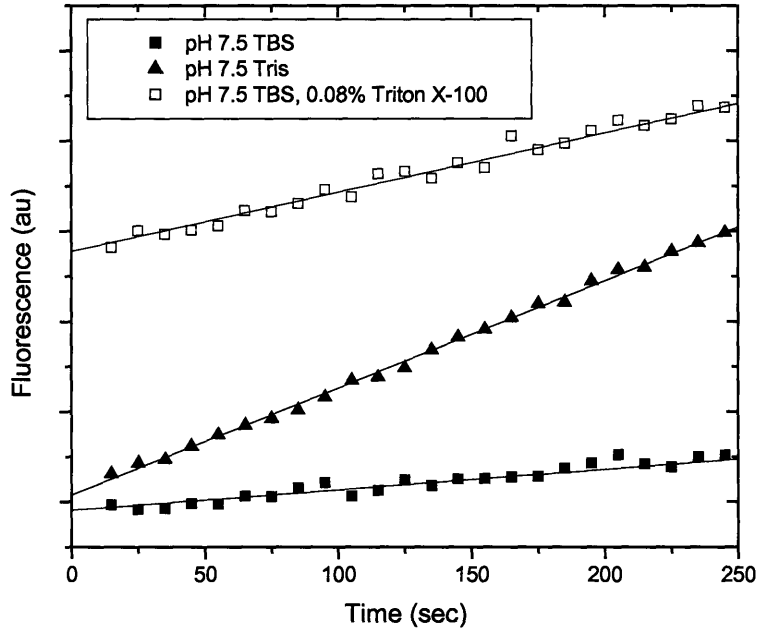

Figure 2.19. Fluorescence generation as a function of time in the digestion of **17′** by trypsin (50 ng/ml) for three different reaction media. Fluorescence was monitored at 475 nm (λ_{ex} 405 nm).

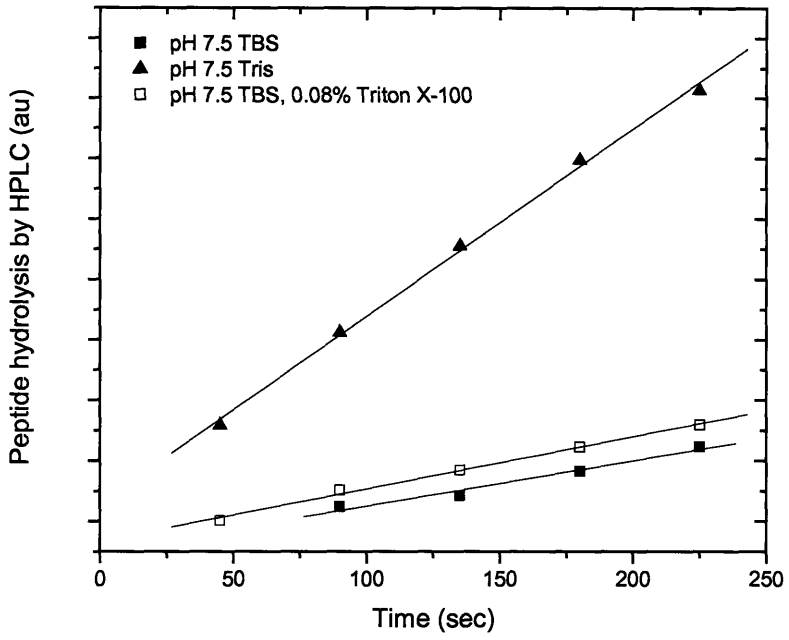

Figure 2.20. Release of the peptide fragment AcHN-LysDNP-GPLGMR as a function of time in the digestion of **17′** by trypsin (50 ng/ml) for three different reaction media. Relative free peptide concentration was determined by HPLC analysis of unbound DNP chromophore.

Rate data from Figures 2.19 and 2.20 are summarized in Table 2.3.

Table 2.3. Relative rates of peptide hydrolysis and fluorescence generation from substrate **17′** under initial-rate conditions, derived from the data of Figures 2.19 and 2.20.

Conditions	Relative rates	
	Peptide hydrolysis	**Fluorescence generation**
pH 7.5 TBS	1	1
pH 7.5 Tris	4.1 ± 0.6	5.3 ± 0.2
pH 7.5 TBS, 0.08% Triton X-100	1.1 ± 0.2	2.9 ± 0.2

The relative rate data shown in Table 2.3 reveal that, in general, the initial rates of fluorescence generation in different reaction media do not scale with the actual rate of peptide hydrolysis as measured by HPLC. For example, the reduction in ionic strength on changing the solvent from Tris-buffered saline to ordinary Tris buffer causes a fourfold increase in the

reaction rate, consistent with previous observations concerning the ionic strength-dependent rate of trypsin-catalyzed peptide hydrolysis.[20] However, the same change in reaction medium causes a greater (5.3-fold) increase in the rate of fluorescence generation. The addition of surfactant has an even greater effect on the disparity between the actual reaction rate and the rate of fluorescence generation: while the presence of 0.08% Triton X-100 does not significantly affect the actual rate of peptide hydrolysis, the rate of fluorescence generation is increased by a factor of three. These observations, together with the effects of the reaction medium on the overall 'on' / 'off' fluorescence enhancement of the system, provide further evidence of the role of ionic strength and surfactant in mediating the interactions between the PPE backbone and fluorescence-quenching peptide in **17**. The general effect of increased ionic strength in this system seems to be the promotion of quencher-polymer interactions, even when the quencher has been cleaved from the polymer backbone (Figure 2.21). Conversely, the addition of surfactant reduces quencher-polymer interactions and enhances the fluorescence of the system in both its 'off' and 'on' states by 'insulating' the hydrophobic peptide and polymer chains from each other (Figure 2.22). The fluorescence enhancement provided to the 'off' state more than offsets the gains achieved in the 'on' state, leading to an overall negative effect on the sensitivity of the system.

Figure 2.21 (following page). Schematic representation of the interaction between the fluorescence-quenching peptide and polymer backbone of **17** before (top) and (after) hydrolysis of the peptide tether by trypsin under conditions of high ionic strength. Hydrophobic effects promote strong quencher-polymer interactions under these conditions.

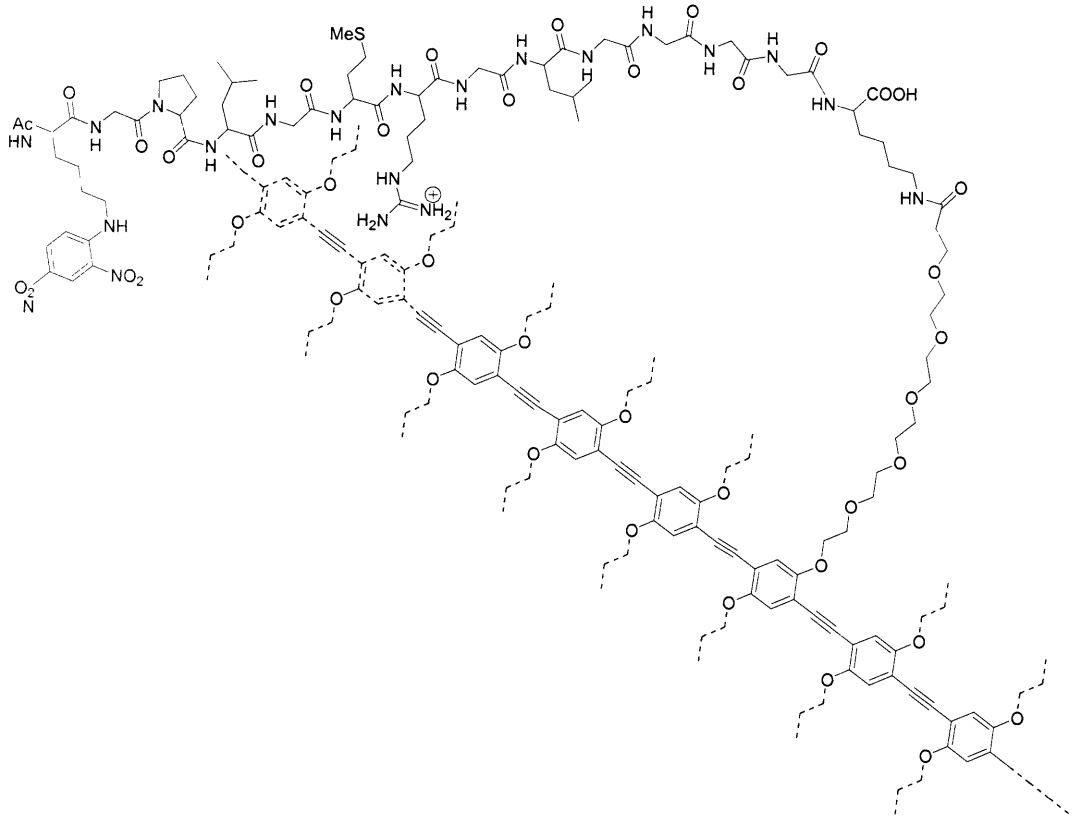

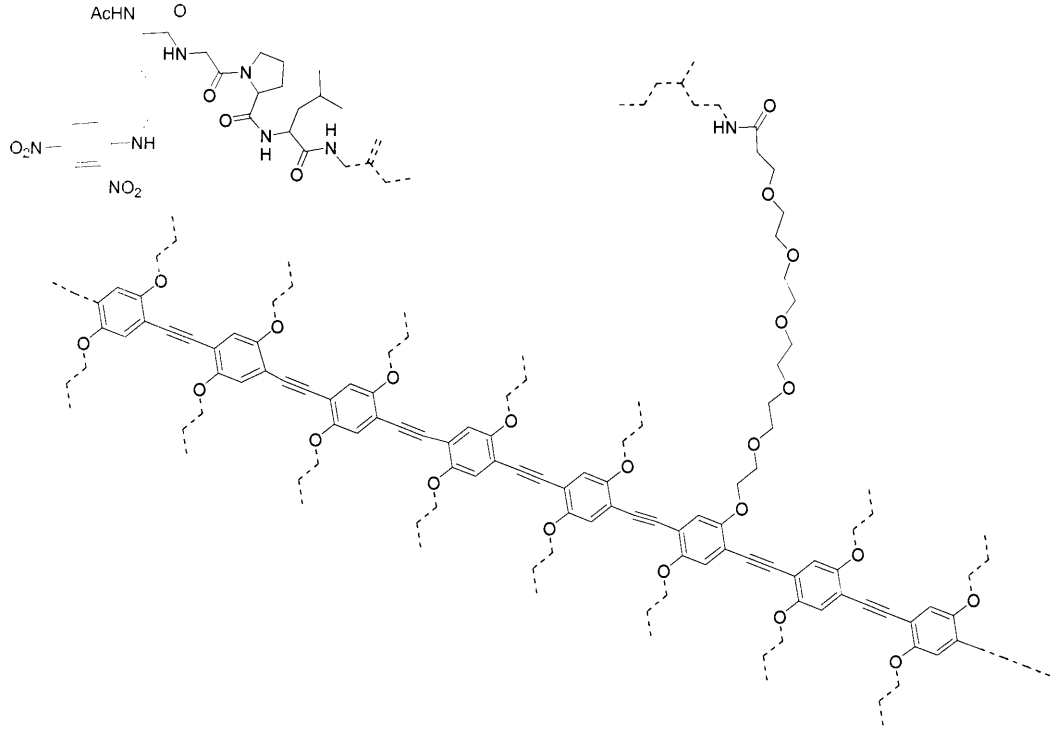

Figure 2.22. Schematic representation of reduced interactions between the fluorescence-quenching peptide and polymer backbone of **17** under conditions of lower ionic strength or in the presence of surfactant. Hydrophobic effects are alleviated by the surfactant and reduce quencher-polymer interactions under these conditions.

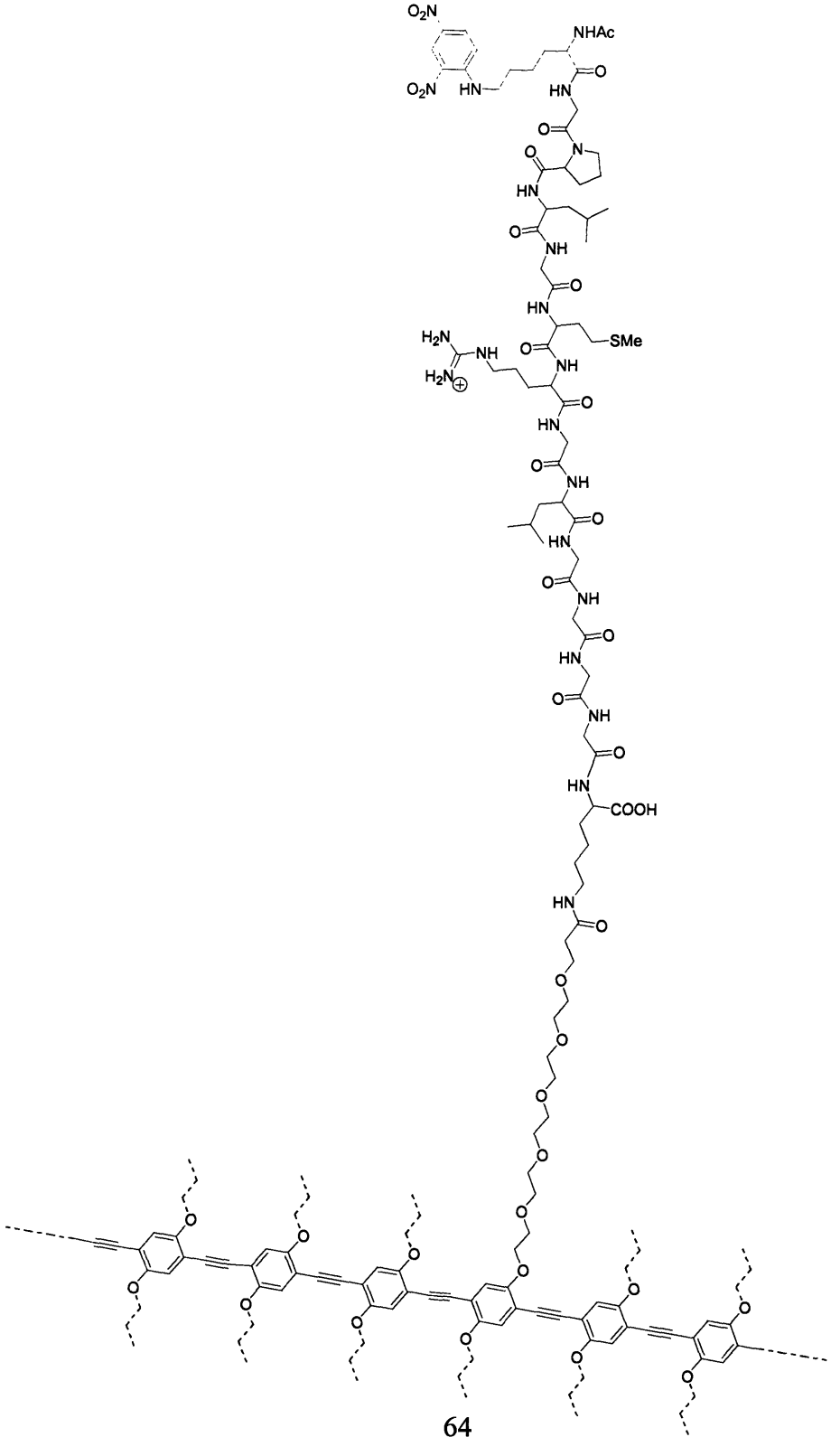

Treatment of* 17 *with MMP-13

As mentioned above, we chose peptide **16** for use as a tether in our quencher-removal protease detection scheme because its core sequence, GPLGMRGL, has been identified as an excellent substrate for the cancer-associated enzyme MMP-13. Unfortunately, subjecting substrate **17** to hydrolysis by an activated commercial preparation of MMP-13 did not result in reproducible increases in fluorescence. This effect is probably a result of the simple steric inaccessibility of the peptide sequence caused by its proximity to the rigid and bulky polymer backbone: while the constricting effects of the polymer itself may not be significant when trypsin (MW ~24 kDa) is used, the much larger MMP-13 enzyme (~60 kDa) may be less tolerant of steric interference. We also suspected that the reagent used to activate the MMP enzyme, 4-aminophenylmercuric acetate (APMA), may interfere with the fluorescene response of **17** to quencher removal. In an independent experiment, we found that 20 μM APMA alone was sufficient to *increase* the fluorescence of **17** in a time-dependent manner. This unexpected result may be due to a reduction in polymer-peptide interactions, perhaps due to oligopeptide chelation of the organomercurial.

PPEs for bioconjugation to antibodies

The exploitation of antibody-antigen interactions represents a critical part of the toolkit used in the study of biological and biochemical phenomena. In particular, the use of fluorescently labeled antibodies for cell staining and the analysis of protein gels has become a standard technique, and a wide variety of both primary and secondary antibodies bearing small-molecule fluorophores are commercially available. In conjunction with the research group of Prof. Alice Ting, we sought to extend the use of labeled antibodies to study protein-protein

interactions that are currently inaccessible with small-molecule dyes. The remainder of this chapter describes a series of PPEs suitable for bioconjugation to antibodies.

While antibodies can be and often are labeled by covalent bond formation between lysine side chains and activated-ester derivatives of small-molecule dyes, they have a number of special structural features that make this form of labeling problematic. Labeling through the side-chains of lysine residues is non-specific and the introduced labels can often interfere with antigen binding. For this reason, it has become popular to take advantage of the fact that antibodies are highly glycosylated, possessing 4-18% carbohydrate by weight, depending on the type of immunoglobulin.[21] Dilute, mildly acidic solutions of periodate can be used to selectively oxidize the vicinal diol groups of carbohydrates to generate aldehydes, which can be condensed with small-molecule amines or hydrazides to form imines or hydrazones. Because antibodies are glycosylated only in regions that do not participate in antigen binding, the binding capacity of the antibodies is preserved. Additionally, the periodate oxidation step can be fine-tuned to change the extent of labeling.[22] Hydrazones are more stable than imines, making the use of hydrazides a preferred method for antibody labeling.[21,23,10] By incorporating hydrazide groups into PPE building blocks, we have designed a series of monomers and polymers suitable for bioconjugation to antibodies (Scheme 2.9).

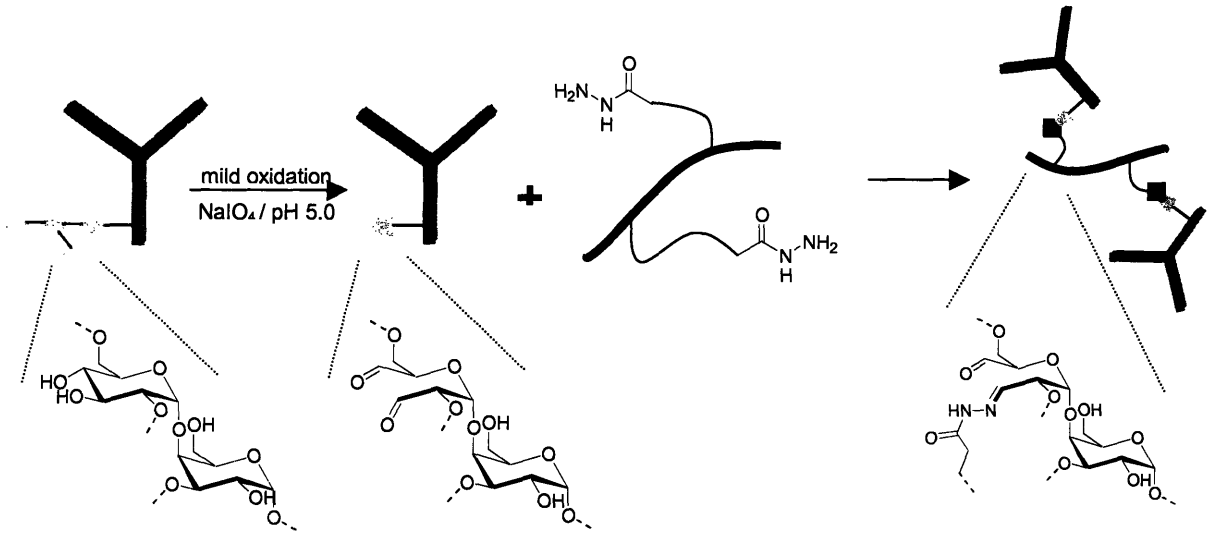

Scheme 2.9. Schematic representation of the oxidation of an immunoglobulin followed by hydrazone formation with a hydrazide-containing polymer.

In our first approach to the preparation of hydrazide-containing PPEs, a hydrazide-containing monomer, **21**, was used to provide a hydrazide-substituted polymer building block suitable for incorporation into a PPE. A similar approach was used for the preparation of **24,** a hydrazide-containing PPE end-capping reagent (Scheme 2.10). Both of these compounds were synthesized by simple hydrazinolysis of the corresponding methyl esters.

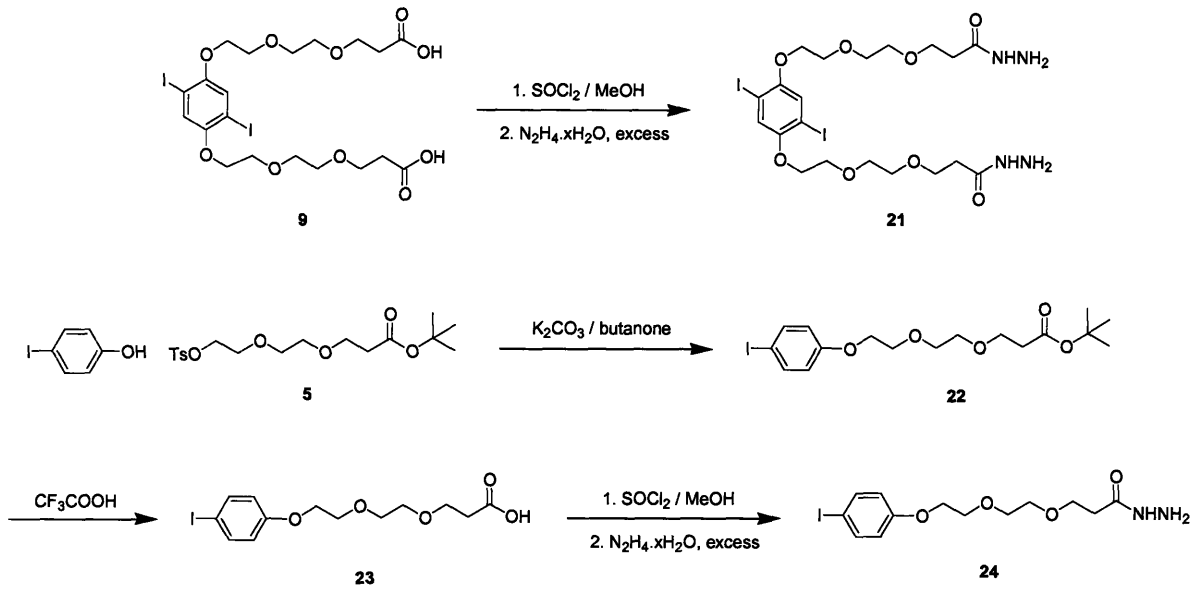

Scheme 2.10. Synthesis of hydrazide-containing monomer **21** and end-cap **24**.

An alternate entry into hydrazide-containing PPEs was based on the activated-ester PPEs used for the preparation of polymer-peptide substrate **17**. In this case, the activated ester was treated with a sub-stoichiometric quantity of an 2-kDa amino-polyethylene glycol to promote solubility, followed by consumption of the remaining activated ester groups with hydrazine hydrate (Scheme 2.11). The polymer was purified by dialysis to remove excess hydrazine and unreacted PEG-amine. Introduction of the hydrazine group in polymers based on **21, 24** and **25** was confirmed by a positive Sanger reaction with 2,4-dinitrofluorobenzene, which covalently derivatizes and quenches the polymer. Methods for antibody labeling with these polymers are currently under development in our laboratory.

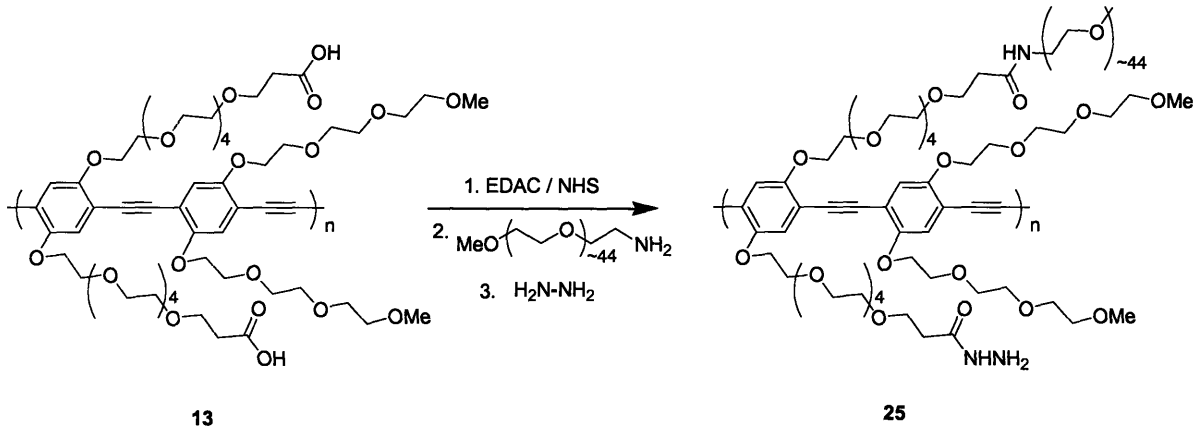

Scheme 2.11. Introduction of hydrazide and PEG groups via post-polymerization modification of **13.**

Conclusions

A family of water-soluble carboxylate-functionalized PPEs has been synthesized for use in bioconjugation schemes. These polymers show strong aggregation effects in aqueous solutions that are reduced at high pH and in the presence of surfactant. Carbodiimide activation of these polymers results in activated-ester PPEs that can be covalently attached to amine-containing biomolecules. This technique has been used to prepare a polymer-peptide substrate in which a trypsin-susceptible oligopeptide chain links an efficient fluorescence quencher to the polymer backbone. Digestion of this substrate with trypsin results in a fluorescence increase of up to an order of magnitude. Ionic strength and surfactant effects play a large role in the photophysical mechanism of fluorescence generation. The PPE bioconjugation technique has also been used to prepare polymers suitable for covalent attachment to oxidized antibodies.

Experimental

Synthetic considerations. Starting materials were purchased from Aldrich Chemical Company or Alfa-Aesar and used without further purification. THF was dried by passing through a 'dry still' column of activated alumina and was stored under argon before use. 2-Butanone was degassed by vigorous sparging with argon immediately before use. Morpholine was dried and degassed by passage through a column of activated alumina, followed by repeated evacuation of the storage flask and re-filling with argon. Melting points were recorded on a Laboratory Instruments Inc. Mel-Temp II and are uncorrected. NMR spectra were measured on Varian Inova-500 and -501 spectrometers at 500 MHz (^{1}H) or 125 MHz (^{13}C) and were referenced to the ^{1}H resonance of internal $SiMe_4$ (^{1}H, 0 ppm) for $CDCl_3$ solutions, and the resonances of naturally occurring ^{13}C and monodeuterated species in the NMR solvent (all other ^{1}H spectra and all ^{13}C spectra). Mass spectra were measured on a Bruker Daltonics Apex II 3T FT-ICR instrument at the MIT Department of Chemistry Instrumentation Facility. Solutions of EDAC (1-(3-dimethylaminopropyl)-3-ethylcarbodiimide hydrochloride) and NHS (*N*-hydroxysuccinimide) were prepared from commercial reagents immediately before use in 0.1 M MES buffer (pH 5.4). Reverse-phase HPLC was carried out on Zorbax SB and Waters Delta Pak C18 columns, eluting with gradients of MeCN and H_2O containing 0.1% CF_3COOH. Compounds were detected on the basis of their UV absorbance as they eluted from the column. Routine absorbance spectra were measured on an Agilent 8453 spectrophotometer. Fluorescence spectra were measured in quartz cuvettes on Spex Fluorolog fluorimeters.

19-Hydroxy-4,7,10,13,16-pentaoxaoctadecanoic acid, *tert*-butyl ester (4). This compound was synthesized based on a modification of a literature procedure for a shorter homolog.[12] A solution of 15 g (63 mmol) pentaethylene glycol in 175 ml of dry THF was treated with *ca.* 100 mg of freshly cut sodium metal chips. The solution was stirred vigorously under argon until gas evolution had ceased (about 1.5 hr). 3.1 ml (2.7 g, 21 mmol) *tert*-butyl acrylate was then added and the reaction mixture stirred overnight under argon. The reaction mixture was quenched by the addition of 8 ml of 1 M aqueous HCl. After stirring for several minutes, the reaction mixture was poured into 200 ml of a saturated NaCl solution and extracted three times with 100 ml portions of EtOAc. The combined EtOAc extracts were washed with saturated aqueous NaCl, separation and dried over anhydrous $MgSO_4$. After filtration, the mixture was concentrated under reduced pressure to provide a clear colorless oil (6.16 g, 80%). ^{1}H NMR ($CDCl_3$, ppm): 1.45 (s, 9H), 2.51 (t, 2H, J = 6.5 Hz), 3.1 (br s, 1H), 3.60-3.74 (m, 22H). ^{13}C NMR ($CDCl_3$, ppm): 28.16, 36.29, 61.72, 66.94, 70.35, 70.40, 70.53, 70.58, 70.60, 70.64, 70.66, 72.69, 80.58, 171.02. HRMS: [$C_{17}H_{34}O_8$+CH_3COO] requires 425.2387, found 425.2389.

19-(*p*-Toluenesulfonyloxy)-4,7,10,13,16-pentaoxaoctadecanoic acid, *tert*-butyl ester (6). Compound **4** (4.5 g, 12.3 mmol) was dissolved in a mixture of 30 ml CH_2Cl_2 and 10 ml Et_3N and cooled in an ice-bath under argon. 3.6 g of solid *p*-toluenesulfonyl chloride (Aldrich) was then added in one portion. The reaction mixture was stirred overnight at room temperature and then poured into 100 ml of 1 M HCl. The organic phase was separated, washed with saturated aqueous NaCl, and dried on anhydrous $MgSO_4$. After filtration, the solution was concentrated to dryness on a small amount of silica gel and chromatographed on silica gel (elution with a gradient of 1:1 EtOAc/hexanes to 3:1 EtOAc/hexanes). The product eluted as a thick, colorless

oil (5.00 g, 78%). ^{1}H NMR ($CDCl_3$, ppm): 1.45 (s, 9H), 2.45 (s, 3H), 2.50 (t, 2H, J = 6.0 Hz), 3.58-3.72 (m, 20H), 4.16 (m, 2H), 7.35 (d, 2H, J = 8.0 Hz), 7.80 (d, 2H, J = 8.0 Hz). ^{13}C NMR ($CDCl_3$, ppm): 21.77, 28.20, 36.36, 66.99, 68.76, 69.38, 70.46, 70.59, 70.62, 70.66, 70.67, 70.68, 70.71, 70.83, 80.60, 128.09, 129.95, 133.05, 144.92, 171.02. HRMS: [$C_{24}H_{40}SO_{10}$+Na] requires 543.2234, found 543.2214.

1,4-diiodo-2,5-bis(17-(*tert*-butoxycarbonyl)-3,6,8,12,15-pentaoxaheptadecyloxy)benzene (8). Compound **6** (1.93 g, 3.71 mmol) and 2,5-diiodohydroquinone (639 mg, 1.77 mmol) was dissolved in air-free 2-butanone. After addition of K_2CO_3 (1.47 g, 10.6 mmol) and a spatula-tip quantity of KI, the reaction mixture was heated at reflux under argon for 20 h. The reaction mixture was evaporated to dryness and re-dissolved in a mixture of CH_2Cl_2 and 1 M HCl. The organic phase was separated, washed with saturated NaCl solution, dried over anhydrous $MgSO_4$ and concentrated to dryness on a small amount of silica gel. Chromatography on silica gel (elution with 7:2 EtOAc/hexanes) gave the product as a thick colorless syrup (0.90 g, 48%). ^{1}H NMR ($CDCl_3$, ppm): 1.44 (s, 9H), 2.50 (t, 2H, J = 6.6 Hz), 3.60-3.77 (m, 18H), 3.87 (t, 2H, J = 4.5 Hz), 4.09 (t, 2H, J = 4.5 Hz), 7.21 (s, 1H). ^{13}C NMR ($CDCl_3$, ppm): 28.29, 36.43, 67.07, 69.76, 70.44, 70.55, 70.68, 70.78, 70.83, 70.91, 80.70, 86.57, 123.56, 153.25, 171.11. HRMS: [$C_{40}H_{68}I_2O_{16}$+Na] requires 1081.2489, found 1081.2477.

1,4-diiodo-2,5-bis(17-carboxy-3,6,8,12,15-pentaoxaheptadecyloxy)benzene (10). Compound **8** (0.90 g, 0.85 mmol) was dissolved in 5 ml neat CF_3COOH and stirred at room temperature overnight. The reaction mixture was evaporated to dryness, dissolved in water, and re-evaporated under reduced pressure to provide an oil which solidified on standing, providing an off-white

powder (0.62 g, 80%). M.p. 64-65°. ^{1}H NMR ($CDCl_3$, ppm): 2.61 (t, 2H, J = 6.0 Hz), 3.63-3.80 (m, 18H), 3.89 (t, 2H, J = 5.0 Hz), 4.11 (t, 2H, J = 5.0 Hz), 7.24 (s, 1H). ^{13}C NMR ($CDCl_3$, ppm): 35.18, 66.66, 69.79, 70.46, 70.69, 70.78, 70.85, 70.89, 71.32, 86.60, 123.62, 153.28, 175.37, 206.05. HRMS: [$C_{32}H_{52}O_{16}I_2$-H] requires 945.1267, found 945.1268.

9-Hydroxy-3,6-dioxanonanoic acid, *tert*-butyl ester (3). This compound was prepared in a manner analogous to that described for **4** above. Diethylene glycol (Aldrich, 31.8 g, 0.3 mol), a small quantity of freshly cut sodium metal, and *tert*-butyl acrylate (13.1 g, 0.1 mol) gave 11.3 g (48%) of a clear, colorless oil. ^{1}H NMR ($CDCl_3$, ppm): 1.45 (s, 9H), 2.52 (t, 2H, J = 6.5 Hz), 2.65 (br s, 1H), 3.6-3.8 (m, 10H). ^{13}C NMR ($CDCl_3$, ppm): 28.2, 36.34, 61.97, 67.02, 70.55, 72.67, 80.87, 106.68, 171.14. HRMS: [$C_{11}H_{25}O_5$+Na] requires 257.1359, found 257.1350.

9-(*p*-Toluenesulfonyloxy)-3,6-dioxanonanoic acid, *tert*-butyl ester (5). Compound **3** (6.5 g, 27.7 mmol) was dissolved in a mixture of 200 ml CH_2Cl_2 and 8 ml Et_3N under argon. The reaction mixture was cooled in an ice bath for 30 min, and then 6.0 g (33.3 mmol) *p*-toluenesulfonyl chloride was added as a solution in 70 ml CH_2Cl_2. The reaction was stirred overnight and poured into 1 M HCl. The organic phase was separated, washed with saturated aqueous $NaHCO_3$ and saturated aqueous NaCl, and dried on anhydrous $MgSO_4$. The residue remaining after concentration under reduced pressure was chromatographed on silica gel (elution with a gradient of 9:1 to 3:1 hexanes/EtOAc) to provide a clear, straw-colored oil (8.9 g, 83%). ^{1}H NMR ($CDCl_3$, ppm): 1.44 (s, 9H), 2.45 (s, 3H), 2.48 (t, 2H, J = 6.5 Hz), 3.55-3.60 (m, 2H), 3.66-3.69 (m, 2H), 4.15 (t, 2H, J = 5.0 Hz), 7.35 (app d, 2H, J = 8.5 Hz), 7.80 (app d, 2H, J = 8.5 Hz). ^{13}C NMR ($CDCl_3$, ppm): 21.76, 28.19, 36.31, 67.00, 68.76, 69.38, 70.41, 70.73, 80.65,

128.09, 129.95, 133.04, 144.93, 170.96. HRMS: [$C_{18}H_{28}SO_7$+Na] requires 411.1448, found 411.1457.

1,4-Diiodo-2,5-bis((8-*tert*-butoxycarbonyl)-3,6-dioxaoctyl)benzene (7). 2,5-Diiodohydroquinone (202 mg, 0.56 mmol) and compound **5** (475 mg, 1.2 mmol, 2.2 eq) were dissolved in air-free 2-butanone (50 ml). K_2CO_3 (465 mg, 3.4 mmol, 6 eq) and a catalytic quantity of KI were added. The reaction was heated at reflux for 16 hr under argon. After cooling to room temperature, the reaction mixture was evaporated to dryness and the residue remaining was taken up in a mixture of $CHCl_3$ and water. The organic layer was separated, washed with saturated aqueous $NaHCO_3$ and saturated aqueous NaCl, dried over anhydrous $MgSO_4$, and filtered. The filtrate was evaporated to dryness onto a small amount of silica gel. Chromatography on silica gel (elution with 5:2 hexanes/EtOAc) provided a clear oil (0.34 g, 75%). ^{1}H NMR ($CDCl_3$, ppm): 1.43 (s, 9H), 2.52 (t, 2H, J = 7.5), 3.64-3.66 (m, 2H), 3.72-3.77 (m, 4H), 3.88 (t, 2H, J = 4.5 Hz), 4.10 (t, 2H, J = 5.0 Hz), 7.23 (s, 1H). ^{13}C NMR ($CDCl_3$, ppm): 28.27, 36.43, 67.11, 69.74, 70.43, 70.66, 71.22, 80.67, 86.55, 123.55, 153.23, 171.09. HRMS: [$C_{28}H_{44}I_2O_{10}$+Na] requires 817.0916, found 817.0928.

1,4-Diiodo-2,5-bis(8-carboxy-3,6-dioxaoctyl)benzene (9). Compound **7** (142 mg, 0.18 mmol) was dissolved in 5 ml neat CF_3COOH and stirred for 1.5 hr at room temperature. The reaction mixture was evaporated to dryness, re-dissolved in water, and concentrated to a white solid (91 mg, 75%). M.p. 100-103°. ^{1}H NMR (DMSO-d_6, ppm): 2.44 (t, 2H, J = 6.0 Hz), 3.51-3.53 (m, 2H), 3.60-3.63 (m, 4H), 3.73 (t, 2H, J = 5.0 Hz), 4.09 (t, 2H, J = 4.5 Hz), 7.37 (s, 1H), 12.2 (br s,

1H). ^{13}C NMR (DMSO-d_6, ppm): 34.80, 66.31, 68.96, 69.68, 69.72, 70.08, 86.94, 122.85, 152.52, 172.65. HRMS [$C_{20}H_{28}O_{10}I_2$-H] requires 680.9688, found 680.9675.

1,4-Bis(4-methylphenylethynyl)-2,5-bis(8-carboxy-3,6-dioxaoctyl)benzene (19). Compound **9** (204 mg, 0.3 mmol) and catalytic amounts of $PdCl_2(PPh_3)_2$ (Strem) and CuI (Aldrich) were dissolved in 5 ml in dry, degassed morpholine under argon. 116 mg (1 mmol) of 4-ethynyltoluene (Gelest) was then added, and the reaction mixture was stirred at room temperature for 2 d. The reaction mixture was then evaporated to dryness under vacuum and re-dissolved in a mixture of CH_2Cl_2 and dilute aqueous HCl. The organic phase was washed with a concentrated NaCl solution containing dilute HCl and dried on $MgSO_4$. After filtration, the solution was evaporated onto a small amount of silica gel and chromatographed on silica gel (7% MeOH/CH_2Cl_2), providing 90 mg (46%) of a dark, oily solid. RP-HPLC (Zorbax SB-C18 column, 40/60 MeCN/H_2O for 2.5 min followed by a gradient to 90/10 MeCN/H_2O over 15 min and a 2.5 min 90/10 MeCN/H_2O hold, all with constant 0.1% CF_3COOH): 18.1 min, absorbance λ_{max} 315 nm and 360 nm. ^1H NMR (DMSO-d_6, ppm): 2.34 (s, 3H), 2.40 (m, 2H), 3.49 (app t, 2H, J = 5.0 Hz), 3.57 (app t, 2H, J = 6.0 Hz), 3.66 (m, 2H), 3.79 (app t, 2H, J = 4.3 Hz), 4.16 (app t, 2H, J = 4.3 Hz), 7.17 (s, 1H), 7.25 (d, 2H, J = 8.0 Hz), 7.41 (d, 2H, J = 8.0 Hz). ^{13}C NMR (DMSO-d_6, ppm): 21.10, 66.13, 66.35, 69.06, 69.75, 70.16, 85.58, 95.04, 113.18, 116.63, 119.54, 129.45, 131.17, 138.67, 152.99, 172.70. HRMS [$C_{38}H_{42}O_{10}$-H] requires 657.2705, found 657.2702.

1-amino-8-(2,4-dinitrophenylamino)-3,6-dioxaoctane (15). Compound **14**[27] (249 mg, 1 mmol) was dissolved in a stirring mixture of 170 mg K_2CO_3 in 5 ml THF. 2,5-dinitrofluorobenzene (186

mg, 1 mmol) was then added *via* syringe. The reaction mixture was stirred for 1 hr, filtered, and evaporated onto a small amount of silica gel. Chromatography on silica gel (elution with 3:1 EtOAc/hexanes) provided 290 mg (71%) of a bright yellow solid. ^{1}H NMR ($CDCl_3$, ppm): 1.43 (s, 9H), 3.34 (m, 2H), 3.56 (m, 2H), 3.62 (m, 2H), 3.67 (m, 2H), 3.71 (m, 2H), 3.84 (t, 2H, J = 5.5 Hz), 5.0 (br s, 1H), 6.94 (d, 1H, J = 9.5 Hz), 8.28 (dd, 1H, J = 9.5, 3.0 Hz), 8.84 (br s, 1H), 9.16 (d, 1H, J = 3.0 Hz). After stirring this compound in neat CF_3COOH (5 ml) overnight, the reaction mixture was evaporated to dryness, resuspended in H_2O, and then re-evaporated under vacuum to form a thick orange oil (compound **15**). ^{1}H NMR (CD_3OD, ppm): 3.14 (t, 2H, J = 5.0 Hz), 3.67 (t, 2H, J = 5.0 Hz), 3.70-3.76 (m, 8H), 3.83 (t, 2H, J = 5.0 Hz), 7.20 (d, 1H, J = 9.5 Hz), 8.28 (dd, 1H, J = 9.5, 3.0 Hz), 9.01 (d, 1H, J = 2.5 Hz). ^{13}C NMR (CD_3OD, ppm): 40.81, 44.09, 68.03, 68.08, 69.79, 71.47, 71.54, 71.62, 116.17, 124.82, 131.24, 149.91. HRMS: [$C_{12}H_{18}N_4O_6$+H] requires 315.1299, found 315.1307.

Polymer synthesis. Monomer **10** (28 mg, 0.03 mmol), 2,5-diethynyl-1,4-bis(3,6-dioxaheptyl)benzene[24] (11 mg, 0.03 mmol), $Pd(PPh_3)_4$ (Strem, catalytic amount) and CuI (Aldrich) were dissolved in dry, degassed morpholine (4 ml) and heated under argon at 60°C for 24 hr. The blue-green fluorescent solution was cooled to room temperature, dissolved in water, and dialyzed (Pierce Snake-Skin, 10,000 MWCO) against several changes of deionized water for 3 d. Lyophilization of the resulting yellow-orange solution gave **12** as a dark solid. ^{1}H NMR (CD_3OD, ppm): broad peaks centered at 2.5, 3.45-3.8, 3.9, 4.3, 7.2. Absorbance λ_{max} (aqueous base, pH 11): 435 nm. Emission λ_{max} (aqueous base, pH 11): 475 nm. Polymer **13** was prepared by an analogous method starting from **10** and using 2,5-diethynyl-1,4-bis(3,6,9-trioxadecyloxy)benzene.[25] ^{1}H NMR for **13** (DMSO-d_6, ppm): broad peaks centered at 2.4, 3.45-

3.55, 3.6, 3.8, 4.2, 7.2. Successful gel permeation chromatographs could not be obtained for these polymers (they did not pass through the GPC column). NMR spectra of these polymers can be found in the Appendix. Based on dialysis and size-exclusion chromatography behavior the molecular weights of these polymers are estimated to be $> 2.5\times10^4$.

Stern-Volmer titrations. Dilute solutions of **13** were titrated with LysDNP in the appropriate medium and the fluorescence spectra measured after each addition of LysDNP. Fluorescence peak heights were used for the construction of Stern-Volmer plots after correcting for the inner-filter effect of the highly colored LysDNP.[26] The slope of the ratio of initial to observed fluorescence (F_0/F) was plotted *versus* the quencher concentration. Linear fits of F_0/F *versus* [LysDNP] provided K_{SV} values as shown in the main text.

Lifetime measurements. Fluorescence lifetimes were measured by the frequency-domain method in a Spex Fluorolog 2 fluorimeter. Phase and modulation data were collected at 10 modulation frequencies between 10 and 220 MHz and fitted to mono- or bi-exponential functions using the instrument software. Colloidal silica ($\tau = 0$) was used as a standard. For lifetime titrations with surfactant, PMT signals were re-balanced after each measurement.

Quantum yield measurements. Quantum yields were measured in the usual manner[1] using a Coumarin 6 standard (QY = 0.78 in EtOH solution) and were corrected for solvent refractive index. Solution optical densities were kept below 0.1 and all measurements were made in triplicate and averaged to reduce error.

Synthesis of peptide AcHN-LysDNP-GPLGMRGLGGGGK (16). Peptide LysDNP-GPLGMRGLGGGGK-OH (without the N-terminal end-cap) was synthesized on an Advanced ChemTech 396 Omega peptide synthesizer using standard Fmoc chemistry. After deprotection of the terminal Fmoc group on the solid support, the collected resin, bearing *ca.* 66 μmol of peptide, was suspended in 8 ml *N*-methylpyrrolidinone (NMP). The swollen resin gave a positive Kaiser test indicating the presence of the free N-terminal amine. $Et(iPr)_2N$ (340 μl) and Ac_2O (185 μl) were added and the resin stirred for 30 min. The resin was collected, rinsed 3x with NMP, and dried. Kaiser tests on the treated beads were negative for free amine. Side-chain protecting group removal and release of the peptide from the resin was performed using standard techniques. The peptide was purified on a Waters Delta Pak C18 column using a gradient of H_2O and MeCN containing constant 0.1% CF_3COOH. Fractions containing **16** were combined and lyophilized to a dark yellow powder. MS: [AcHN-LysDNP-GPLGMRGLGGGGK+OH] requires 1508.7, found 1508.8. The peptide was made up to 10 mM in water for use.

Small-molecule mimic 20. Compound **19** (231 μg, 0.35 μmol) was dissolved in 231 μl of DMF. 14 μl each (1.4 μmol) of freshly-prepared 0.1 M solutions of EDAC and NHS in 0.1 M MES buffer were then added, and the mixture was stirred for 3 hr. Then 0.1 ml of a 10 mM solution of AcHN-Lys(DNP)-GPLGMRGLGGGGK-OH was added in dilute borate buffer (pH 8.5). After stirring overnight, the solution was purified by HPLC (one product peak, isolated through repeated injections on a semi-preparative Zorbax SB-C18 column) using 2.5 min at 90/10 H_2O/MeCN, followed by a gradient to 85/15 MeCN/H_2O over 20 min and a 4.5 min 85/15 MeCN/H_2O hold, all with constant 0.1% CF_3COOH. Compound **4** eluted at 19.1 min,

absorbance λ_{max} 360 nm with an additional peak at 315 nm. Fractions containing the compound of interest were combined and lyophilized to a dark filmy solid.

Preparation of substrates 17 and 18. 500 μl of solution containing 0.25 mM (repeat unit basis) **12** in DMF was treated with 25 μl each of freshly prepared 0.1 M solutions of EDAC and NHS in 0.1 M MES buffer (*ca.* 20 eq EDAC/NHS per repeat unit). After 1 hr, a mixture of 65 μl 10 mM **16** (for **17**) or **15** (for **18**) with 500 μl pH 8.5 borate buffer was added and the resulting reaction mixture was stirred overnight. The reaction mixture was diluted with water and dialyzed (Pierce Snake-Skin, 10,000 MWCO) for several days against water. An analogous procedure was used for the preparation of **17′** using 150 μl of activated **12** solution diluted into 250 μl pH 8.5 borate buffer containing 10 μl 10 mM **16.** The resulting yellow-orange, non-fluorescent solutions were used as stock concentrates for trypsin assays.

Trypsin digestion of substrates. TPCK-treated trypsin (Sigma, 11,000 units/mg) was made up as a 1 mg/ml stock solution in 1 mM HCl and stored frozen in working aliquots. In a typical fluorescence assay, a portion of a stock solution of substrate was diluted into assay buffer to a total volume of 3 ml. The fluorescence spectrum of the sample was measured (with λ_{ex} 405 nm for polymer substrates and 345 nm for **20**). After addition of trypsin (3 μl), the fluorescence of the sample (at 475 nm for polymer substrates, 400 nm for **20**) was collected every 10 s for 30 min. When fluorescence generation was complete, the final fluorescence spectrum was collected. The ratio of the areas of the final and initial fluorescence spectra provided the degree of fluorescence enhancement on hydrolysis. Control experiments using the trypsin inhibitor benzamidine hydrochloride were carried out using 0.4 mg/ml of inhibitor in the reaction mixture.

Collection of data for kinetic analysis. Dilute solutions of trypsin were used in the collection of initial rate data to minimize the effects of product inhibition. All experiments were carried out at 23.4 +/- 0.1°C. In a typical experiment, a portion of stock solution of **17′** was diluted into assay medium (Tris-buffered saline, plain Tris buffer, or Tris-buffered saline containing 0.08% Triton X-100 – 500 μl total volume in all cases) and treated with 2.5 μl of a 10 μg/ml solution of trypsin. The fluorescence of the reaction mixture (measured at 475 nm) was collected every 7.5 s for 6 min. The slope of a plot of F_{475} *versus* time was used to determine the rate of fluorescence generation under each of the three assay medium conditions. For the determination of the peptide cleavage rate, parallel experiments were run at the same concentration and temperature. Aliquots of reaction mixture were removed at 45-s intervals and quenched by acidification with one volume of 10% aqueous CF_3COOH for every 25 volumes of reaction mixture. The resulting solutions were analyzed for the peptide fragment AcHN-LysDNP-GPLGMR on a Zorbax SB-C8 100x4.5 mm reverse-phase HPLC column (the polymer with bound peptide does not pass through the column) monitoring for the absorbance of the LysDNP chromophore at 360 nm. Integration of the elution peaks provided a relative measure of the concentration of LysDNP in each sample. The slope of a plot of the peak integration (in mAU-s) *versus* time was used to determine the actual rate of peptide cleavage under each of the three assay medium conditions.

1,4-Diiodo-2,5-bis((8-*tert*-butoxycarbonyl)-3,6-dioxaoctyl)benzene bis-hydrazide (21). Diacid **9** (209 mg, 0.31 mmol) was suspended in MeOH and treated dropwise with 0.5 ml $SOCl_2$ (CAUTION! Violent reaction.) The reaction mixture was stirred for 30 min at room temperature and then heated at reflux for 2 h. The reaction mixture was evaporated to dryness *in vacuo*, then

re-suspended in EtOH. Hydrazine hydrate (1 ml) was added and the reaction mixture heated at reflux overnight. The resulting suspension was concentrated to dryness and recrystallized from hot EtOH, providing a white solid (113 mg, 52%). ^{1}H NMR (DMSO-d_6, ppm): 2.25 (t, 2H, J = 6.5 Hz), 3.50 (app t, 2H, J = 5.0 Hz), 3.58-3.62 (m, 4H), 3.72 (app t, 2H, J = 4.0 Hz), 4.09 (t, 2H, 4.0 Hz), 4.17 (br s, 2H), 7.37 (s, 1H), 8.99 (s, 1H). ^{13}C NMR (DMSO-d_6, ppm): 34.31, 66.72, 68.94, 69.58, 69.65, 70.03, 86.94, 122.83, 152.51, 169.49. HRMS: [$C_{20}H_{32}N_4O_8I_2$+H] requires 711.0832, found 711.0839.

9-(4-Iodophenyloxy)-3,6-dioxanonanoic acid, *tert*-butyl ester (22). 4-Iodophenol (4.4 g, 20 mmol), tosylate **5** (8.54 g, 22 mmol), and K_2CO_3 (5.54 g, 40 mmol) were heated at reflux in 2-butanone (200 ml) under argon for 48 h. After cooling to room temperature, the reaction mixture was diluted with CH_2Cl_2 and washed with dilute aqueous HCl. The organic phase was washed with saturated NaCl solution, dried over anhydrous $MgSO_4$, filtered, and chromatographed on silica gel (elution with 4:1 hexanes/EtOAc) to provide a clear oil that solidifed on standing (5.51 g, 63%). M.p. < 40°. ^{1}H NMR ($CDCl_3$, ppm): 1.44 (s, 9H), 2.50 (t, 2H, J = 6.3 Hz), 3.62-3.74 (m, 6H), 3.83 (app t, 2H, J = 4.8 Hz), 4.08 (t, 2H, J = 4.2 Hz), 6.79 (d, 2H, J = 8.7 Hz), 7.54 (d, 2H, J = 8.8 Hz). ^{13}C NMR ($CDCl_3$, ppm): 28.26, 36.40, 67.09, 67.67, 69.76, 70.58, 70.92, 80.71, 83.09, 117.20, 138.31, 158.83, 171.07. HRMS: [$C_{17}H_{25}IO_5$+Na] requires 459.0639, found 459.0622.

9-(4-Iodophenyloxy)-3,6-dioxanonanoic acid (23). Compound **22** was stirred in neat CF_3COOH (5 ml) at room temperature overnight. The reaction mixture was concentrated to dryness, re-suspended in water, and dried *in vacuo* to provide a white, flaky solid (212 mg,

89%). M.p. 65-67°. ^{1}H NMR (DMSO-d_6, ppm): 2.43 (t, 2H, J = 6.5 Hz), 3.49-3.57 (m, 4H), 3.58 (t, 2H, J = 6.5 Hz), 3.71 (m, 2H), 4.05 (m, 2H), 6.80 (d, 2H, J = 9.0 Hz), 7.58 (d, 2H, J = 9.0 Hz), 12.17 (br s, 1H). ^{13}C NMR (DMSO-d_6, ppm): 35.89, 67.40, 68.40, 69.93, 70.78, 70.97, 84.33, 118.44, 139.10, 159.53, 173.81. HRMS: [$C_{13}H_{17}IO_5$-H] requires 379.0048, found 379.0038.

9-(4-Iodophenyloxy)-3,6-dioxanonanoic acid hydrazide (24). $SOCl_2$ (10 drops) was added dropwise (CAUTION! Violent reaction.) to a suspension of **23** (209 mg, 0.55 mmol) in MeOH. The reaction mixture was heated at reflux for 2 h, cooled, and concentrated to dryness under reduced pressure to provide a clear, colorless oil: ^{1}H NMR ($CDCl_3$, ppm): 2.61 (t, 2H, J = 6.5 Hz), 3.62-3.71 (m, 7H), 3.75 (t, 2H, J = 7.0 Hz), 3.83 (app t, 2H, J = 5.0 Hz), 4.08 (app t, 2H, J = 5.0 Hz), 6.70 (d, 2H, J = 9.0 Hz), 7.54 (d, 2H, J = 9.0 Hz). This oil was re-dissolved in EtOH, and 30 drops of hydrazine hydrate were added. The reaction mixture was heated at reflux overnight, concentrated to dryness, re-suspended in toluene and dried *in vacuo* to provide a waxy white solid (92%). M.p. 70-75°. ^{1}H NMR ($CDCl_3$, ppm): 2.48 (t, 2H, J = 5.5 Hz), 3.65-3.73 (m, 8H), 3.85 (m, 2H), 4.14 (app t, 2H, J = 5.0 Hz), 6.71 (d, 2H, J = 8.0 Hz), 7.55 (d, 2H, J = 8.0 Hz), 7.78 (br s, 1H). ^{13}C NMR ($CDCl_3$, ppm): 35.48, 66.95, 67.66, 69.82, 70.32, 70.64, 83.25, 101.93, 117.19, 138.42, 158.77. HRMS: [$C_{13}H_{19}N_2O_4I$+H] requires 395.0462, found 395.0462.

References

(1) Lakowicz, J. R.; *Principles of fluorescence spectroscopy;* Kluwer Academic: New York, 1999.

(2) Schanze has reviewed the field of conjugated polyelectrolytes to 2002: Pinto, M. R.; Schanze, K. S. *Synthesis* **2002,** *9,* 1293.

(3) Chen, L.; McBranch, D. W.; Wang, H.-L.; Helgeson, R.; Wudl, F.; Whitten, D. G. *Proc. Natl. Acad. Sci. USA* **1999,** *96,* 12287.

(4) DiCesare, N.; Pinto, M. R.; Schanze, K. S.; Lakowicz, J. R. *Langmuir* **2002,** *18,* 7785.

(5) (a) Ho, H. A.; Boissinot, M.; Bergeron, M. G.; Corbeil, G.; Dore, K.; Boudreau, D.; Leclerc, M. *Angew. Chem. Int. Ed. Engl.* **2002,** *41,* 1548. (b) Dore, K.; Dubus, S.; Ho, H. A.; Levesque, I.; Brunette, M.; Corbeil, G.; Boissinot, M.; Boivin, G.; Bergeron, M. G.; Boudreau, D.; Leclerc, M. *J. Am. Chem. Soc.* **2004,** *126,* 4240.

(6) Nilsson, K. P. R.; Inganaes, O. *Nature Materials* **2003,** *2,* 419.

(7) (a) Gaylord, B. S.; Heeger, A. J.; Bazan, G. C. *Proc. Natl. Acad. Sci. USA* **2002,** *99,* 10954. (b) Gaylord, B. S.; Heeger, A. J.; Bazan, G. C. *J. Am. Chem. Soc.* **2003,** *125,* 896. (c) Wang, S.; Bazan, G. C. *Adv. Mater.* **2003,** *15,* 1425.

(8) (a) Kushon, S. A.; Ley, K. D.; Bradford, K.; Jones, R. M.; McBranch, D.; Whitten, D. *Langmuir* **2002,** *18,* 7425. (b) Kushon, S. A.; Bradford, K.; Marin, V.; Suhrada, C.; Armitage, B. A.; McBranch, D.; Whitten, D. *Langmuir* **2003,** *19,* 6456.

(9) Kuroda, K.; Swager, T. M. *Chem. Commun.* **2003,** 26.

(10) (a) Aslam, M.; Dent, A.; Eds. *Bioconjugation;* Macmillan Reference: New York, 1998. (b) Hermanson, G.; *Bioconjugate techniques;* Academic Press: San Diego, 1996.

(11) While this dissertation was being prepared, a related approach to a PPE-based fluorogenic protease assay based on quencher removal was reported. Pinto, M. R.; Schanze, K. S. *Proc. Natl. Acad. Sci. USA* **2004,** *101,* 7505.

(12) Seitz, O.; Kunz, H. *J. Org. Chem.* **1997,** *62,* 813.

(13) (a) Pinto, M. R.; Kristal, B. M.; Schanze, K. S. *Langmuir* **2003,** *19,* 6523. (b) Tan, C.; Pinto, M. R.; Schanze, K. S. *Chem. Commun.* **2002,** 446.

(14) (a) Stracke, M. L.; Liotta, L. A. In *The molecular basis of cancer;* Mendelsohn, J.; Howley, P. M.; Israel, M. A.; Liotta, L. A.; Eds. Philadelphia: Saunders, 2000. (b) Brinckerhoff, C. E.; Matrisian, L. M. *Nature Rev. Mol. Cell Biol.* **2002,** *3,* 207.

(15) (a) Mahmood, U.; Tung, C.-H.; Bogdanov Jr., A.; Weissleder, R. *Radiology* **1999,** *213,* 866. (b) Weissleder, R.; Tung, C.-H.; Mahmood, U.; Bogdanov Jr., A. *Nature Biotechnol.* **1999,** *17,* 375. (c) Bremer, C.; Tung, C.-H.; Weissleder, R. *Nature Med.* **2001,** *7,* 743. (d) Funovics, M.; Weissleder, R.; Tung, C.-H. *Anal. Bioanal. Chem.* **2003,** *377,* 956.

(16) McIntyre, J. O.; Fingleton, B.; Wells, K. S.; Piston, D. W.; Lynch, C. C.; Gautam, S.; Matrisian, L. M. *Biochem. J.* **2004,** *377,* 617.

(17) (a) Freije, J. M. P.; Díez-Itza, I.; Balbín, M.; Sánchez, L. M.; Blasco, R.; Tolivia, J.; López-Otín, C. *J. Biol. Chem.* **1994,** *269,* 16766. (b) Knäuper, V.; López-Otín, C.; Smith, B.; Knight, G.; Murphy, G. *J. Biol. Chem.* **1996,** *271,* 1544. (c) Leeman, M. F.; Curran, S.; Murray, G. I. *Crit. Rev. Biochem. Mol. Biol.* **2002,** *37,* 149.

(18) Deng, S. J.; Bickett, D. M.; Mitchell, J. L.; Lambert, M. H.; Blackburn, R. K.; Carter, H. L.; Neugebauer, J.; Pahel, G.; Weiner, M. P.; Moss, M. L. *J. Biol. Chem.* **2000,** *275,* 31422.

(19) Knight, C. G.; Willenbrock, F.; Murphy, G. *FEBS Lett.* **1992,** *296,* 263.

(20) (a) Béchet, J. J.; Chevallier, J.; Labouesse, J.; Arnould, B.; Aldin-Cicarelli, S.; Yon, J. *Biochem. Biophys. Acta* **1968,** *151,* 165. (b) Castañeda-Agulló, M.; Del Castillo, L. M.; Whitaker, J. R.; Tappel, A. L. *J. Gen. Physiol.* **1961,** *44,* 1103.

(21) O'Shannessy, D. J.; Quarles, R. H. *J. Immunol. Methods* **1987,** *99,* 153.

(22) Wolfe, C. A. C.; Hage, D. S. *Anal. Biochem.* **1995,** *231,* 123.

(23) Duijndam, W. A. L.; Wiegant, J.; Van Duijn, P.; Haaijman, J. J. *J. Immunol. Methods* **1988,** *109,* 289.

(24) Koishi, K.; Ikeda, T.; Kondo, K.; Sakaguchi, T.; Kamada, K.; Tawa, K.; Ohta, K. *Macromol. Chem. Phys.* **2000,** *201,* 525.

(25) Kim, J.; Levitsky, I. A.; McQuade, D. T.; Swager, T. M. *J. Am. Chem. Soc.* **2002,** *124,* 7710.

(26) Zheng, M.; Bai, F.; Li, F.; Li, Y.; Zhu, D. *J. Appl. Poly. Sci.* **1998,** *70,* 599.

(27) Beer, P. D.; Cadman, J.; Lloris, J. M.; Martínez-Máñez, R.; Soto J., Pardo, T.; Marcos, M. D. *J. Chem. Soc. Dalton Trans.* **2000,** *11,* 1805.

Chapter 3

Layer-by-layer PPE films on silica substrates for enhanced sensory amplification

Introduction

The use of conjugated polymers in thin-film form has a number of advantages over polymer solutions in sensory schemes. As described in Chapter 1, these stem from inherent limitations in energy migration along a one-dimensional structure such as a dissolved PPE in solution. Excitons generated in one segment of the polymer chain are free to migrate along the length of the polymer backbone, but the random nature of the exciton 'walk' means that the excited state is likely to re-visit the same portions of the polymer chain several times during its lifetime. By depositing the polymer as a two-dimensional thin film, excitons are allowed a greater degree of migrational freedom in which the chances of re-visiting the same polymer segment are greatly reduced. If each polymer segment is thought of as a receptor for a particular photophysically active analyte — one that either serves as a fluorescence quencher or an emissive trap — this means that a larger number of potential receptor sites can be visited by the exciton, resulting in greater signal amplification and lower detection limits.

There has been long-standing interest in the Swager group in optimizing the structure of PPE thin films to maximize energy migration and boost signal amplification. Spin-coating is one of the most popular methods of making conjugated polymer thin films but suffers from limited reproducibility and the requirement for large quantities of material (much of which is 'spun off' the substrate in the spin-coating process). In contrast, the Langmuir-Blodgett (LB) technique, which deposits aligned polymers onto substrates in a highly controlled fashion, is capable of producing PPE films of precisely controlled thickness and alignment. Former Swager group graduate student Jinsang Kim and postdoc Igor Levitsky made use of these features to determine the effects of PPE film thickness on energy migration and analyte sensing.[1,2] While unparalleled in the degree of control it provides, the LB technique has disadvantages of its own: foremost

among these are the high cost of the equipment needed to produce LB films and the time-consuming nature of LB film deposition onto substrates.

The initial motivation for the work described in this chapter was the desire to produce PPE-coated silica microspheres for use in laser applications. Microspheres are well known as efficient cavities for the generation of lasing behavior due to the presence of so-called 'whispering-gallery modes' (WGMs)[3] in which total internal reflection causes the constructive interference of certain wavelengths of light. In the case of microspheres, light is guided around the inside of the spherical structure and the microsphere takes on the role of the internal 'cavity' necessary for lasing to take place. In most cases, microsphere lasers are constructed from a dielectric material such as silica internally 'doped' with a laser dye or lanthanide ion.[4] However, microsphere lasing can also occur when the optically active material is coated on the outside of a transparent microsphere. In order to use PPEs as the gain medium in microsphere lasers, we sought a method to evenly coat silica microspheres (5 μm and smaller in diameter) with PPE thin films. Spin-coating and LB techniques were ruled out for obvious practical reasons, and initial efforts by former Swager graduate student Aimee Rose to coat microspheres with conjugated polymer using solvent-driven physisorption met with limited success. The fact that commercial silica microspheres are mostly sold as aqueous suspensions discouraged the use of water-sensitive silane chemistry. For these reasons, we elected to use the alternating layer-by-layer (LBL) deposition technique to accomplish the required PPE deposition onto microspheres. This chapter describes the use of a polyelectrolyte PPE to generate thin films on glass slides and silica microspheres and the use of these PPE thin films for various energy-transfer and amplified quenching applications.

The layer-by-layer (LBL) technique

The layer-by-layer technique was pioneered by Decher[5] and Rubner and is based on the sequential adsorption of oppositely charged polyelectrolytes (Figure 3.1).

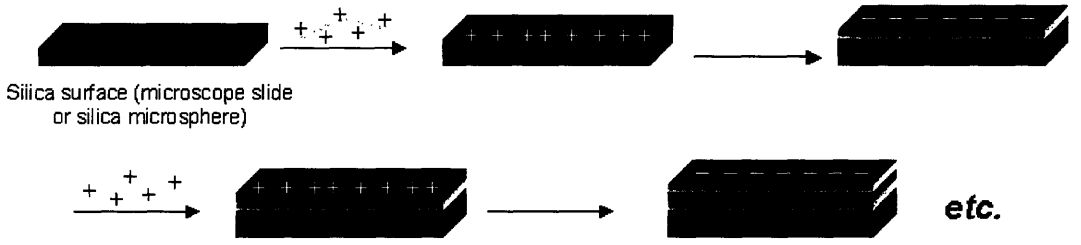

Figure 3.1. Schematic illustration of the layer-by-layer deposition process. For clarity, deposition is shown on only one side of the substrate.

To construct a thin film using LBL methods, a charged substrate is first immersed in a solution of an oppositely charged polyelectrolyte (polymer A). Over-compensation of the surface charge on the substrate gives the thin film an overall charge of the same type as polymer A. Subsequent immersion of the polymer A-coated substrate into a polyelectrolyte solution of opposite charge (polymer B) results in the deposition of polymer B as a new layer. This A/B 'layer pair' can then be subjected to additional adsorption cycles as needed to generate films of desired thickness. Numerous studies employing X-ray techniques, ellipsometry and profilometry have shown that the thickness of the resulting films is directly proportional to the number of deposited A/B layer pairs.[5]

Since its introduction in the early 1990s, the LBL technique has become very popular as a method for constructing thin films. Its principal advantages center on its extreme operational simplicity — the only equipment required to create LBL thin films is three beakers and a source of water for rinsing the substrate between immersions. Any substrate to which a polyelectrolyte

can be adsorbed is usable, including glass, which contains mildly acidic silanol groups that are easily deprotonated in base to give a negatively charged surface. The LBL technique has also been extended beyond polyelectrolytes to include gold nanoparticles, colloids of various descriptions, and charged biomolecules such as proteins and DNA in the film structure. These and other applications of the LBL technique have been reviewed in the compilation edited by Tripathy *et al.*[6]

Sensory and conjugated-polymer applications of LBL

The simplicity of the LBL technique has led to interest in using thin films assembled using this method for sensory purposes. For example, Lee *et al.* deposited films containing a pH-sensitive pyrene dye on silica supports in both native form and as pendant chromophores. The fluorescence of the LBL-assembled films was found to be sensitive to quenching analytes such as DNT, Fe^{3+} and Hg^{2+} as well as to changes in pH.[7] Leblanc and co-workers fabricated an unusual LBL structure based on alternating layers of the biological polycation chitosan and highly luminescent CdSe 'quantum dots' capped with anionic head-groups. These authors found that inclusion into the LBL structure had beneficial effects on the fluorescence properties of the quantum dots, and the resulting structures were used in the fluorescence-based detection of the nerve agent paraoxon.[8]

Several groups have studied the behavior of LBL-assembled thin films incorporating a conjugated polymers as a component polyelectrolyte. Rubner and co-workers examined energy transfer in LBL films made up of an anionic poly(phenylene) donor separated from a cationic poly(phenylene vinylene) acceptor by non-conjugated spacer layers of varying thickness.[9] They observed efficient Förster energy transfer (FRET) between these two conjugated polymers even

when thick spacer groups were used and concluded that significant layer interpenetration occurs in this system. Richter and Kirstein carried out a similar study using a poly(phenylene vinylene) donor separated from a layer of dye-modified poly(allylamine) (PAH) acceptor by PAH-poly(styrenesulfonate) (PSS) spacers.[10] They also observed efficient energy transfer between the two photophysically active layers, although the observed Förster radii were not self-consistent and they similarly attributed these results to significant layer interpenetration. Schanze *et al.* recently reported an LBL film based on an anionic PPE bearing short phosphonate-terminated side chains.[11] A quaternary ammonium polycation (see below) and a Zr(IV) species were used as co-polyelectrolytes, and the Zr(IV)-containing film was used in the construction of an electroluminescent device. These authors did not report the photoluminescence properties of the resulting films. Thunemann also created electroluminescent devices derived from a PPE with integrated benzoic acid side-groups, but in this case the PPE was pre-aggregated with polyelectrolyte counterions before deposition onto substrates.[12]

Previous research in the Swager group has made use of PPE-containing LBL films for sensory purposes. Former Swager group postdoc Tyler McQuade fabricated films based on a polycationic PPE donor and a fluorescein-modified polyanion.[13] The resulting assembly functioned as a polymer-amplified pH sensor in which energy transfer between the PPE and fluorescein was modulated by the pH-sensitive photophysical properties of the fluorescein acceptor.

This chapter describes the preparation of highly fluorescent PPE thin films using the LBL technique. The PPE chosen was designed to satisfy a number of requirements to ensure appropriate LBL behavior while retaining optimal fluorescence properties. The LBL technique was used to deposit thin films of this polymer on glass slides and silica microspheres. Glass

slides LBL-coated with PPE showed excellent donor characteristics toward dye-modified derivatives of poly(allylamine) (PAH). The LBL-coated silica microspheres were used in a series of 'suspension-phase' Stern-Volmer quenching assays and exhibited greatly enhanced sensitivities relative to PPEs in solution.

Results and Discussion

Synthesis of a polyelectrolyte PPE for LBL deposition

Initial efforts to create LBL films using simple carboxylate PPEs like those described in Chapter 2 produced films with well-controlled thickness (measured in terms of the film absorbance) but very poor fluorescence properties. This suggested that the weakly acidic carboxylic acid groups present on each repeating unit did not provide sufficient electrostatic repulsion to prevent π-stacking and polymer aggregation. For this reason, we sought to include a pentiptycene units[14] (described in Chapter 1) into the PPE structure to reduce aggregation effects and ensure high fluorescence quantum yields in the resulting films. The use of a carboxylate-containing diiodophenylene monomer (described in Chapter 2) and this pentiptycene co-monomer provided polymer **1** in good yield (Scheme 3.1).

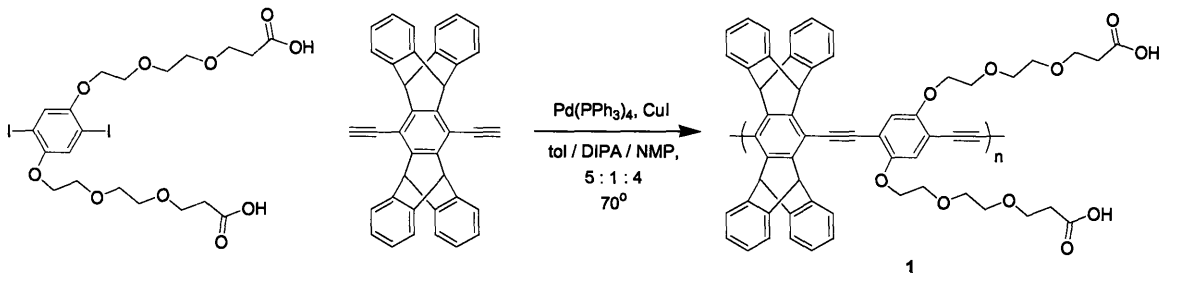

Scheme 3.1. Synthesis of polymer **1**.

Remarkably, we found that the use of 50% *N*-methylpyrrolidinone (NMP) in the polymerization mixture together with the usual 4:1 toluene/DIPA combination was essential for successful polymerization: the use of toluene/DIPA alone, neat morpholine, NMP/DIPA, or other solvent combinations led to no visible polymerization, even at high temperatures and prolonged reaction times. This strong solvent dependency may arise from the different solubility requirements of the two monomers and the growing polymer chain.

Characteristics of LBL PPE films on glass slides and microspheres

Polymer **1** was deposited on glass microscope slides (previously cleaned with concentrated nitric acid followed by 3 N KOH) from DMF solutions after first adsorbing a layer of the commercially available polycation poly(diallyldimethylammonium chloride) (PDAC, Scheme 3.2) to render the substrate cationic. The high water soubility and pH-independent charge of this polyelectrolyte make it especially suitable for our application.

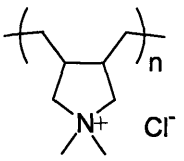

Scheme 3.2. Structure of poly(diallyldimethylammonium chloride) (PDAC).

LBL films were built up by successive immersion of the polymer-coated substrates in DMF solutions of **1** and aqueous solutions of PDAC. The use of DMF as a solvent for the deposition of **1** was necessary due to the insolubility of this polymer in water. To avoid contaminating the dipping solutions, exhaustive rinsing steps with appropriate solvents were used between substrate immersions or before transferring substrates from one solvent to another.

Qualitatively, films of PDAC/**1** produced by the LBL technique showed a deep-yellow color and bright, homogeneous fluorescence under illumination by a hand-held UV lamp. The

growth in film thickness, represented by the absorbance of the film, was monitored after each dipping cycle using a standard spectrophotometer. Figure 3.2 shows the spectra of consecutive (PDAC/**1**) layer pairs after each immersion in **1**.

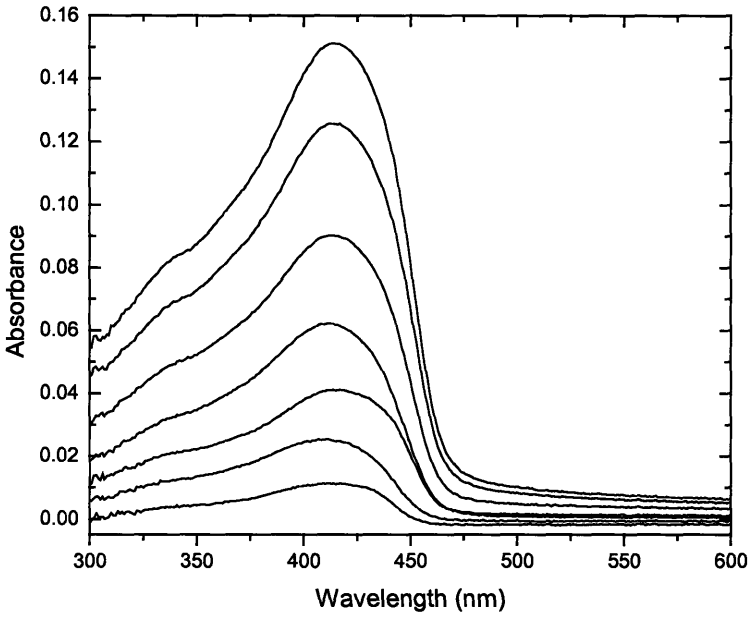

Figure 3.2. UV-vis spectra of a PDAC/**1** LBL film on a glass microscope slide, measured after the deposition of each layer pair. The lowest trace represents one PDAC/**1** layer pair, with each subsequent trace representing an additional PDAC/**1** cycle. Polymer **1** was deposited from a 0.01 wt% solution in DMF, while PDAC was deposited from a 2 wt% solution in water. Each immersion was approximately 3 minutes in duration.

Figure 3.3 shows the buildup of absorbance after each layer pair for the system shown above.

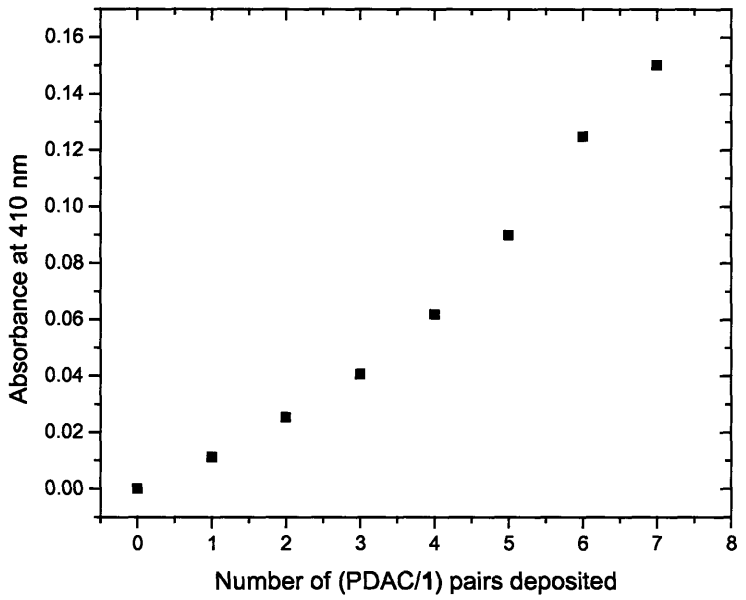

Figure 3.3. A_{410} *versus* number of (PDAC/**1**) layer pairs deposited for the system shown in Figure 3.2.

The pattern of absorbance growth shown in Figure 3.2 is typical of LBL film deposition and shows that the essential absorbance features of polymer **1** are maintained as the film is built up. The relationship of film absorbance to the number of layer pairs deposited (Figure 3.3) was found to be linear at early stages in the deposition process, but deviated significantly from linearity at later stages. The use of longer immersion times (up to 20 minutes) was found to restore linearity in most cases, suggesting that depletion or contamination of the dipping solutions over time may interfere with the kinetics of the adsorption process.

While PDAC itself has no absorption bands in the visible region, the adsorption of a layer of this material onto a pre-existing PPE layer was found to influence the spectroscopic characteristics of the PPE layer itself (Figure 3.4). The slight absorbance red-shift seen on capping a layer of **1** with PDAC likely arises from perturbations in the bandgap of **1** brought on by the strongly charged environment created by the additional PDAC layer. Immersion-induced

annealing of the polymer film is also consistent with these spectral shifts, which may be indicative of a small amount of polymer aggregation.

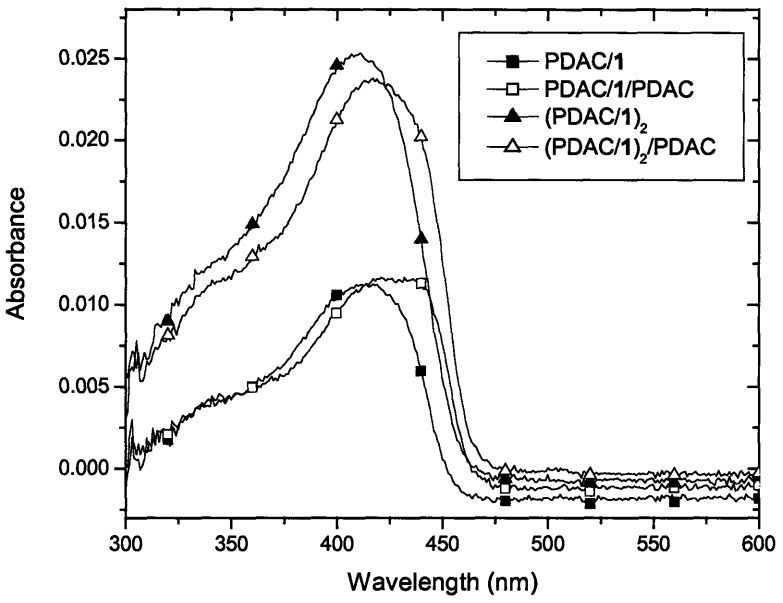

Figure 3.4. Build-up of absorbance of polymer **1** in the construction of two PDAC/**1** layer pairs, showing the spectroscopic effects of the addition of PDAC layers.

In contrast to the absorbance build-up behavior seen in Figures 3.2 and 3.3, the growth of fluorescence with dipping cycles was much less regular. Following the build-up of fluorescence for a (**1**/PDAC) LBL film through three layer pairs (Figure 3.5) shows that while the overall fluorescence of the film does increase as the number of immersions in polymer **1** is increased, the growth is not regular, with strong fluorescence effects seen after PDAC immersions.

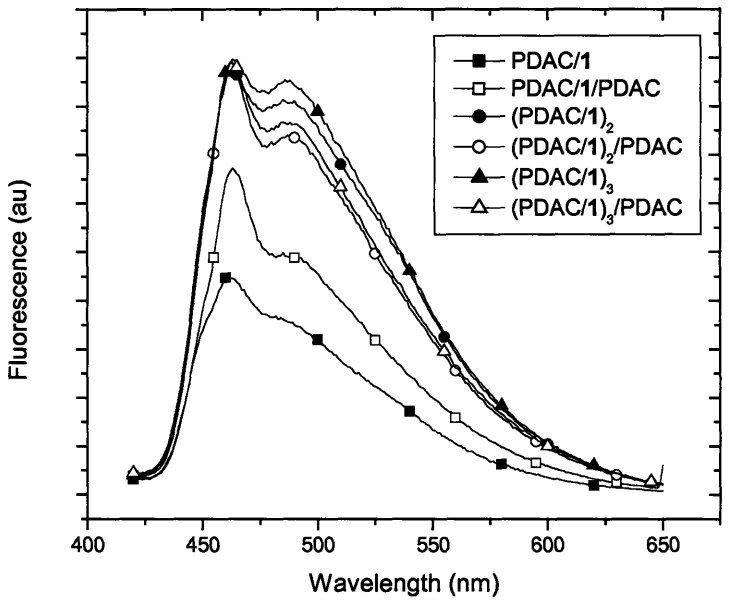

Figure 3.5. Fluorescence of a (PDAC/**1**) LBL film followed after each immersion. Growth of film fluorescence is not regular with respect to the number of layers of **1** deposited.

One notable feature of the fluorescence spectra shown in Figure 3.5 is the layer-dependent increase in the intensity of the fluorescence band at 490 nm relative to the main emission at 460 nm (Figure 3.5). This result suggests that the deposition of multiple layer pairs promotes the formation of an emissive aggregate or excimer. The dramatic irregularity of the fluorescence intensities in the face of the highly regular absorbance data may also be due to physical effects such as the waveguiding of light in the glass substrates. Problems arising from fluorescence intensity inconsistencies were minimized in our applications by the use of single layer-pair PDAC/**1** films, in which film-to-film variations in fluorescence intensity were less than 10%.

LBL polymer films were deposited on silica microsphere substrates by a simple extension of the methodology described above. Commercially available suspensions of monodisperse silica microspheres ranging in size from 0.64 to 5.00 μm were centrifuged, the supernatant decanted,

and the microsphere pellet ultrasonicated in 3 N KOH for 30-60 minutes to render the microsphere surfaces anionic. The LBL deposition of PDAC/**1** films on these microspheres was then simply carried out by treatment of the microspheres with the appropriate polymer solution with continuous ultrasonication or stirring. Excess polymer was removed by repeated centrifugation and ultrasonication steps using fresh solvent. By visual inspection, microspheres coated with **1** were bright yellow in color and could be dispersed in solvent to provide a bright blue-green fluorescent, turbid suspension (Figure 3.6).

Figure 3.6. 5.0-μm silica microspheres coated with polymer **1**. Left: Microspheres in suspension in DMF with a pellet of settled microspheres at the bottom of the test tube, illuminated by normal room light. Right: The same microspheres suspended in DMF and illuminated by a hand-held UV lamp.

PPE-coated microspheres were examined by scanning electron microscopy by Swager group graduate student Jessica Liao. The resulting micrographs confirmed that the LBL process left an even coating of polymer on the microsphere surface, although indentations can be seen in some cases.

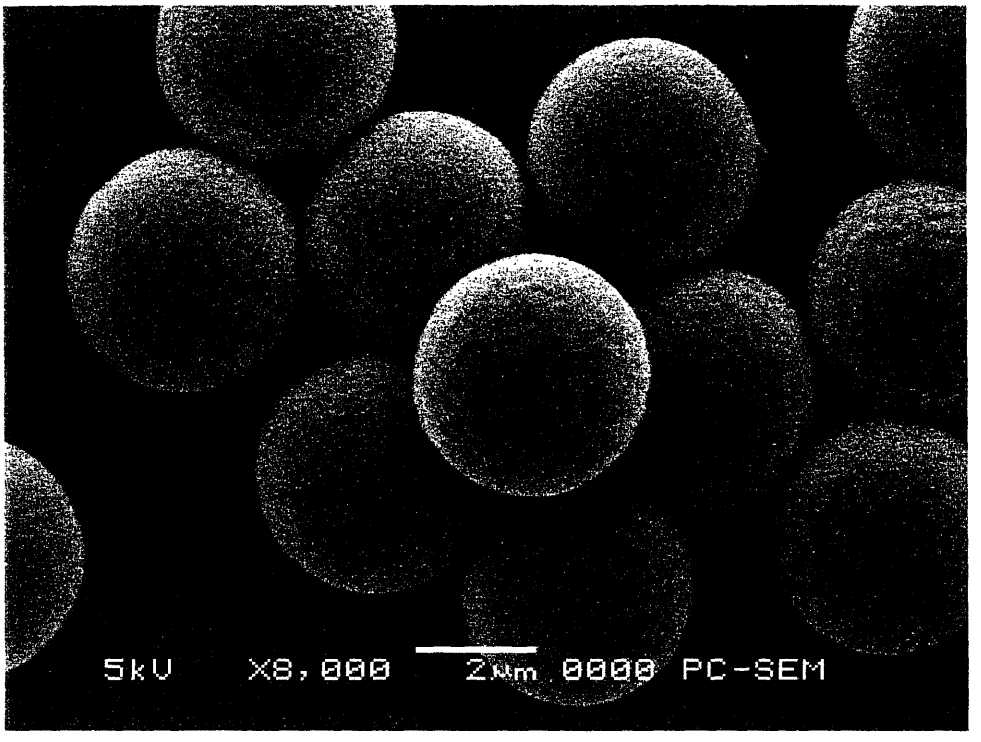

Figure 3.7. Scanning electron micrograph of 5.0-μm microspheres coated with polymer **1**. Image courtesy of Jessica Liao.

Confocal laser scanning microscopy was used to confirm the surface-confined nature of the polymer film on 5.0-μm silica microspheres (Figure 3.8). Because confocal microscopy only reveals fluorescent objects through thin 'slices' in the x-y plane, the polymer-coated microspheres appear as bright rings, indicating that the fluorescent material (polymer **1**) is located only at the outer surfaces of the microspheres.

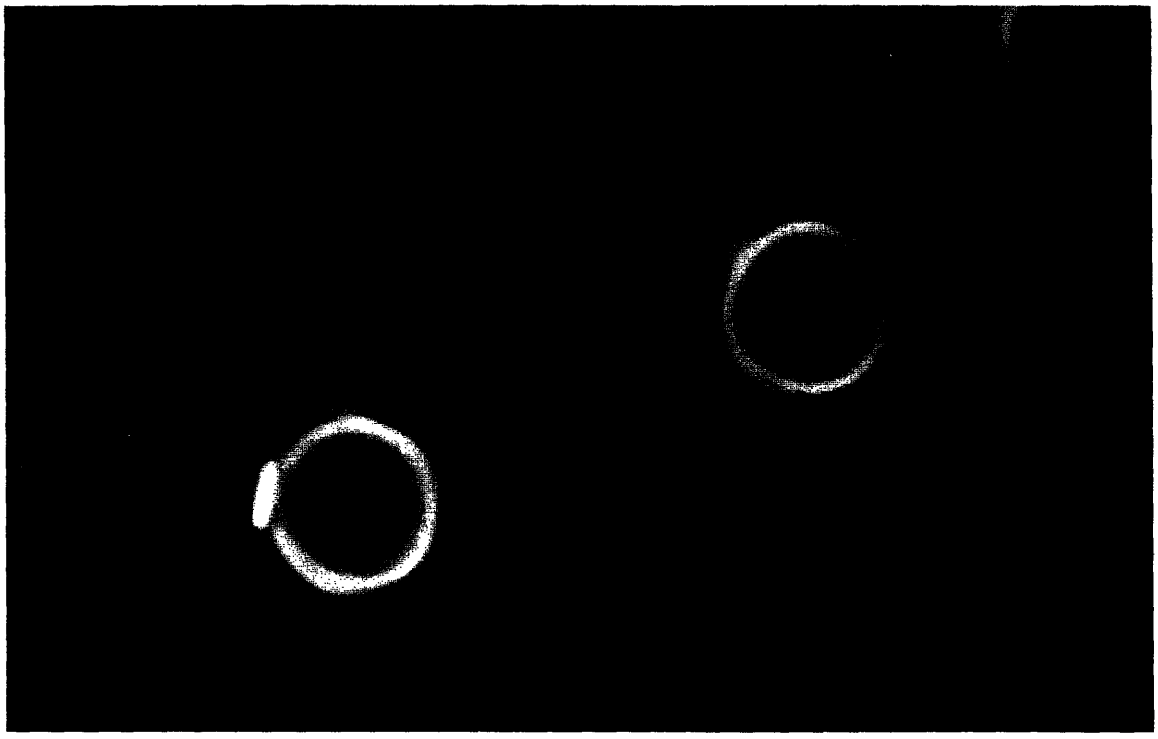

Figure 3.8. Confocal micrograph of silica microspheres coated with polymer **1.** Confocal microscopy only reveals fluorescent objects. The microspheres are imaged at a thin 'slice' along the z-axis and appear as rings due to confinement of the fluorescent PPE to the outer surface of the microsphere.

Confocal micrographs of polymer-coated microspheres also revealed that microsphere aggregation increased as the microspheres with subjected to more numerous layer-pair depositions (Figure 3.9). This increased aggregation could be avoided by thorough sonication while adding polyelectrolyte solutions to the microsphere suspensions, suggesting that aggregation was caused by polyelectrolyte-promoted adhesion of closely packed microspheres.

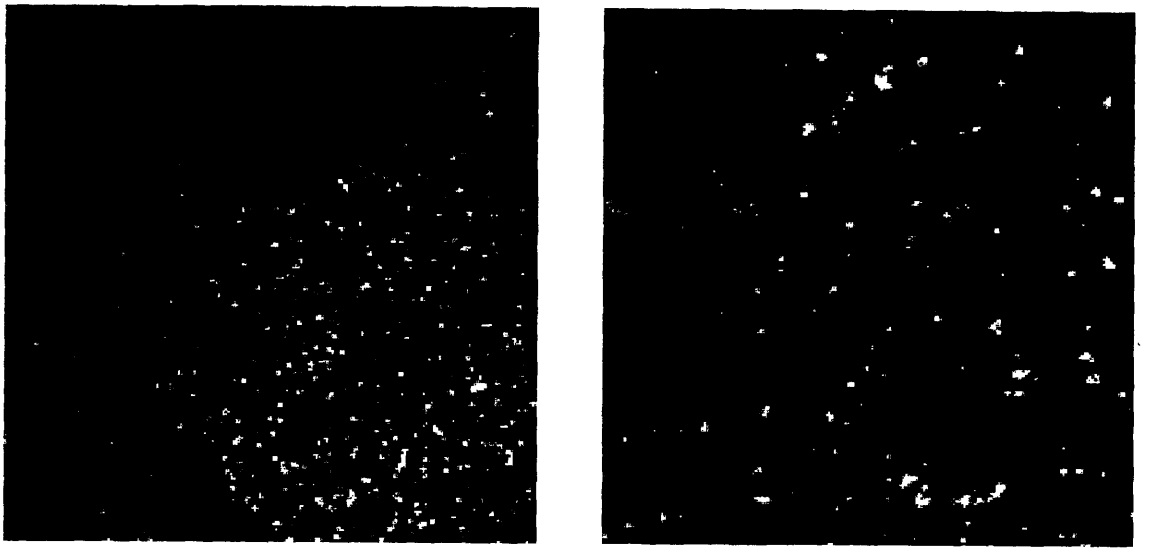

Figure 3.9. Confocal micrograph of silica microspheres coated with polymer **1**. *Left:* One PDAC/**1** layer pair. *Right:* Four PDAC/**1** layer pairs.

Spectroscopic analysis of confocal micrographs demonstrated that the fluorescence spectrum of a single layer of polymer **1** on microspheres is substantially the same as that for **1** in DMF solution, indicating that the microsphere-coated form does not suffer from the effects of π-stacking and aggregation (Figure 3.10). Differences at the blue edge of the emission band are suggestive of greater conformational disorder in the LBL-deposited polymer relative to isolated polymer chains in solution.

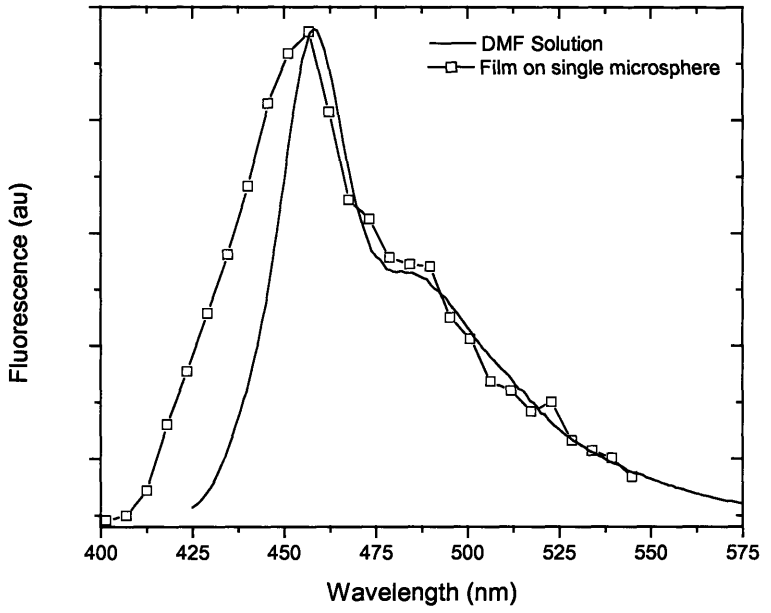

Figure 3.10. Spectrum of polymer **1** in DMF measured in a fluorimeter (λ_{ex} 405 nm) and coated as a film on a single 5.0-μm silica microsphere (λ_{ex} 364 nm).

Energy transfer effects in LBL films

The simplicity with which films of **1** can be constructed using the LBL method provided an opportunity to use this technique to investigate energy transfer and quenching phenomena in multilayer films. In particular, we sought to use the strong electrostatic forces present in LBL films to examine the efficiency of energy transfer from a single layer of **1** to a dye-labeled polycation adsorbed on top of it. Derivatives of PAH derivatized with fluorescein, tetramethylrhodamine, and carboxy-X-rhodamine (a Texas Red analog) were prepared as shown in Scheme 3.3. These polymeric dye derivatives were synthesized so as to have an extremely small fluorophore loading (one equivalent of fluorophore per 415 polymer repeat units) to minimize interference by the pendant dye groups in the LBL adsorption process.

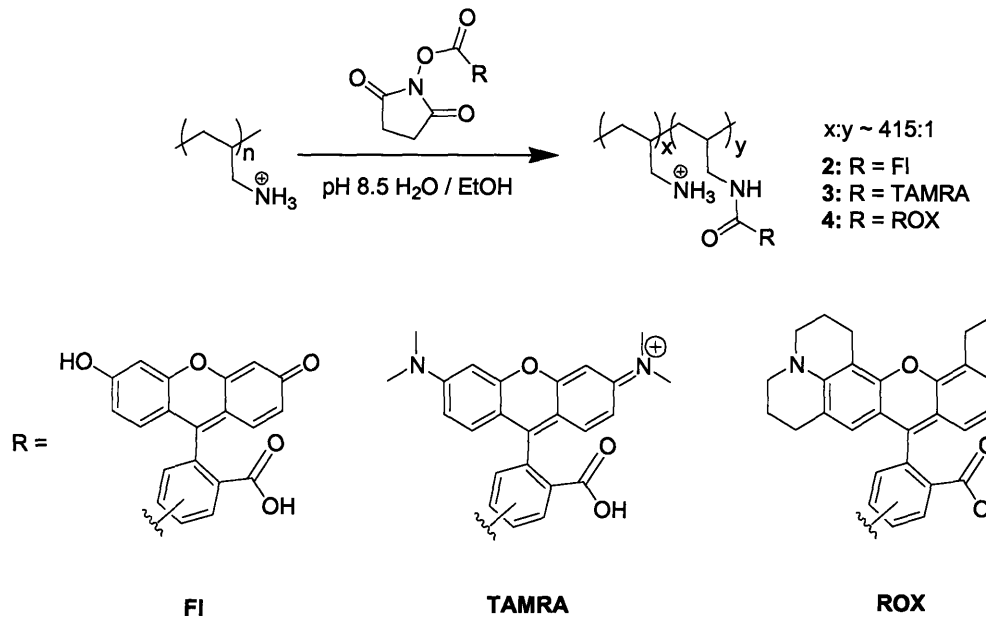

Scheme 3.3. Synthesis of dye-labeled derivatives of PAH using fluorophore succinimide esters. For simplicity, only one isomer of each dye is shown; mixtures of the 5'- and 6'-carboxylate succinimide esters were used in each case.

Previous investigations (not shown here) in conjunction with former Swager group postdoc Tyler McQuade had revealed that energy transfer between spin-coated films of polymers structurally related to **1** and fluorophores adsorbed to the film surface was remarkably efficient even in cases where the spectral overlap between the PPE and dye was small. This result deviates from predictions based on simple Förster energy transfer (FRET), which dictates that energy transfer between donor and acceptor chromophores should be strongly dependent on spectral overlap, and suggested that an electron-exchange (Dexter-type) energy transfer mechanism may be operative. To verify if this effect could be reproduced in an LBL system, a film of **1** on a glass microscope slide was dipped into a solution of **4** for 5 seconds. Fluorescence spectra were measured before and after immersion (Figure 3.11).

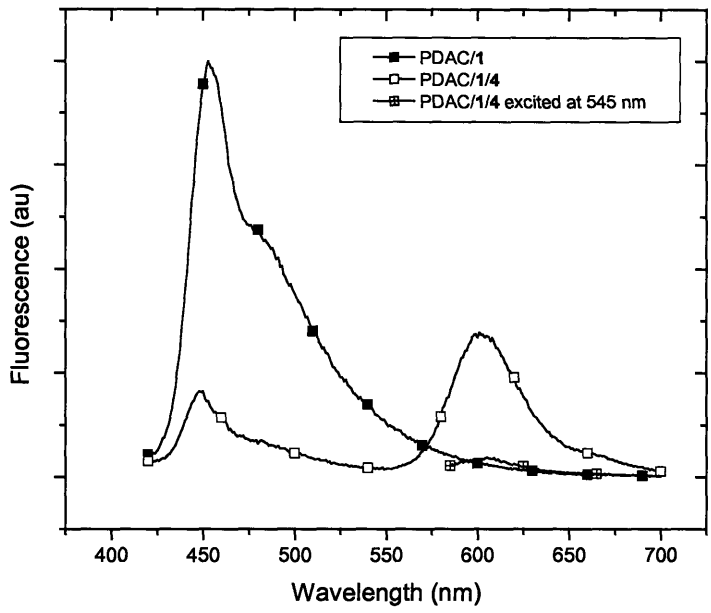

Figure 3.11. Spectra of an LBL film of **1** before and after a 5-s immersion in a solution of **4.**

The spectrum of the PDAC/**1**/**4** system in Figure 3.11 clearly shows a strong emission band centered around 600 nm due to the fluorescence of the ROX fluorophore, even with excitation at 405 nm. Concomitant with the appearance of this new band is a marked reduction in the intensity of the emission due to **1** — the remaining emission is blue-shifted to about 445 nm and is dominated by Raman scattering from water trapped in the polymer film. Because the ROX fluorophore has no absorbance at the wavelength used to excite the polymer (405 nm), the new emission band is entirely due to energy transfer from **1** to **4.** Direct excitation of the ROX fluorophore at 545 nm gave rise to a ROX emission about 8 times weaker than that produced by excitation of **1.** While this degree of signal amplification is significant, previous experiments with spin-cast films using TAMRA surface-trapped dyes provided energy-harvesting amplifications about one order of magnitude greater than this.

To investigate the effect of film thickness on energy transfer, a layer of **4** was deposited as the top layer on films composed of one to five layers of **1**. The ratios of emission intensities of the ROX fluorophore (F_4) and PPE **1** (F_1) generated on excitation of **1** were plotted *versus* the number of layer pairs (Figure 3.12).

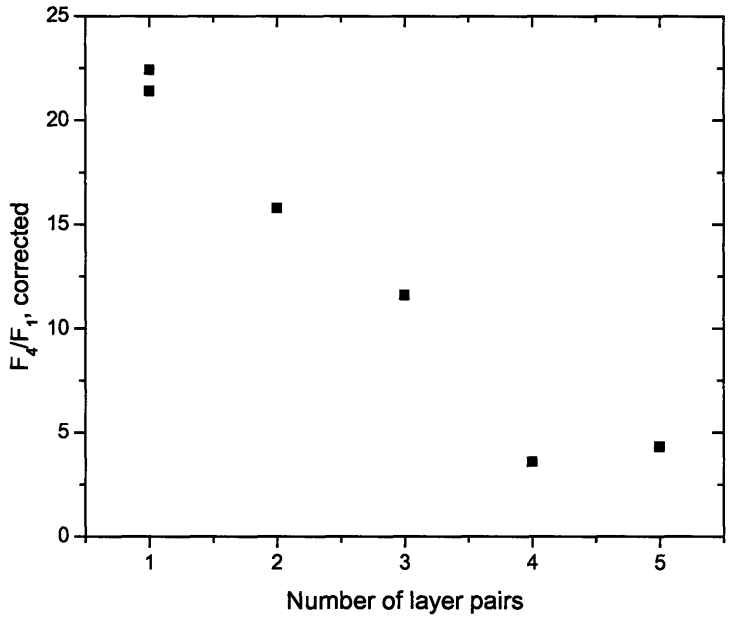

Figure 3.12. Ratio of fluorescence emission intensity arising from the ROX-substituted PAH derivative **4** and PPE **1** in (PDAC/**1**) films containing different numbers of layer pairs underneath a layer of **4**. Ratios are corrected for thickness-dependent changes in peak shape. Two experiments were carried out for the simple one-layer-pair system.

Figure 3.12 shows a steady monotonic decrease in the ROX/PPE emission ratio as the number of layer pairs of PDAC/**1** is increased from one to four. This result implies that energy harvesting and transfer by **1** to the fluorophore in **4** is most efficient for the layer of **1** immediately adjacent to **4**. In this case, it is probable that there is some interpenetration of the top layer of **4** into the underlying (PDAC/**1**) LBL structure, but that energy transfer from lower layers to the emissive traps present in **4** is inefficient owing to poor inter-layer exciton migration in these films. Although layer interpenetration is known to be significant in systems such as PDAC/PSS and

PAH/PAA, the vast structural differences between **1** and PDAC may limit this effect in the films studied here. In all cases, it is obvious for this system that the use of more than one underlying layer of PPE provides no advantage in sensory applications.

In order to facilitate exciton migration through LBL films, we attempted to prepare a series of pentiptycene-containing cationic polymers based on imidazolium-substituted monomers such as those shown in Scheme 3.4. It was hoped that the construction of an all-PPE film would enable facile three-dimensional exciton migration and overcome the problems posed by the presence of interleaved non-conjugated layers of PDAC.

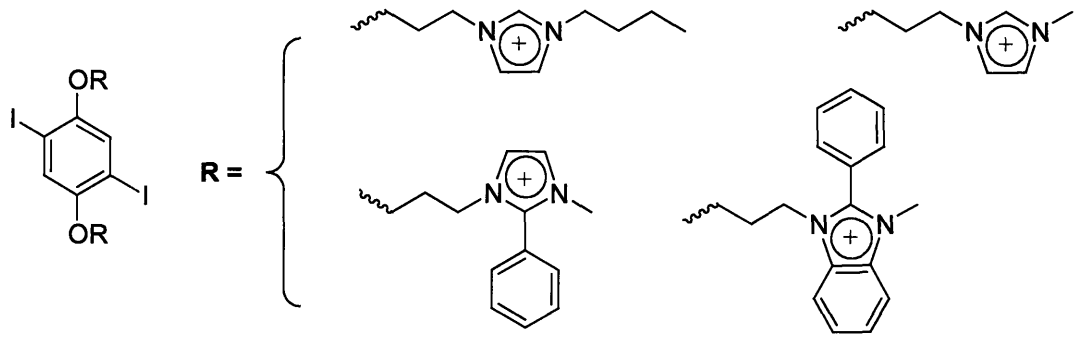

Scheme 3.4. Monomers used in the attempted synthesis of cationic, imidazolium-containing PPEs. Counterions used include OTf, BF_4^- and I^-.

Unfortunately, polymerization of these monomers was unsuccessful under every set of conditions used. However, a cationic PPE could be obtained by microwave heating of a PPE containing bromoalkane-substituted sidechains in neat *N*-methylimidazole (not shown). While this PPE could be adsorbed to a layer of PSS on a glass slide, all attempts to co-adsorb this polymer with **1** failed.

PPE-dye energy transfer in LBL films was further examined using polymers **2** and **3** in a manner similar to that described above for **4** (see above, Figure 3.11). In this experiment, a single layer-pair PDAC/**1** film was immersed for 10 minutes in solutions of **2, 3** and **4** of comparable concentration. As shown in Figure 3.13, all three polymers were found to be efficient quenchers

of the PPE fluorescence of **1** in the LBL film, but the fluorescein derivative **2** showed the largest dye emission overall.

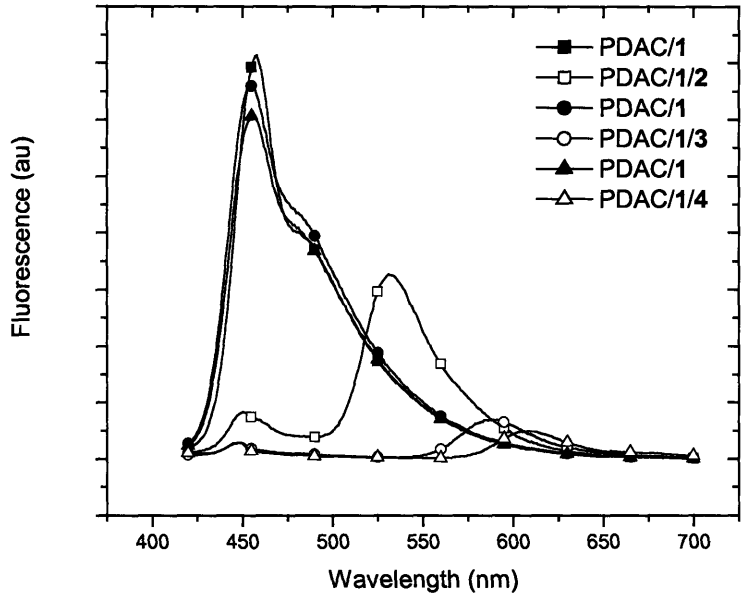

Figure 3.13. Fluorescence spectra of PDAC/**1** films (solid symbols) and after adsorption of a top layer of a PAH fluorescein (**2**), tetramethylrhodamine (**3**) or carboxy-X-rhodamine (**4**) derivative (open symbols).

It is instructive to compare the PDAC/**1**/**4** curves of Figure 3.11 and Figure 3.13, which represent the same dipping experiment but differ in the length of time the PDAC/**1** film was immersed in **4** (5 seconds and 10 minutes, respectively). Emission from the ROX fluorophore is much weaker after extended immersion in **4**, implying that prolonged exposure of the film to the dye-labeled polycation results in a reduction in the effective quantum yield of the pendant fluorophores. This may arise from simple aggregation and self-quenching effects as the layer of **4** is allowed to accumulate on top of the PDAC/**1** film. If so, the observed trend of dye emission intensities in Figure 3.13 may reflect enhanced self-quenching in the hydrophobic TAMRA and ROX dyes *versus* the more hydrophilic fluorescein unit.

Quenching effects in LBL PPE-coated microspheres

Quantitative or semi-quantitative assessment of the relative sensory advantages of PPE thin films over PPEs in solution is made difficult by the manner in which a thin-film Stern-Volmer experiment is carried out. For films that are immersed into an analyte solution, removed, and dried, calculation of the quenching constant K_{SV} is complicated by the uncertainty surrounding the effective 'concentration' of analyte in the dried film. The use of LBL polymer-coated microspheres suspended in solvent — essentially a micron-sized 'suspension' of thin films — should allow for the quantitative determination of an effective K_{SV} for thin films while keeping the polymer surface in equilibrium with the quencher solution. Comparison of the observed K_{SV} values for the suspended microspheres with those determined for polymers in solution thus allows a semi-quantitative assignment of sensory amplification provided by thin films.

Preliminary experiments in this area revealed a strong solvent dependence in the quenching of PPE-coated microspheres. A suspension of 1.87-μm (PDAC/**1**)$_2$-coated microspheres in $CHCl_3$ showed a K_{SV} of approximately 70 M^{-1} with the quencher 2,4-dinitrotoluene (DNT), somewhat larger than values seen for comparable PPEs in solution (see Chapter 4). This value is consistent with mostly dynamic interactions between well-solvated quenchers and the efficiently 'wetted' organic surface. In contrast, PDAC/**1**-coated microspheres suspended in 50 mM pH 7.5 Tris buffer showed a K_{SV} of 9.2×10^3 with the electronically similar, negatively charged quencher 3,5-dinitrobenzoate. In order to test the effect of microsphere charge on the quenching efficiency, the latter experiment was repeated with PDAC/**1**/PDAC-coated microspheres having a positive surface charge. In this case the observed K_{SV} was 4.5×10^3,

indicating that any pre-concentration effects arising from greater surface adsorption of the quencher are more than offset by the presence of an extra PDAC 'spacer' layer between the fluorescent PPE **1** and the electron-accepting quencher.

Following up on this result, K_{SV} values were determined for suspensions of PDAC/**1** and $(PDAC/1)_2$-coated 5.0 μm microspheres using 4-nitrobenzylamine, ε-*N*-(2,4-dinitrophenyl)lysine (LysDNP) and dinitrophenyl-labeled bovine serum albumin (BSA-DNP) as quenchers. Stern-Volmer experiments were carried out in 0.1 M pH 7.3 phosphate-buffered saline (PBS) and polymer **5** (see Chapter 2) was used as a water-soluble analog of **1** for comparison purposes (Scheme 3.5).

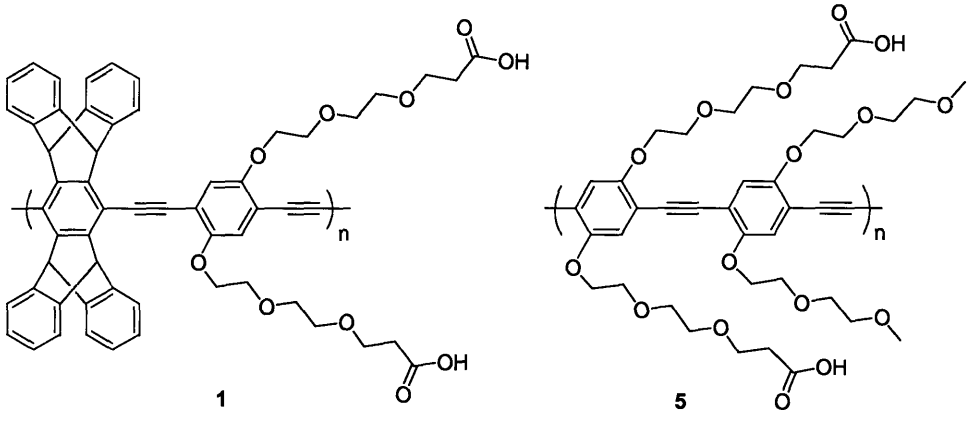

Scheme 3.5. Structures of LBL polymer **1** and water-soluble analog **5**.

K_{SV} data are listed in Table 3.1.

Table 3.1. Observed K_{SV} values (in M^{-1}) PPE-microsphere systems and PPE **5** in solution using 4-nitrobenzylamine, LysDNP and DNP-labeled BSA as quenchers. DNP-labeled BSA values are expressed in terms of equivalents of DNP. All Stern-Volmer determinations were carried out in 0.1 M PBS, pH 7.3.

System / Quencher	4-nitrobenzylamine	LysDNP	BSA-DNP
PDAC/1 microspheres	$(1.45 \pm 0.4) \times 10^3$	$(1.13 \pm 0.04) \times 10^5$	$(6.6 \pm 0.4) \times 10^4$
$(PDAC/1)_2$ microspheres	$(2.69 \pm 0.07) \times 10^3$	$(1.81 \pm 0.04) \times 10^5$	$(9.9 \pm 0.5) \times 10^4$
Polymer 5 in solution	$(5.91 \pm 0.08) \times 10^2$	$(1.48 \pm 0.07) \times 10^4$	$(3 \pm 2) \times 10^2$

The most notable trend in Table 3.1 is that, for all cases, the PPE-coated microsphere systems show larger K_{SV} values than polymer **5**. The enhancement provided by a single PDAC/**1** layer pair on a microsphere ranges from about threefold for the small, soluble 4-nitrobenzylamine to over 200-fold for BSA-DNP. In the latter case, this large difference may be originate from co-operative static binding of the protein's multiple DNP groups to the microsphere surface. Quenching efficiency towards PPE-coated microspheres proceeds in the order LysDNP > BSA-DNP > nitrobenzylamine, while in the case of polymer **5** the quenching efficiencies of BSA-DNP and nitrobenzylamine are comparable. It is likely that the greater quenching efficiency of LysDNP is a result of hydrophobic interactions between this quencher and the polymer surface that are stronger than those possible with the labeled protein derivative, which is partially solubilized by other charged and hydrophilic amino-acid side chains. Finally, it is interesting to note that in all cases the microspheres coated with two layer pairs show larger K_{SV} values than those coated with one layer pair. This result is surprising given the energy-transfer layer effects described in Figure 3.12 may reflect a different energy-transfer mechanism or stronger quencher-surface binding in thicker films.

Conclusions

A carboxylate-functionalized PPE suitable for use in layer-by-layer deposition has been synthesized and used with the non-conjugated polycation PDAC to create PPE films on glass slides and silica microspheres. These films show excellent spectral properties and are capable of transferring excitation energy to polycationic dye-labeled acceptors adsorbed to the film surface. In addition, PPE-coated microspheres have been used for the detection of water-soluble

quenchers in solution and show quenching enhancements of up to 200-fold *versus* water-soluble PPEs in solution.

Experimental

Synthesis of polymer 1. Diethynylpentiptycene (Nomadics Life Sciences Inc.) (75 mg, 0.154 mmol), 2,5-bis(9-carboxy-3,6-dioxaoctyloxy)-1,4-diiodobenzene (see Chapter 2) (105 mg, 0.154 mmol) $Pd(PPh_3)_4$ and CuI (catalytic amounts) were dissolved in a degassed mixture of 50% NMP, 40% toluene and 10% DIPA and stirred at 60° overnight under argon. After cooling to room temperature, the polymer was precipitated into EtOAc, collected by centrifugation and washed several times with EtOAc yielding 100 mg (72%) of a yellow solid **1**. The molecular weight of polymer **1** could not be determined using gel-permeation chromatography. The ^1H NMR spectrum of **1** can be found in the Appendix.

Synthesis of dye-labeled PAH derivatives 2-4. Poly(allylamine hydrochloride) (Alfa-Aesar, M_n 70,000) and the succinimide esters of the 5(6)-carboxy derivatives of fluorescein (Molecular Probes, for **2**), tetramethylrhodamine (Sigma, for **3**) or carboxy-X-rhodamine (Molecular Probes, for **4**) were combined in a 415:1 molar ratio (based on amine equivalents in PAH) in *ca.* 10 ml of a solution of 10% EtOH in pH 8.3 borate buffer. The reaction mixtures were stirred overnight in the dark and then transferred to dialysis tubing (Pierce SnakeSkin, 10,000 MWCO) and dialyzed exhaustively against deionized water for a minimum of two days. Solutions were stored in the dark before use.

Layer-by-layer deposition. Glass microscope slides were generally cleaned by soaking in concentrated HNO_3 for at least 1 hr before use, followed by rinsing with deionized water and ethanol. In some cases the acid cleaning step was replaced by vigorous sonication with a detergent solution followed by sonication in absolute ethanol. Slides were soaked in 3 N KOH before the deposition of the first layer. LBL films were built up by alternating immersion of the glass slides for a minimum of 10 minutes into solutions of 1-2 wt% PDAC (Dajac Laboratories) in deionized H_2O and saturated solutions of **1** in DMF (filtered before use). Slides were washed with the copious quantities of the immersion solvent followed by ethanol after each immersion and were air-dried.

Silica microspheres were obtained from Bangs Labs and shaken with 3 N KOH for a minimum of 20 minutes before deposition of the first layer. Excess KOH solution was removed by centrifugation of the microspheres, removal of the supernatant, and vigorous shaking with fresh deionized water. This process was repeated as necessary until the washings reached neutral pH. Polymer solutions were added to microsphere suspensions while ultrasonicating, and ultrasonication or vigorous shaking was continued throughout the adsorption process. Excess polymer solution was removed by the process described above and microspheres were washed several times between immersions. Microspheres were stored under a DMF supernatant before use and could be re-suspended by vigorous shaking or ultrasonication.

Microsphere characterization. Confocal micrographs were obtained using a Leica Microsystems confocal laser scanning microscope with excitation from a laser line at 364 nm. Care was taken to avoid prolonged exposure of microspheres to the UV laser light to minimize photobleaching. Microsphere spectra were obtained using the software provided as a histogram

from 5-nm intensity 'bins'. Scanning electron micrographs were acquired by Jessica Liao at the SEM facility of the MIT Institute for Soldier Nanotechnologies.

Fluorescence measurements. Fluorescence spectra for films on glass slides and microsphere suspensions were obtained on Spex Fluorolog 2 and 3 fluorimeters. Spectra of suspended microspheres were obtained in quartz cuvettes in the right-angle detection mode. Microsphere suspensions were magnetically stirred during fluorescence experiments to prevent sedimentation. Quenchers were obtained from Aldrich (4-nitrobenzylamine HCl) or Sigma (LysDNP and BSA-DNP) and used without further purification. For Stern-Volmer quenching experiments, quenchers were added as concentrated solutions to minimize intensity effects from dilution (under 0.5%). Polymer films on glass slides were allowed to air-dry before acquiring spectra. All spectra from flat substrates were obtained in the front-face detection mode.

References

(1) Levitsky, I. A.; Kim, J.; Swager, T. M. *J. Am. Chem. Soc.* **1999,** *121,* 1466.

(2) Levitsky, I. A.; Kim, J.; Swager, T. M. *Macromolecules* **2001,** *34,* 2315.

(3) For a brief review of one prominent group's contributions, see Lefèvre-Seguin, V. *Opt. Mater.* **1999,** *11,* 153.

(4) For example, see (a) Fujiwara, H.; Sasaki, K. *J. Appl. Phys.* **1999,** *86,* 2385. (b) Arai, Y.; Yano, T.; Shibata, S. *Appl. Phys. Lett.* **2003,** *82,* 3173.

(5) Decher has reviewed the basic concepts of LBL deposition and early work in the area. Decher, G. *Science* **1997,** *277,* 1232.

(6) *Handbook of Polyelectrolytes and their Applications;* Tripathy, S. K.; Kumar, J.; Nalwa, H. S.; Eds.; American Scientific Publishers: Stevenson Ranch, Calif., 2002.

(7) Lee, S.-H.; Kumar, J.; Tripathy, S. K. *Langmuir* **2000,** *16,* 10482.

(8) Constantine, C. A.; Gattás-Asfura, K. M.; Mello, S. V.; Crespo, G.; Rastogi, V.; Cheng, T.-C.; DeFrank, J. J.; Leblanc, R. M. *Langmuir* **2003,** *19,* 9863.

(9) Baur, J. W.; Rubner, M. F.; Reynolds, J. R.; Kim, S. *Langmuir* **1999,** *15,* 6460.

(10) Richter, B.; Kirstein, S. *J. Chem. Phys.* **1999,** *111,* 5191.

(11) Pinto, M. R.; Kristal, B. M.; Schanze, K. S. *Langmuir* **2003,** *19,* 6523.

(12) Thünemann, A. F.; Ruppelt, D. *Langmuir* **2001,** *17,* 5098.

(13) McQuade, D. T.; Hegedus, A. H.; Swager, T. M. *J. Am. Chem. Soc.* **2000,** *122,* 12389.

(14) Yang, J.-S.; Swager, T. M. *J. Am. Chem. Soc.* **1998,** *120,* 11864.

Chapter 4

Synthesis and properties of calix[4]arene-substituted poly(phenylene ethynylene)s

Introduction

The research described in this chapter concerns the synthesis and properties of new calix[4]arene-based poly(phenylene ethynylene)s. Because of the somewhat unusual nature of calixarenes, this chapter begins with a primer on the structure and basic properties of calixarenes, followed by more detailed discussions concerning particular aspects of calixarene chemistry relevant to this research — the use of the calix[4]arene skeleton as an organizing element for crown ethers and the complexation of organic cations within the calix[4]arene basket. For reasons of brevity, only those aspects of calix[4]arene chemistry that are immediately relevant to the work presented in this chapter are discussed. Readers interested in learning more about calixarenes are referred to the monographs by Gutsche[1,2] and to the review compilations edited by Mandolini and Ungaro[3] and Asfari[4] for more information.

Synthesis and general properties of calixarenes

Calixarenes are broadly defined as a class of cyclophane-like macrocycles consisting of a series of aromatic rings *meta*-linked by methylene bridging groups. Synthesized by the base-catalyzed condensation of substituted phenols with formaldehyde, the calixarene family features a surprising degree of structural diversity.

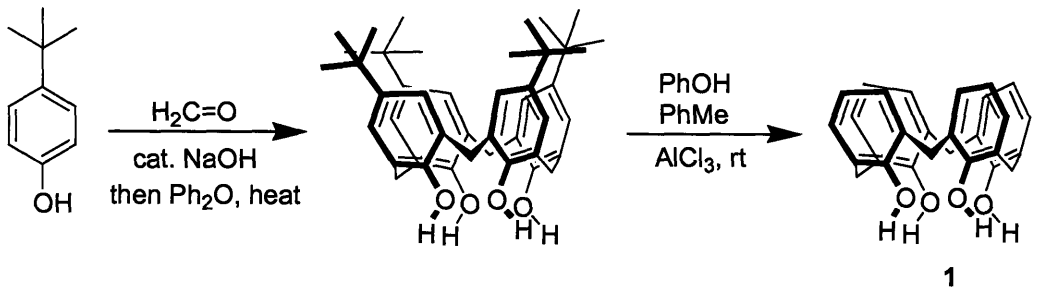

Scheme 4.1. Synthesis of calix[4]arene (**1**) *via* the *p-tert*-butyl derivative.

Calixarenes can come in a variety of different sizes based on the number of component aromatic rings in the macrocycle and are named accordingly — for example, the molecule shown in Figure 5.1 is known as calix[4]arene due to the presence of four aromatic rings in the overall structure. Theoretically, any calix[*n*]arene with $n \geq 4$ can be prepared, but those in which *n* is 4, 6 or 8 are easiest to synthesize and are most commonly used in literature applications. The simplest route to these molecules involves the preparation of their *p-tert*-butyl derivatives using *p-tert*-butylphenol and formaldehyde. The precise conditions of solvent, reaction temperature and (especially) the nature and concentration of the alkali metal hydroxide used in the reaction determine the size of the resulting macrocycle. Unsubstituted calix[*n*]arenes can be obtained from the *p-tert*-butyl derivatives using an $AlCl_3$-mediated Friedel-Crafts-like de-alkylation procedure.[5] In the late 1980s the group of Gutsche, which had been involved in much of the systematic investigation into the structural and chemical properties of calixarenes, published methods for high-yielding syntheses of the n = 4, 6 and 8 *p-tert*-butylcalix[n]arenes that could easily provide hundred-gram quantities of these compounds in one-pot procedures.[6,7] Although the general structure of the calixarenes had been known since the 1940s, the publication of these procedures roughly corresponded with an increase in the number of calixarene-related research articles appearing in the literature. As Mandolini and Ungaro[3] point out, access to these

simplified methods for calixarene synthesis also coincided with the surge of interest in supramolecular chemistry caused by the awarding of the 1987 Nobel Prize in Chemistry for work in this area.

The primary attraction of calixarenes in supramolecular chemistry lies in their basket-like shape and the presence of two distinct 'rims' defining this basket — an 'upper rim' comprising the edges of the aromatic rings making up the calixarene skeleton, and a 'lower rim' made up of the phenolic OH groups. Early research in this area also recognized the presence of multiple conformational isomers arising from flipping motions involving individual rings within the calixarene system. Higher calixarenes can possess a large number of distinct conformations, but in the parent calix[4]arene molecule these motions give rise to four possible isomers (Scheme 4.2).

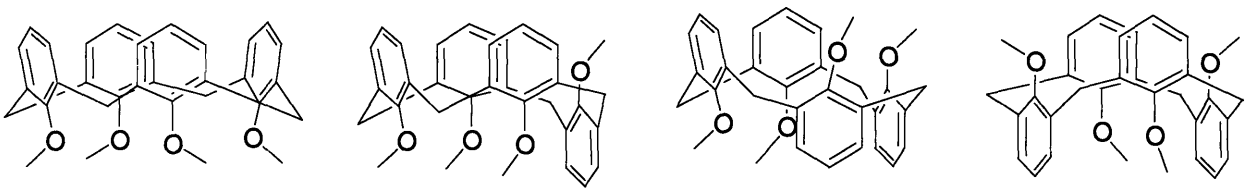

Scheme 4.2. The four possible conformations of the calix[4]arene skeleton, shown for the tetramethyl ether. Abbreviations are shown in parentheses.

It has been generally concluded that the mechanism of calix[4]arene conformational interconversion involves the motion of the phenolic end of one of the aromatic units through the center of the macrocycle cavity.[1] Modification of the phenolic OH groups on the aromatic rings with carbon-based substituents (such as the methyl ether groups shown in Scheme 4.2) changes

the barrier for conformational interconversion, with substituents larger than ethyl completely preventing the interconversion of isomers. In addition to these steric factors, hydrogen bonding throughout the lower rim plays a significant role in restricting the conformational mobility of the calix[4]arene skeleton.

It is notoriously difficult to predict the conformational outcome of a reaction that converts a flexible calix[4]arene derivative into one with a locked conformation. No hard and fast rules exist for determining the distribution of conformational isomers arising from such reactions, although some general trends exist.[8,9] In the case of the synthesis of lower-rim ether derivatives of calix[4]arene, the nature of the alkylating agent (tosylates or halides), base (carbonates, hydrides, alkoxides, alkyllithiums), solvent (THF, DMF, MeCN, acetone) and upper-rim substituents (hydrogens, *tert*-butyl groups, other substituents) all play significant roles. For example, while the reaction of unmodified calix[4]arene with excess 1-iodopropane gives exclusively the *cone* conformation of tetrapropoxycalix[4]arene with the NaH / DMF base-solvent combination, a mixture of *cone* and *paco* is obtained when a 9:1 THF:DMF mixture is used. When the alkylation is carried out using propyl tosylate and Cs_2CO_3 in MeCN, a mixture of conformations is obtained from which large quantities of the *1,3-alt* conformation can be isolated. These conformational outcomes have been explained as arising from a combination of steric effects, metal-ion templation, hydrogen bonding, and cation-π interactions. While some classes of calix[4]arene lower-rim derivatization reactions are 'reliable' in their conformational outcomes — for example, the use of alkyl halides with NaH as a base in DMF seems to always provide *cone* products — it remains difficult to predict *a priori* what the outcome of a given derivatization reaction will be in more complex cases or when the calixarene scaffold is already partially derivatized.

The task of identifying calix[4]arene conformations experimentally is facilitated by the unique NMR signatures characteristic of each conformation. These signatures differ most in the number and nature of the peaks arising from hydrogen atoms attached to the methylene 'hinge' carbons. In the case of the *cone* conformation, the two hydrogens on each methylene carbon are inequivalent (one points away from the macrocyle while the other points roughly parallel to its axis), differ in their ^{1}H NMR chemical shift by about 1 ppm, and couple to each other strongly, providing a classic 'AB quartet'-type pattern. In the *1,3-alt* conformation, which is much more flexible and higher in symmetry, these two hydrogens become equivalent and a singlet is seen. The *paco* form is much lower in symmetry than either of these conformations and the presence of multiple inequivalent aromatic rings leads to highly complex NMR spectra. Further characterization difficulties can arise in cases where a mixture of conformations is present. For example, the *1,3-alt* and *cone* conformations of tetrapropoxycalix[4]arene can be separated by column chromatography only with great difficulty.

Calixarene-based ionophores

While the most obvious structural feature of the calix[4]arene skeleton is the basket-like shape of its inner cavity, many promising molecular recognition applications of these molecules have resulted not from exploitation of this cavity but from the use of the calix[4]arene framework to pre-organize ligands or receptor groups in desired geometries. The availability of the geometrically well-defined and (more-or-less) accessible conformations already mentioned, the presence of the two chemically distinct 'rims', and the development of procedures for regioselective calixarene modification all faciliate these applications, and these synthetic possibilities have allowed the preparation of a wide variety of calixarene-based ionophores. One

of the most popular derivatization strategies for the synthesis of ligands for small ions involves the modification of the calixarene lower rim with amide or ester linkages, as shown in Scheme 4.3.

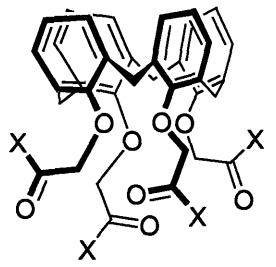

Scheme 4.3. A common motif for calix[4]arene-based ionophores. X = OH, OR, or NR_2.

In these cases, the calixarene is fixed in the *cone* conformation and interaction with the metal ion takes place through the ether and carbonyl oxygens on the lower rim. Systems such as the one shown in Scheme 4.3 are generally excellent Na^+ binders and have been used in a variety of sensory schemes.[10]

The incorporation of ionophoric crown ether groups into calixarenes was pioneered by the group of Ungaro.[11] In contrast to the systems described above, these 'calixcrowns' show a preference for larger alkali metal cations, and some derivatives are remarkably efficient ligands for Cs^+ and even Fr^+.[12] Much of the research in this area has been motivated by the need for ligands that selectively extract heavier alkali metal cations from solutions containing Na^+. This application is of special importance in the treatment of aqueous nuclear waste containing mixtures of radioactive ^{137}Cs and non-radioactive Na isotopes.

As in the case of simple crown ethers, interactions between metal ions and the oxygen atoms of singly-bridged calixcrowns are important in guest binding, and the size of the crown ether ring is a key factor in determining the selectivity of the calixcrown toward various ions.

However, the presence of multiple aromatic units in the calixarene moiety introduces an additional consideration for metal binding that often leads to unusual selectivity. When the substituents on the non-bridged rings are suitably chosen, the interactions between these aromatic rings and metal ion guests can lead to interesting conformational effects. For example, the two closely related calixcrowns shown in Scheme 4.4 each undergo a different conformational interconversion on binding K^+.[13]

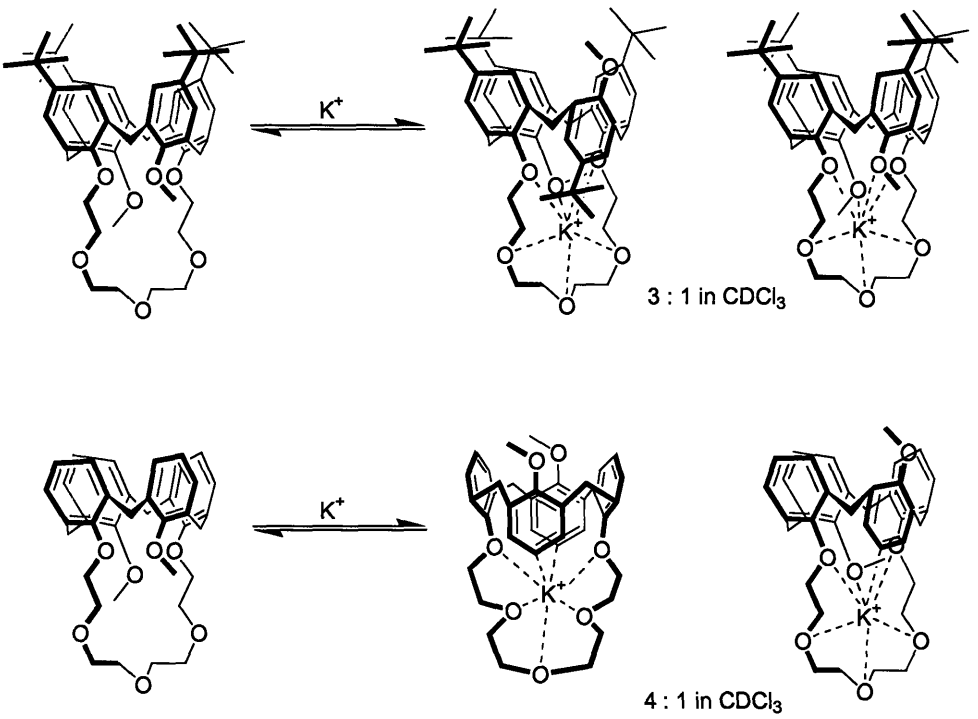

Scheme 4.4. Conformational interconversions on binding K^+ for two calixcrown[4] derivatives. The *paco* isomer is preferred for the *tert*-butyl deriavtive, while the de-*tert*-butylated version shows a strong preference for the *1,3-alt* conformation.

While they appear somewhat random at first glance, the outcomes shown in Scheme 4.4 can be explained as arising from a combination of steric and cation-π interactions,[14] of which the latter prove to be especially potent in these systems.[15] In the case of the *tert*-butyl derivative, a cation-π interaction stabilizes the *paco* conformation, while the smaller steric hindrance of the de-*tert*-

butylated derivative allows the interaction of both mobile aromatic edges with the metal cation. The presence of these interactions has been further confirmed using X-ray crystallography.

In the structures shown in Scheme 4.4, the conformational mobility provided by the presence of two methyl-substituted rings allows the calixcrown ligand to adopt the conformations most conducive to ion binding. Ungaro and co-workers synthesized calixcrown derivatives locked in the *cone, paco* and *1,3-alt* conformations by substitution of the rings not forming part of the crown ether chain with bulky isopropyl groups. Using these fixed conformational isomers, they determined that, in general, the *paco* and *1,3-alt* conformations are excellent ligands for the larger alkali metal ions (K^+ and larger), with a *paco* calixcrown[5] derivative showing a K^+/Na^+ binding constant ratio of over 10^5. In a similar vein, locked *1,3-alt* conformations of calixcrowns have proven to be efficient ligands for Cs^+.[13,16]

Part of the research described in this chapter involves the synthesis of calixarene-modified PPEs in which the PPE backbone is connected to the calixarene through a direct calixcrown linkage containing a PPE monomer unit. A small number of calixcrown derivatives have been reported in which the crown ether portion of the molecule contains embedded benzene rings (Scheme 4.5).[17] These derivatives, all of which are of the bis-crown variety (conformationally-locked *1,3-alt* isomers containing two crown ether bridges), were studied for their ability to transport $^{137}Cs^+$ across a supported liquid membrane. The incorporation of *ortho*-linked aromatic rings into the crown ether had beneficial effects on ion binding and particularly on Cs^+/Na^+ selectivity ratios, a phenomenon attributed to the inability of the rigidified crown ether portion to re-organize around the Na^+ ion. Cs^+ binding in the *para*-linked version was about three orders of magnitude weaker than in the *ortho*-linked version.

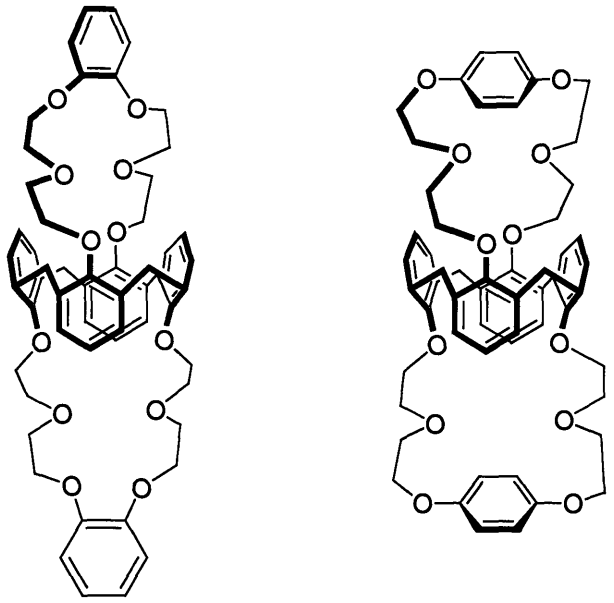

Scheme 4.5. Calixarene-bis(crown) ethers containing aromatic rings embedded in the crown ether portion of the molecule *via ortho* (left) or *para* (right) linkages. Both molecules are locked in the *1,3-alt* conformation. The *ortho* derivative is a much stronger Cs^+ binder than the *para* derivative.

Within the Swager group, former postdoc Khushrav Crawford and graduate student Marc Goldfinger prepared calixarene-based conjugated polymers containing a bithiophene-linked calixcrown unit.[18] These polymers were found to undergo Na^+-specific emission changes which were attributed to the confomational rigidification of the bithiophene moiety. No fluorescence changes were observed for K^+, Li^+ or Ca^{2+}.

Complexation of organic salts inside the calix[4]arene cavity

The prospect of using the basket-like cavity of calix[4]arenes for the complexation of organic molecules is immediately suggested by the structure of the molecules themselves. Most efforts in this area have been directed at developing systems that bind either neutral molecules or organic ions within the calixarene cavity. Calixarene complexes with neutral molecules are somewhat rare and are generally weak, although the well-known strong complexation of C_{60} by calix[8]arenes is a notable exception.[19] In contrast, many organic cations, especially modified

ammonium and pyridinium derivatives, are known to bind within the calixarene cavity.[20] The driving force for this binding interaction is generally explained as a co-operative effect of multiple cation-π interactions between the aromatic units of the calixarene and the ion itself. In addition, much of the early work in this area used water-soluble calixarenes bearing negatively charged groups (sulfonates or phenoxides), introducing significant electrostatic and hydrophobic binding forces.

As in the case of the calixcrowns, steric factors also play a role in the binding of analytes in the calixarene cavity, and many of the most interesting organic cation-binding calixarene systems are derived from the larger calix[*n*]arenes ($n \geq 5$). Depending on the pattern of lower-rim substitution, such molecules can bind organic cations such as acetylcholine with binding constants on the order of 10^2-10^3.[20] In contrast, no evidence has been observed for the complexation of trimethylalkylammonium cations by calix[4]arenes locked in the *cone* conformation. Additionally, the presence of bulky substituents at the upper rim has been found to have a deleterious effect on analyte binding in these systems.

Relative to organic ammonium derivatives, *N*-methylpyridinium salts are better guests for calix[4]arenes, though binding constants are small – around 5-7 M^{-1} for *N*-methylpyridinium iodide with *cone* tetraalkoxycalix[4]arenes in $CDCl_3$-CD_3CN mixtures.[21] Rigidification of the *cone* structure by the elimination of "pinching" motions increases these binding constants, as does the use of calix[4]arene 'capsules' formed by linking two calix[4]arene units *via* their upper rims (Scheme 4.6).[22]

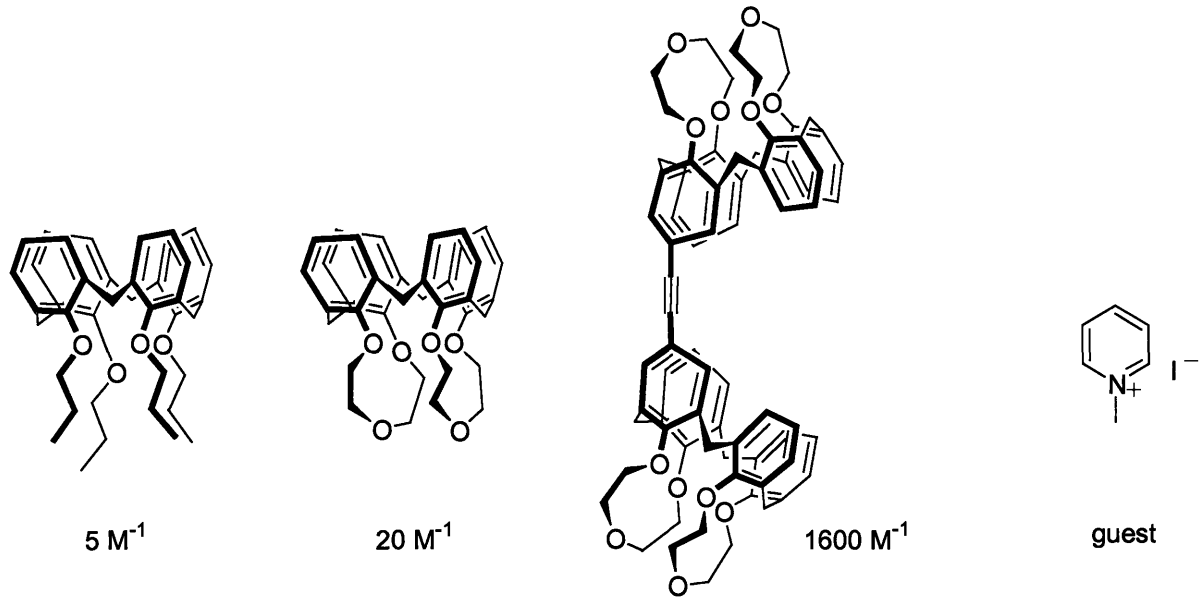

Scheme 4.6. Approximate binding constants for calix[4]arenes in the *cone* conformation with *N*-methylpyridinium iodide in $CDCl_3$-CD_3CN mixtures. Both rigidification of the calixarene conformation (through the formation of 1,2 ring bridges) and capsule formation (using a calixarene-calixarene bridge) have dramatic effects on the binding constant.

Araki *et al.* have studied the interaction of *cone* tetrapropoxycalix[4]arene with various *N*-methylpyridinium iodide salts and with *N*-methylquinolinium iodide.[23] Their observations confirm the expected steric limitations on guest binding, in that the introduction of extra methyl groups onto the pyridinium core results in a reduction in K_a and that the formation of a double-calixarene 'capsule' results in even greater binding selectivity. The bulkier *N*-methylquinolinium iodide was found to bind to the *cone* calix[4]arene with a K_a of 3.6 ± 1.3 and was not bound at all by a doubly linked calix[4]arene capsule.

The goal of the research described in this chapter was to apply some of the guest-binding properties of calix[4]arene receptors to the design of new PPE-based sensors. Two calixcrown-based monomers were designed in order to provide PPEs in which the polymer backbone is intimately associated with the calixcrown cavity. The crystal structures of these monomers were determined and show interesting structural features. A PPE prepared from one of these

monomers showed a small spectral response to Ba^{2+}. In addition, an upper-rim-linked, *cone*-locked monomer was designed in which the PPE backbone is forced to pass alongside the opening of the basket-like *cone* calix[4]arene cavity. A PPE formed from this monomer is strongly quenched by the analyte *N*-methylquinolinium hexafluorophosphate.

Results and Discussion

Synthesis and structural characterization of calixarene-based monomers

Calix[4]arene-crown ether monomers were synthesized as shown in Scheme 4.7.

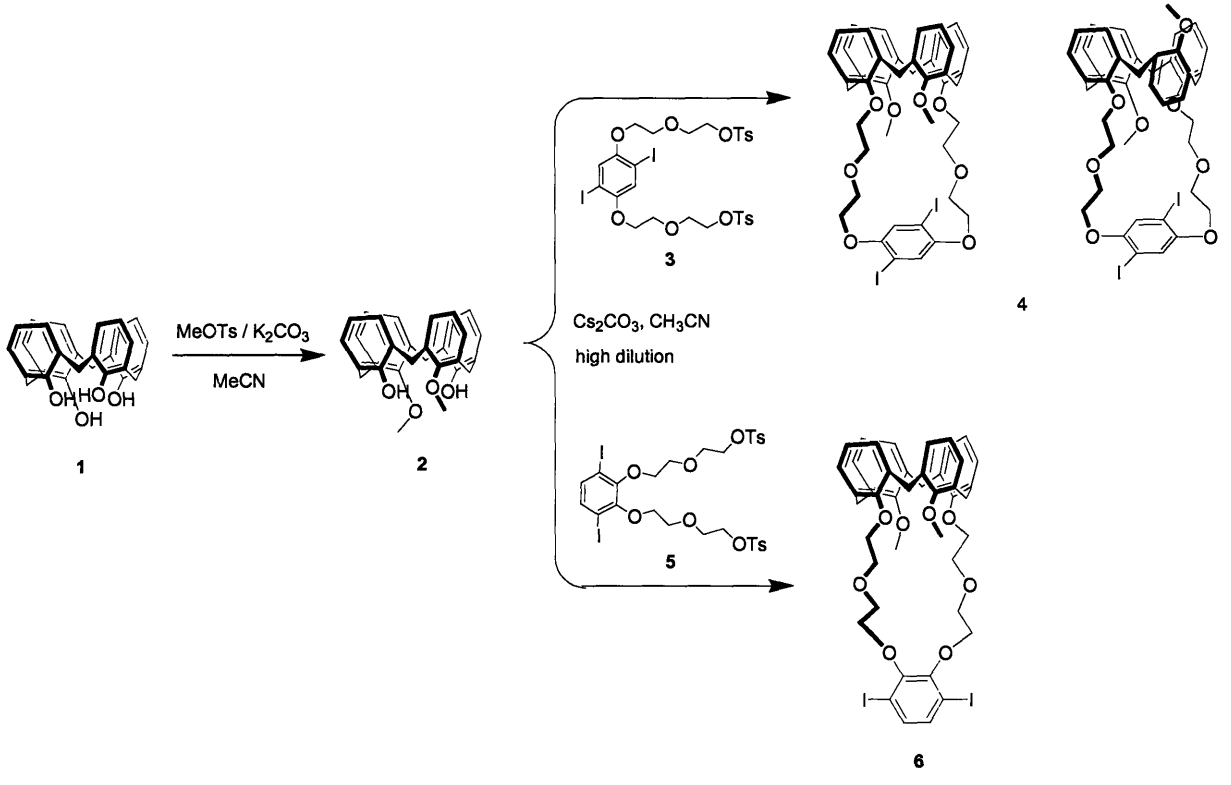

Scheme 4.7. Synthesis of calixcrown monomers **4** and **6.**

Following a well-known literature route, reaction of the unmodified calix[4]arene **1** with two equivalents of methyl tosylate in MeCN using K_2CO_3 as a base provided the 1,3-ring

disubstituted calix[4]arene dimethyl ether.[24] This derivative has a sharp ^{1}H NMR spectrum, clearly indicating the presence of a rigid *cone* isomer stabilized by intramolecular hydrogen bonding around the lower rim of the calixarene. Reaction of **2** with the ditosylate **3**[25] under high-dilution conditions provided a product that eluted as one compound in column chromatography and HPLC. The ^{1}H NMR spectrum of the product mixture was highly complex, suggesting the presence of multiple calixarene conformations, and a variable-temperature NMR study did not show any significant changes in the spectrum of the product mixture between –10° and 50°. High-resolution mass spectral analysis of the product mixture indicated the presence of one compound consistent with the desired molecular formula $C_{44}H_{44}I_2O_8$. These observations suggested that two or more non-interconverting conformations were present, and the complexity of the ^{1}H NMR spectrum strongly implied the presence of a highly asymmetric *paco* isomer. To obtain a more definitive structural assignment, crystals suitable for X-ray crystal structure determination were grown by slow evaporation of a CH_2Cl_2/MeOH solution of the product. The structure of **4** revealed that this compound crystallizes somewhat unusually as a mixture of *paco* and *cone* conformations, resulting in a crystal consisting of *paco* and *cone* conformations at a 3:1 ratio. Structures of these isomers are shown in Figures 4.1 and 4.2.

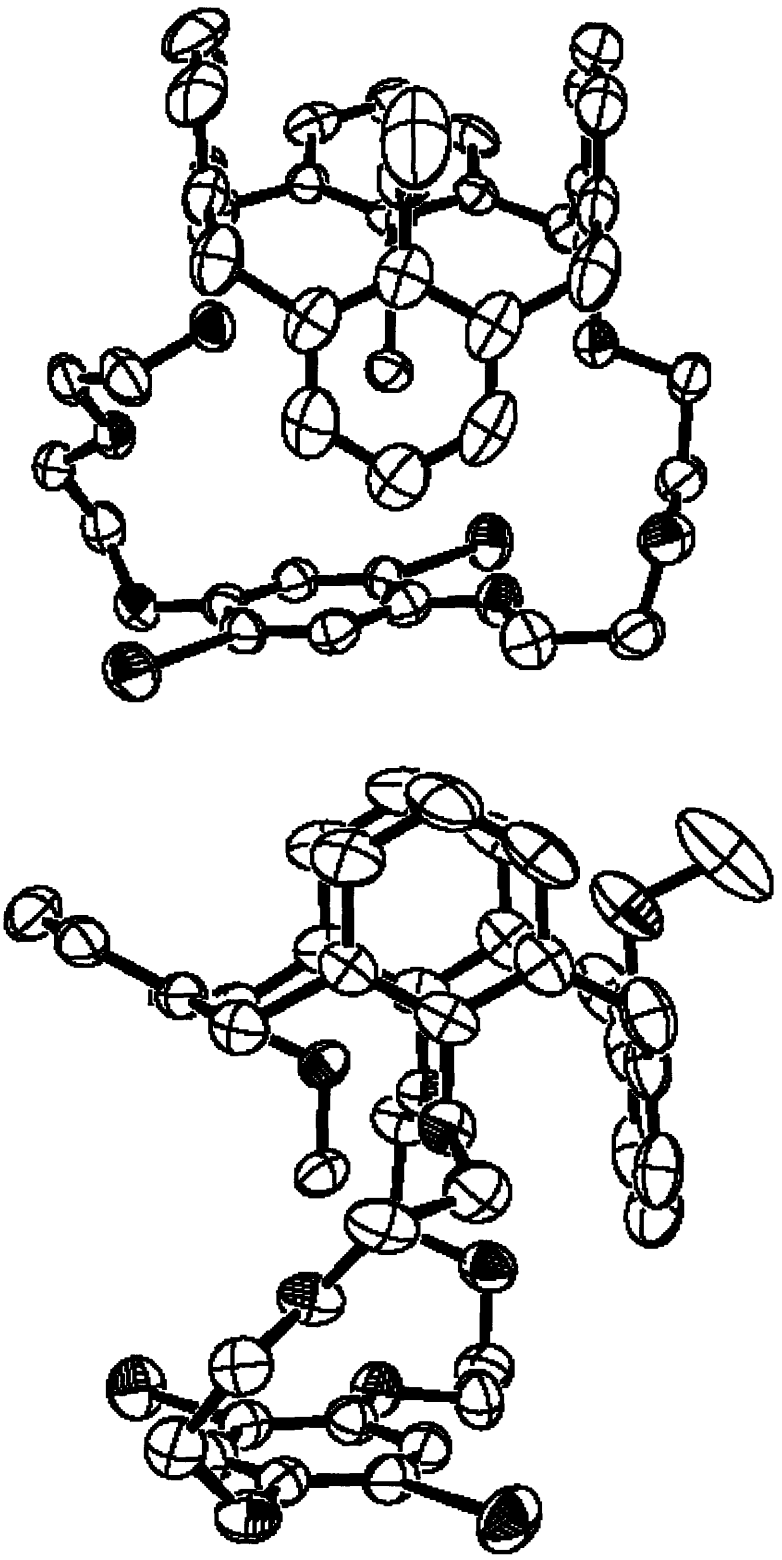

Figure 4.1. Crystal structure of the *paco* isomer of **4** from two orthogonal side views. One molecule of the asymmetric unit is shown. Ellipsoids are drawn at 50% probability.

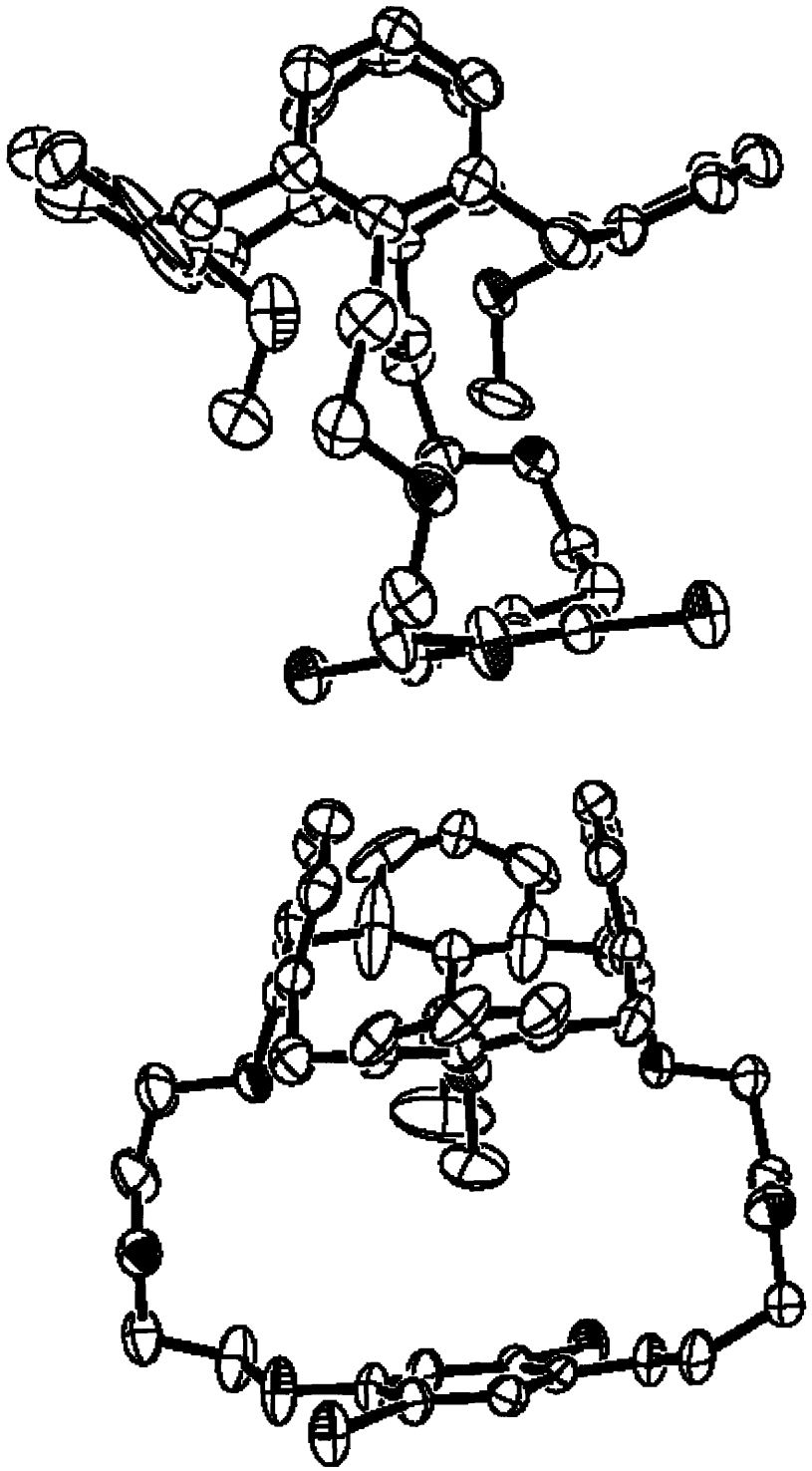

Figure 4.2. Crystal structure of the *cone* isomer of **4** from two orthogonal side views. One molecule of the asymmetric unit is shown. Ellipsoids are drawn at 50% probability.

The structure of the *paco* isomer of **4** (Figure 4.1) shows the classic features of this conformation. The three 'upright' or *syn* rings roughly define the sides of a pinched partial cone in which the aromatic rings attached to the crown ether moiety are nearly parallel to each other and sharply angled relative to the *syn* methoxy-bearing ring. The 'inverted' or *anti* methoxy-bearing ring is almost perpendicular to the crown-ether-bearing rings and directs the *anti* methoxy group sharply away from the partial-cone cavity, while the diiodophenylene unit is oriented approximately perpendicular to the axis of the cavity. In contrast, the structure of the *cone* isomer (Figure 4.2) represents a highly distorted pinched cone in which the crown-ether-bearing rings are actually tilted toward one another. Removal of the methoxy groups of **4** using Me_3SI in $CHCl_3$ provided a product **4'** in which only the *cone* conformation could be detected (see Appendix). This suggests that the abundance of the *paco* isomer in **4** may be due to steric repulsion between the *para*-linked diiodophenylene unit and methyl ether groups.

Reaction of the dimethyl ether **2** with the ditosylate **5**, prepared in two steps from 2,5-diiodocatechol, provided the calix[4]arene monomer **6** by an analogous procedure. In contrast to **4**, the ^1H NMR spectrum of **6** features a series of somewhat broad peaks consistent with a flexible *cone* conformation. Confirmation of the *cone* structure of **6** was provided by X-ray single crystal analysis (Figure 4.3).

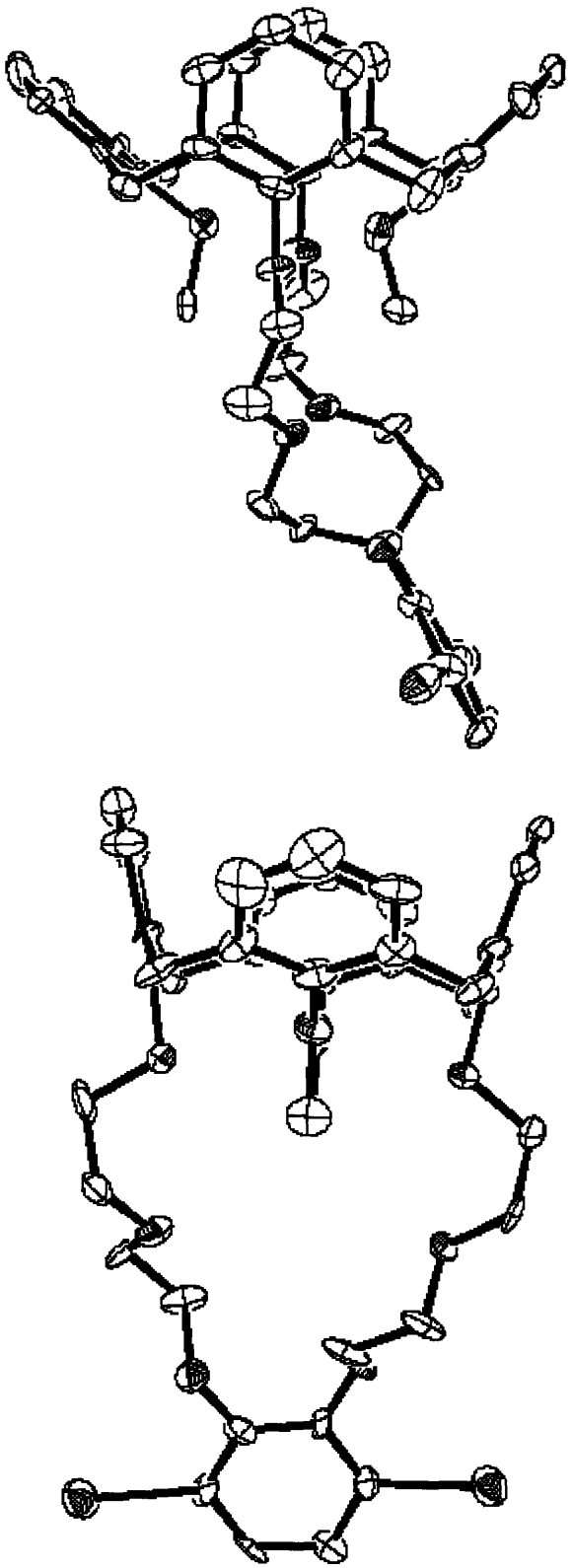

Figure 4.3. Crystal structure of **6** from two orthogonal side views. One molecule of the asymmetric unit is shown. Ellipsoids are drawn at 50% probability.

The structure of **6** is that of a standard pinched-*cone* calixarene, with the crown-ether-bearing rings oriented parallel to one another and the methoxy-bearing rings angled strongly away. The crown ether linker suspends the diiodophenylene group at an oblique angle below the calixarene and at a much larger calixarene-diiodophenylene distance than seen in either of the conformations of **4**. This is a predictable consequence of the differences in connectivity between the diiodophenylene units of **4** and **6** and suggests that PPEs based on **4** will have a smaller calixarene-backbone distance than those based on **6**. In addition, the structures support the prediction that the calixcrown ionophore in polymers based on **4** will be much less accessible than that in those based on **6.**

Synthesis of a basket-like calix[4]arene-based monomer locked in the *cone* conformation was carried out according to the sequence shown in Scheme 4.8.

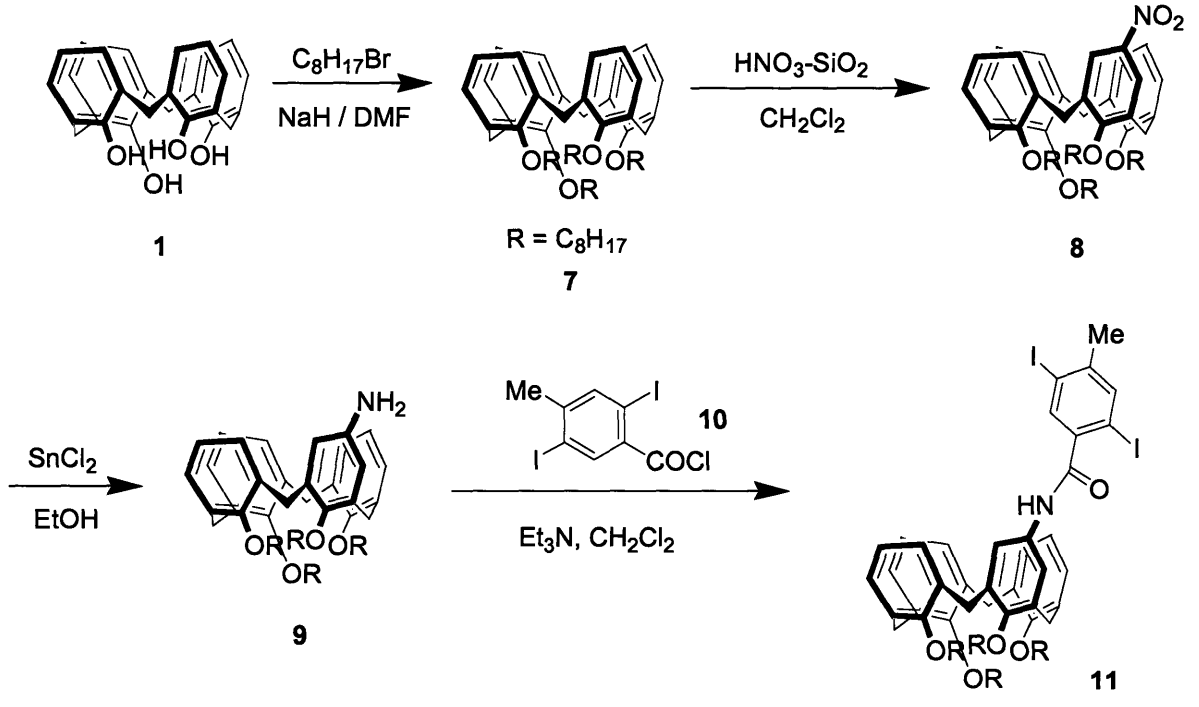

Scheme 4.8. Synthesis of monomer **11.**

Treatment of the parent calix[4]arene **1** with 1-bromooctane in DMF using NaH as a base provided the tetraoctyl ether **7**[26] in the *cone* conformation. The use of silica-supported HNO_3 allowed for mild nitration[27] of **7**, which was monitored by TLC and quenched when the starting material had been completely consumed. The product mixture contained mostly **8** along with small quantities of di- and trinitrocalixarenes, which were easily removed by column chromatography. The NMR spectrum of **8** shows the expected pattern for a calix[4]arene with one *para*-substituted ring, including two overlapping 'AB quartets' in the bridging methylene region. Reduction of **8** using $SnCl_2$ provided the calix-aniline[28] derivative **9**, which was condensed with acid chloride **10**[25] to provide the amide-based monomer **11**.

Synthesis and characterization of calixarene-based PPEs

Monomers **4, 6** and **11** were co-polymerized with 2,5-diethynyl-1,4-bis(hexadecyloxy)benzene in toluene-diisopropylamine mixtures in the standard manner. Polymers **12, 13** and **14** (Scheme 4.9) were isolated by precipitation from MeOH. GPC *versus* polystyrene standards indicated molecular weights on the order of $1\text{-}2\times10^4$. Overall, it was found that monomer purity was essential for the prevention of gel formation during polymerization, especially in the case of **12** and **13**. This gelation process presumably results from cross-linking caused by impurities containing two diiodophenylene units per monomer.

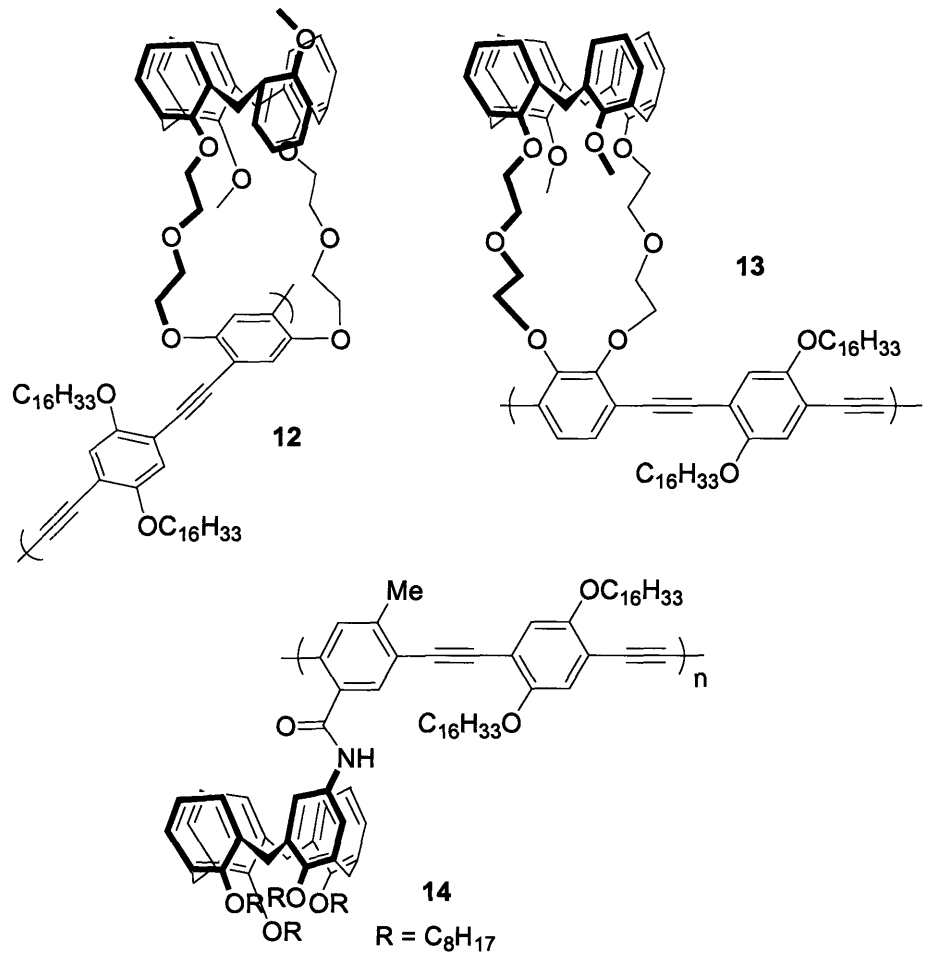

Scheme 4.9. Structures of polymers **12, 13** and **14.**

Spectroscopic response of calixcrown-based PPEs to Ba^{2+} and other analytes

The absorbance and emission spectra of polymers **12** and **13** are shown in Figures 4.4 and 4.5.

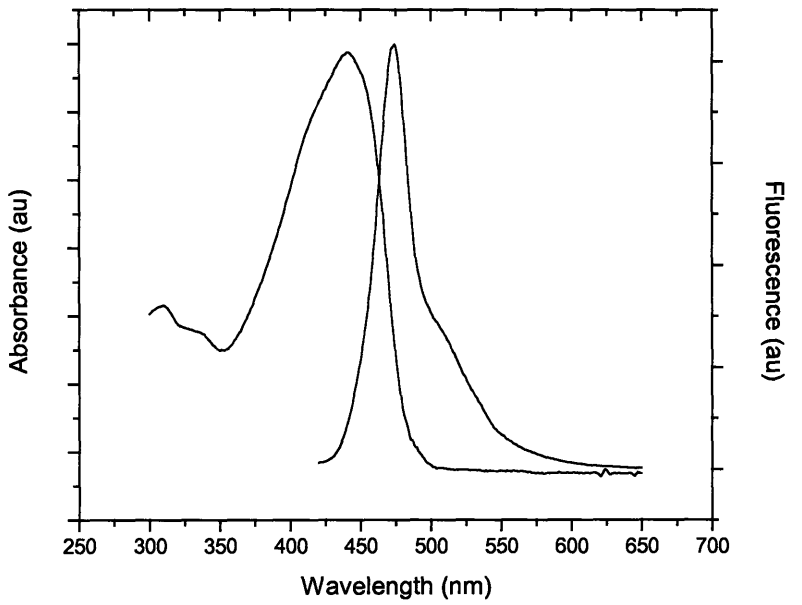

Figure 4.4. Absorbance (left) and fluorescence (right) spectra of polymer **12** in CH_2Cl_2 solution.

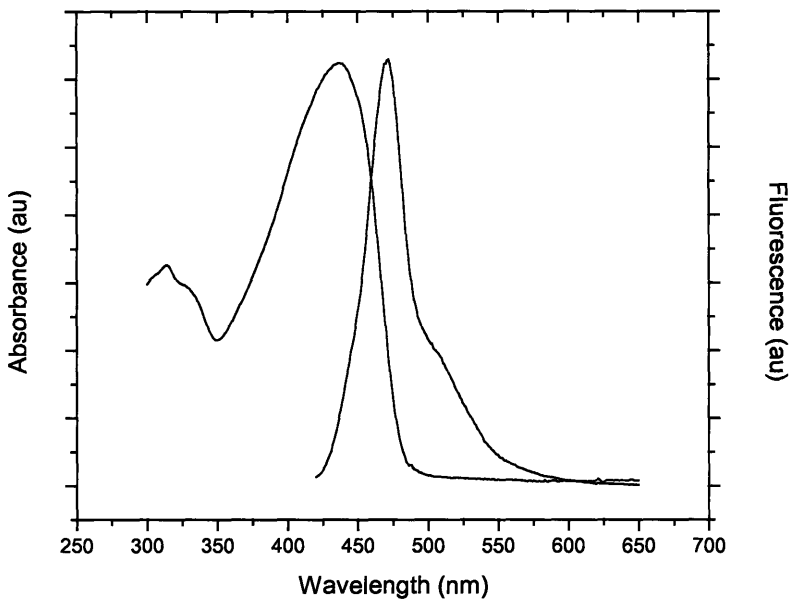

Figure 4.5. Absorbance (left) and fluorescence (right) spectra of polymer **13** in CH_2Cl_2 solution.

Determination of the fluorescence response of these polymers to metal salts is complicated by the insolubility of these salts in 'good' (i.e. non-aggregating) solvents for PPEs. To overcome this problem, we chose to use $Ba(ClO_4)_2$, which is commercially available and highly soluble in MeCN. Small aliquots of a concentrated solution of $Ba(ClO_4)_2$ in MeCN were added to solutions of the PPEs in CH_2Cl_2. As shown in Figure 4.6, **12** showed no response to Ba^{2+} at millimolar concentrations. However, a small decrease in the fluorescence intensity of **13** is observed at small concentrations of Ba^{2+}, with subsequent concentration increases causing no further changes (Figure 4.7).

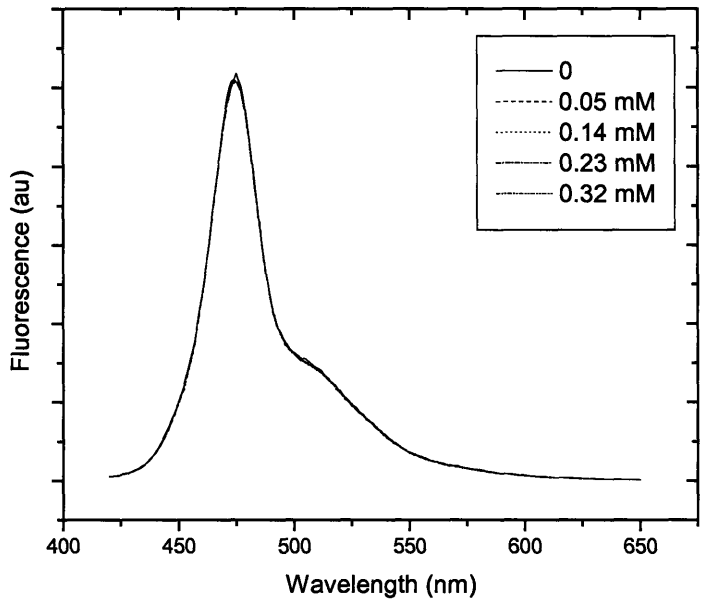

Figure 4.6. Response of polymer **12** to Ba^{2+} in CH_2Cl_2 solution.

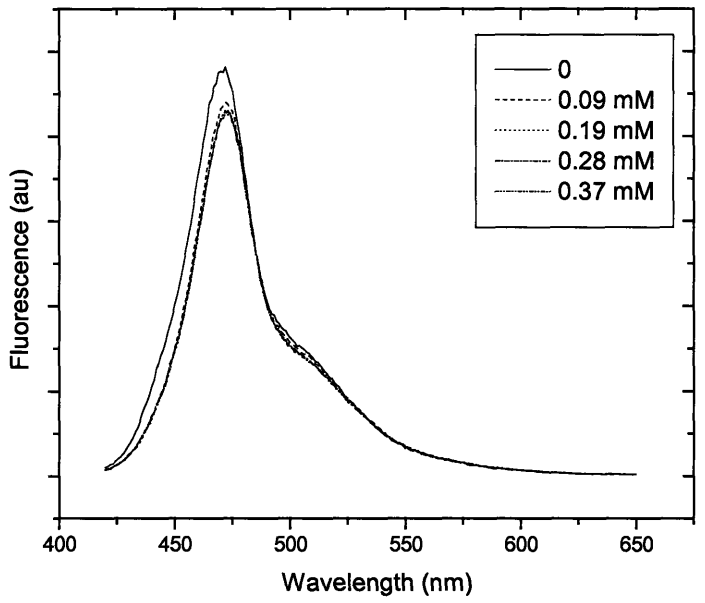

Figure 4.7. Response of polymer **13** to Ba^{2+} in CH_2Cl_2 solution.

The behavior of these polymers in response to Ba^{2+} can be explained as arising through a combination of factors. Although there have been no literature reports on the interactions between calixcrowns and Ba^{2+}, former Swager group graduate student Hsiao-hua Yu found that Ba^{2+} exerted a template-like effect on the electropolymerization of a calixcrown-based bithiophene derivative.[29] The ionophoric cavity of **12** seems ideal for a large, fairly soft cation such as Ba^{2+} due to the proximity of the crown ether donors and multiple π electron-donating aromatic rings, but access to the calixcrown ionophore is likely hindered by the steric crowding caused by the connectivity of the *para*-linked phenylene unit. In contrast, the more accessible crown ether moieties of polymer **13** are able to bind Ba^{2+}, and it is plausible that the interaction of this ion with the crown-ether oxygen atoms connected directly to the PPE backbone causes the observed spectral shifts.

Polymer **12** was screened against a variety of nitroaromatic compounds, including some with relatively acidic protons, in order to determine if any abnormally large Stern-Volmer quenching interactions were present. Such large K_{SV} values would be indicative of a static binding interaction between a fluorescence-quenching guest molecule and the PPE, possibly through hydrogen bonding between the guest and the calixcrown moiety (see Chapter 1). The observed K_{SV} values are typical of those observed for PPE quenching by nitroaromatics, and although dinitroaromatics are better overall quenchers than mononitroaromatics, no further trends can be discerned among the data (Table 4.1).

Table 4.1. Stern-Volmer quenching constants for polymer **12** with a variety of analytes.

Analyte	K_{SV}, M^{-1} (solvent)
2,4-dinitrotoluene	29 ± 1 (CH_2Cl_2)
2,6-dinitrotoluene	32 ± 1 (CH_2Cl_2)
4-nitrotoluene	15.0 ± 0.5 (CH_2Cl_2)
2-nitrobenzenesulfonamide	11.2 ± 0.5 (THF)
3-nitrophthalimide	18.2 ± 0.6 (THF)
3,5-dinitrobenzoic acid	24.1 ± 0.9 (CH_2Cl_2)
4-nitrobenzylamine	20 ± 2 (CH_2Cl_2)

Spectroscopic effects of guest binding in basket-like calixarene-PPEs

Polymer **14** possesses a basket-like calix[4]arene cavity locked in the *cone* conformation attached directly to the PPE backbone by means of an amide linkage of limited flexibility. In order to see whether the known organic cation-binding properties of rigid *cone* calixarenes could be applied to the PPE-mediated detection of a photophysically active guest, we elected to use the electron-poor *N*-methylquinolinium (NMQ) ion as a prototypical quencher. This ion contains the same structural features as the known calix[4]arene guest *N*-methylpyridinium, with the added advantage of a more extended aromatic system that should promote larger π-stacking interactions

with the PPE backbone. We chose to use the hexafluorophosphate (PF_6) salt of NMQ to avoid complications from strong charge-transfer interactions between NMQ and most halide ions. The *N*-methylacridinium ion, which might seem to be an even better target analyte for a calixarene-PPE system, has absorbance and emission spectra that strongly overlap with those of **14** and thus preclude its use as a quencher.

To determine the contribution of the host-guest interaction to the fluorescence quenching, polymer **15** was prepared from monomer **16.** This model system was designed to provide an electronic environment identical the one present in polymer **14** (Scheme 4.10).

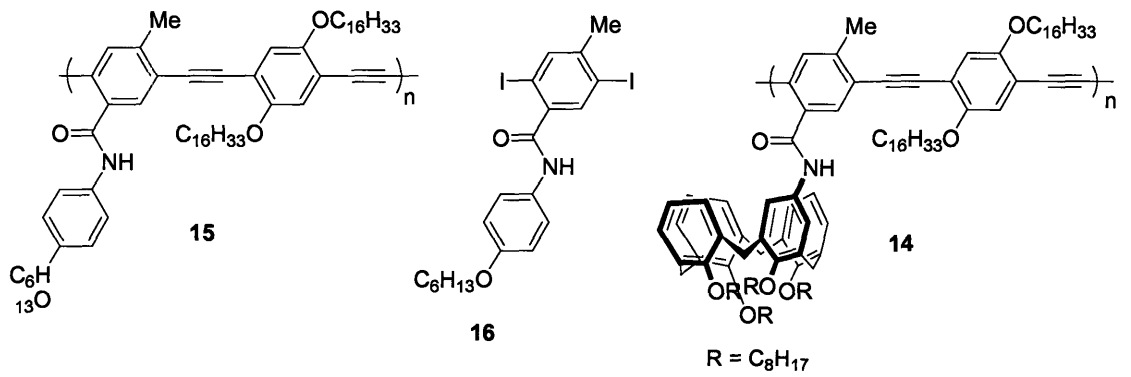

Scheme 4.10. Structures of model polymer **15**, derived from monomer **16**. This monomer unit has an electronic structure analogous to that of the calixarene-based monomer in **14**.

The Stern-Volmer quenching plots for these polymers with NMQ are shown in Figure 4.8.

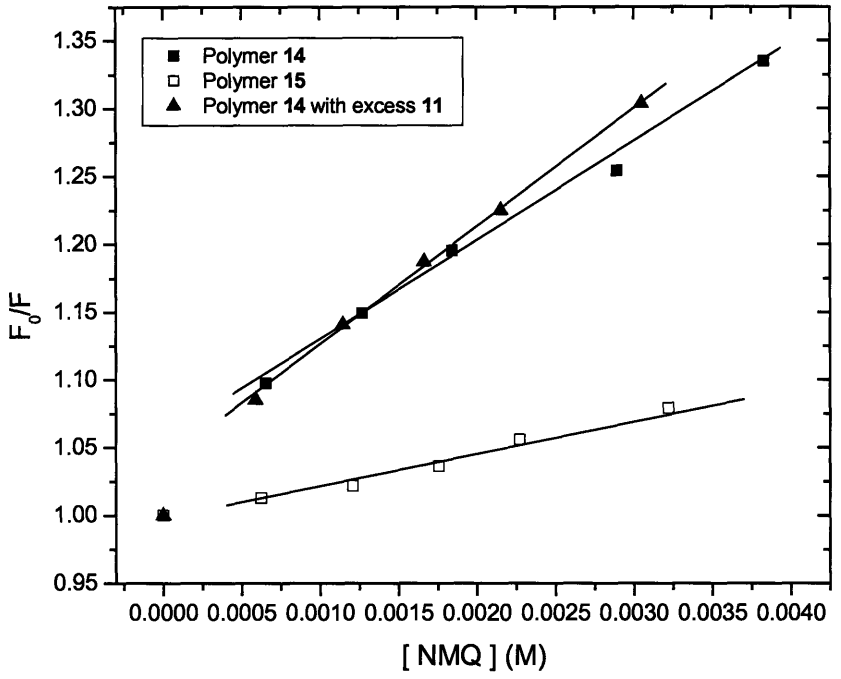

Figure 4.8. Stern-Volmer quenching of polymers **14** and **15** with *N*-methylquinolinium PF_6 as a function of quencher concentration.

Polymer **14** is quenched by NMQ with a K_{SV} of 82 ± 7 M^{-1}, while the control polymer **15** shows a K_{SV} of 25 ± 2 M^{-1}. The Stern-Volmer quenching constant for polymer **14** was very slightly increased (to 97 ± 6 M^{-1}) in the presence of a large excess of exogenous monomer **11**. However, the fluorescence lifetimes τ of polymers **14** and **15** were found to be completely insensitive to quencher concentration. Because dynamic quenching would imply that larger quencher concentrations should give rise to smaller τ values (Chapter 1), this result demonstrates that static PPE-quencher interactions are at play in all of the above systems. The fact that even the model polymer **15** shows completely static quenching with NMQ suggests that there is a strong electrostatic interaction between the electron-rich PPE backbone and NMQ that does not depend on the presence of a calix[4]arene host system. 'Modification' of the PPE structure with

the *cone* calixarene roughly triples the observed K_{SV}, reflecting the additional enthalpic driving force of multiple cation-π interactions between the analyte and the calixarene 'baskets' in **14**. Without the aid of an electron-rich extended π-structure, monomer **11** is unable to efficiently compete with the polymer for NMQ and its presence does not significantly change the Stern-Volmer constant. It is worth re-iterating that *cone* calix[4]arenes are known to interact only very weakly with the *N*-methylquinolinium ion. Nonetheless, it is probable that the quenching of polymer **14** by NMQ arises from a synergistic combination of cation-π interactions within the calixarene cavity and electrostatic interactions between the PPE and the electron-poor π-system of NMQ.

Conclusions

A series of structurally unusual calix[4]arene-crown ether monomers have been synthesized, and a PPE based on one of these monomers shows small spectral shifts on exposure to Ba^{2+}. Additionally, a PPE has been prepared in which the polymer backbone passes along the upper rim of a fixed *cone* calix[4]arene. Enhanced quenching of this polymer by the *N*-methylpyridinium cation is attributed to cation-π interactions between the guest and the calix[4]arene host.

Experimental

Synthetic considerations. Reagents were purchased commercially and generally used without further purification. Dichloromethane was reagent grade or better and used without further purification. DMF was dried by storage over activated molecular sieves before use. MeCN was

dried immediately before use by passage through a column of freshly activated alumina. Toluene-diisopropylamine mixtures used for polymerization reactions were degassed by vigorous sparging with argon before use. Compound **3**,[25] 2,5-diiodocatechol,[30] and 2,5-diethynyl-1,4-bis(hexadecyloxy)benzene[31] have been previously reported and were generously provided by Phoebe Kwan, Zhengguo Zhu, and Irina Gorodetskaya, respectively. Compounds **2**,[24] **10**,[25] and *N*-methylquinolinium hexafluorophosphate[32] were prepared by literature procedures. Melting points were recorded on a Laboratory Devices Inc. Mel-Temp II and are uncorrected. NMR spectra were recorded on Varian INOVA 500 MHz or Varian UNITY 300 MHz spectrometers and referenced to the ^{1}H resonance of internal Me_4Si or the ^{13}C resonance of the solvent. High-resolution mass spectra were recorded on a Bruker Daltonics Apex II 3T FT-ICR instrument. HPLC analyses were carried out on a Dynamax 250×9.5 column using degassed EtOAc/C_7H_{16} eluents at a 4 ml/min flow rate. Compound elution was monitored at 265 nm.

***Para*-linked calixcrown 4.** Compound **2** (200 mg, 0.44 mmol), compound **3** (302 mg, 0.44 mmol) and Cs_2CO_3 (500 mg) were heated at reflux in dry MeCN (175 ml) under argon for 4 d. After cooling to room temperature, the reaction mixture was concentrated to dryness and re-dissolved in a mixture of $CHCl_3$ and 1 N HCl. The organic layer was separated, washed with water and saturated NaCl solution, and dried on anhydrous $MgSO_4$. Column chromatography (4:1 hexanes/EtOAc) provided a white solid (179 mg, 43%). M.p. >130°, broad. HPLC: 10.9 min (10% EtOAc/C_7H_{16}). ^{1}H NMR and ^{13}C NMR ($CDCl_3$, ppm): extremely complex spectra, see appendix. HRMS: [$C_{44}H_{44}I_2O_8$+Na] requires 977.1018, found 977.1049.

Demethylation of 4. A solution of calixcrown **4** (40 mg, 0.042 mmol) in $CHCl_3$ (5 ml) was treated with 15 μl Me_3SI under argon. After stirring at 60° for 1.5 h, the reaction mixture was cooled to room temperature and washed with 1 N HCl, dilute $Na_2S_2O_3$, and saturated NaCl solution. The reaction mixture was dried over anhydrous $MgSO_4$, filtered, and concentrated to dryness. The white residue remaining was recrystallized from $CHCl_3$-MeOH and then chromatographed on silica gel (elution with 4:1 hexanes/EtOAc) to provide **4'** as a white solid (7 mg, 18%). HPLC: 16.2 min (10% EtOAc/C_7H_{16}). ^1H NMR ($CDCl_3$, ppm): 3.27 (d, 2H, 13.0 Hz), 3.86 (m, 2H), 3.90 (m, 2H), 4.13 (m, 2H), 4.30 (m, 2H), 4.34 (d, 2H, 13.0 Hz), 6.62-6.66 (m, 2H), 6.76 (d, 2H, 7.5 Hz), 7.01 (s, 1H), 7.03 (d, 2H, 7.5 Hz), 7.37 (s, 1H). ^{13}C NMR ($CDCl_3$, ppm): 69.99, 70.52, 71.47, 75.55, 87.38, 118.85, 124.77, 125.10, 128.40, 128.64, 128.88, 133.55, 151.85, 153.45, 153.81. HRMS: [$C_{42}H_{40}O_8I_2$-H] requires 925.0740, found 925.0744.

1,4-diiodo-2,3-bis(2-(2-hydroxyethoxy)ethyl)benzene. 2,5-Diiodocatechol (543 mg, 1.50 mmol), 2-(2-chloroethoxy)ethanol (375 μl, 2.55 mmol), K_2CO_3 (830 mg) and a few crystals of KI were combined in dry DMF in a Schlenk tube and stirred at 80° under argon for 4 d. After cooling to room temperature, the reaction mixture was extracted with CH_2Cl_2 and the organic extract washed with dilute HCl, water, and NH_4Cl solution (three times). The organic layer was dried on anhydrous $MgSO_4$ and chromatographed on silica gel (elution with 4% MeOH in CH_2Cl_2) to provide a slightly pink-colored solid (510 mg, 63%). M.p. 87°. ^1H NMR ($CDCl_3$, ppm): 3.2 (br s, 1H), 3.69 (m, 2H), 3.76 (app d, 2H, 4.2 Hz), 3.91 (m, 2H), 4.24 (m, 2H), 7.25 (s, 1H). ^{13}C NMR ($CDCl_3$, ppm): 61.91, 70.66, 72.92, 73.26, 93.25, 135.83, 152.32. HRMS: [$C_{14}H_{20}I_2O_6$+CH_3COO] requires 596.9488, found 596.9495.

1,4-diiodo-2,3-bis(2-(2-(*p*-toluenesulfonyloxy)ethoxy)ethyl)benzene (5). *Para*-toluenesulfonyl chloride (400 mg, 2.2 mmol) was added to a cold solution of 1,4-diiodo-2,3-bis(2-(2-hydroxyethoxy)ethyl)benzene (155 mg, 0.29 mmol) in a mixture of 20 ml CH_2Cl_2 and 3 ml Et_3N. After stirring under argon overnight, the reaction mixture was diluted with EtOAc and washed with 1 N HCl and saturated NaCl solution. The organic layer was dried over anhydrous $MgSO_4$ and purified by column chromatography on silica gel (elution with 2:1 hexanes/EtOAc) to provide **5** as a white solid (152 mg, 62%). M.p. 74°-76°. ^{1}H NMR ($CDCl_3$, ppm): 2.43 (s, 3H), 3.75 (m, 4H), 4.09 (m, 2H), 4.18 (m, 2H), 7.22 (s, 1H), 7.33 (d, 2H, 8.0 Hz), 7.78 (d, 2H, 8.0 Hz). ^{13}C NMR ($CDCl_3$, ppm): 21.78, 68.70, 69.45, 70.45, 72.45, 93.21, 128.05, 130.00, 132.95, 135.63, 144.97, 152.02. HRMS: [$C_{28}H_{32}S_2O_{10}I_2$+Na] requires 868.9418, found 868.9437.

***Ortho*-linked calixcrown 6.** Compound **2** (76 mg, 0.17 mmol), compound **5** (143 mg, 0.17 mmol), and Cs_2CO_3 (155 mg) were heated at reflux in dry MeCN (75 ml) under argon for 4 d. The reaction mixture was concentrated to dryness and re-dissolved in a mixture of CH_2Cl_2 and 1 N HCl. The organic layer was separated, washed with saturated NaCl solution, and dried over anhydrous $MgSO_4$. Purification by column chromatography (elution with 3:1 hexanes/EtOAc) provided a white solid (85 mg, 53%). M.p. dec. HPLC: 6.8 min (10% EtOAc/C_7H_{16}). ^{1}H NMR (CD_3CN, ppm): broad peaks. 3.25 (d, 2H, 12.5 Hz), 3.40 (m, 2H), overlapping peaks 3.90 (br m), 4.01 (m), 4.08 (m), 4.16 (s), 4.22 (m) total integration *ca.* 11H, 4.41 (d, 2H, 12.5 Hz), 6.49 (t, 1H, 7.5 Hz), 6.61 (d, 2H, 7.5 Hz), 6.90 (t, 1H, 7.0 Hz), 7.17 (d, 2H, 7.0 Hz), 7.31 (s, 1H). ^{13}C NMR ($CDCl_3$, ppm): 31.18, 64.46, 70.39, 72.13, 73.45, 73.76, 93.36, 122.76, 122.84, 127.98, 128.65, 133.92, 135.75, 136.58, 152.49. HRMS: [$C_{44}H_{44}I_2O_8$+CH_3COO] requires 1013.1264, found 1013.1249.

Mononitrotetra(octyloxy)calix[4]arene 8. Silica-supported HNO_3 was prepared by stirring a suspension of 40 g silica gel in 100 ml of 8 N HNO_3 for 3 h. The silica was recovered by filtration and air-dried overnight before use. Calix[4]arene tetraoctyl ether **7** (1.00 g, 1.15 mmol) was dissolved in 40 ml CH_2Cl_2 and treated with *ca.* 1 g of HNO_3-SiO_2. A purple color developed immediately. After 50 min TLC analysis (9:1 hexanes/EtOAc) indicated complete consumption of **7**. After removal of the silica by filtration, the reaction mixture was washed with aqueous $NaHCO_3$ and saturated NaCl solution. The organic phase was separated, dried over anhydrous $MgSO_4$, and filtered through a small pad of silica gel. The oil remaining after concentration of the eluate was chromatographed on silica gel (elution with 3% EtOAc/hexanes) to provide 365 mg (35%) of **8** as an oily orange solid. ^{1}H NMR ($CDCl_3$, ppm): 0.89 (m, 12H), 1.30 (m, 36H), 1.49 (m, 4H), 1.88 (m, 8H), 3.16 (d, 2H, 14.0 Hz), 3.19 (d, 2H, 14.0 Hz), 3.75 (t, 2H, 6.5 Hz), 3.84-3.92 (m, 4H), 3.92-4.02 (m, 2H), 4.41 (d, 2H, 14 Hz), 4.46 (d, 2H, 14 Hz), 6.23 (br s, 2H), 6.83 (t, 1H, 7.5 Hz), 6.93 (t, 2H, 8.3 Hz), 7.11 (s, 1H). ^{13}C NMR ($CDCl_3$, ppm): 14.32, 22.91, 22.91, 22.94, 26.32, 26.60, 26.77, 29.71, 29.78, 29.90, 29.93, 30.04, 30.20, 30.44, 30.60, 30.69, 31.16, 31.31, 32.16, 32.18, 32.19, 75.34, 75.39, 75.71, 121.87, 122.61, 123.41, 127.89, 128.70, 129.65, 134.18, 135.17, 136.19, 136.87, 142.73, 156.04, 157.41, 161.66, 163.15. HRMS: [$C_{60}H_{87}NO_6$] requires 917.6528, found 917.6501.

Monoaminotetra(octyloxy)calix[4]arene 9. Nitro compound **8** (129 mg, 0.14 mmol) was dissolved in EtOH containing *ca.* 5% EtOAc to promote solubility. 2 g of $SnCl_2$ were added and the reaction mixture heated at reflux under argon overnight. The reaction mixture was concentrated to dryness, re-dissolved in CH_2Cl_2 and washed with 1 N NaOH followed by

saturated NaCl solution. The organic phase was dried over anhydrous $MgSO_4$ and filtered, and the solvent was removed under reduced pressure to afford a dark red oil that was used without further purification (86 mg, 69%). ^{1}H NMR ($CDCl_3$, ppm): 0.89 (app t, 12H, 6.0 Hz), 1.25-1.40 (br m, 40H), 1.89 (m, 8H), 3.02 (d, 2H, 13.5 Hz), 3.14 (d, 2H, 13.5 Hz), 3.78 (t, 2H, 7.5 Hz), 3.86 (m, 6H), 4.36 (d, 2H, 13.0 Hz), 4.44 (d, 2H, 13.5 Hz), 5.94 (s, 2H), 6.54-6.65 (m, 9H). ^{13}C NMR ($CDCl_3$, ppm): 14.34, 22.95, 26.54, 26.60, 26.66, 29.87, 29.88, 30.16, 30.52, 30.57, 30.58, 31.19, 31.23, 31.25, 32.22, 71.19, 75.34, 75.37, 75.40, 115.57, 121.72, 121.99, 122.05, 128.23, 128.24, 128.28, 128.29, 135.38, 135.44, 135.58, 140.47, 149.99, 156.80, 156.89. HRMS: [$C_{60}H_{89}NO_4$+H] requires 888.6864, found 888.6881.

Calix[4]arene monomer 11. A solution of **10** (161 mg, 0.40 mmol) in CH_2Cl_2 was added dropwise over 30 min to an ice-cold solution of **9** (353 mg, 0.40 mmol) in 40 ml CH_2Cl_2 containing 1 ml Et_3N. The reaction mixture was allowed to stir overnight while warming to room temperature, then was poured into dilute HCl. The organic phase was separated, washed with water and saturated NaCl solution, and dried over anhydrous $MgSO_4$. The residue remaining after concentration to dryness was subjected to column chromatography (6:1 hexanes/EtOAc) and the product recrystallized from a $CHCl_3$-MeOH-hexane mixture, yielding 103 mg (21%) of a cream-colored solid. M.p. 100° dec. HPLC: 4.3 min (10% EtOAc/C_7H_{16}). ^{1}H NMR ($CDCl_3$, ppm): 0.89 (m, 12H), 1.30-1.42 (m, 40H), 1.89 (m, 8H), 2.40 (s, 3H), 3.15 (d, 2H, 13.0 Hz), 3.17 (d, 2H, 14.0 Hz), 3.84 (t, 2H, 7.0 Hz), 3.90 (m, 6H), 3.44 (app d, 4H, 13.5 Hz), 6.53 (m, 3H), 6.63-6.75 (m, 8H), 6.89 (s, 1H), 7.72 (s, 1H), 7.83 (s, 1H). ^{13}C NMR ($CDCl_3$, ppm): numerous peaks (see Appendix); major peaks at 14.34, 22.95, 26.52, 26.65, 29.89, 30.19, 30.54, 32.21,

75.40, 100.00, 120.92, 122.21, 128.21, 128.61, 135.39, 157.09. HRMS: [$C_{68}H_{93}NO_5I_2$+Na] requires 1280.5035, found 1280.5075.

2,5-Diiodo-4-methylbenzoic acid, (4-hexyloxy)phenylamide (16). A solution of **10** (418 mg, 1.03 mmol) in CH_2Cl_2 was added dropwise to an ice-cold solution of 4-hexyloxyaniline (203 mg, 1.05 mmol) in a mixture of 20 ml CH_2Cl_2 and 4 ml Et_3N. After stirring for 8 hr under argon, the reaction mixture was washed with 1 N NaOH followed by 1 N HCl and saturated NaCl solution. The organic layer was dried over anhydrous $MgSO_4$, filtered, and concentrated to dryness. The residue remaining was recrystallized from hot EtOH to give **16** as pale pink plates (208 mg, 37%). ^{1}H NMR ($CDCl_3$, ppm): 0.91 (m, 3H), 1.33-1.37 (m, 4H), 1.78 (m, 2H), 2.41 (s, 3H), 3.95 (t, 2H, 6.8 Hz), 6.89 (app dd, 2H, 2.0 Hz, 6.5 Hz), 7.44 (s, 1H), 7.50 (app dd, 2H, 2.0 Hz, 6.5 Hz), 7.73 (s, 1H), 7.90 (s, 1H). ^{13}C NMR ($CDCl_3$, ppm): 14.27, 22.83, 25.92, 27.70, 29.43, 31.80, 68.53, 92.25, 100.80, 115.08, 122.13, 130.37, 138.58, 140.63, 141.22, 145.60, 156.72, 165.44. HRMS: [$C_{20}H_{23}NO_2I_2$-H] requires 561.9745, found 561.9729.

Polymer synthesis. PPEs were synthesized by standard methods. In a typical synthesis, monomer **4** (17 mg, 0.018 mmol), 2,5-diethynyl-1,4-bis(hexadecyloxy)benzene (11 mg, 0.018 mmol), $Pd(PPh_3)_4$ and CuI (catalytic amounts) were dissolved in freshly degassed 4:1 toluene/diisopropylamine (2 ml) under argon and stirred at 60° overnight. The reaction mixture was diluted with a small quantity of CH_2Cl_2, washed with saturated $NaHCO_3$ and NaCl solutions, dried over anhydrous $MgSO_4$ and concentrated. Slow addition of the concentrated CH_2Cl_2 solution to MeOH resulted in the precipitation of the PPE as a yellow solid. Polymer **12** was collected by centrifugation, washed several times with fresh MeOH, and allowed to air-dry.

Polymers **13** and **14** were prepared and purified by an analogous method using 2,5-diethynyl-1,4-bis(hexadecyloxy)benzene and monomers **6** and **11,** respectively. Polymer M_n values were on the order of $1\text{-}2\times10^4$ with PDI values of 1.3-2.0. ^{1}H NMR spectra of these polymers are included in the appendix.

Fluorescence studies. Fluorescence spectra were measured on a Spex Fluorolog 2 fluorimeter in quartz cuvettes. Fluorescence lifetimes were measured using phase modulation at 10 frequencies between 10 and 220 MHz and referenced to a colloidal-silica standard ($\tau = 0$). For Stern-Volmer quenching studies, quenchers were dissolved in solutions equal in polymer concentration to the assay solution. Lifetime Stern-Volmer studies showed consistent τ values in each case (0.55 ± 0.02 ns) regardless of quencher concentration.

X-ray crystal structure determination. Crystals suitable for X-ray analysis were grown by slow evaporation of CH_2Cl_2-MeOH solutions of **4** and **6.** Crystal structure determination was performed by Dr. William Davis (MIT X-ray Crystallography Facility) using a Bruker Smart diffractometer equipped with a Kappa CCD area detector using radiation from a Mo-Kα source monochromated through graphite ($\lambda = 0.71073$ Å). Structures were solved and refined using the Bruker SHELXTL package. Crystal structure numbering schemes and data are reproduced below.

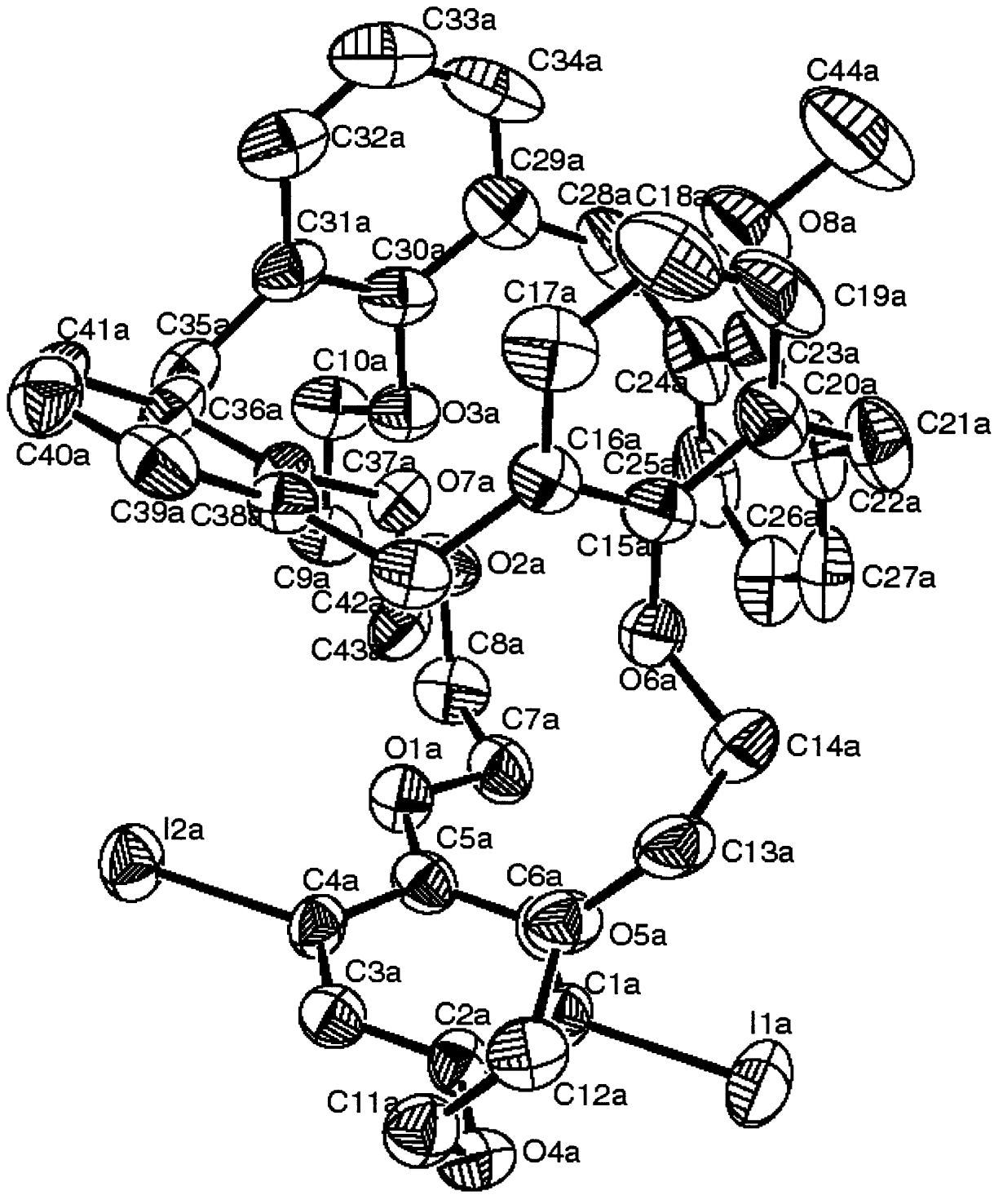

Figure 4.9. The *paco* conformation of **4**, showing the crystallographic numbering scheme. The structure depicted above represents half of the molecules in the crystal. In the numbering scheme, atoms belonging to the above molecule take the suffix 'a' while those belonging to the *paco* isomer of the other molecule take the suffix 'c'.

Table 4.2. Crystal data and structure refinement for **4.**

Empirical formula	$C_{44.125}\ H_{44}\ C_{10.25}\ I_2\ O_8$	
Formula weight	964.96	
Temperature	193(2) K	
Wavelength	0.71073 Å	
Crystal system	Orthorhombic	
Space group	Pbca	
Unit cell dimensions	a = 21.553(2) Å	α= 90°.
	b = 16.1747(17) Å	β= 90°.
	c = 47.940(5) Å	γ = 90°.
Volume	16712(3) $Å^3$	
Z	16	
Density (calculated)	1.534 Mg/m^3	
Absorption coefficient	1.572 mm^{-1}	
F(000)	7728	
Theta range for data collection	1.27 to 23.00°.	
Index ranges	-22<=h<=23, -17<=k<=17, -52<=l<=33	
Reflections collected	71892	
Independent reflections	11637 [R(int) = 0.0463]	
Completeness to theta = 23.00°	100.0 %	
Absorption correction	None	
Refinement method	Full-matrix least-squares on F^2	
Data / restraints / parameters	11637 / 3 / 1038	
Goodness-of-fit on F^2	2.107	
Final R indices [I>2sigma(I)]	R1 = 0.0607, wR2 = 0.1209	
R indices (all data)	R1 = 0.0699, wR2 = 0.1223	
Largest diff. peak and hole	0.674 and -0.639 $e.Å^{-3}$	

Table 4.3. Atomic coordinates (x 10^4) and equivalent isotropic displacement parameters ($Å^2$x 10^3) for **4.** U(eq) is defined as one third of the trace of the orthogonalized U^{ij} tensor.

	x	y	z	U(eq)
I(1A)	3006(1)	7720(1)	3215(1)	67(1)
I(2A)	4763(1)	9131(1)	2096(1)	56(1)
O(1A)	4840(2)	7490(3)	2436(1)	47(1)
O(2A)	6033(2)	6501(3)	2462(1)	57(1)
O(3A)	6588(2)	7850(2)	2769(1)	45(1)
O(4A)	2939(2)	9407(3)	2871(1)	50(1)
O(5A)	3810(2)	9802(3)	3301(1)	47(1)
O(6A)	4987(2)	9096(3)	3514(1)	46(1)
O(7A)	5910(2)	9407(2)	3065(1)	37(1)
O(8A)	6793(3)	7896(4)	3726(1)	77(2)
C(1A)	3533(3)	8155(4)	2875(1)	43(2)
C(2A)	3417(3)	8931(4)	2767(1)	39(2)
C(3A)	3768(3)	9189(4)	2544(1)	43(2)
C(4A)	4240(3)	8704(4)	2436(1)	40(2)
C(5A)	4364(3)	7932(4)	2551(1)	45(2)
C(6A)	4002(3)	7650(4)	2772(1)	46(2)
C(7A)	4920(3)	6640(4)	2519(2)	55(2)

C(8A)	5437(3)	6264(4)	2354(2)	57(2)
C(9A)	6271(3)	7242(4)	2339(1)	52(2)
C(10A)	6810(3)	7537(4)	2507(1)	51(2)
C(11A)	3085(3)	10227(4)	2953(1)	51(2)
C(12A)	3272(3)	10275(4)	3255(1)	47(2)
C(13A)	3981(3)	9774(5)	3589(1)	54(2)
C(14A)	4388(3)	9039(5)	3639(2)	63(2)
C(15A)	5435(3)	9481(4)	3678(1)	43(2)
C(16A)	5614(3)	10277(4)	3609(1)	41(2)
C(17A)	6065(3)	10664(5)	3775(1)	59(2)
C(18A)	6326(4)	10256(5)	3998(2)	75(2)
C(19A)	6153(4)	9456(6)	4054(2)	76(2)
C(20A)	5718(3)	9034(4)	3890(1)	52(2)
C(21A)	5585(4)	8132(4)	3944(1)	65(2)
C(22A)	5719(4)	7571(4)	3695(1)	57(2)
C(23A)	6307(4)	7479(4)	3590(1)	55(2)
C(24A)	6454(4)	7022(4)	3354(1)	60(2)
C(25A)	5965(5)	6615(4)	3228(2)	70(2)
C(26A)	5368(4)	6660(5)	3328(2)	70(2)
C(27A)	5245(4)	7143(5)	3561(2)	67(2)
C(28A)	7105(4)	7007(5)	3229(2)	72(2)
C(29A)	7333(3)	7847(5)	3140(1)	55(2)
C(30A)	7054(3)	8261(4)	2918(1)	47(2)
C(31A)	7199(3)	9073(4)	2848(1)	47(2)
C(32A)	7680(3)	9456(5)	3000(2)	60(2)
C(33A)	7987(3)	9044(7)	3202(2)	75(3)
C(34A)	7815(4)	8248(7)	3276(2)	74(3)
C(35A)	6819(3)	9558(4)	2643(1)	50(2)
C(36A)	6526(3)	10307(4)	2778(1)	42(2)
C(37A)	6080(3)	10196(4)	2987(1)	39(2)
C(38A)	5825(3)	10874(3)	3133(1)	36(1)
C(39A)	6044(3)	11664(4)	3061(1)	50(2)
C(40A)	6480(3)	11783(4)	2859(1)	52(2)
C(41A)	6716(3)	11115(4)	2720(1)	53(2)
C(42A)	5353(3)	10736(4)	3356(1)	44(2)
C(43A)	5409(3)	9058(4)	2907(1)	43(2)
C(44A)	7095(5)	7378(8)	3939(2)	134(5)
I(1B)	5159(1)	2846(1)	10294(1)	45(1)
I(2B)	2022(1)	1868(1)	10358(1)	50(1)
O(1B)	3995(2)	3910(2)	10148(1)	41(1)
O(2B)	4033(2)	4764(3)	9597(1)	47(1)
O(3B)	4455(2)	3277(2)	9289(1)	40(1)
O(4B)	3173(2)	777(2)	10430(1)	53(1)
O(5B)	3007(2)	-739(2)	10101(1)	44(1)
O(6B)	3509(2)	-205(2)	9540(1)	44(1)
O(7B)	3346(2)	1923(2)	9332(1)	42(1)
O(8B)	4665(5)	1078(6)	9357(3)	81(3)
C(1B)	4206(2)	2552(3)	10298(1)	32(1)
C(2B)	3773(3)	3165(3)	10235(1)	31(1)
C(3B)	3146(3)	2966(3)	10259(1)	34(1)
C(4B)	2967(3)	2167(4)	10327(1)	37(1)
C(5B)	3399(3)	1551(3)	10378(1)	36(1)
C(6B)	4026(3)	1758(3)	10371(1)	37(1)
C(7B)	3546(3)	4509(3)	10046(1)	45(2)
C(8B)	3887(3)	5112(3)	9861(1)	41(2)
C(9B)	4649(3)	4485(4)	9568(1)	43(2)

C(10B)	4722(3)	4090(4)	9285(1)	46(2)
C(11B)	3598(3)	99(4)	10423(2)	53(2)
C(12B)	3218(3)	-666(4)	10380(1)	48(2)
C(13B)	3450(3)	-1147(4)	9923(1)	55(2)
C(14B)	3285(3)	-1003(4)	9625(1)	55(2)
C(15B)	3463(3)	-89(3)	9254(1)	37(2)
C(16B)	2936(3)	296(4)	9147(1)	40(2)
C(17B)	2890(3)	402(4)	8858(1)	44(2)
C(18B)	3353(3)	138(4)	8685(1)	45(2)
C(19B)	3883(3)	-211(4)	8795(1)	49(2)
C(20B)	3955(3)	-322(3)	9083(1)	39(2)
C(21B)	2441(3)	664(4)	9341(1)	45(2)
C(22B)	2288(3)	1541(3)	9246(1)	39(2)
C(23B)	2768(3)	2120(4)	9225(1)	38(2)
C(24B)	2693(3)	2881(4)	9090(1)	41(2)
C(25B)	2108(3)	3060(4)	8982(1)	51(2)
C(26B)	1616(3)	2527(4)	9010(2)	59(2)
C(27B)	1713(3)	1755(4)	9146(1)	47(2)
C(28B)	3240(3)	3451(4)	9054(1)	45(2)
C(29B)	3777(3)	3049(3)	8900(1)	41(2)
C(30B)	4359(3)	2958(3)	9023(1)	36(1)
C(31B)	4833(3)	2507(4)	8895(1)	43(2)
C(32B)	4718(3)	2198(4)	8627(1)	53(2)
C(33B)	4156(4)	2311(4)	8498(1)	54(2)
C(34B)	3687(3)	2719(4)	8634(1)	49(2)
C(35B)	5415(3)	2251(4)	9048(2)	50(2)
C(36B)	5503(9)	1350(11)	9099(5)	84(7)
C(37B)	5109(3)	787(4)	9156(1)	40(2)
C(38B)	5089(9)	-50(11)	9139(5)	112(9)
C(39B)	5628(9)	-354(12)	8936(4)	86(6)
C(40B)	6020(7)	191(10)	8842(3)	52(2)
C(41B)	6047(9)	1006(12)	8901(3)	91(6)
C(42B)	4574(3)	-595(3)	9199(1)	41(2)
C(43B)	3418(4)	2125(5)	9627(1)	72(2)
C(44B)	4928(15)	1060(30)	9655(6)	134(5)
C(36C)	5251(5)	1604(7)	9245(3)	22(3)
C(37C)	5109(3)	787(4)	9156(1)	40(2)
C(38C)	4853(6)	203(8)	9335(3)	36(1)
C(39C)	4846(5)	356(8)	9608(2)	26(3)
C(40C)	5039(9)	1116(11)	9702(5)	52(2)
C(41C)	5235(5)	1737(6)	9522(2)	23(2)
C(44C)	5627(8)	289(10)	8764(3)	64(5)
O(8C)	5110(3)	624(4)	8859(1)	24(2)
Cl(2S)	7238(6)	-220(9)	8800(3)	141(5)
C(101)	7344(13)	573(15)	8881(7)	47(2)
Cl(1S)	7030(11)	1278(14)	8962(4)	490(30)

Table 4.4. Bond lengths [Å] and angles [°] for **4.**

I(1A)-C(1A)	2.105(6)	O(1A)-C(7A)	1.442(7)
I(2A)-C(4A)	2.097(6)	O(2A)-C(9A)	1.430(8)
O(1A)-C(5A)	1.365(7)	O(2A)-C(8A)	1.437(7)

O(3A)-C(30A)	1.401(7)
O(3A)-C(10A)	1.436(7)
O(4A)-C(2A)	1.377(7)
O(4A)-C(11A)	1.419(8)
O(5A)-C(12A)	1.407(7)
O(5A)-C(13A)	1.429(7)
O(6A)-C(15A)	1.392(7)
O(6A)-C(14A)	1.427(7)
O(7A)-C(37A)	1.378(7)
O(7A)-C(43A)	1.433(7)
O(8A)-C(23A)	1.406(9)
O(8A)-C(44A)	1.470(10)
C(1A)-C(2A)	1.382(8)
C(1A)-C(6A)	1.391(9)
C(2A)-C(3A)	1.374(8)
C(3A)-C(4A)	1.387(8)
C(4A)-C(5A)	1.391(8)
C(5A)-C(6A)	1.392(9)
C(7A)-C(8A)	1.495(9)
C(9A)-C(10A)	1.489(8)
C(11A)-C(12A)	1.504(8)
C(13A)-C(14A)	1.498(9)
C(15A)-C(16A)	1.384(9)
C(15A)-C(20A)	1.389(9)
C(16A)-C(17A)	1.402(9)
C(16A)-C(42A)	1.529(8)
C(17A)-C(18A)	1.376(10)
C(18A)-C(19A)	1.373(11)
C(19A)-C(20A)	1.402(10)
C(20A)-C(21A)	1.510(9)
C(21A)-C(22A)	1.529(9)
C(22A)-C(23A)	1.370(9)
C(22A)-C(27A)	1.390(10)
C(23A)-C(24A)	1.389(9)
C(24A)-C(25A)	1.384(11)
C(24A)-C(28A)	1.525(10)
C(25A)-C(26A)	1.374(11)
C(26A)-C(27A)	1.389(10)
C(28A)-C(29A)	1.508(10)
C(29A)-C(34A)	1.388(10)
C(29A)-C(30A)	1.392(9)
C(30A)-C(31A)	1.392(9)
C(31A)-C(32A)	1.411(9)
C(31A)-C(35A)	1.503(9)
C(32A)-C(33A)	1.348(11)
C(33A)-C(34A)	1.385(12)
C(35A)-C(36A)	1.512(8)
C(36A)-C(41A)	1.399(9)
C(36A)-C(37A)	1.400(8)
C(37A)-C(38A)	1.412(8)
C(38A)-C(39A)	1.407(8)
C(38A)-C(42A)	1.492(8)
C(39A)-C(40A)	1.360(9)
C(40A)-C(41A)	1.368(9)
I(1B)-C(1B)	2.109(5)
I(2B)-C(4B)	2.100(5)
O(1B)-C(2B)	1.362(6)
O(1B)-C(7B)	1.454(7)
O(2B)-C(9B)	1.408(7)
O(2B)-C(8B)	1.418(7)
O(3B)-C(30B)	1.393(7)
O(3B)-C(10B)	1.436(7)
O(4B)-C(5B)	1.367(7)
O(4B)-C(11B)	1.429(7)
O(5B)-C(12B)	1.419(7)
O(5B)-C(13B)	1.440(7)
O(6B)-C(15B)	1.388(7)
O(6B)-C(14B)	1.437(7)
O(7B)-C(23B)	1.383(7)
O(7B)-C(43B)	1.459(7)
O(8B)-C(37B)	1.438(12)
O(8B)-C(44B)	1.54(3)
C(1B)-C(6B)	1.385(8)
C(1B)-C(2B)	1.395(8)
C(2B)-C(3B)	1.394(8)
C(3B)-C(4B)	1.388(8)
C(4B)-C(5B)	1.385(8)
C(5B)-C(6B)	1.393(8)
C(7B)-C(8B)	1.508(8)
C(9B)-C(10B)	1.506(8)
C(11B)-C(12B)	1.499(8)
C(13B)-C(14B)	1.490(9)
C(15B)-C(16B)	1.393(8)
C(15B)-C(20B)	1.394(8)
C(16B)-C(17B)	1.400(8)
C(16B)-C(21B)	1.536(8)
C(17B)-C(18B)	1.366(8)
C(18B)-C(19B)	1.381(8)
C(19B)-C(20B)	1.399(8)
C(20B)-C(42B)	1.510(8)
C(21B)-C(22B)	1.525(8)
C(22B)-C(27B)	1.372(8)
C(22B)-C(23B)	1.399(8)
C(23B)-C(24B)	1.401(8)
C(24B)-C(25B)	1.392(8)
C(24B)-C(28B)	1.507(8)
C(25B)-C(26B)	1.374(9)
C(26B)-C(27B)	1.425(9)
C(28B)-C(29B)	1.518(8)
C(29B)-C(30B)	1.394(8)
C(29B)-C(34B)	1.398(8)
C(30B)-C(31B)	1.397(8)
C(31B)-C(32B)	1.399(9)
C(31B)-C(35B)	1.512(9)
C(32B)-C(33B)	1.373(9)
C(33B)-C(34B)	1.371(9)
C(35B)-C(36B)	1.490(18)
C(36B)-C(37B)	1.275(18)
C(36B)-C(41B)	1.61(3)
C(37B)-C(38B)	1.357(18)
C(38B)-C(42B)	1.446(18)
C(38B)-C(39B)	1.59(3)

C(39B)-C(40B)	1.30(2)	C(40C)-C(41C)	1.39(2)
C(40B)-C(41B)	1.35(2)	C(44C)-O(8C)	1.318(17)
C(36C)-C(41C)	1.346(16)	Cl(2S)-C(101)	1.36(2)
C(38C)-C(39C)	1.332(16)	C(101)-Cl(1S)	1.38(2)
C(39C)-C(40C)	1.37(2)		

C(5A)-O(1A)-C(7A)	118.6(5)	C(25A)-C(24A)-C(23A)	115.9(8)
C(9A)-O(2A)-C(8A)	113.4(5)	C(25A)-C(24A)-C(28A)	121.4(7)
C(30A)-O(3A)-C(10A)	112.1(5)	C(23A)-C(24A)-C(28A)	122.6(8)
C(2A)-O(4A)-C(11A)	117.2(5)	C(26A)-C(25A)-C(24A)	122.3(7)
C(12A)-O(5A)-C(13A)	112.2(4)	C(25A)-C(26A)-C(27A)	119.3(8)
C(15A)-O(6A)-C(14A)	114.9(5)	C(26A)-C(27A)-C(22A)	120.7(8)
C(37A)-O(7A)-C(43A)	115.1(4)	C(29A)-C(28A)-C(24A)	113.4(6)
C(23A)-O(8A)-C(44A)	112.1(7)	C(34A)-C(29A)-C(30A)	117.3(7)
C(2A)-C(1A)-C(6A)	122.1(6)	C(34A)-C(29A)-C(28A)	122.0(7)
C(2A)-C(1A)-I(1A)	119.7(5)	C(30A)-C(29A)-C(28A)	120.7(7)
C(6A)-C(1A)-I(1A)	118.2(5)	C(31A)-C(30A)-C(29A)	122.7(6)
C(3A)-C(2A)-O(4A)	121.5(6)	C(31A)-C(30A)-O(3A)	119.1(6)
C(3A)-C(2A)-C(1A)	117.9(6)	C(29A)-C(30A)-O(3A)	118.1(6)
O(4A)-C(2A)-C(1A)	120.5(5)	C(30A)-C(31A)-C(32A)	117.1(7)
C(2A)-C(3A)-C(4A)	121.6(6)	C(30A)-C(31A)-C(35A)	121.8(6)
C(3A)-C(4A)-C(5A)	120.0(6)	C(32A)-C(31A)-C(35A)	120.7(7)
C(3A)-C(4A)-I(2A)	120.0(5)	C(33A)-C(32A)-C(31A)	121.0(8)
C(5A)-C(4A)-I(2A)	120.0(5)	C(32A)-C(33A)-C(34A)	120.8(8)
O(1A)-C(5A)-C(4A)	117.0(6)	C(33A)-C(34A)-C(29A)	120.9(8)
O(1A)-C(5A)-C(6A)	123.7(6)	C(31A)-C(35A)-C(36A)	111.3(5)
C(4A)-C(5A)-C(6A)	119.2(6)	C(41A)-C(36A)-C(37A)	117.7(6)
C(1A)-C(6A)-C(5A)	119.1(6)	C(41A)-C(36A)-C(35A)	122.7(6)
O(1A)-C(7A)-C(8A)	109.4(5)	C(37A)-C(36A)-C(35A)	119.4(5)
O(2A)-C(8A)-C(7A)	111.6(6)	O(7A)-C(37A)-C(36A)	119.6(5)
O(2A)-C(9A)-C(10A)	109.1(6)	O(7A)-C(37A)-C(38A)	118.8(5)
O(3A)-C(10A)-C(9A)	109.0(5)	C(36A)-C(37A)-C(38A)	121.5(5)
O(4A)-C(11A)-C(12A)	112.2(5)	C(39A)-C(38A)-C(37A)	116.8(6)
O(5A)-C(12A)-C(11A)	109.9(5)	C(39A)-C(38A)-C(42A)	122.8(5)
O(5A)-C(13A)-C(14A)	109.4(5)	C(37A)-C(38A)-C(42A)	120.3(5)
O(6A)-C(14A)-C(13A)	114.2(6)	C(40A)-C(39A)-C(38A)	122.5(6)
C(16A)-C(15A)-C(20A)	122.4(6)	C(39A)-C(40A)-C(41A)	119.5(6)
C(16A)-C(15A)-O(6A)	118.4(5)	C(40A)-C(41A)-C(36A)	122.0(6)
C(20A)-C(15A)-O(6A)	119.0(6)	C(38A)-C(42A)-C(16A)	112.9(5)
C(15A)-C(16A)-C(17A)	118.3(6)	C(2B)-O(1B)-C(7B)	117.3(4)
C(15A)-C(16A)-C(42A)	122.5(6)	C(9B)-O(2B)-C(8B)	115.2(4)
C(17A)-C(16A)-C(42A)	119.2(6)	C(30B)-O(3B)-C(10B)	112.8(4)
C(18A)-C(17A)-C(16A)	120.6(7)	C(5B)-O(4B)-C(11B)	118.1(5)
C(19A)-C(18A)-C(17A)	119.6(7)	C(12B)-O(5B)-C(13B)	112.6(5)
C(18A)-C(19A)-C(20A)	121.9(7)	C(15B)-O(6B)-C(14B)	112.2(4)
C(15A)-C(20A)-C(19A)	116.9(7)	C(23B)-O(7B)-C(43B)	113.7(5)
C(15A)-C(20A)-C(21A)	123.0(6)	C(37B)-O(8B)-C(44B)	111.8(15)
C(19A)-C(20A)-C(21A)	120.1(7)	C(6B)-C(1B)-C(2B)	121.8(5)
C(20A)-C(21A)-C(22A)	113.9(6)	C(6B)-C(1B)-I(1B)	118.9(4)
C(23A)-C(22A)-C(27A)	117.2(7)	C(2B)-C(1B)-I(1B)	119.3(4)
C(23A)-C(22A)-C(21A)	121.6(7)	O(1B)-C(2B)-C(3B)	124.7(5)
C(27A)-C(22A)-C(21A)	121.1(7)	O(1B)-C(2B)-C(1B)	117.5(5)
C(22A)-C(23A)-C(24A)	124.5(8)	C(3B)-C(2B)-C(1B)	117.8(5)
C(22A)-C(23A)-O(8A)	118.0(7)	C(4B)-C(3B)-C(2B)	120.1(5)
C(24A)-C(23A)-O(8A)	117.5(7)	C(5B)-C(4B)-C(3B)	121.7(5)

C(5B)-C(4B)-I(2B) 118.3(4)
C(3B)-C(4B)-I(2B) 120.0(4)
O(4B)-C(5B)-C(4B) 116.9(5)
O(4B)-C(5B)-C(6B) 124.7(5)
C(4B)-C(5B)-C(6B) 118.4(5)
C(1B)-C(6B)-C(5B) 119.9(5)
O(1B)-C(7B)-C(8B) 107.8(5)
O(2B)-C(8B)-C(7B) 112.1(5)
O(2B)-C(9B)-C(10B) 109.0(5)
O(3B)-C(10B)-C(9B) 109.5(5)
O(4B)-C(11B)-C(12B) 106.6(5)
O(5B)-C(12B)-C(11B) 111.9(5)
O(5B)-C(13B)-C(14B) 109.7(5)
O(6B)-C(14B)-C(13B) 109.4(6)
O(6B)-C(15B)-C(16B) 118.9(5)
O(6B)-C(15B)-C(20B) 119.4(5)
C(16B)-C(15B)-C(20B) 121.7(6)
C(15B)-C(16B)-C(17B) 118.4(6)
C(15B)-C(16B)-C(21B) 121.1(6)
C(17B)-C(16B)-C(21B) 120.3(5)
C(18B)-C(17B)-C(16B) 120.9(6)
C(17B)-C(18B)-C(19B) 119.9(6)
C(18B)-C(19B)-C(20B) 121.4(6)
C(15B)-C(20B)-C(19B) 117.5(6)
C(15B)-C(20B)-C(42B) 122.3(6)
C(19B)-C(20B)-C(42B) 119.9(6)
C(22B)-C(21B)-C(16B) 109.2(5)
C(27B)-C(22B)-C(23B) 118.3(6)
C(27B)-C(22B)-C(21B) 122.2(5)
C(23B)-C(22B)-C(21B) 119.0(5)
O(7B)-C(23B)-C(22B) 119.1(5)
O(7B)-C(23B)-C(24B) 118.5(5)
C(22B)-C(23B)-C(24B) 122.4(6)
C(25B)-C(24B)-C(23B) 117.4(6)
C(25B)-C(24B)-C(28B) 122.5(6)
C(23B)-C(24B)-C(28B) 120.0(6)
C(26B)-C(25B)-C(24B) 122.1(6)
C(25B)-C(26B)-C(27B) 118.7(6)
C(22B)-C(27B)-C(26B) 120.9(6)
C(24B)-C(28B)-C(29B) 113.0(5)
C(30B)-C(29B)-C(34B) 118.0(6)
C(30B)-C(29B)-C(28B) 121.7(6)
C(34B)-C(29B)-C(28B) 120.1(6)
O(3B)-C(30B)-C(29B) 118.8(5)
O(3B)-C(30B)-C(31B) 119.2(5)
C(29B)-C(30B)-C(31B) 121.8(6)
C(30B)-C(31B)-C(32B) 117.4(6)
C(30B)-C(31B)-C(35B) 122.4(6)
C(32B)-C(31B)-C(35B) 119.7(6)
C(33B)-C(32B)-C(31B) 121.5(6)
C(34B)-C(33B)-C(32B) 120.0(6)
C(33B)-C(34B)-C(29B) 121.0(6)
C(36B)-C(35B)-C(31B) 116.9(8)
C(37B)-C(36B)-C(35B) 130.5(16)
C(37B)-C(36B)-C(41B) 111.5(16)
C(35B)-C(36B)-C(41B) 109.5(16)
C(36B)-C(37B)-C(38B) 136.2(16)
C(36B)-C(37B)-O(8B) 110.8(13)
C(38B)-C(37B)-O(8B) 110.2(14)
C(37B)-C(38B)-C(42B) 128(2)
C(37B)-C(38B)-C(39B) 108.7(16)
C(42B)-C(38B)-C(39B) 119.5(17)
C(40B)-C(39B)-C(38B) 118.5(15)
C(39B)-C(40B)-C(41B) 128.0(16)
C(40B)-C(41B)-C(36B) 115.4(15)
C(38B)-C(42B)-C(20B) 115.2(7)
C(38C)-C(39C)-C(40C) 119.0(13)
C(39C)-C(40C)-C(41C) 122.3(16)
C(36C)-C(41C)-C(40C) 120.3(12)
Cl(2S)-C(101)-Cl(1S) 141(3)

Table 4.5. Anisotropic displacement parameters ($Å^2 x\ 10^3$) for **4.** The anisotropic displacement factor exponent takes the form: $-2\pi^2[\ h^2\ a^{*2}U^{11} + ... + 2\ h\ k\ a^*\ b^*\ U^{12}\ ]$

	U^{11}	U^{22}	U^{33}	U^{23}	U^{13}	U^{12}
I(1A)	70(1)	74(1)	59(1)	9(1)	15(1)	-17(1)
I(2A)	63(1)	63(1)	43(1)	4(1)	11(1)	2(1)
O(1A)	51(3)	40(2)	50(3)	-1(2)	6(2)	6(2)
O(2A)	53(3)	49(3)	68(3)	-8(2)	-13(2)	10(2)
O(3A)	37(3)	50(3)	47(3)	-10(2)	1(2)	5(2)
O(4A)	34(3)	60(3)	55(3)	-5(2)	1(2)	1(2)
O(5A)	36(2)	62(3)	42(3)	-10(2)	2(2)	3(2)
O(6A)	42(3)	58(3)	38(3)	1(2)	5(2)	0(2)
O(7A)	36(2)	37(2)	39(2)	-2(2)	5(2)	-4(2)
O(8A)	80(4)	107(4)	44(3)	-6(3)	-13(3)	32(3)
C(1A)	42(4)	55(4)	33(4)	2(3)	4(3)	-10(3)
C(2A)	44(4)	43(4)	30(4)	-3(3)	0(3)	-6(3)
C(3A)	44(4)	43(4)	42(4)	-3(3)	-4(3)	-1(3)
C(4A)	42(4)	50(4)	30(4)	0(3)	4(3)	-6(3)
C(5A)	48(4)	44(4)	42(4)	-2(3)	-7(3)	0(3)
C(6A)	53(4)	45(4)	39(4)	-1(3)	-5(3)	-6(3)
C(7A)	58(5)	48(4)	60(5)	11(4)	-1(4)	10(4)
C(8A)	60(5)	47(4)	64(5)	-13(4)	-6(4)	1(4)
C(9A)	50(4)	53(4)	52(4)	-12(4)	-7(3)	6(4)
C(10A)	46(4)	60(4)	47(4)	-19(3)	0(3)	11(3)
C(11A)	46(4)	51(4)	55(5)	-1(3)	7(3)	6(3)
C(12A)	45(4)	44(4)	52(4)	-10(3)	4(3)	7(3)
C(13A)	32(4)	88(5)	41(4)	-7(4)	6(3)	1(4)
C(14A)	44(4)	85(6)	59(5)	8(4)	10(3)	-5(4)
C(15A)	36(4)	62(5)	32(4)	-11(3)	4(3)	11(3)
C(16A)	41(4)	51(4)	31(4)	-9(3)	4(3)	10(3)
C(17A)	67(5)	60(5)	48(5)	-29(4)	-3(4)	6(4)
C(18A)	89(6)	80(6)	56(5)	-24(5)	-29(4)	7(5)
C(19A)	84(6)	107(7)	36(5)	-10(5)	-21(4)	22(5)
C(20A)	59(5)	61(5)	37(4)	-4(3)	4(3)	14(4)
C(21A)	86(6)	73(5)	36(4)	7(4)	8(4)	18(4)
C(22A)	86(6)	50(4)	33(4)	9(3)	5(4)	7(4)
C(23A)	72(5)	52(4)	40(4)	14(3)	-3(4)	14(4)
C(24A)	92(6)	47(4)	40(4)	6(3)	-2(4)	22(4)
C(25A)	118(8)	51(5)	42(5)	-2(4)	11(5)	18(5)
C(26A)	87(6)	62(5)	60(5)	6(4)	9(5)	-4(4)
C(27A)	91(6)	62(5)	49(5)	18(4)	21(4)	2(4)
C(28A)	88(6)	80(6)	49(5)	-7(4)	-3(4)	44(5)
C(29A)	55(5)	65(5)	46(4)	-10(4)	6(4)	24(4)
C(30A)	36(4)	58(5)	46(4)	-17(3)	1(3)	6(3)
C(31A)	34(4)	64(5)	43(4)	-12(4)	11(3)	-2(3)
C(32A)	46(5)	76(5)	58(5)	-27(4)	9(4)	-6(4)
C(33A)	44(5)	110(8)	72(6)	-37(6)	-6(4)	4(5)
C(34A)	52(5)	122(8)	49(5)	-28(5)	-19(4)	37(5)
C(35A)	45(4)	57(4)	48(4)	-5(3)	15(3)	-10(3)
C(36A)	38(4)	45(4)	44(4)	-5(3)	6(3)	-13(3)
C(37A)	37(4)	38(4)	42(4)	6(3)	-5(3)	-11(3)
C(38A)	35(3)	32(3)	43(3)	-4(3)	-4(3)	3(3)
C(39A)	61(5)	37(4)	53(4)	-5(3)	-20(4)	4(3)

C(40A)	60(4)	40(3)	57(4)	-2(3)	0(3)	-11(3)
C(41A)	36(4)	68(5)	54(5)	12(4)	1(3)	-20(4)
C(42A)	41(4)	40(4)	50(4)	-10(3)	0(3)	12(3)
C(43A)	41(4)	45(4)	44(4)	-1(3)	4(3)	-11(3)
C(44A)	114(8)	230(13)	59(6)	-2(7)	-18(5)	80(8)
I(1B)	35(1)	41(1)	58(1)	5(1)	0(1)	-5(1)
I(2B)	36(1)	36(1)	79(1)	12(1)	-1(1)	-4(1)
O(1B)	40(2)	26(2)	58(3)	6(2)	2(2)	-4(2)
O(2B)	43(3)	54(3)	45(3)	-5(2)	-6(2)	1(2)
O(3B)	47(3)	31(2)	42(3)	1(2)	1(2)	-11(2)
O(4B)	36(3)	28(2)	93(4)	17(2)	-8(2)	-2(2)
O(5B)	40(3)	48(3)	45(3)	5(2)	-4(2)	-6(2)
O(6B)	49(3)	39(3)	43(3)	12(2)	-4(2)	-10(2)
O(7B)	32(2)	48(3)	45(3)	4(2)	-6(2)	2(2)
O(8B)	56(7)	73(7)	114(10)	6(7)	2(6)	10(6)
C(1B)	26(3)	33(3)	37(3)	-1(3)	0(3)	-4(3)
C(2B)	42(4)	23(3)	29(3)	-4(2)	1(3)	-1(3)
C(3B)	35(4)	33(4)	35(4)	0(3)	1(3)	5(3)
C(4B)	31(3)	36(4)	43(4)	2(3)	1(3)	-6(3)
C(5B)	39(4)	22(3)	48(4)	5(3)	-7(3)	-3(3)
C(6B)	34(4)	28(3)	48(4)	4(3)	0(3)	2(3)
C(7B)	51(4)	24(3)	61(4)	6(3)	1(3)	1(3)
C(8B)	48(4)	34(4)	40(4)	2(3)	1(3)	-1(3)
C(9B)	45(4)	43(4)	39(4)	-6(3)	2(3)	-10(3)
C(10B)	52(4)	38(4)	47(4)	-3(3)	8(3)	-13(3)
C(11B)	37(4)	32(4)	90(5)	10(3)	-19(3)	0(3)
C(12B)	47(4)	38(4)	60(5)	16(3)	-9(3)	-5(3)
C(13B)	61(5)	47(4)	56(5)	21(3)	6(4)	9(4)
C(14B)	69(5)	38(4)	58(5)	14(3)	6(4)	-1(4)
C(15B)	47(4)	23(3)	42(4)	7(3)	-8(3)	-8(3)
C(16B)	41(4)	31(3)	48(4)	-1(3)	5(3)	-4(3)
C(17B)	40(4)	38(4)	54(5)	-1(3)	-12(3)	-2(3)
C(18B)	45(4)	51(4)	38(4)	3(3)	-4(3)	4(3)
C(19B)	46(4)	42(4)	58(5)	-9(3)	-3(3)	-5(3)
C(20B)	45(4)	27(3)	46(4)	8(3)	-2(3)	-3(3)
C(21B)	37(4)	49(4)	47(4)	3(3)	-6(3)	-9(3)
C(22B)	35(4)	32(3)	50(4)	-7(3)	-2(3)	0(3)
C(23B)	33(4)	41(4)	38(4)	-7(3)	2(3)	4(3)
C(24B)	50(4)	29(4)	45(4)	-12(3)	-3(3)	4(3)
C(25B)	51(5)	42(4)	60(5)	-9(3)	-14(3)	14(3)
C(26B)	51(5)	52(4)	75(5)	-26(4)	-24(4)	11(4)
C(27B)	36(4)	44(4)	62(5)	-20(3)	-10(3)	-2(3)
C(28B)	53(4)	27(3)	56(4)	-5(3)	-9(3)	0(3)
C(29B)	54(4)	24(3)	47(4)	1(3)	-1(3)	-3(3)
C(30B)	45(4)	30(3)	33(4)	4(3)	1(3)	-9(3)
C(31B)	51(4)	30(3)	46(4)	4(3)	10(3)	-16(3)
C(32B)	65(5)	40(4)	53(5)	-4(3)	25(4)	-9(3)
C(33B)	85(6)	39(4)	39(4)	4(3)	-4(4)	-5(4)
C(34B)	65(5)	36(4)	47(4)	7(3)	-14(4)	-7(3)
C(35B)	38(4)	45(4)	68(5)	1(3)	12(3)	-11(3)
C(36B)	71(14)	47(11)	130(20)	24(12)	-64(13)	-16(11)
C(37B)	24(3)	40(4)	55(4)	1(3)	9(3)	4(3)
C(38B)	89(15)	58(12)	190(20)	62(14)	-115(16)	-41(11)
C(39B)	78(13)	85(14)	97(15)	-63(12)	-23(10)	34(11)
C(40B)	60(4)	40(3)	57(4)	-2(3)	0(3)	-11(3)
C(41B)	112(16)	109(16)	52(11)	16(10)	14(10)	-32(12)

C(42B)	49(4)	27(3)	48(4)	1(3)	-9(3)	0(3)
C(43B)	68(5)	115(7)	34(4)	0(4)	-20(4)	-6(5)
C(44B)	114(8)	230(13)	59(6)	-2(7)	-18(5)	80(8)
C(36C)	11(6)	22(7)	32(8)	-2(5)	10(5)	6(5)
C(37C)	24(3)	40(4)	55(4)	1(3)	9(3)	4(3)
C(38C)	35(3)	32(3)	43(3)	-4(3)	-4(3)	3(3)
C(39C)	11(6)	43(7)	25(7)	12(5)	-6(4)	5(5)
C(40C)	60(4)	40(3)	57(4)	-2(3)	0(3)	-11(3)
C(41C)	28(6)	21(6)	21(6)	-8(5)	-5(5)	-1(5)
C(44C)	80(13)	77(12)	34(9)	22(8)	-29(9)	-18(10)
O(8C)	25(4)	28(4)	18(4)	-2(3)	9(3)	3(3)
Cl(2S)	95(8)	140(11)	187(14)	27(10)	-8(8)	7(8)
C(101)	45(4)	44(4)	52(4)	-10(3)	4(3)	7(3)
Cl(1S)	550(50)	820(70)	101(15)	190(30)	-100(20)	-520(60)

Table 4.6. Hydrogen coordinates (x 10^4) and isotropic displacement parameters ($Å^2$x 10^3) for **4.**

	x	y	z	U(eq)
H(3A)	3685	9713	2462	52
H(6A)	4075	7120	2851	55
H(7A1)	4531	6329	2486	66
H(7A2)	5018	6611	2721	66
H(8A1)	5399	5654	2359	68
H(8A2)	5403	6443	2157	68
H(9A1)	5944	7671	2336	62
H(9A2)	6404	7133	2145	62
H(10A)	7103	7076	2539	62
H(10B)	7031	7979	2404	62
H(11A)	2719	10585	2922	61
H(11B)	3428	10438	2836	61
H(12A)	3352	10858	3307	57
H(12B)	2931	10066	3374	57
H(13A)	3604	9736	3706	65
H(13B)	4205	10286	3640	65
H(14A)	4440	8966	3843	75
H(14B)	4177	8540	3566	75
H(17A)	6192	11212	3733	70
H(18A)	6624	10527	4112	90
H(19A)	6334	9181	4209	91
H(21A)	5143	8071	3997	78
H(21B)	5839	7946	4104	78
H(25A)	6044	6293	3066	84
H(26A)	5043	6363	3239	84
H(27A)	4833	7182	3630	81
H(28A)	7396	6778	3369	87
H(28B)	7107	6633	3066	87
H(32A)	7790	10012	2960	72
H(33A)	8324	9303	3295	90
H(34A)	8030	7972	3422	89

H(35A)	6489	9199	2565	60
H(35B)	7087	9739	2486	60
H(39A)	5883	12132	3156	60
H(40A)	6618	12325	2815	63
H(41A)	7018	11204	2579	63
H(42A)	5003	10414	3278	52
H(42B)	5188	11278	3418	52
H(43A)	5025	9358	2949	65
H(43B)	5359	8475	2958	65
H(43C)	5500	9103	2708	65
H(44A)	6785	7193	4074	201
H(44B)	7416	7699	4034	201
H(44C)	7284	6895	3849	201
H(3B)	2840	3379	10228	41
H(6B)	4331	1355	10416	44
H(7B1)	3352	4804	10204	55
H(7B2)	3216	4225	9939	55
H(8B1)	3626	5609	9833	49
H(8B2)	4274	5287	9954	49
H(9B1)	4745	4078	9716	51
H(9B2)	4939	4956	9586	51
H(10C)	4513	4433	9142	55
H(10D)	5168	4054	9237	55
H(11C)	3831	64	10601	64
H(11D)	3899	169	10268	64
H(12C)	3471	-1157	10428	58
H(12D)	2856	-654	10507	58
H(13C)	3450	-1748	9962	66
H(13D)	3871	-930	9960	66
H(14C)	3474	-1438	9507	66
H(14D)	2829	-1029	9601	66
H(17B)	2533	660	8782	53
H(18B)	3309	195	8488	54
H(19B)	4207	-380	8673	58
H(21C)	2061	319	9336	53
H(21D)	2597	674	9536	53
H(25B)	2048	3566	8885	61
H(26B)	1217	2672	8941	71
H(27B)	1376	1382	9168	57
H(28C)	3385	3634	9239	54
H(28D)	3105	3948	8949	54
H(32B)	5036	1903	8532	63
H(33B)	4092	2107	8314	65
H(34B)	3295	2777	8545	59
H(35C)	5777	2454	8941	60
H(35D)	5419	2536	9231	60
H(39B)	5662	-919	8885	104
H(40B)	6324	-10	8715	63
H(41B)	6367	1353	8831	109
H(42C)	4534	-651	9404	50
H(42D)	4671	-1150	9123	50
H(43D)	3223	2660	9665	109
H(43E)	3861	2153	9673	109
H(43F)	3219	1696	9740	109
H(44D)	5000	490	9713	201
H(44E)	4632	1323	9783	201

H(44F)	5321	1368	9660	201
H(39C)	4709	-54	9735	40
H(40C)	5038	1221	9897	79
H(41C)	5359	2258	9595	35
H(44G)	5970	683	8786	95
H(44H)	5578	149	8567	95
H(44I)	5719	-214	8871	95

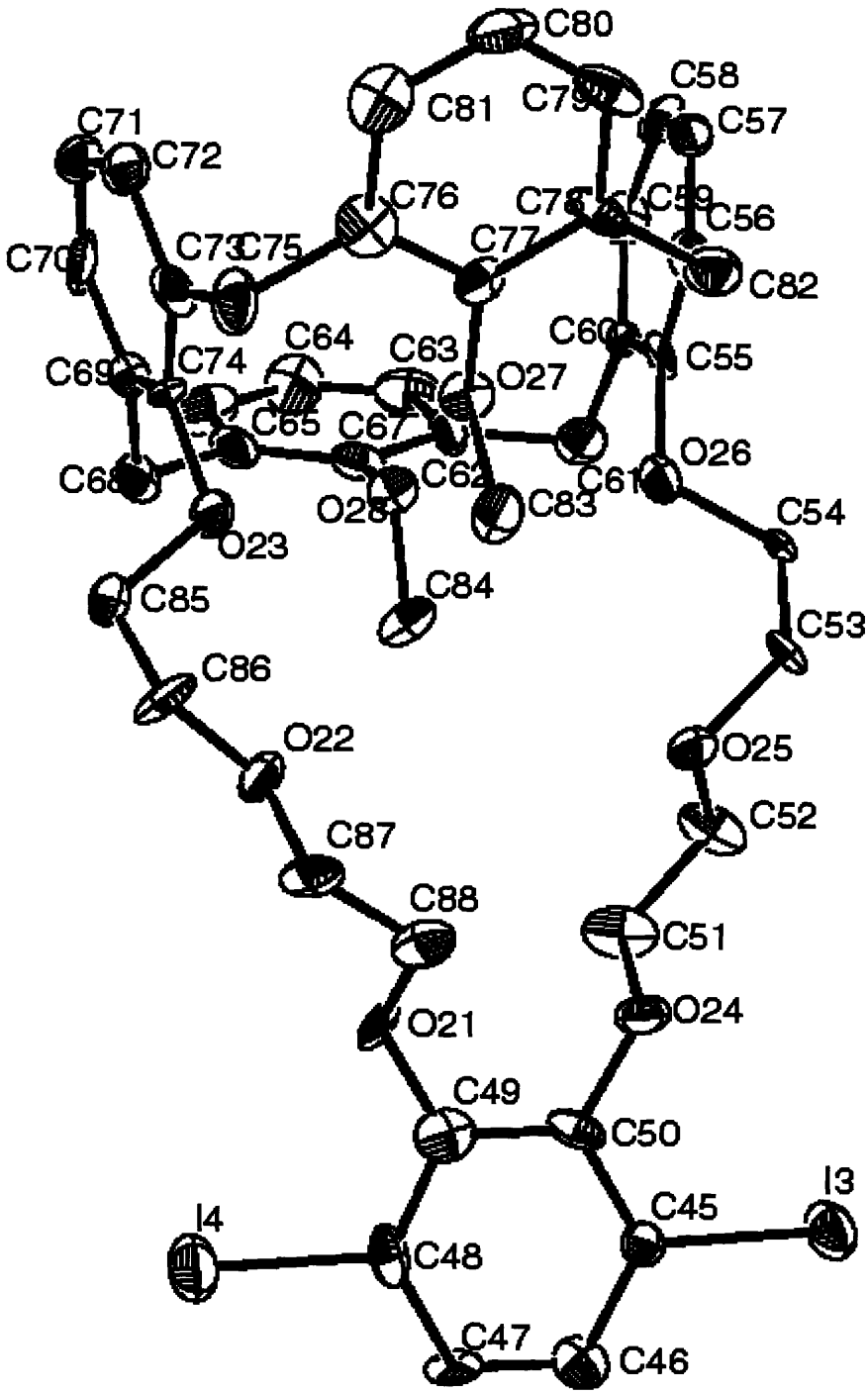

Figure 4.10. One molecule of **6**, showing the crystallographic numbering scheme. Numbering of the other molecule in the asymmetric unit is by an analogous scheme.

Table 4.7. Crystal data and structure refinement for **6.**

Empirical formula	$C_{44.50}\ H_{44}\ Cl\ I_2\ O_8$	
Formula weight	996.05	
Temperature	193(2) K	
Wavelength	0.71073 Å	
Crystal system	Monoclinic	
Space group	P2(1)/c	
Unit cell dimensions	a = 14.7132(7) Å	α= 90°.
	b = 29.5179(14) Å	β= 108.0870(10)°.
	c = 19.9111(10) Å	γ = 90°.
Volume	8220.1(7) $Å^3$	
Z	8	
Density (calculated)	1.610 Mg/m^3	
Absorption coefficient	1.648 mm^{-1}	
F(000)	3984	
Theta range for data collection	1.75 to 22.50°.	
Index ranges	-14<=h<=15, -27<=k<=31, -21<=l<=21	
Reflections collected	33599	
Independent reflections	10740 [R(int) = 0.1131]	
Completeness to theta = 22.50°	99.9 %	
Absorption correction	None	
Refinement method	Full-matrix least-squares on F^2	
Data / restraints / parameters	10740 / 0 / 975	
Goodness-of-fit on F^2	1.349	
Final R indices [I>2sigma(I)]	R1 = 0.0841, wR2 = 0.1466	
R indices (all data)	R1 = 0.1389, wR2 = 0.1587	
Extinction coefficient	0.00014(5)	
Largest diff. peak and hole	0.819 and -0.684 $e.Å^{-3}$	

Table 4.8. Atomic coordinates (x 10^4) and equivalent isotropic displacement parameters ($Å^2$x 10^3) for **6.** U(eq) is defined as one third of the trace of the orthogonalized U^{ij} tensor.

	x	y	z	U(eq)
I(1)	2923(1)	10103(1)	6380(1)	43(1)
I(2)	2833(1)	10366(1)	9827(1)	44(1)
I(3)	11693(1)	7138(1)	6111(1)	38(1)
I(4)	11462(1)	7226(1)	9531(1)	50(1)
Cl(1)	1413(3)	2003(1)	5688(2)	66(1)
Cl(2)	2893(3)	1314(1)	5995(2)	69(1)
O(11)	3555(6)	9446(2)	7685(4)	32(2)
O(12)	3833(6)	8585(2)	7116(4)	26(2)
O(13)	5119(6)	7848(2)	7330(4)	30(2)
O(14)	3352(6)	9523(2)	9038(4)	33(2)
O(15)	3935(6)	8644(2)	9534(4)	34(2)
O(16)	5148(6)	7863(3)	9820(4)	35(2)
O(17)	4695(6)	7353(2)	8483(4)	31(2)
O(18)	6201(7)	8115(3)	8799(4)	32(2)
O(21)	10922(6)	7960(2)	8317(4)	27(2)
O(22)	10546(6)	8866(2)	8814(4)	29(2)

O(23)	9301(6)	9630(2)	8573(4)	26(2)
O(24)	11106(6)	7933(2)	6942(4)	33(2)
O(25)	10460(6)	8806(2)	6409(4)	28(2)
O(26)	9315(5)	9633(2)	6099(4)	26(2)
O(27)	9935(5)	10103(2)	7481(3)	23(2)
O(28)	8172(6)	9466(2)	7083(4)	25(2)
C(1)	3051(9)	10207(4)	7453(6)	36(4)
C(2)	2758(9)	10630(4)	7665(7)	30(3)
C(3)	2752(8)	10665(4)	8349(6)	28(3)
C(4)	2974(9)	10303(4)	8808(6)	26(3)
C(5)	3206(8)	9891(4)	8578(6)	24(3)
C(6)	4333(9)	9402(4)	9381(6)	36(2)
C(7)	4358(10)	9038(4)	9886(6)	41(4)
C(8)	3867(11)	8288(4)	9983(7)	44(4)
C(9)	4769(11)	8057(4)	10346(6)	45(4)
C(10)	5854(10)	7543(4)	10101(6)	25(2)
C(11)	5592(9)	7083(4)	10111(5)	24(2)
C(12)	6289(11)	6773(4)	10449(7)	41(4)
C(13)	7204(11)	6906(5)	10764(7)	45(4)
C(14)	7509(10)	7348(4)	10717(6)	40(4)
C(15)	6813(10)	7665(4)	10387(6)	25(3)
C(16)	7168(9)	8148(4)	10275(6)	36(3)
C(17)	7687(9)	8163(4)	9744(7)	27(3)
C(18)	8658(10)	8170(4)	9955(7)	37(3)
C(19)	9161(9)	8163(4)	9444(6)	32(3)
C(20)	8667(10)	8166(4)	8745(8)	41(4)
C(21)	7656(10)	8162(4)	8505(6)	33(3)
C(22)	7196(10)	8160(3)	9013(6)	24(3)
C(23)	7097(10)	8138(4)	7725(6)	36(4)
C(24)	6763(10)	7661(4)	7499(6)	28(3)
C(25)	7442(10)	7328(4)	7465(6)	35(4)
C(26)	7178(10)	6891(4)	7291(6)	31(3)
C(27)	6233(10)	6764(4)	7202(6)	33(3)
C(28)	5525(9)	7063(4)	7251(6)	31(3)
C(29)	5826(9)	7524(4)	7355(6)	25(3)
C(30)	4520(9)	6911(4)	7178(6)	32(3)
C(31)	4504(8)	6653(4)	7820(6)	29(2)
C(32)	4419(9)	6186(4)	7834(7)	37(4)
C(33)	4381(10)	5957(5)	8445(8)	52(4)
C(34)	4409(10)	6203(5)	9019(8)	50(4)
C(35)	4492(9)	6671(4)	9055(6)	28(2)
C(36)	4541(9)	6880(4)	8450(6)	31(3)
C(37)	4558(9)	6928(4)	9711(6)	40(4)
C(38)	3833(9)	7621(4)	8281(6)	34(3)
C(39)	5699(9)	8531(4)	8693(6)	37(3)
C(40)	4786(9)	8104(4)	6665(6)	34(3)
C(41)	3815(10)	8283(4)	6571(6)	39(4)
C(42)	2940(9)	8767(4)	7053(7)	37(4)
C(43)	2976(9)	9043(3)	7674(7)	34(3)
C(44)	3272(9)	9829(4)	7916(6)	25(3)
C(45)	11626(8)	7155(4)	7139(6)	22(3)
C(46)	11889(9)	6780(4)	7588(6)	29(3)
C(47)	11828(9)	6806(3)	8262(7)	28(3)
C(48)	11499(8)	7193(4)	8485(6)	27(3)
C(49)	11230(9)	7575(4)	8076(7)	31(3)
C(50)	11285(8)	7553(4)	7373(6)	23(3)

C(51)	10102(9)	8038(4)	6601(6)	36(2)
C(52)	10052(9)	8401(4)	6074(6)	33(3)
C(53)	10537(8)	9156(4)	5943(6)	29(3)
C(54)	9688(9)	9407(3)	5580(6)	25(3)
C(55)	8707(9)	9999(4)	5830(5)	24(2)
C(56)	9103(10)	10427(4)	5880(6)	32(3)
C(57)	8467(10)	10787(4)	5598(6)	28(3)
C(58)	7489(11)	10715(4)	5294(6)	37(4)
C(59)	7106(10)	10285(4)	5304(6)	37(4)
C(60)	7725(9)	9913(4)	5579(5)	25(2)
C(61)	7297(9)	9452(4)	5598(6)	30(3)
C(62)	6724(10)	9434(4)	6120(6)	26(3)
C(63)	5713(10)	9432(4)	5906(7)	39(4)
C(64)	5191(10)	9413(4)	6365(7)	41(4)
C(65)	5680(10)	9417(4)	7083(8)	37(4)
C(66)	6663(10)	9424(3)	7337(6)	29(3)
C(67)	7204(9)	9423(3)	6858(6)	25(3)
C(68)	7260(8)	9434(4)	8133(6)	27(3)
C(69)	7687(10)	9902(4)	8362(6)	27(3)
C(70)	7117(10)	10250(5)	8396(6)	37(4)
C(71)	7477(10)	10688(4)	8560(6)	33(3)
C(72)	8420(10)	10777(4)	8692(6)	29(3)
C(73)	9051(10)	10419(4)	8690(5)	28(3)
C(74)	8661(10)	9986(4)	8555(6)	29(3)
C(75)	10086(10)	10526(4)	8799(6)	36(4)
C(76)	10209(8)	10781(4)	8166(6)	29(2)
C(77)	10163(8)	10552(4)	7533(6)	23(3)
C(78)	10229(9)	10784(4)	6939(6)	28(2)
C(79)	10428(8)	11242(4)	7006(7)	35(3)
C(80)	10508(9)	11480(4)	7617(7)	39(4)
C(81)	10393(9)	11249(4)	8189(7)	35(3)
C(82)	10137(9)	10528(4)	6257(6)	31(3)
C(83)	10745(10)	9802(4)	7669(6)	39(4)
C(84)	8650(8)	9039(4)	7197(6)	27(3)
C(85)	9586(9)	9390(4)	9236(6)	30(3)
C(86)	10553(9)	9188(4)	9335(6)	35(4)
C(87)	11467(9)	8667(4)	8935(6)	29(3)
C(88)	11459(10)	8372(4)	8327(7)	40(4)
C(1S)	2653(10)	1892(4)	5939(7)	47(4)

Table 4.9. Bond lengths [Å] and angles [°] for **6.**

I(1)-C(1)	2.109(11)	O(12)-C(42)	1.388(13)
I(2)-C(4)	2.112(11)	O(12)-C(41)	1.400(12)
I(3)-C(45)	2.080(10)	O(13)-C(29)	1.402(13)
I(4)-C(48)	2.103(11)	O(13)-C(40)	1.471(12)
Cl(1)-C(1S)	1.766(14)	O(14)-C(5)	1.395(13)
Cl(2)-C(1S)	1.740(12)	O(14)-C(6)	1.436(13)
O(11)-C(44)	1.336(12)	O(15)-C(7)	1.399(12)
O(11)-C(43)	1.461(12)	O(15)-C(8)	1.403(13)

O(16)-C(10)	1.388(13)
O(16)-C(9)	1.449(12)
O(17)-C(36)	1.414(12)
O(17)-C(38)	1.440(13)
O(18)-C(22)	1.398(14)
O(18)-C(39)	1.416(12)
O(21)-C(49)	1.363(13)
O(21)-C(88)	1.447(13)
O(22)-C(86)	1.405(11)
O(22)-C(87)	1.427(13)
O(23)-C(74)	1.406(12)
O(23)-C(85)	1.440(12)
O(24)-C(50)	1.388(12)
O(24)-C(51)	1.456(13)
O(25)-C(52)	1.411(12)
O(25)-C(53)	1.416(12)
O(26)-C(55)	1.399(12)
O(26)-C(54)	1.473(11)
O(27)-C(77)	1.364(12)
O(27)-C(83)	1.439(13)
O(28)-C(67)	1.360(13)
O(28)-C(84)	1.429(12)
C(1)-C(44)	1.417(15)
C(1)-C(2)	1.429(15)
C(2)-C(3)	1.369(15)
C(3)-C(4)	1.379(14)
C(4)-C(5)	1.377(15)
C(5)-C(44)	1.365(14)
C(6)-C(7)	1.465(15)
C(8)-C(9)	1.468(17)
C(10)-C(15)	1.395(16)
C(10)-C(11)	1.413(15)
C(11)-C(12)	1.382(16)
C(11)-C(37)	1.550(16)
C(12)-C(13)	1.356(17)
C(13)-C(14)	1.392(16)
C(14)-C(15)	1.392(16)
C(15)-C(16)	1.558(15)
C(16)-C(17)	1.485(15)
C(17)-C(18)	1.359(16)
C(17)-C(22)	1.409(15)
C(18)-C(19)	1.433(16)
C(19)-C(20)	1.354(16)
C(20)-C(21)	1.415(17)
C(21)-C(22)	1.380(16)
C(21)-C(23)	1.517(16)
C(23)-C(24)	1.511(14)
C(24)-C(29)	1.379(16)
C(24)-C(25)	1.420(16)
C(25)-C(26)	1.359(15)
C(26)-C(27)	1.397(17)
C(27)-C(28)	1.392(16)
C(28)-C(29)	1.426(16)
C(28)-C(30)	1.508(16)
C(30)-C(31)	1.494(15)
C(31)-C(32)	1.385(14)
C(31)-C(36)	1.409(15)
C(32)-C(33)	1.408(17)
C(33)-C(34)	1.345(17)
C(34)-C(35)	1.385(15)
C(35)-C(36)	1.376(15)
C(35)-C(37)	1.487(16)
C(40)-C(41)	1.478(16)
C(42)-C(43)	1.468(15)
C(45)-C(46)	1.401(14)
C(45)-C(50)	1.410(14)
C(46)-C(47)	1.374(15)
C(47)-C(48)	1.367(15)
C(48)-C(49)	1.375(15)
C(49)-C(50)	1.429(15)
C(51)-C(52)	1.486(14)
C(53)-C(54)	1.439(15)
C(55)-C(56)	1.381(15)
C(55)-C(60)	1.397(16)
C(56)-C(57)	1.414(16)
C(56)-C(82)	1.502(16)
C(57)-C(58)	1.393(16)
C(58)-C(59)	1.392(16)
C(59)-C(60)	1.423(15)
C(60)-C(61)	1.506(15)
C(61)-C(62)	1.528(15)
C(62)-C(63)	1.414(16)
C(62)-C(67)	1.420(15)
C(63)-C(64)	1.365(16)
C(64)-C(65)	1.386(17)
C(65)-C(66)	1.375(16)
C(66)-C(67)	1.420(15)
C(66)-C(68)	1.557(15)
C(68)-C(69)	1.528(15)
C(69)-C(70)	1.342(15)
C(69)-C(74)	1.386(17)
C(70)-C(71)	1.397(16)
C(71)-C(72)	1.355(16)
C(72)-C(73)	1.407(15)
C(73)-C(74)	1.391(15)
C(73)-C(75)	1.503(17)
C(75)-C(76)	1.529(15)
C(76)-C(81)	1.406(15)
C(76)-C(77)	1.413(15)
C(77)-C(78)	1.397(14)
C(78)-C(79)	1.382(14)
C(78)-C(82)	1.521(15)
C(79)-C(80)	1.378(16)
C(80)-C(81)	1.382(15)
C(85)-C(86)	1.499(15)
C(87)-C(88)	1.489(14)

C(44)-O(11)-C(43)	116.9(9)
C(42)-O(12)-C(41)	112.8(9)
C(29)-O(13)-C(40)	114.8(8)
C(5)-O(14)-C(6)	115.6(9)

C(7)-O(15)-C(8)	114.3(9)
C(10)-O(16)-C(9)	112.7(8)
C(36)-O(17)-C(38)	114.5(9)
C(22)-O(18)-C(39)	114.4(9)
C(49)-O(21)-C(88)	117.7(9)
C(86)-O(22)-C(87)	111.4(9)
C(74)-O(23)-C(85)	113.1(8)
C(50)-O(24)-C(51)	115.5(8)
C(52)-O(25)-C(53)	114.7(8)
C(55)-O(26)-C(54)	114.4(7)
C(77)-O(27)-C(83)	114.5(9)
C(67)-O(28)-C(84)	112.5(8)
C(44)-C(1)-C(2)	121.7(10)
C(44)-C(1)-I(1)	118.4(9)
C(2)-C(1)-I(1)	119.0(8)
C(3)-C(2)-C(1)	117.1(10)
C(2)-C(3)-C(4)	121.8(10)
C(5)-C(4)-C(3)	119.8(10)
C(5)-C(4)-I(2)	120.4(8)
C(3)-C(4)-I(2)	119.6(9)
C(44)-C(5)-C(4)	122.5(11)
C(44)-C(5)-O(14)	119.2(10)
C(4)-C(5)-O(14)	118.2(10)
O(14)-C(6)-C(7)	108.4(10)
O(15)-C(7)-C(6)	110.7(9)
O(15)-C(8)-C(9)	115.4(12)
O(16)-C(9)-C(8)	108.6(10)
O(16)-C(10)-C(15)	121.6(11)
O(16)-C(10)-C(11)	119.1(12)
C(15)-C(10)-C(11)	119.2(11)
C(12)-C(11)-C(10)	118.5(12)
C(12)-C(11)-C(37)	121.1(11)
C(10)-C(11)-C(37)	120.3(10)
C(13)-C(12)-C(11)	121.0(13)
C(12)-C(13)-C(14)	122.3(14)
C(15)-C(14)-C(13)	117.1(14)
C(14)-C(15)-C(10)	121.5(11)
C(14)-C(15)-C(16)	116.9(12)
C(10)-C(15)-C(16)	121.3(10)
C(17)-C(16)-C(15)	113.5(9)
C(18)-C(17)-C(22)	118.2(12)
C(18)-C(17)-C(16)	120.2(12)
C(22)-C(17)-C(16)	121.6(11)
C(17)-C(18)-C(19)	120.3(12)
C(20)-C(19)-C(18)	120.0(13)
C(19)-C(20)-C(21)	121.3(12)
C(22)-C(21)-C(20)	117.1(12)
C(22)-C(21)-C(23)	121.2(13)
C(20)-C(21)-C(23)	121.7(12)
C(21)-C(22)-O(18)	118.8(11)
C(21)-C(22)-C(17)	123.1(13)
O(18)-C(22)-C(17)	117.9(11)
C(24)-C(23)-C(21)	111.9(9)
C(29)-C(24)-C(25)	117.3(11)
C(29)-C(24)-C(23)	123.2(11)
C(25)-C(24)-C(23)	119.4(12)
C(26)-C(25)-C(24)	121.3(13)
C(25)-C(26)-C(27)	118.9(12)
C(28)-C(27)-C(26)	123.8(12)
C(27)-C(28)-C(29)	114.2(12)
C(27)-C(28)-C(30)	122.5(12)
C(29)-C(28)-C(30)	123.3(11)
C(24)-C(29)-O(13)	119.3(11)
C(24)-C(29)-C(28)	123.8(11)
O(13)-C(29)-C(28)	116.9(11)
C(31)-C(30)-C(28)	110.2(10)
C(32)-C(31)-C(36)	115.7(11)
C(32)-C(31)-C(30)	123.4(11)
C(36)-C(31)-C(30)	120.9(11)
C(31)-C(32)-C(33)	121.5(12)
C(34)-C(33)-C(32)	118.5(13)
C(33)-C(34)-C(35)	124.1(13)
C(36)-C(35)-C(34)	115.4(12)
C(36)-C(35)-C(37)	122.2(10)
C(34)-C(35)-C(37)	122.3(11)
C(35)-C(36)-C(31)	124.7(11)
C(35)-C(36)-O(17)	117.0(10)
C(31)-C(36)-O(17)	118.2(10)
C(35)-C(37)-C(11)	112.8(11)
O(13)-C(40)-C(41)	109.7(9)
O(12)-C(41)-C(40)	110.1(10)
O(12)-C(42)-C(43)	110.6(10)
O(11)-C(43)-C(42)	109.4(10)
O(11)-C(44)-C(5)	124.7(10)
O(11)-C(44)-C(1)	118.4(10)
C(5)-C(44)-C(1)	116.9(11)
C(46)-C(45)-C(50)	120.2(10)
C(46)-C(45)-I(3)	121.4(8)
C(50)-C(45)-I(3)	118.4(8)
C(47)-C(46)-C(45)	119.3(11)
C(48)-C(47)-C(46)	120.1(11)
C(47)-C(48)-C(49)	124.0(11)
C(47)-C(48)-I(4)	118.7(9)
C(49)-C(48)-I(4)	117.3(9)
O(21)-C(49)-C(48)	122.7(11)
O(21)-C(49)-C(50)	120.6(10)
C(48)-C(49)-C(50)	116.6(11)
O(24)-C(50)-C(45)	119.1(10)
O(24)-C(50)-C(49)	120.7(10)
C(45)-C(50)-C(49)	119.8(10)
O(24)-C(51)-C(52)	107.6(10)
O(25)-C(52)-C(51)	110.9(10)
O(25)-C(53)-C(54)	118.0(10)
C(53)-C(54)-O(26)	109.6(9)
C(56)-C(55)-C(60)	124.0(11)
C(56)-C(55)-O(26)	118.2(11)
C(60)-C(55)-O(26)	117.6(10)
C(55)-C(56)-C(57)	116.5(12)
C(55)-C(56)-C(82)	124.0(11)
C(57)-C(56)-C(82)	119.4(11)
C(58)-C(57)-C(56)	121.7(11)
C(59)-C(58)-C(57)	120.1(12)

C(58)-C(59)-C(60)	119.7(13)
C(55)-C(60)-C(59)	117.7(11)
C(55)-C(60)-C(61)	123.4(10)
C(59)-C(60)-C(61)	118.9(12)
C(60)-C(61)-C(62)	111.8(9)
C(63)-C(62)-C(67)	116.7(11)
C(63)-C(62)-C(61)	123.1(11)
C(67)-C(62)-C(61)	120.2(12)
C(64)-C(63)-C(62)	123.8(13)
C(63)-C(64)-C(65)	118.0(14)
C(66)-C(65)-C(64)	121.9(13)
C(65)-C(66)-C(67)	119.8(12)
C(65)-C(66)-C(68)	124.9(11)
C(67)-C(66)-C(68)	115.3(12)
O(28)-C(67)-C(66)	121.8(11)
O(28)-C(67)-C(62)	118.2(11)
C(66)-C(67)-C(62)	119.6(12)
C(69)-C(68)-C(66)	111.8(9)
C(70)-C(69)-C(74)	117.2(12)
C(70)-C(69)-C(68)	120.2(13)
C(74)-C(69)-C(68)	122.6(11)
C(69)-C(70)-C(71)	121.6(13)
C(72)-C(71)-C(70)	120.9(12)
C(71)-C(72)-C(73)	119.5(12)
C(74)-C(73)-C(72)	117.2(12)
C(74)-C(73)-C(75)	124.0(11)
C(72)-C(73)-C(75)	118.8(11)
C(69)-C(74)-C(73)	123.2(11)
C(69)-C(74)-O(23)	120.0(11)
C(73)-C(74)-O(23)	116.7(12)
C(73)-C(75)-C(76)	111.0(10)
C(81)-C(76)-C(77)	117.2(11)
C(81)-C(76)-C(75)	121.9(11)
C(77)-C(76)-C(75)	120.9(10)
O(27)-C(77)-C(78)	119.5(10)
O(27)-C(77)-C(76)	118.5(10)
C(78)-C(77)-C(76)	121.5(10)
C(79)-C(78)-C(77)	117.8(11)
C(79)-C(78)-C(82)	122.0(11)
C(77)-C(78)-C(82)	120.1(10)
C(80)-C(79)-C(78)	122.8(12)
C(79)-C(80)-C(81)	118.6(11)
C(80)-C(81)-C(76)	121.8(11)
C(56)-C(82)-C(78)	109.9(10)
O(23)-C(85)-C(86)	108.0(9)
O(22)-C(86)-C(85)	112.5(10)
O(22)-C(87)-C(88)	109.7(10)
O(21)-C(88)-C(87)	111.7(10)
Cl(2)-C(1S)-Cl(1)	111.8(7)

Table 4.10. Anisotropic displacement parameters ($Å^2 x\ 10^3$) for **6.** The anisotropic displacement factor exponent takes the form: $-2\pi^2[\ h^2\ a^{*2}U^{11} + ... + 2\ h\ k\ a^*\ b^*\ U^{12}\ ]$

	U^{11}	U^{22}	U^{33}	U^{23}	U^{13}	U^{12}
I(1)	59(1)	35(1)	44(1)	5(1)	29(1)	3(1)
I(2)	41(1)	52(1)	37(1)	-11(1)	11(1)	2(1)
I(3)	59(1)	32(1)	25(1)	0(1)	15(1)	-3(1)
I(4)	89(1)	35(1)	37(1)	-2(1)	35(1)	-5(1)
Cl(1)	70(3)	64(3)	61(3)	-4(2)	17(2)	0(2)
Cl(2)	110(4)	43(2)	57(3)	-2(2)	30(3)	10(2)
O(11)	36(6)	26(5)	45(6)	0(4)	29(5)	7(4)
O(12)	35(6)	19(4)	23(5)	-5(4)	10(4)	6(4)
O(13)	37(6)	25(5)	28(5)	3(4)	12(4)	13(4)
O(14)	42(7)	26(5)	31(5)	4(4)	12(5)	5(4)
O(15)	38(6)	26(5)	35(5)	9(4)	7(5)	6(4)
O(16)	42(6)	41(5)	22(5)	4(4)	10(4)	18(5)
O(17)	26(6)	28(5)	38(5)	-3(4)	10(4)	-1(4)
O(18)	43(7)	33(5)	18(5)	-1(4)	5(5)	-11(5)
O(21)	26(6)	22(5)	46(5)	-6(4)	31(5)	-1(4)
O(22)	32(6)	31(5)	26(5)	-4(4)	14(4)	9(4)
O(23)	34(6)	30(5)	14(4)	0(4)	5(4)	9(4)
O(24)	35(6)	18(5)	53(6)	7(4)	25(5)	7(4)
O(25)	30(6)	27(5)	29(5)	4(4)	11(4)	12(4)
O(26)	29(6)	28(5)	20(5)	6(4)	9(4)	3(4)
O(27)	21(5)	19(5)	27(5)	-8(4)	2(4)	-11(4)
O(28)	18(6)	27(5)	26(5)	-2(4)	2(4)	1(4)
C(1)	37(10)	51(9)	26(8)	13(7)	20(7)	11(7)
C(2)	36(9)	18(7)	46(9)	5(6)	26(7)	-2(6)
C(3)	28(9)	18(7)	51(9)	-19(6)	29(7)	-5(6)
C(4)	30(9)	27(7)	26(7)	14(6)	15(7)	-3(6)
C(5)	8(8)	32(8)	33(8)	-3(7)	7(6)	-3(6)
C(6)	11(6)	32(5)	49(6)	2(5)	-11(5)	-3(4)
C(7)	59(11)	23(8)	19(8)	4(6)	-18(7)	8(7)
C(8)	70(13)	32(8)	44(9)	12(7)	40(9)	25(8)
C(9)	80(13)	39(8)	31(8)	-7(7)	38(9)	11(8)
C(10)	41(7)	24(5)	13(5)	7(4)	13(5)	18(5)
C(11)	32(6)	35(6)	7(4)	14(4)	6(4)	13(5)
C(12)	36(11)	31(8)	57(10)	12(7)	14(8)	13(8)
C(13)	56(13)	48(10)	38(9)	4(7)	23(9)	9(9)
C(14)	41(10)	50(10)	28(8)	5(7)	11(7)	-9(8)
C(15)	38(10)	20(7)	13(7)	0(5)	0(7)	14(7)
C(16)	38(10)	47(9)	14(7)	-12(6)	-4(7)	3(7)
C(17)	8(9)	24(7)	48(10)	-10(6)	7(7)	-2(6)
C(18)	33(10)	35(8)	40(9)	-3(6)	8(8)	-4(7)
C(19)	28(9)	26(8)	27(8)	-4(6)	-12(7)	-7(6)
C(20)	23(10)	44(9)	63(11)	-9(8)	24(9)	-7(7)
C(21)	47(11)	29(8)	22(8)	12(6)	8(8)	12(7)
C(22)	40(10)	12(7)	15(7)	-2(5)	2(7)	-2(6)
C(23)	65(11)	28(8)	24(8)	3(6)	29(8)	-10(7)
C(24)	47(11)	22(7)	17(7)	-6(5)	13(7)	2(7)
C(25)	50(11)	35(9)	27(8)	-5(6)	23(7)	-2(7)
C(26)	42(11)	33(9)	15(7)	3(6)	3(7)	13(7)
C(27)	48(11)	28(8)	21(7)	0(6)	10(7)	12(8)

C(28)	29(10)	36(9)	20(7)	1(6)	-5(6)	15(7)
C(29)	21(9)	34(8)	22(7)	6(6)	9(6)	12(7)
C(30)	26(9)	34(8)	26(8)	8(6)	-8(7)	3(7)
C(31)	6(6)	41(6)	35(6)	1(5)	-1(4)	-4(4)
C(32)	23(9)	19(8)	61(10)	-10(7)	1(7)	1(6)
C(33)	32(11)	51(10)	62(11)	6(9)	0(9)	-20(8)
C(34)	29(10)	55(10)	73(12)	4(9)	27(9)	-17(8)
C(35)	29(6)	20(5)	34(6)	10(4)	5(5)	-11(4)
C(36)	31(9)	11(7)	43(9)	1(6)	2(7)	-3(6)
C(37)	43(10)	31(8)	38(9)	20(7)	0(7)	7(7)
C(38)	24(9)	24(7)	53(9)	0(6)	11(7)	-14(7)
C(39)	27(9)	32(8)	52(9)	-4(7)	11(7)	7(7)
C(40)	46(11)	36(8)	17(8)	-1(6)	5(7)	13(7)
C(41)	51(11)	54(9)	7(7)	11(6)	3(7)	16(8)
C(42)	15(9)	41(8)	51(9)	-27(7)	4(7)	7(7)
C(43)	28(9)	11(7)	70(10)	-6(6)	26(8)	3(6)
C(44)	24(9)	39(8)	17(7)	13(6)	13(6)	5(6)
C(45)	19(8)	24(7)	25(7)	3(6)	9(6)	1(6)
C(46)	34(9)	20(7)	31(8)	-3(6)	7(7)	-9(6)
C(47)	41(10)	1(6)	48(9)	-2(6)	21(7)	-1(6)
C(48)	19(8)	41(8)	24(7)	4(7)	12(6)	-10(7)
C(49)	22(9)	24(8)	50(9)	-1(7)	15(7)	-9(6)
C(50)	21(8)	14(7)	26(8)	6(6)	-3(6)	-5(6)
C(51)	11(6)	32(5)	49(6)	2(5)	-11(5)	-3(4)
C(52)	13(8)	37(8)	36(8)	15(7)	-10(6)	-3(6)
C(53)	13(8)	40(8)	42(8)	35(7)	22(7)	20(6)
C(54)	47(10)	16(6)	20(7)	11(5)	22(7)	12(6)
C(55)	32(6)	35(6)	7(4)	14(4)	6(4)	13(5)
C(56)	52(11)	30(8)	12(7)	0(6)	9(7)	0(8)
C(57)	48(11)	15(7)	25(8)	-4(6)	19(7)	-5(7)
C(58)	61(13)	30(8)	23(8)	-9(6)	19(8)	10(8)
C(59)	42(10)	38(9)	34(8)	1(7)	16(7)	5(8)
C(60)	41(7)	24(5)	13(5)	7(4)	13(5)	18(5)
C(61)	28(9)	35(8)	23(7)	3(6)	2(6)	12(6)
C(62)	35(10)	26(7)	18(7)	3(6)	11(7)	-4(6)
C(63)	36(11)	25(8)	47(9)	-1(6)	0(8)	-4(7)
C(64)	37(10)	42(9)	45(10)	-8(7)	12(9)	-10(7)
C(65)	19(10)	34(8)	62(11)	-4(7)	18(8)	1(7)
C(66)	46(11)	15(7)	24(8)	0(5)	10(8)	-8(6)
C(67)	21(9)	17(7)	37(9)	6(6)	8(7)	0(6)
C(68)	20(8)	33(8)	35(8)	12(6)	17(7)	3(6)
C(69)	35(10)	26(7)	23(7)	5(6)	14(7)	9(7)
C(70)	44(10)	56(10)	19(8)	-1(7)	21(7)	12(8)
C(71)	39(11)	36(9)	26(8)	7(6)	14(7)	21(7)
C(72)	37(10)	30(8)	16(7)	-1(6)	4(7)	6(7)
C(73)	40(10)	30(8)	11(7)	7(6)	2(6)	3(7)
C(74)	50(11)	16(7)	29(8)	8(6)	26(7)	20(7)
C(75)	51(11)	37(8)	24(8)	-10(6)	18(7)	-13(7)
C(76)	6(6)	41(6)	35(6)	1(5)	-1(4)	-4(4)
C(77)	17(8)	18(7)	40(8)	-6(6)	17(7)	-6(6)
C(78)	29(6)	20(5)	34(6)	10(4)	5(5)	-11(4)
C(79)	18(9)	31(8)	54(10)	23(7)	7(7)	3(6)
C(80)	43(11)	21(7)	56(10)	-2(7)	18(8)	8(7)
C(81)	23(9)	40(9)	38(9)	-14(7)	5(7)	-14(7)
C(82)	29(9)	28(7)	35(8)	5(6)	8(7)	6(6)
C(83)	51(11)	33(8)	42(9)	-3(6)	27(8)	2(7)

C(84)	17(8)	29(7)	30(8)	-13(6)	-1(6)	4(6)
C(85)	44(10)	29(7)	19(7)	-4(6)	14(7)	5(7)
C(86)	34(10)	31(8)	40(9)	-14(7)	12(7)	15(7)
C(87)	22(9)	27(7)	29(8)	1(6)	-4(6)	13(6)
C(88)	37(10)	35(8)	49(9)	5(7)	16(8)	16(7)
C(1S)	63(12)	46(9)	33(8)	-6(7)	16(8)	-6(8)

Table 4.11. Hydrogen coordinates (x 10^4) and isotropic displacement parameters ($Å^2$x 10^3) for **6.**

	x	y	z	U(eq)
H(2)	2580	10872	7352	36
H(3)	2593	10941	8509	34
H(6A)	4684	9663	9626	43
H(6B)	4627	9302	9034	43
H(7A)	5016	8975	10160	49
H(7B)	4019	9133	10210	49
H(8A)	3418	8066	9708	52
H(8B)	3603	8407	10337	52
H(9A)	5223	8270	10638	54
H(9B)	4659	7819	10649	54
H(12)	6127	6469	10460	50
H(13)	7645	6694	11020	54
H(14)	8150	7428	10899	48
H(16A)	6622	8350	10126	43
H(16B)	7587	8259	10723	43
H(18)	8998	8178	10435	44
H(19)	9825	8158	9591	38
H(20)	9000	8170	8417	49
H(23A)	6547	8337	7627	43
H(23B)	7498	8243	7451	43
H(25)	8081	7409	7564	42
H(26)	7618	6681	7232	37
H(27)	6067	6461	7104	39
H(30A)	4105	7173	7118	39
H(30B)	4284	6721	6763	39
H(32)	4387	6020	7430	44
H(33)	4337	5643	8451	62
H(34)	4370	6050	9418	60
H(37A)	4325	6739	10021	48
H(37B)	4148	7193	9590	48
H(38A)	3434	7527	7822	50
H(38B)	3995	7935	8265	50
H(38C)	3498	7579	8619	50
H(39A)	6016	8739	9062	56
H(39B)	5058	8481	8701	56
H(39C)	5681	8656	8244	56
H(40A)	4776	7909	6272	41
H(40B)	5221	8353	6675	41
H(41A)	3581	8437	6119	47

H(41B)	3385	8034	6572	47
H(42)	2395	8721	6669	45
H(43A)	2334	9131	7657	41
H(43B)	3252	8867	8101	41
H(46)	12101	6515	7432	35
H(47)	12011	6561	8567	34
H(51A)	9810	8140	6949	43
H(51B)	9763	7771	6370	43
H(52A)	10390	8304	5751	39
H(52B)	9390	8454	5801	39
H(53)	11119	9222	5873	35
H(54A)	9207	9203	5290	30
H(54B)	9835	9631	5273	30
H(57)	8707	11080	5615	33
H(58)	7091	10954	5084	44
H(59)	6448	10240	5131	45
H(61A)	7804	9228	5731	36
H(61B)	6881	9375	5129	36
H(63)	5385	9445	5425	47
H(64)	4527	9398	6201	49
H(65)	5334	9415	7402	44
H(68A)	6855	9349	8415	33
H(68B)	7773	9213	8219	33
H(70)	6467	10199	8308	44
H(71)	7063	10923	8579	39
H(72)	8649	11071	8784	35
H(75A)	10450	10246	8867	43
H(75B)	10333	10708	9222	43
H(79)	10512	11397	6622	42
H(80)	10636	11789	7644	47
H(81)	10439	11408	8602	42
H(82A)	10399	10710	5955	37
H(82B)	10496	10248	6364	37
H(83A)	11173	9884	7411	58
H(83B)	10530	9496	7554	58
H(83C)	11071	9825	8166	58
H(84A)	9036	9014	7683	40
H(84B)	9051	9015	6899	40
H(84C)	8186	8799	7086	40
H(85A)	9127	9153	9232	36
H(85B)	9611	9597	9620	36
H(86A)	10998	9428	9323	42
H(86B)	10777	9046	9796	42
H(87A)	11633	8489	9366	35
H(87B)	11943	8903	8991	35
H(88A)	11180	8536	7890	48
H(88B)	12112	8295	8357	48
H(1S1)	2918	2027	5597	56
H(1S2)	2962	2031	6394	56

References

(1) Gutsche, C. D. *Calixarenes*; Royal Society of Chemistry: Cambridge, 1989.

(2) Gutsche, C. D. *Calixarenes Revisited;* Royal Society of Chemistry: Cambridge, 1998.

(3) *Calixarenes in Action;* Mandolini, L., Ungaro, R., Eds.; Imperial College Press: London, 2000.

(4) *Calixarenes 2001;* Asfari, Z., Ed.; Kluwer Academic Publishers: Dordrecht, 2001.

(5) Gutsche, C. D.; Levine, J. A.; Sujeeth, P. K. *J. Org. Chem.* **1985,** *50,* 5802.

(6) Gutsche, C. D.; Iqbal, M. *Org. Synth.* **1989,** *68*, 234 (collective volume *8,* 75).

(7) A good source of practical procedures for calixarene syntheses can be found in Arduini, A.; Casnati, A.; in *Macrocycle Synthesis: a Practical Approach;* Parker, D., Ed.; Oxford University Press: Oxford, 1996, chapter 7.

(8) van Loon, J.-D.; Verboom, W.; Reinhoudt, D. N. *Org. Prep. Proc. Int.* **1992,** *24,* 437.

(9) Boehmer, V. *Agnew. Chem. Int. Ed. Engl.* **1995,** *34*, 713. Also see relevant sections of references 1 and 2.

(10) Selected examples: (a) Arnaud-Neu, F.; Barboso, S.; Berny, F.; Casnati, A.; Muzet, N.; Pinalli, A.; Ungaro, R.; Schwing-Weill, M.-J.; Wipff, G. *J. Chem. Soc. Perkin Trans. 2,* **1999,** 1727. (b) Casnati, A.; Ting, Y.; Berti, D.; Fabbi, M.; Pochini, A.; Ungaro, R.; Sciotto, D.; Lombardo, G. G. *Tetrahedron* **1993,** *49,* 9815. (c) van der Veen, N. J.; Egberink, R. J. M.; Engbersen, J. F. J.; van Veggel, F. J. C. M.; Reinhoudt, D. N. *J. Chem. Soc. Chem. Commun.* **1999,** 681. (d) Sato, N.; Shinkai, S. *J. Chem. Soc. Perkin Trans. 2*, **1993,** 621. See also Ikeda, A.; Shinkai, S. *Chem. Rev.* **1997,** *97,* 1713.

(11) For an early example, see Arduini, A.; Pochini, A.; Reverberi, S.; Ungaro, R. *Tetrahedron* **1986,** *42,* 2089.

(12) Haverlock, T. J.; Mirzadeh, S.; Moyer, B. A. *J. Am. Chem. Soc.* **2003,** *125,* 1126.

(13) Casnati, A.; Pochini, A.; Ungaro, R; Bocchi, C; Ugozzoli, F; Egberink, R. J. M.; Struijk, H; Lugtenberg, R.; de Jong, F.; Reinhoudt, D. N. *Chem. Eur. J.* **1996,** *2,* 436.

(14) (a) Ma, J. C.; Dougherty, D. A. *Chem. Rev.* **1997,** *97,* 1303. (b) Dougherty, D. A. *Science* **1996,** *271,* 163.

(15) Lhotak, P.; Shinkai, S. *J. Phys. Org. Chem.* **1997,** *10,* 273.

(16) (a) Ghidini, E.; Ugozzoli, F.; Ungaro, R.; Harkema, S.; El-Fadl, A.-A.; Reinhoudt, D. N. *J. Am. Chem. Soc.* **1990,** *112,* 6979. (b) Guillon, J.; Léger, J.-M.; Sonnet, P.; Jarry, C.; Robba, M. *J. Org. Chem.* **2000,** *65,* 8283.

(17) (a) Asfari, Z.; Bressot, C.; Vicens, J.; Hill, C.; Dozol, J.-F.; Rouquette, H.; Eymard, S.; Lamare, V.; Toumois, B. *Anal. Chem.* **1995,** *67,* 3133. (b) Thuéry, P.; Nierlich, M.; Bryan, J. C.; Lamare, V.; Dozol, J.-F.; Asfari, Z.; Vicens, J. *J. Chem. Soc. Dalton Trans.* **1997,** 4191.

(18) Crawford, K. B.; Goldfinger, M. B.; Swager, T. M. *J. Am. Chem. Soc.* **1998,** *120,* 5187.

(19) Atwood, J. L.; Koutsantonis, G. A.; Raston, C. L. *Nature* **1994,** *368,* 229.

(20) See Dalla Cort, A.; Mandolini, L. Chapter 5 in reference 3.

(21) Araki, K.; Hisaichi, K.; Kanai, T.; Shinkai, S. *Chem. Lett.* **1995,** 569.

(22) Arduini, A.; Pochini, A.; Secchi, A. *Eur. J. Org. Chem.* **2000,** 2325.

(23) (a) Araki, K.; Hayashida, H. *Tet. Lett.* **2000,** *41,* 1209. (b) Araki, K.; Watanabe, T.; Oda, M.; Hayashida, H.; Yasutake, M.; Shinmyozu, T. *Tet. Lett.* **2001,** *42,* 7465.

(24) van Loon, J.-D.; Arduini, A.; Coppi, L.; Verboom, W.; Pochini, A.; Ungaro, R.; Harkema, S.; Reinhoudt, D. N. *J. Org. Chem.* **1990,** *55,* 5639.

(25) Zhou, Q.; Swager, T. M. *J. Am. Chem. Soc.* **1995,** *117,* 12593.

(26) Vreekamp, R. H.; Verboom, W.; Reinhoudt, D. N. *J. Org. Chem.* **1996,** *61,* 4282.

(27) A related procedure has been published: Kelderman, E.; Derhaeg, L.; Heesink, G. J. T.; Verboom, W.; Engbersen, J. F. J.; van Hulst, N. F.; Persoons, A.; Reinhoudt, D. N. *Agnew. Chem. Int. Ed. Engl.* **1992,** *31,* 1075.

(28) Reduction of a related nitrocalixarene: Zeng, C.-C.; Zheng, Q.-Y.; Tang, Y.-L.; Huang, Z.-T. *Tetrahedron* **2003,** *59,* 2539.

(29) Yu, H.-H. Ph.D. Thesis, Massachusetts Institute of Technology, 2003.

(30) Zhu, Z.; Swager, T. M. *Org. Lett.* **2001,** *3,* 3471.

(31) Swager, T. M.; Gil, C. J.; Wrighton, M. S. *J. Phys. Chem.* **1995,** *99,* 4886.

(32) Dockery, K. P.; Dinnocenzo, J. P.; Farid, S.; Goodman, J. L.; Gould, I. R.; Todd, W. P. *J. Am. Chem. Soc.* **1997,** *119,* 1876.

Jordan H. Wosnick

EDUCATION

Ph.D., organic chemistry (2004)
Massachusetts Institute of Technology, Cambridge, MA, USA
Thesis title: New sensor applications of poly(phenylene ethynylene)s
Advisor: Prof. Timothy Swager

B.Sc. (Hons. First Class), chemistry (1998)
McGill University, Montreal, QC, Canada
Thesis title: Reactions of cubane derivatives with sulfur and bivalent sulfur compounds
Advisors: Profs. David Harpp and Patrick Farrell

PROFESSIONAL EXPERIENCE

Graduate assistant, Massachusetts Institute of Technology (1998-2004)
Advisor: Prof. Timothy Swager
· Prepared and studied new electronically conjugated polymers modified with biomolecules and synthetic macrocycles
· Co-authored two short reviews related to ongoing research in the field
· Responsible for research group computer facilities
· *Teaching assistant activities:* Taught several sections of general and introductory organic chemistry, assisted in preparing and grading exams

Teaching assistant, McGill University (1997-98)
· Responsible for supervision of introductory organic chemistry laboratory classes in both regular and summer school term

Research Assistant, McGill University (1995-97)
Advisors: Prof. Denis Gilson, Profs. David Harpp and Patrick Farrell
· Synthesized and analyzed solid-state magnetic resonance properties of tin- and phosphorus-substituted transition metal carbonyl complexes (Gilson group)
· Studied methods for the preparation of sulfur-substituted cubane compounds (Harpp and Farrell groups)

AWARDS

MIT Wyeth-Ayerst Scholar (2002)
MIT Chemistry Dept Award for Excellence in Graduate Teaching (1999)
NSERC Post-Graduate Scholarship (1998, declined)
ICI Award in Chemistry, McGill University (1998)
Canada Scholarship in Science and Engineering (1994-98)
J.W. McConnell Scholarship, McGill University (1994-98)

PUBLICATIONS AND PRESENTATIONS

Wosnick, Jordan H.; Swager, Timothy M. Poly(phenylene ethynylene)-based systems for biosensing. Oral presentation at the 226th American Chemical Society National Meeting, New York, September 2003.

Wosnick, Jordan H.; Swager, Timothy M. Synthesis and properties of calix[4]arene-containing poly(phenylene ethynylene)s. Oral presentation at the 224th American Chemical Society National Meeting, Boston, August 2002.

Swager, Timothy M.; **Wosnick, Jordan H.** Self-amplifying semiconducting polymers for chemical sensors. Review article in *MRS Bulletin* (2002), 27(6), 446-450.

Priefer, Ronny; Lee, Yoon Joo; Barrios, Fabiola; **Wosnick, Jordan H.;** Lebuis, Anne-Marie; Farrell, Patrick G.; Harpp, David N.; Sun, Aiming; Wu, Shaoxiong; Snyder, James P. Dicubyl disulfide. *Journal of the American Chemical Society* (2002), 124(20), 5626-5627.

Geller, Jordan M.; **Wosnick, Jordan H.;** Butler, Ian S.; Gilson, Denis F.R.; Morin, Frederick G.; Bélanger-Gariépy, Françoise. X-ray diffraction, Raman spectroscopic, and solid-state NMR studies of the group 14 metal-(tetracarbonyl)cobalt complexes $Ph_3MCo(CO)_4$ (M = Si, Sn, Pb). *Canadian Journal of Chemistry* (2002), 80(7), 813-820.

Christendat, Dharamdat; **Wosnick, Jordan H.;** Butler, Ian S.; Gilson, Denis F.R.; Lebuis, Anne-Marie; Morin, Frederick G. Structural and spectroscopic studies of bis(pentacarbonylmanganese)diphenyltin(IV) and bis(pentacarbonylmanganese)diphenyllead(IV). *Journal of Molecular Structure* (2001), 559(1-3), 235-243.

Wosnick, Jordan H.; Swager, Timothy M. Molecular photonic and electronic circuitry for ultra-sensitive chemical sensors. Review article in *Current Opinion in Chemical Biology* (2000), 4(6), 715-720.

Wosnick, Jordan H.; Morin, Frederick G.; Gilson, Denis F.R. 31P chemical shift anisotropies of trimethyl- and triphenylphosphine-substituted Group VIB metal pentacarbonyl complexes. *Canadian Journal of Chemistry* (1998), 76(9), 1280-1283.

Acknowledgements

> Joshua the son of Perachyah used to say: Find a teacher for yourself, acquire a friend for yourself, and give every person the benefit of the doubt.
>
> — *Mishnah Avot (Ethics of the Fathers) 1:6*

I don't think that I really knew what I was getting into when I decided to come to MIT for graduate school. In fact, I'm still not completely sure that I know what I'm doing, even so many years on. Just the same, I'm willing to put my faith in the fact that in life, things usually work out for the best. The reason this happens is because of the good will and friendship of the people we meet along the way, I think — that's why we thank them in our Ph.D. dissertations, even though the acknowledgements may be sandwiched in between lists of references and mind-numbing pages of NMR spectra.

That said, the first person to thank has to be Prof. Tim Swager. I was initially drawn to his group by the interdisciplinary nature of his research, but was quickly won over by his creative ideas and easy-going nature. It was clear right from the beginning that I was dealing with someone who operated on a different mental plane than most people you're likely to meet. Over time I realised that doing a Ph.D. is as much about apprenticeship as it is about research or classes, and I couldn't have found a better mentor than Tim in that regard. His creativity and open-mindedness in research are inspiring, and the way he interacts with the group — openly and honestly, and with a perpetually upbeat attitude — explains why he has so many fans among his students and in the wider world of chemistry. I've learned a tremendous amount from him and will always be grateful for his help and guidance.

Day-to-day life in the lab was made interesting and entertaining by the seemingly endless stream of students and post-docs that came and went during my time in the group. Although they all made contributions to my MIT experience, there are several people that I have to single out. Alex Paraskos and I joined the group together after a somewhat overwhelming first semester at MIT and went through the various grad-school rites of passage at the same time. I had fun sharing a bay with him for a few years and really appreciated having someone in the group to commiserate and listen to loud jazz with. Bruce Yu taught me a lot about the practical side of chemistry and Broadway musicals. He and the rest of the crowd one year ahead of me — Tim Long, J.D. Tovar and Aimee Rose — also provided lots of valuable tips about how to survive grad school. Among the many post-docs that came through the group, I have to especially thank Tyler McQuade, whose mentorship and honest advice have meant a lot to me. His approach to science and life is inspiring and I'm glad that we had a chance to work together, however brief our collaboration was.

I got to know a different group of people after moving into the newly renovated labs down the hall. As the research in our shared space in 18-144 began to coalesce around some common goals, the easy-going rapport among our little biosensor crowd grew

stronger, and the support and friendship of Kenichi Kuroda, Jessica Liao, and Vanessa Perez was really valuable to me. Sam Thomas didn't share our physical space, but was a frequent visitor who was always willing to answer my questions about fluorescence and to be a sounding-board for some crazy ideas. I particularly have to thank Juan Zheng and Gigi Bailey, whose tolerance of my messy habits in our closely shared lab and office quarters continues to amaze me. I really enjoyed the time I spent with them, and their companionship and support made a huge difference to me in my last couple of years at MIT. I'll always be thankful for that.

Karen Warren, Richard Lay and Rebekah Bjork made things run smoothly around the lab and helped me considerably. Outside of the Swager group, Dr. Charlene Mello and Jen Burzycki of the US Army Natick Soldier Center helped me take my first baby-steps in the world of biochemistry, provided me with a lot of advice, and generously devoted a lot of their time to helping me out. Prof. Alice Ting and Marta Fernandez Suarez also taught me a lot of biochemistry through our collaboration on the antibody project, and I'm grateful for their patience and efforts in that area. I must thank Dr. Mark Wall of the MIT DCIF for his help with experimental aspects of NMR spectrometry, Dr. Bill Davis of the MIT X-ray crystallography lab for solving the tricky calixarene crystal structures presented in Chapter 4, and the MIT Institute for Soldier Nanotechnologies for the use of their HPLC instrument. Outside of the chemistry world, my good friend Arvind Govindarajan taught me biology and provided a lot of valuable experimental and moral support.

Of course, none of this would have been possible without the support and encouragement of my whole family, who have always helped see me through the rough spots and kept me moving forward. They were always patient with my prolonged absence, even when I was needed back home, and I'm glad that we'll now be able to spend more time together.

Most of all, I have to thank Caroline. She made the difference when it really mattered and it is her love, support, and patience that has gotten me through this experience. I can't even begin to tell how much that means to me, but I think she knows.

The research described in this dissertation was supported primarily by the Office of Naval Research and by the NASA Fundamental Technologies for Biomolecular Sensors program.

Appendix
^{1}H and ^{13}C NMR spectra

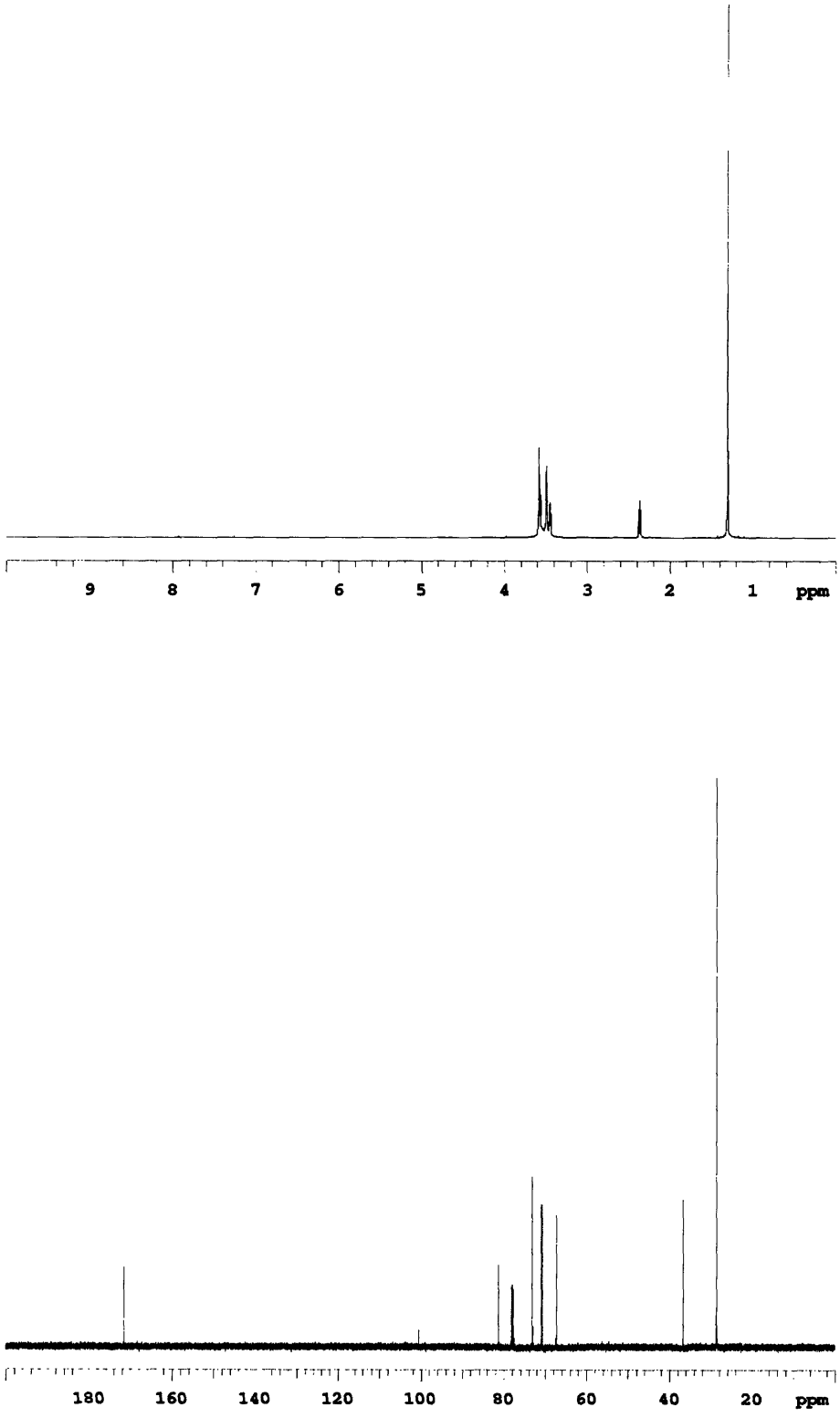

^{1}H (top) and ^{13}C (bottom) NMR spectra of **3** (Chapter 2).

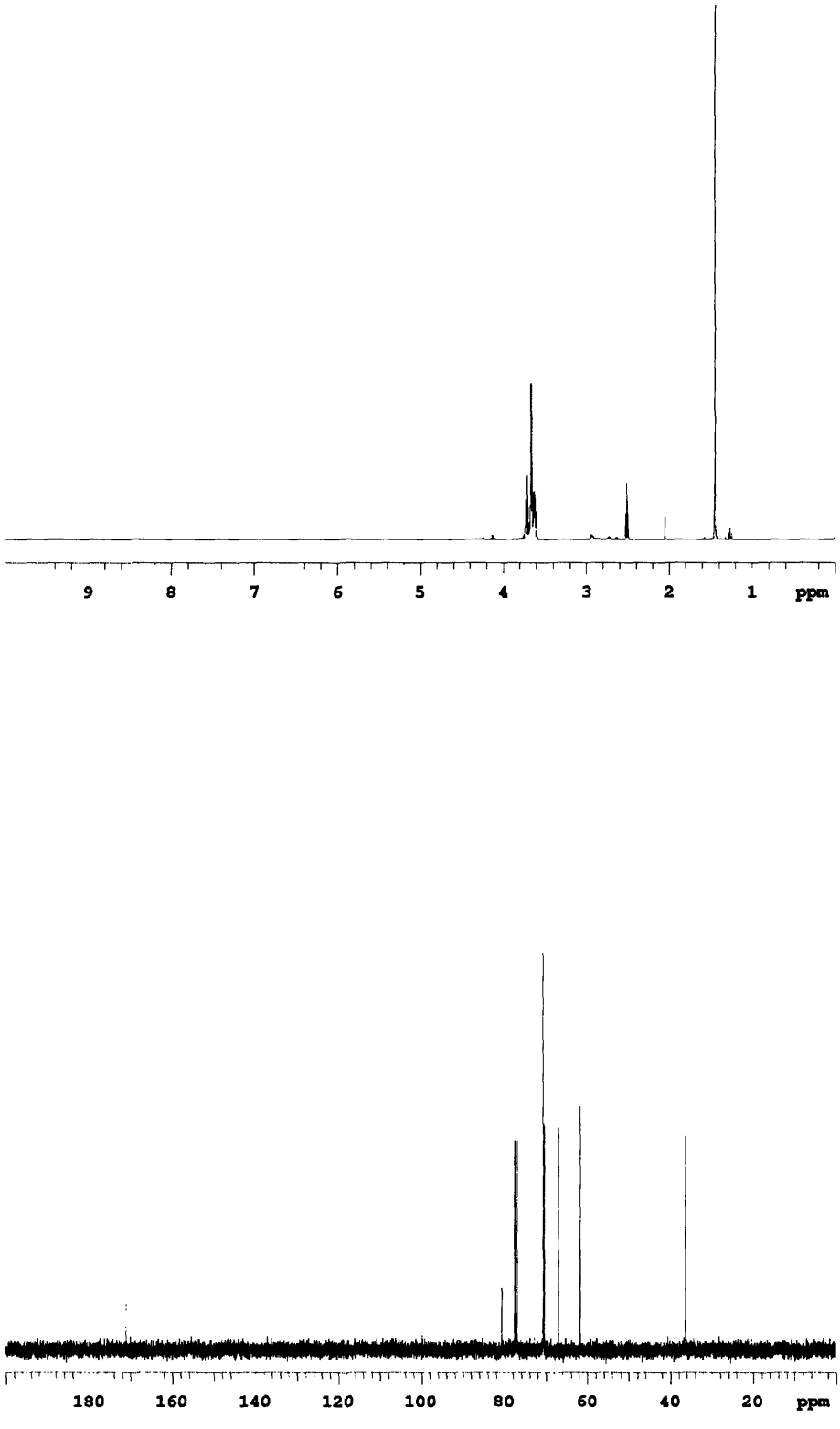

^{1}H (top) and ^{13}C (bottom) NMR spectra of **4** (Chapter 2).

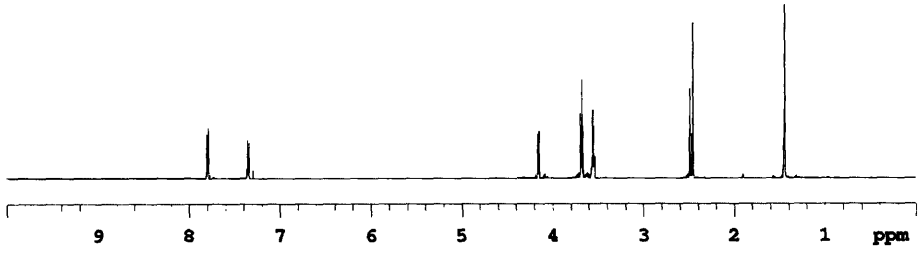

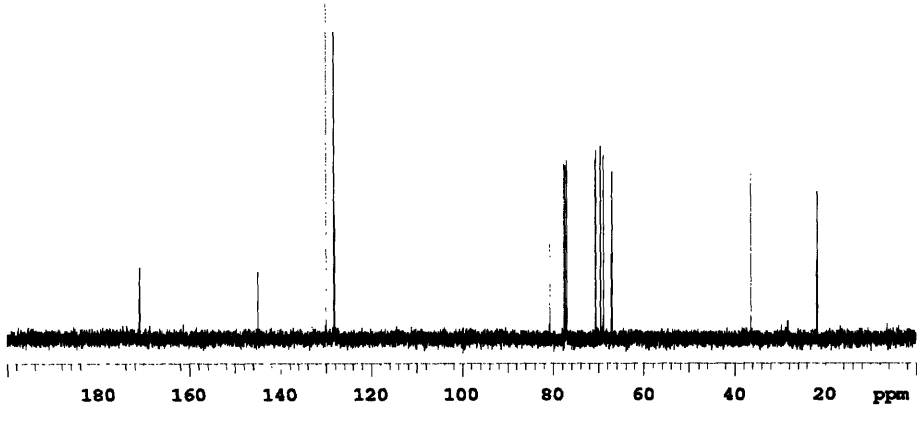

^{1}H (top) and ^{13}C (bottom) NMR spectra of **5** (Chapter 2).

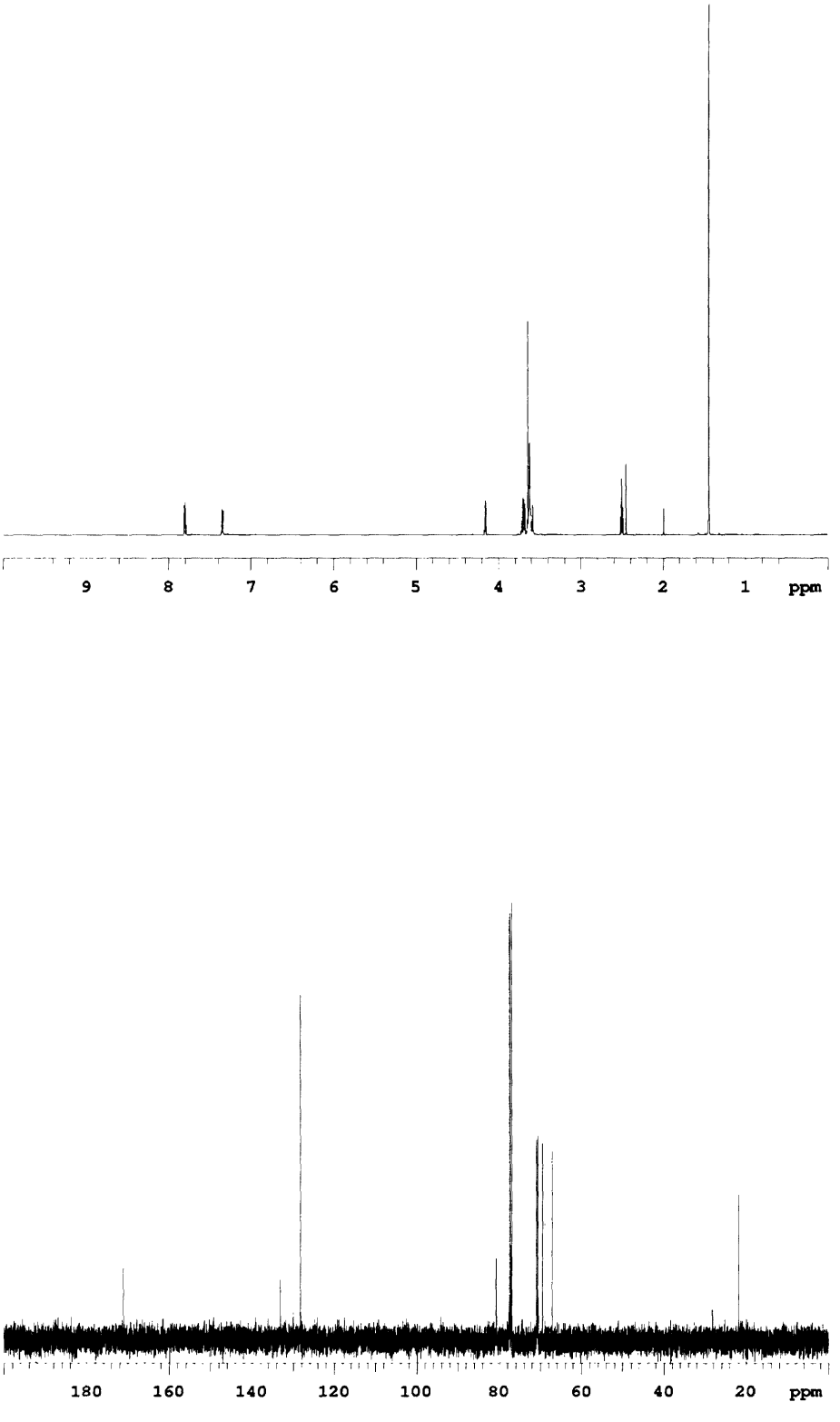

^{1}H (top) and ^{13}C (bottom) NMR spectra of **6** (Chapter 2).

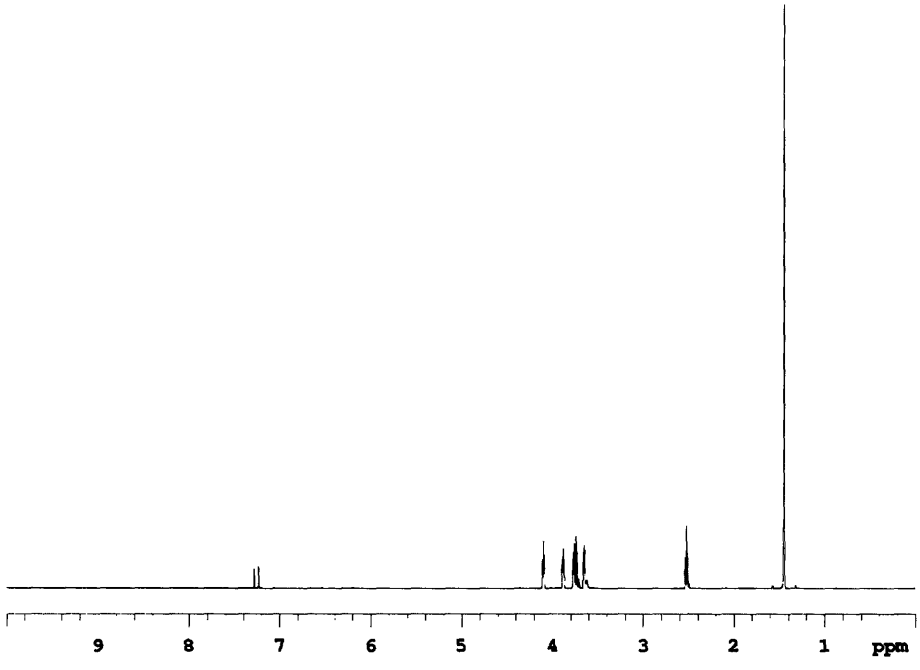

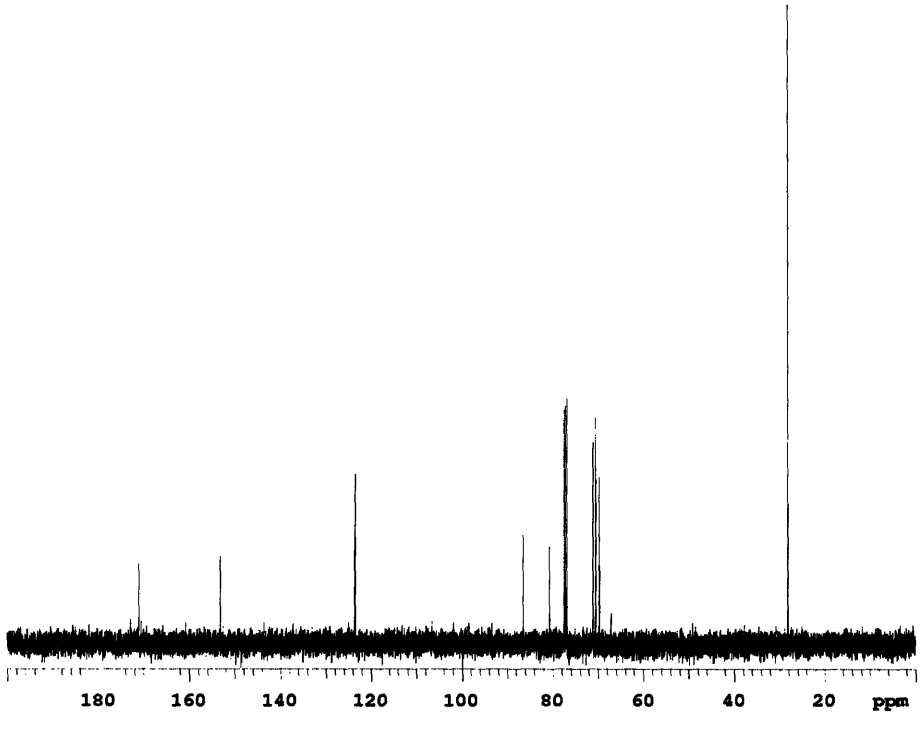

^{1}H (top) and ^{13}C (bottom) NMR spectra of **7** (Chapter 2).

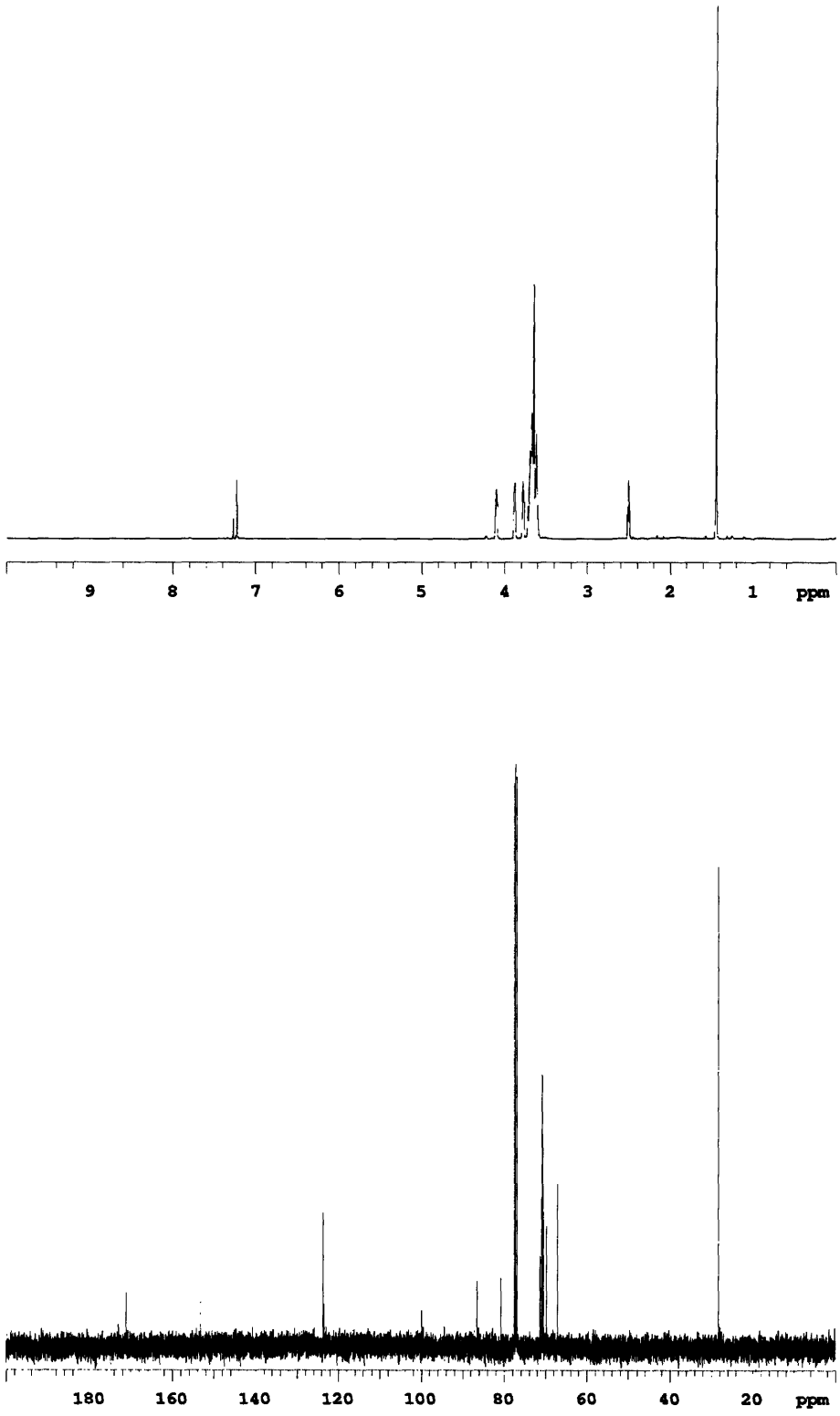

^{1}H (top) and ^{13}C (bottom) NMR spectra of **8** (Chapter 2).

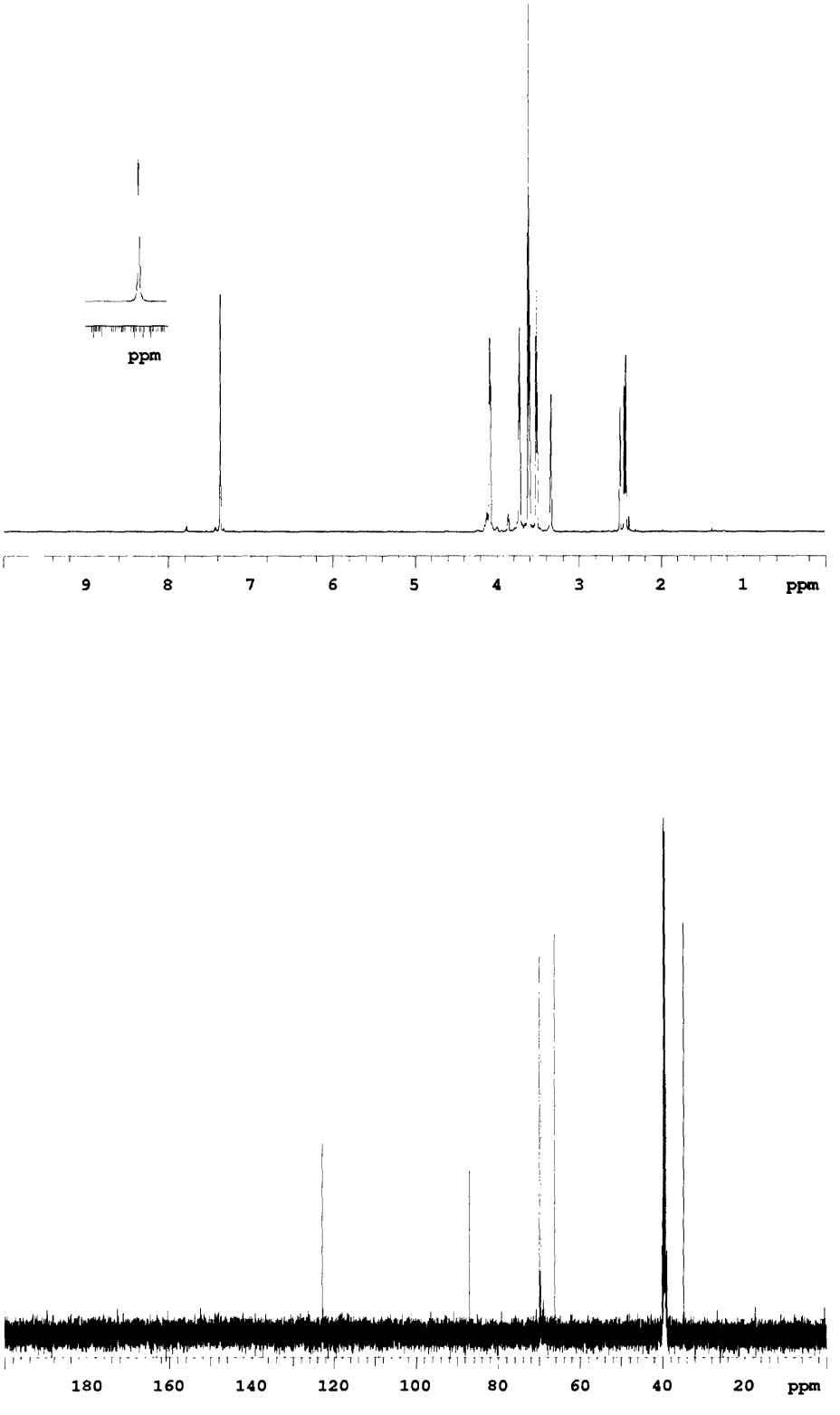

^{1}H (top) and ^{13}C (bottom) NMR spectra of **9** (Chapter 2).

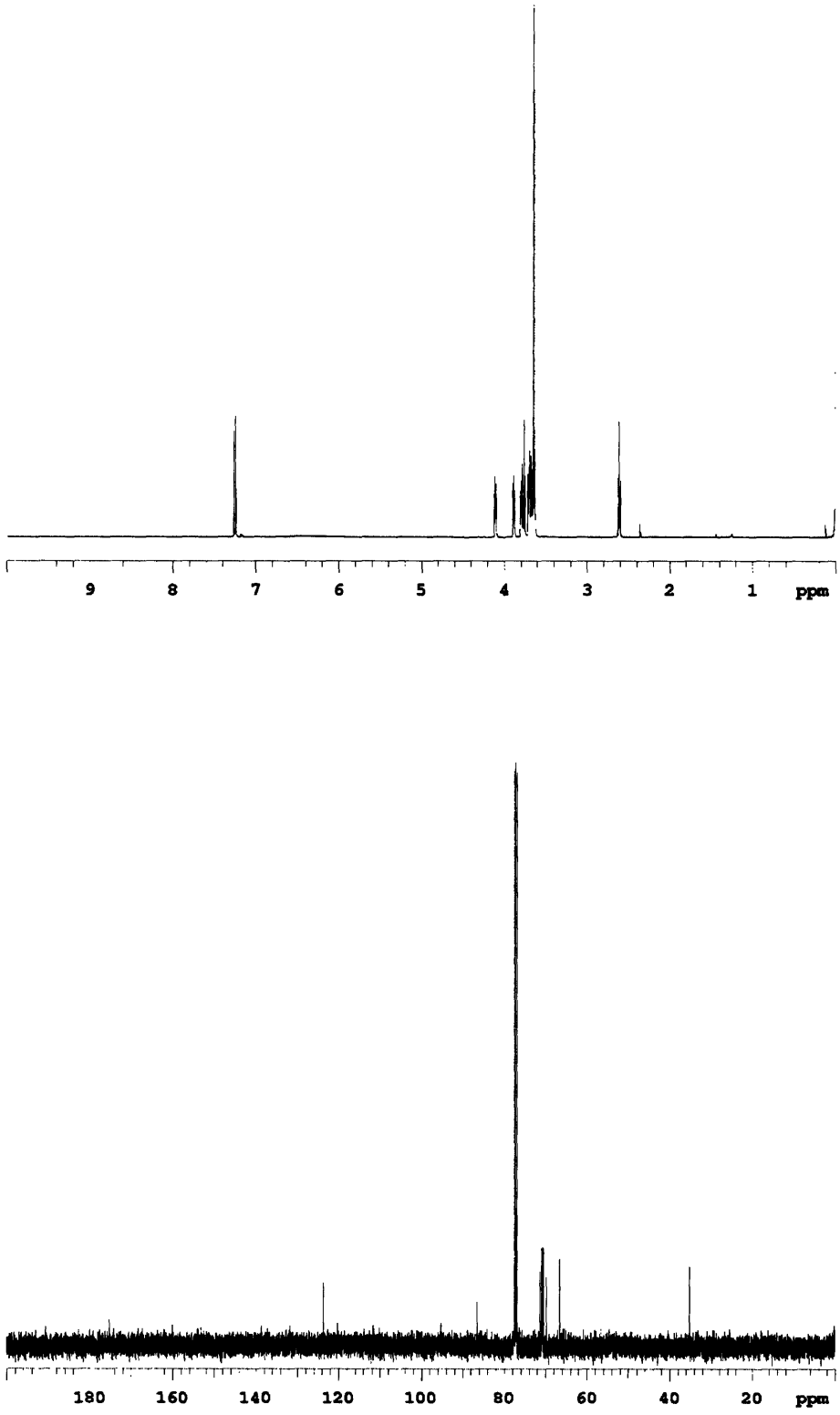

^{1}H (top) and ^{13}C (bottom) NMR spectra of **10** (Chapter 2).

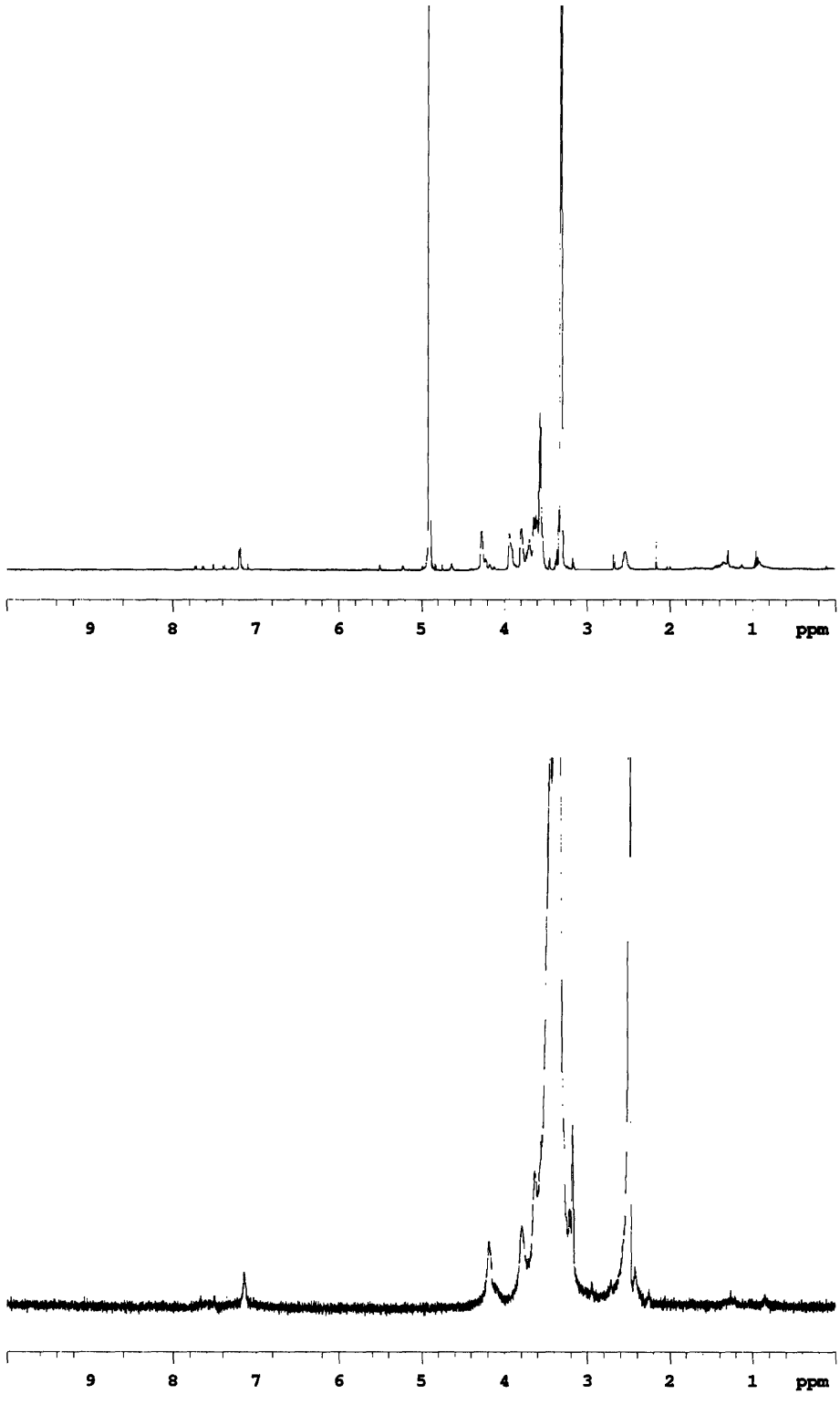

^{1}H NMR spectra of **12** (top) and **13** (bottom) (Chapter 2).

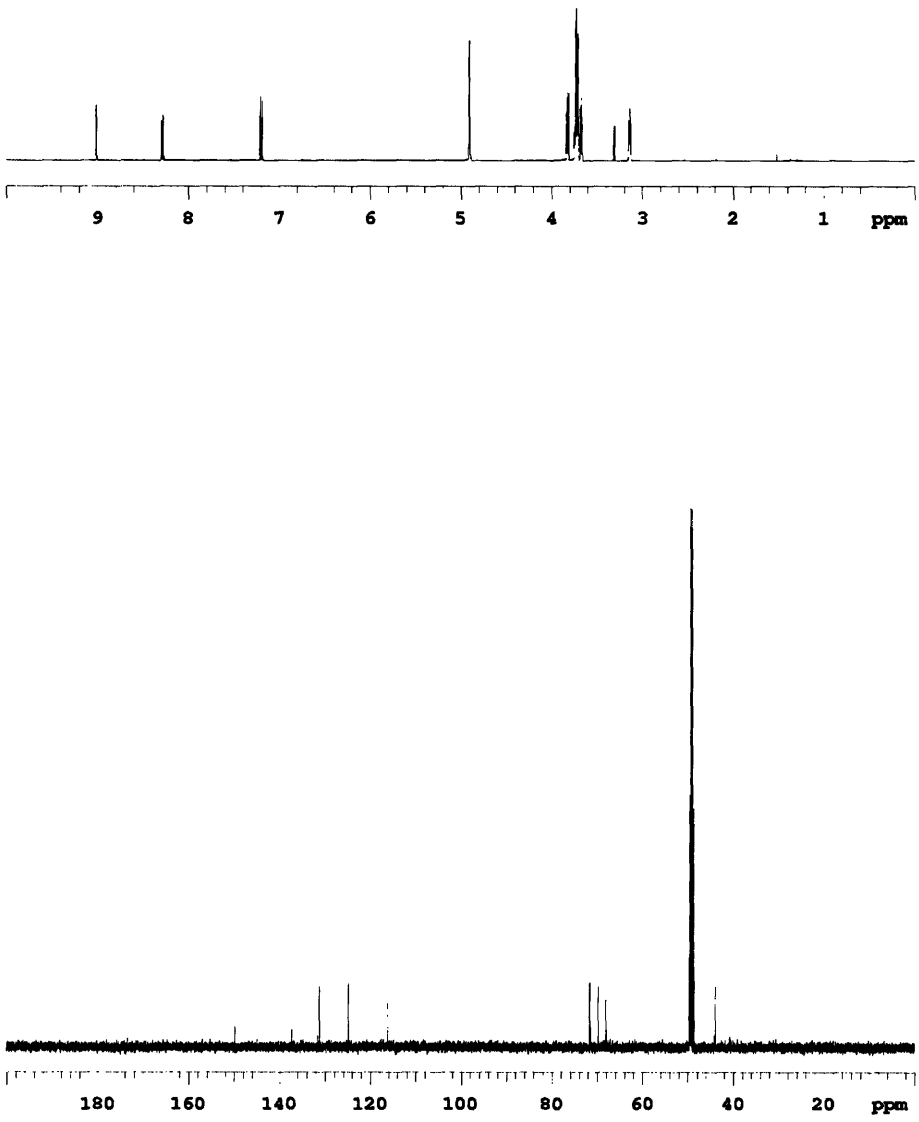

^{1}H (top) and ^{13}C (bottom) NMR spectra of **15** (Chapter 2).

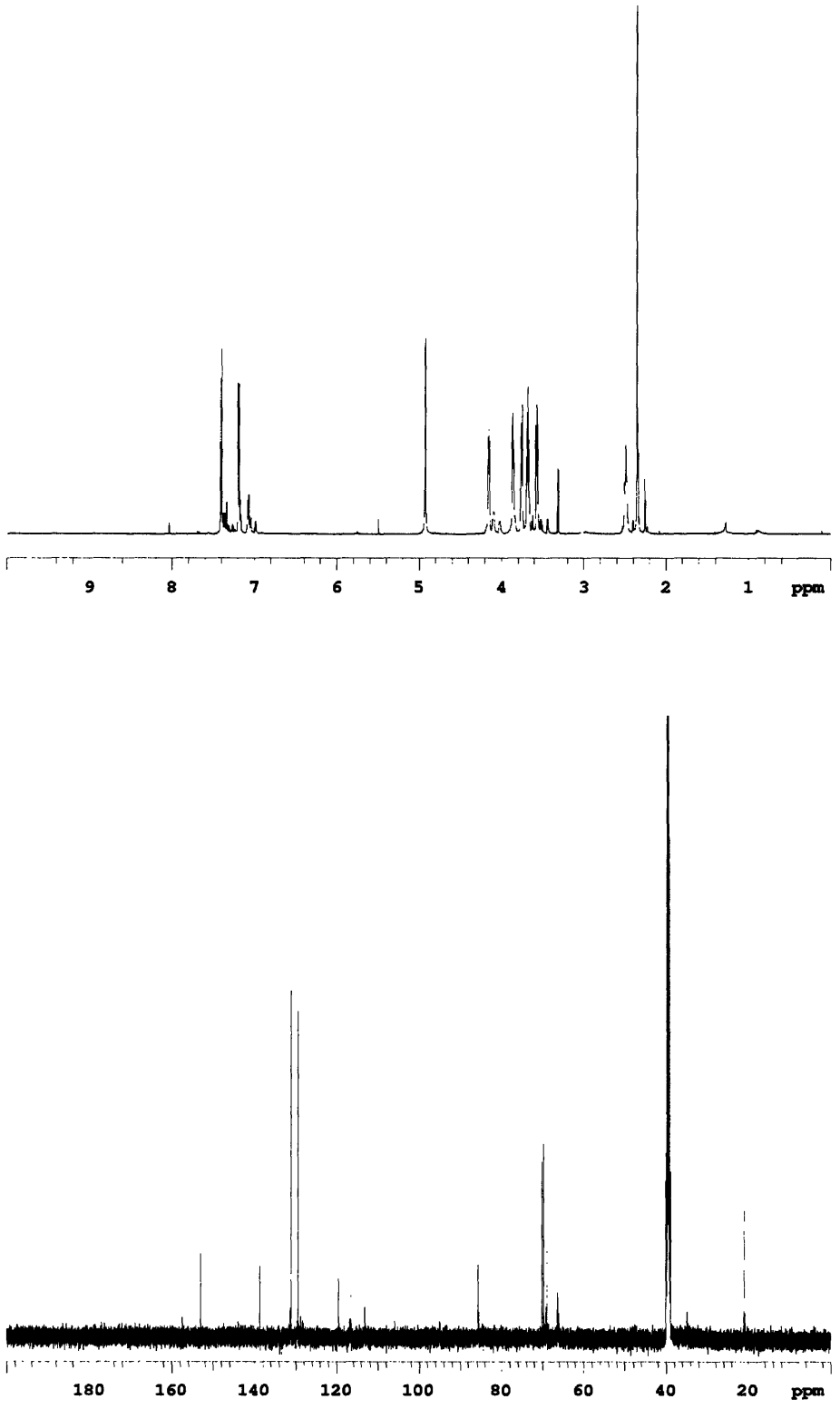

^{1}H (top) and ^{13}C (bottom) NMR spectra of **19** (Chapter 2).

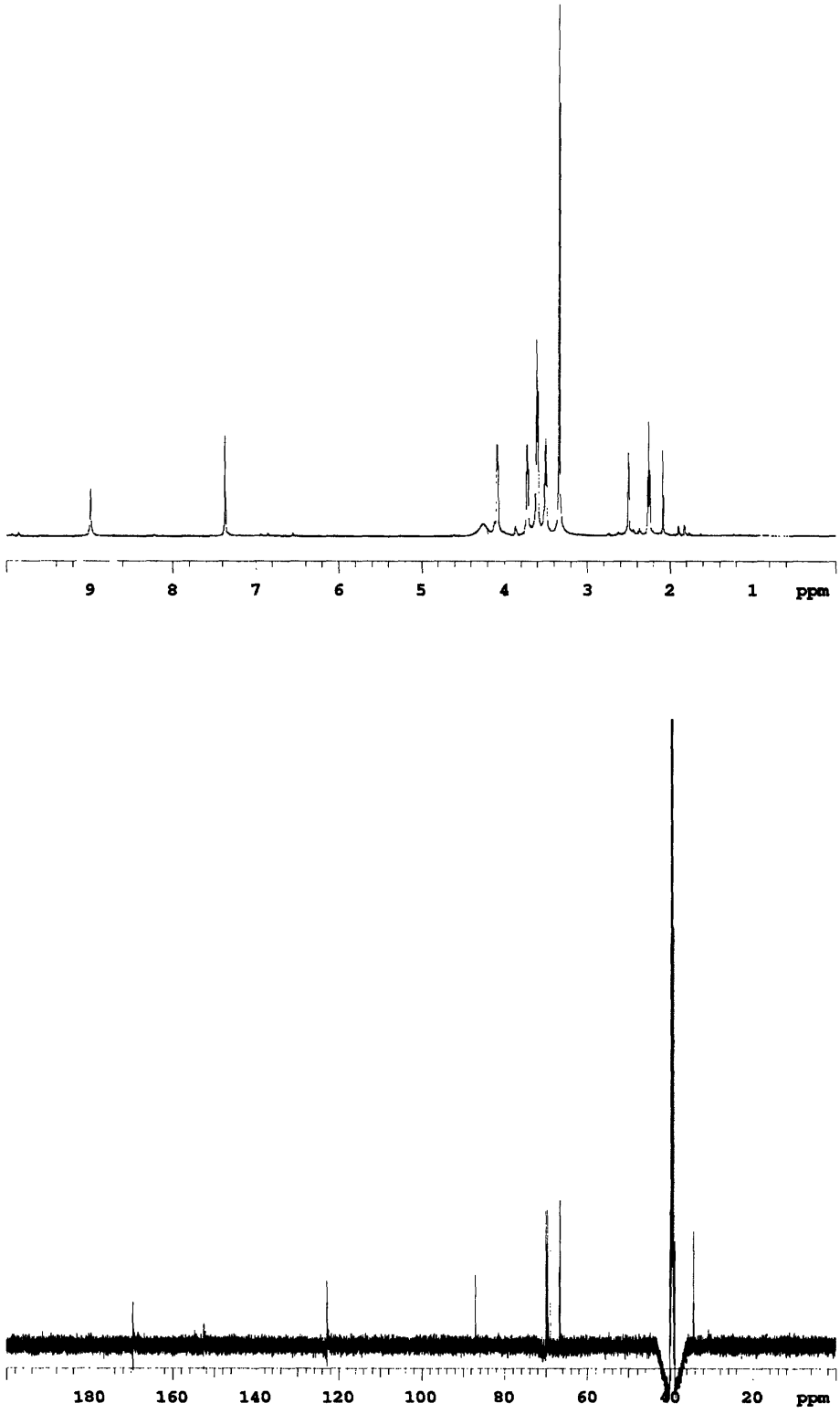

^{1}H (top) and ^{13}C (bottom) NMR spectra of **21** (Chapter 2).

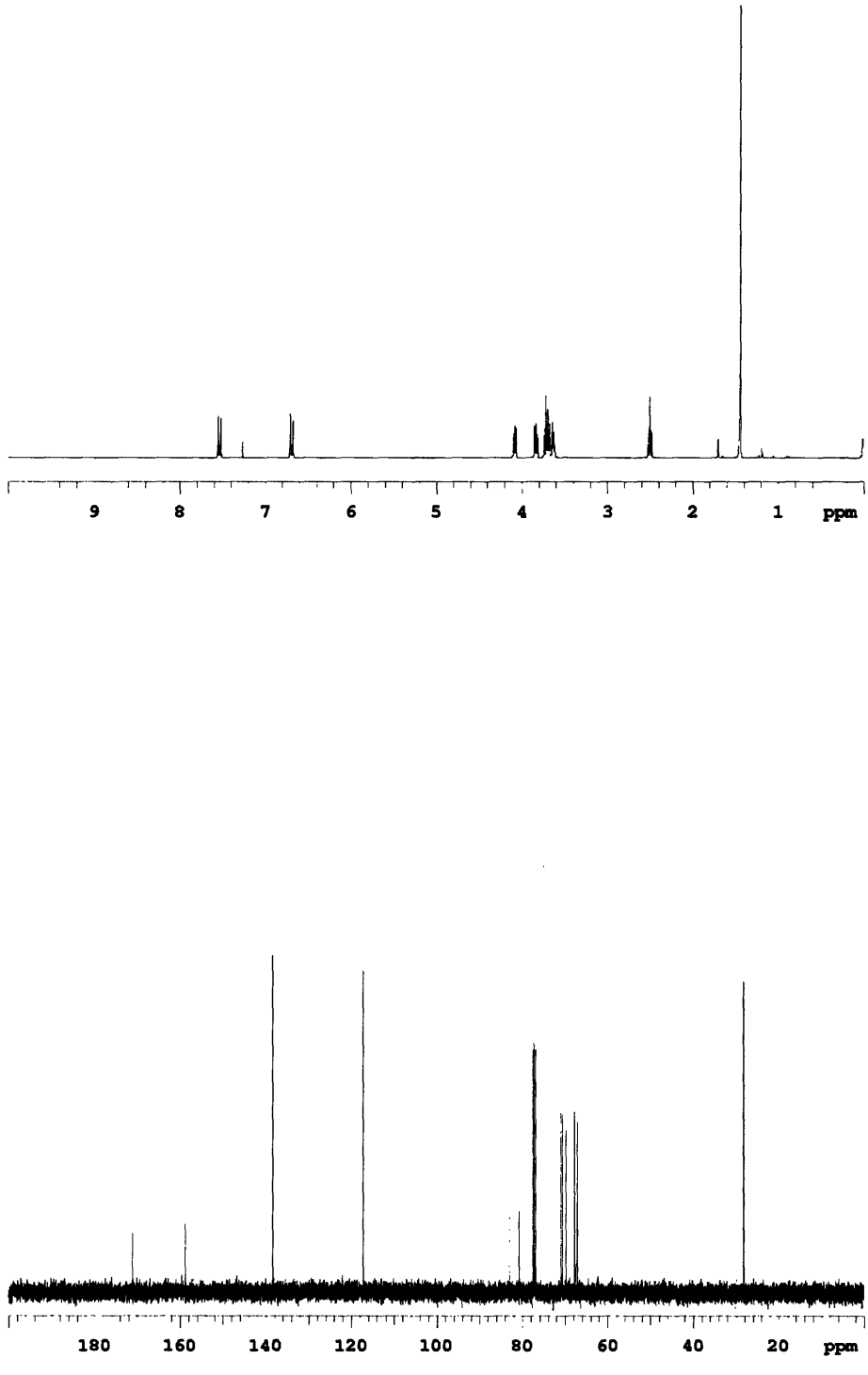

^{1}H (top) and ^{13}C (bottom) NMR spectra of **22** (Chapter 2).

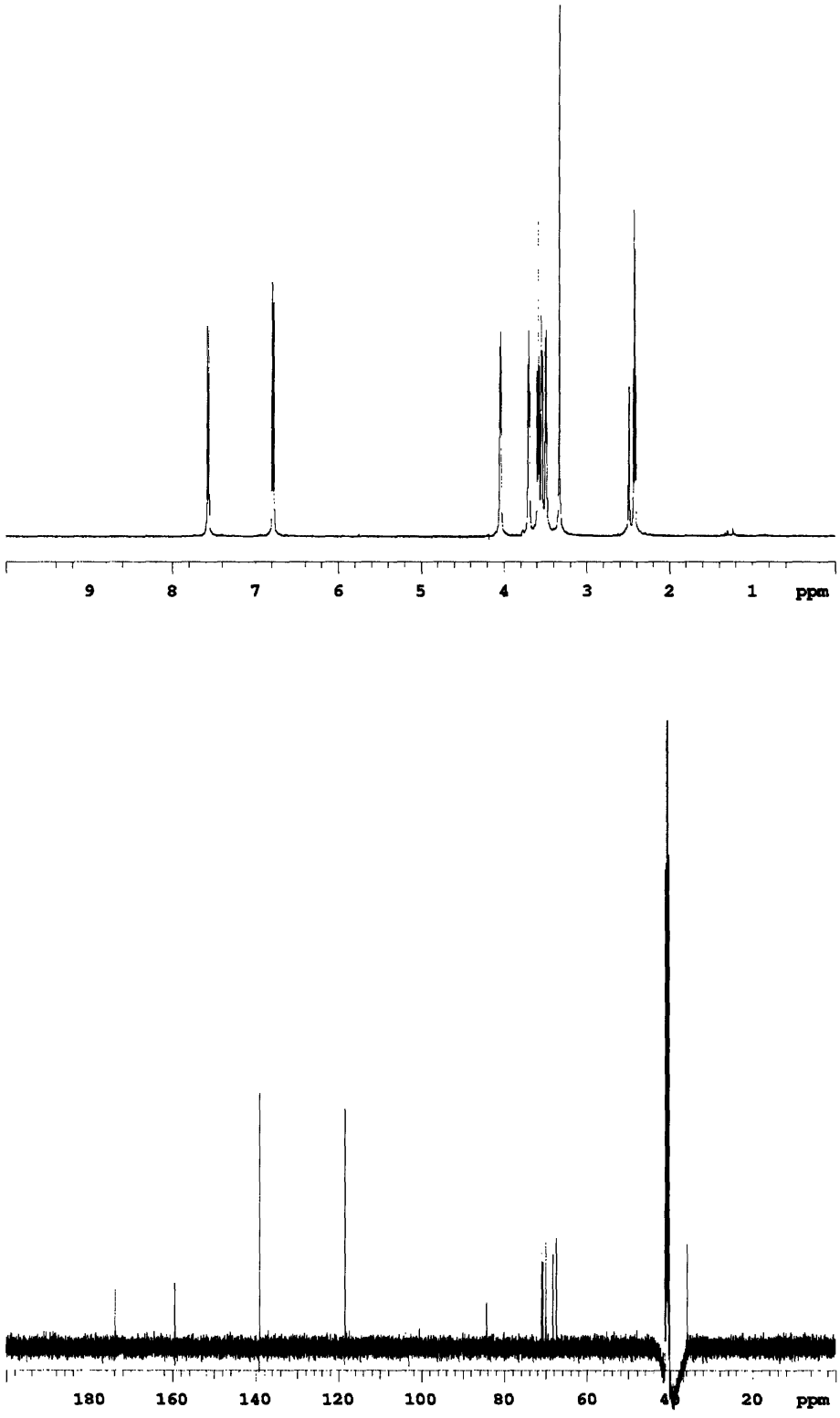

^{1}H (top) and ^{13}C (bottom) NMR spectra of **23** (Chapter 2).

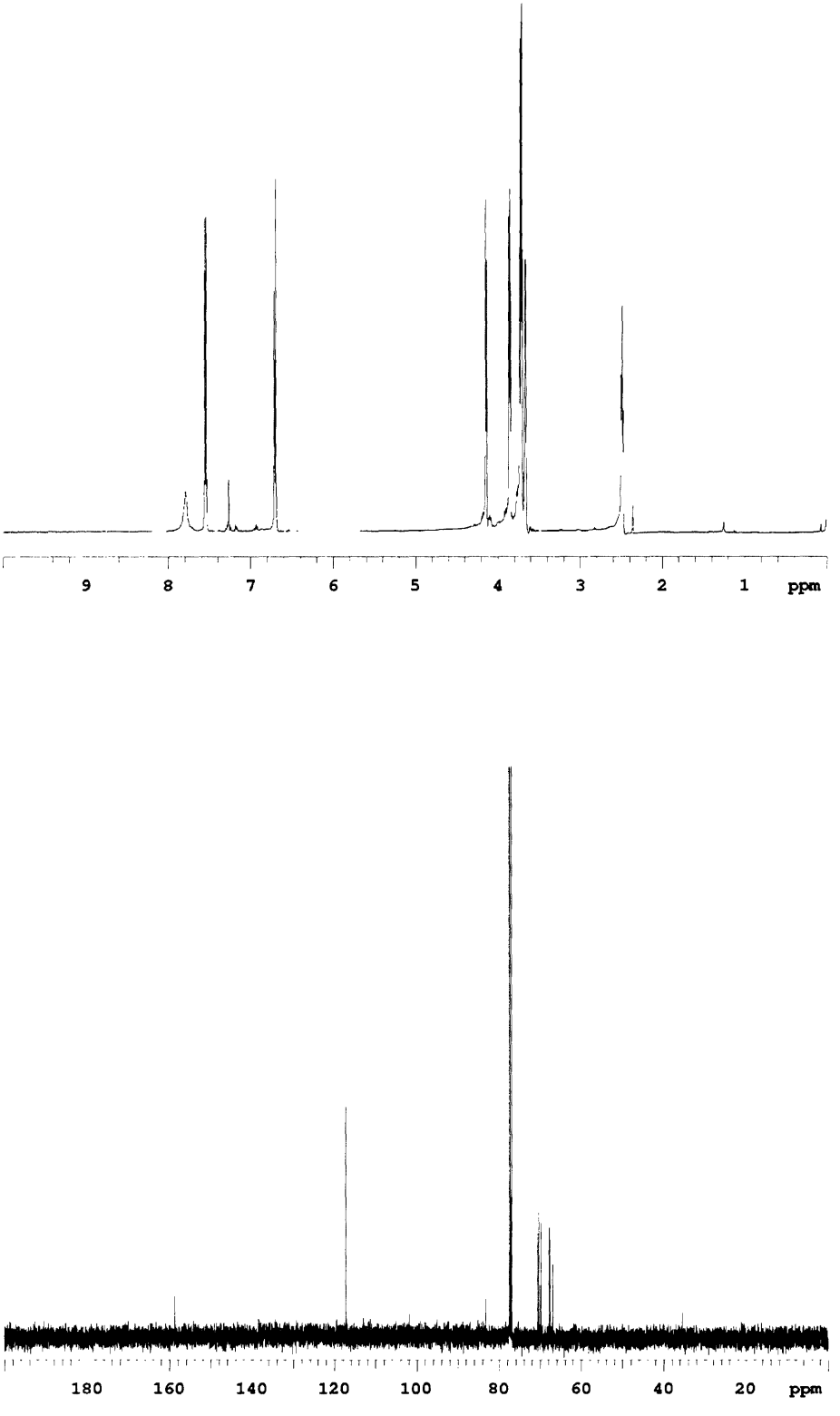

^{1}H (top) and ^{13}C (bottom) NMR spectra of **24** (Chapter 2).

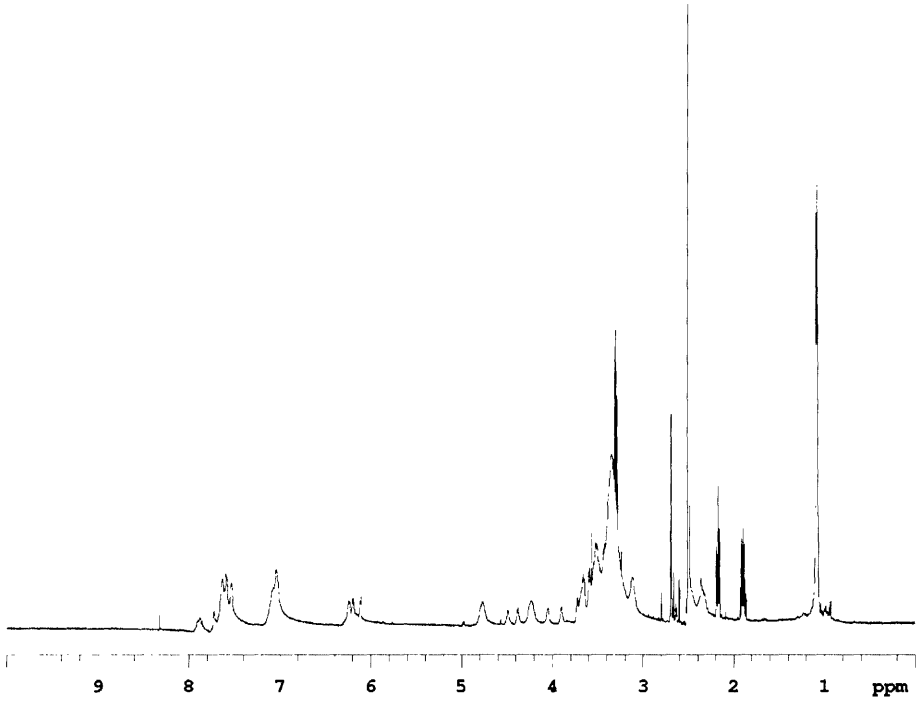

^{1}H NMR spectrum of **1** (Chapter 3).

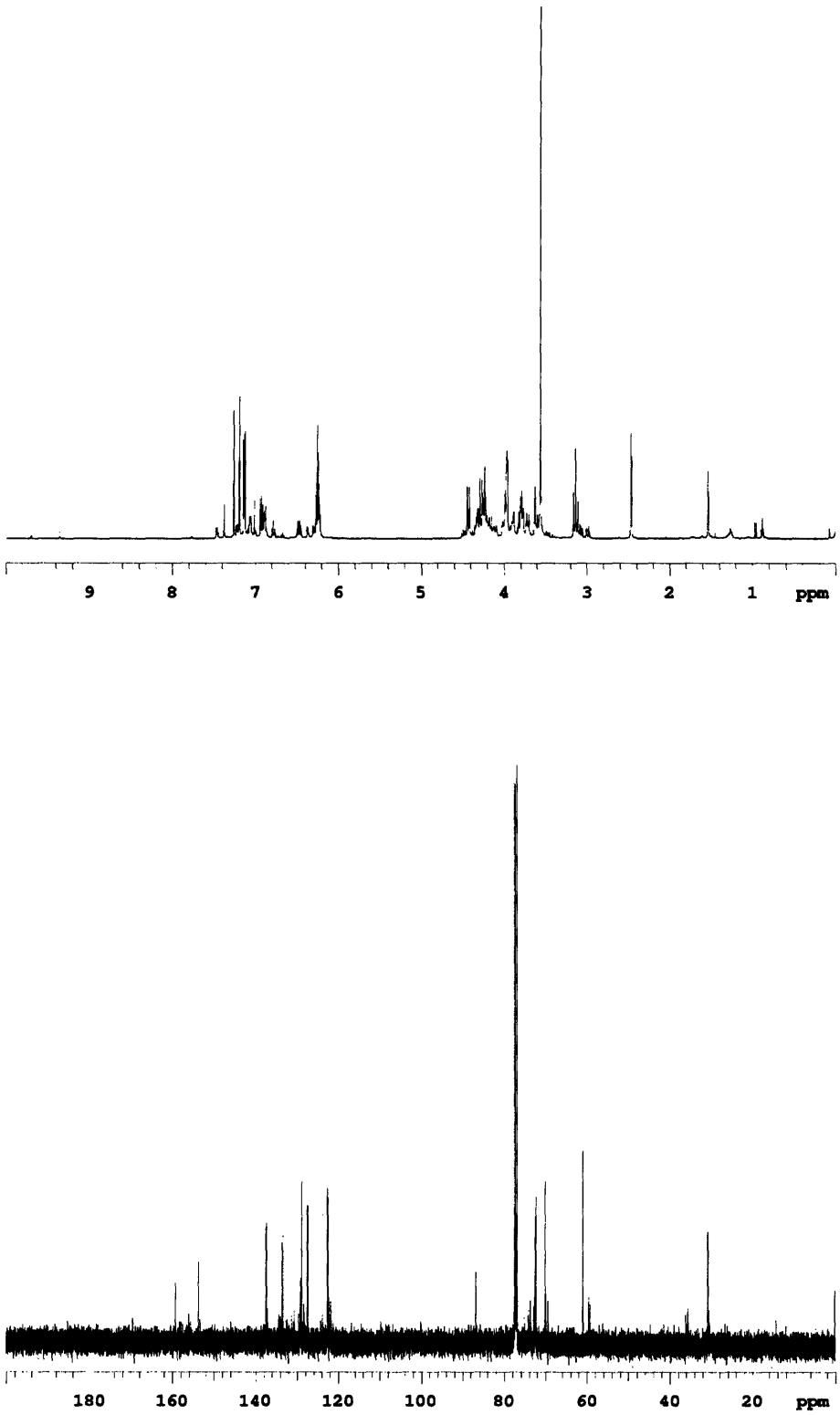

^{1}H (top) and ^{13}C (bottom) NMR spectra of **4** (Chapter 4).

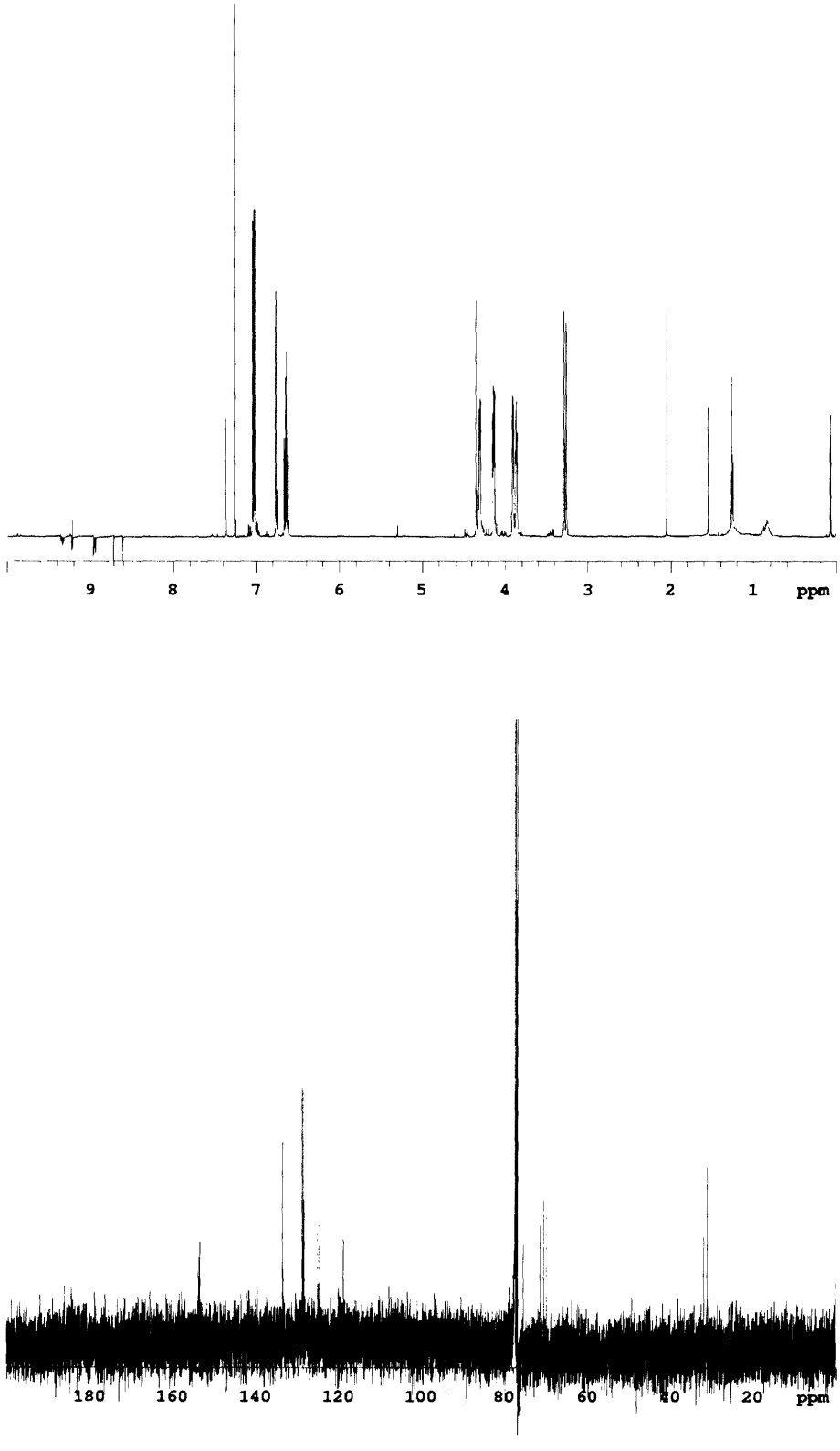

^{1}H (top) and ^{13}C (bottom) NMR spectra of **4′** (Chapter 4).

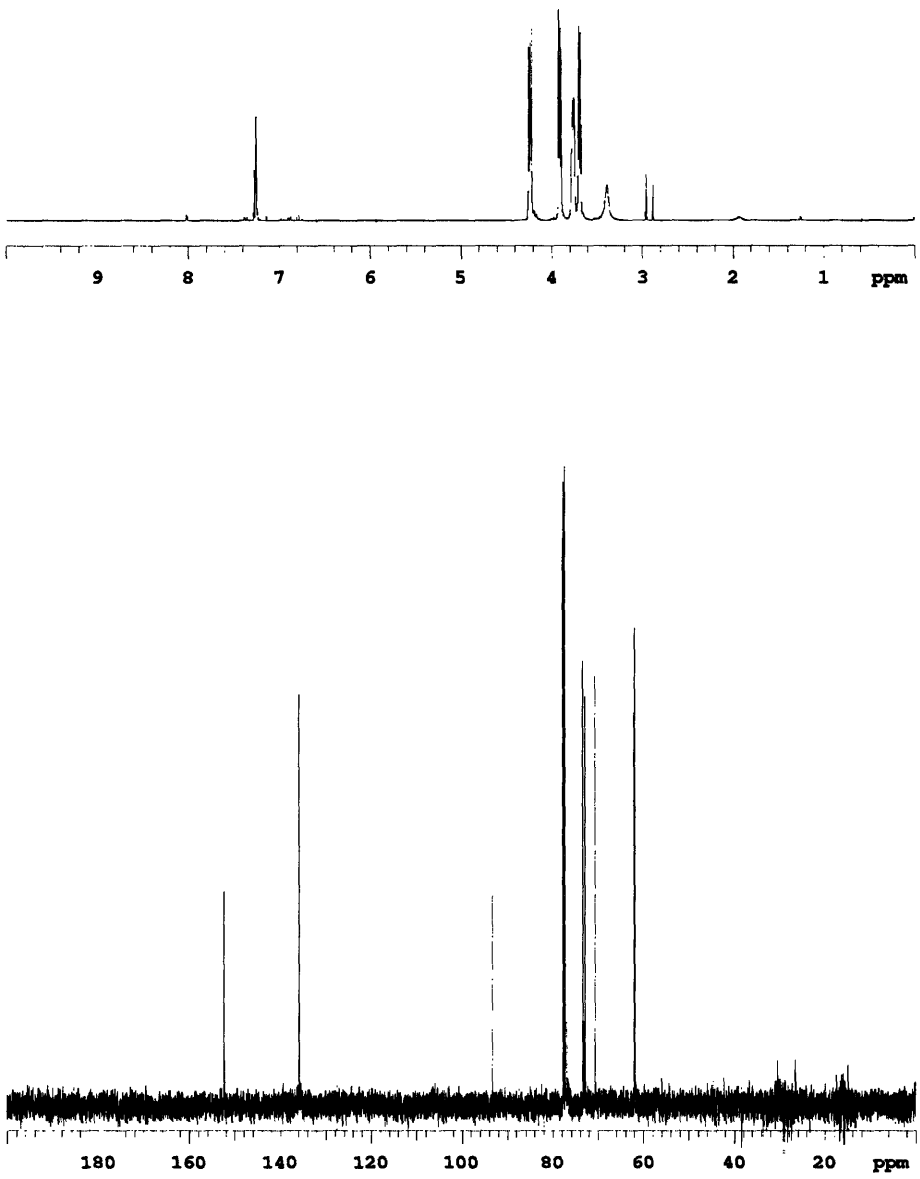

^{1}H (top) and ^{13}C (bottom) NMR spectra of the dihydroxy precursor to **5** (Chapter 4).

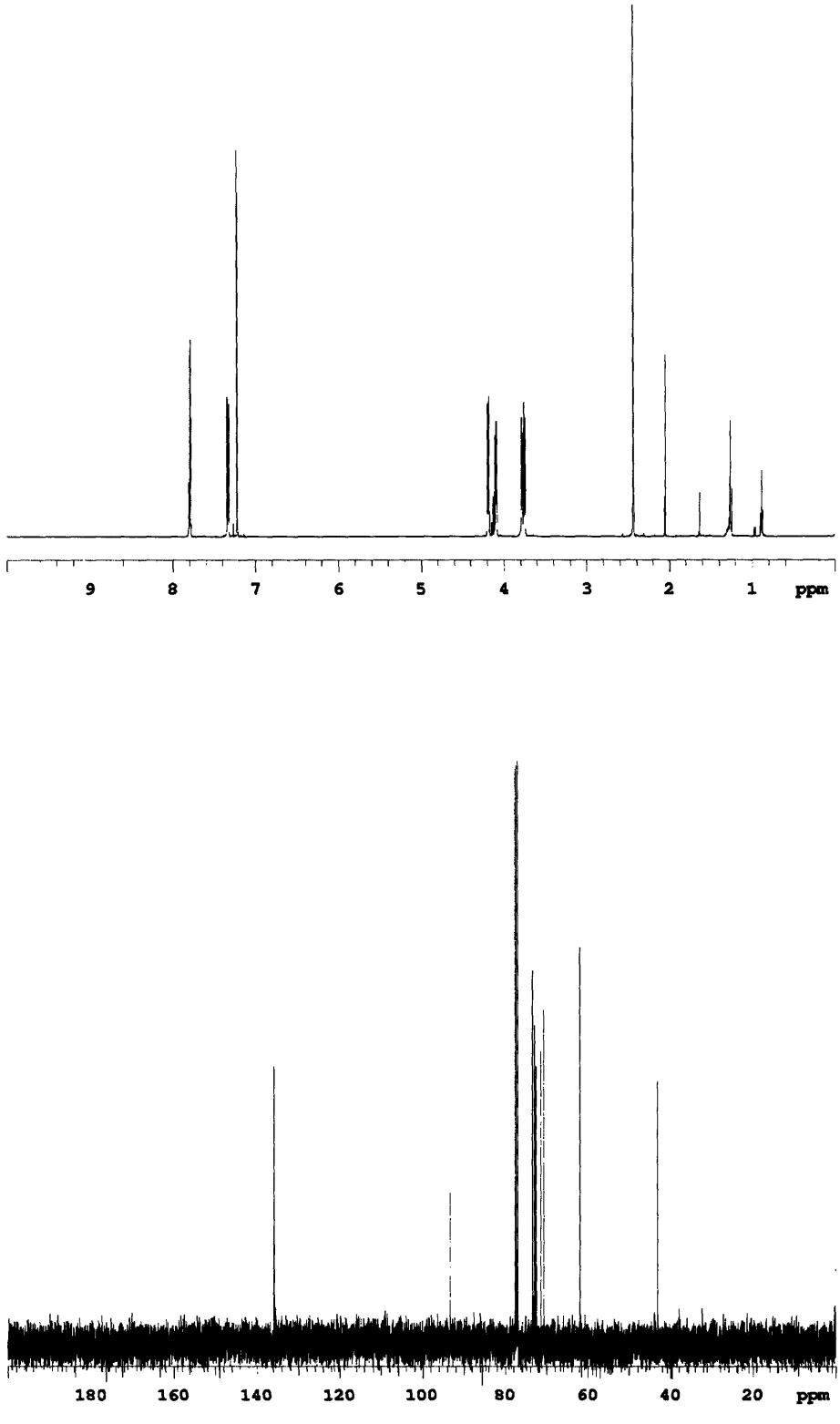

^{1}H (top) and ^{13}C (bottom) NMR spectra of **5** (Chapter 4).

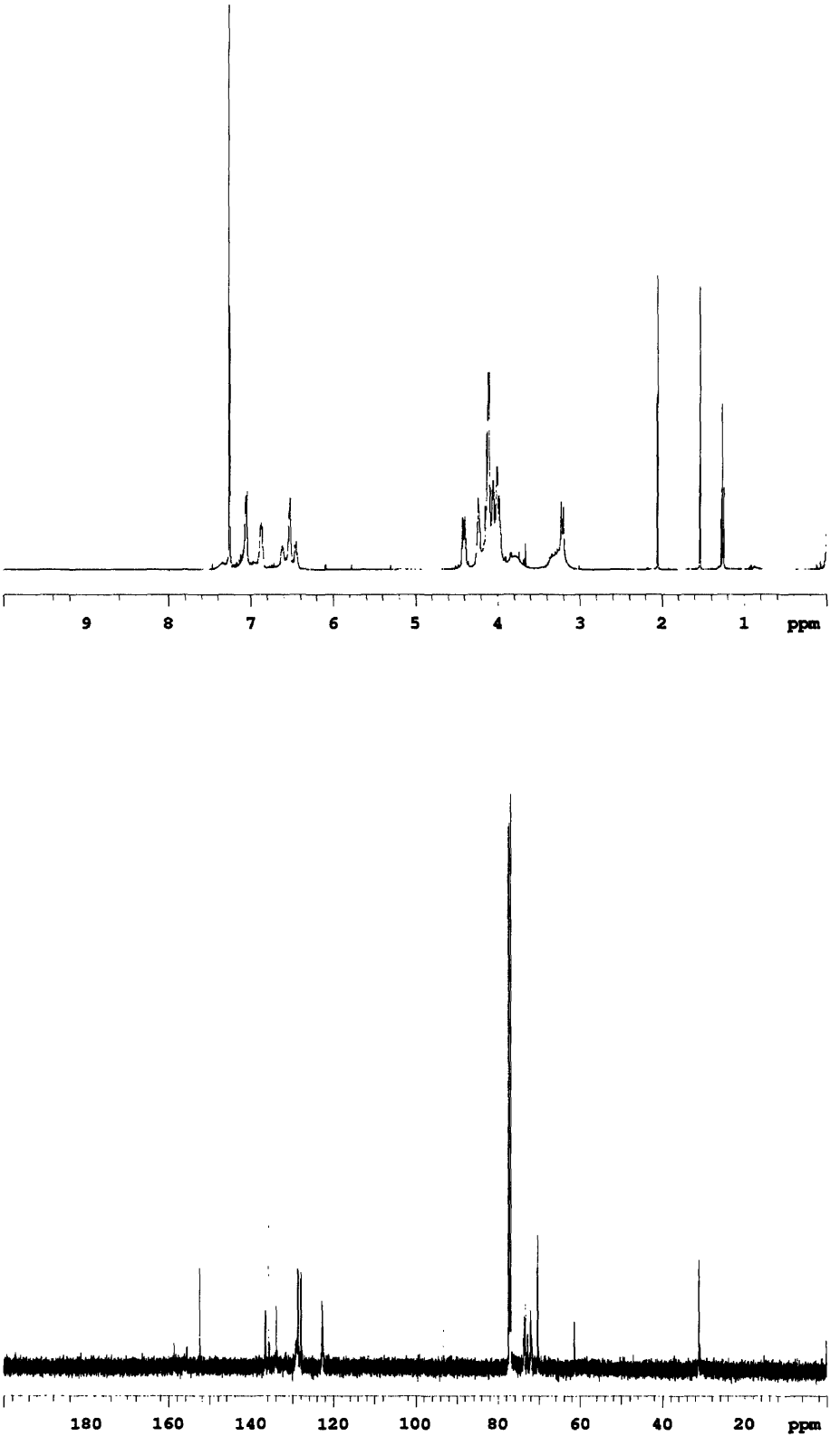

^{1}H (top) and ^{13}C (bottom) NMR spectra of **6** (Chapter 4).

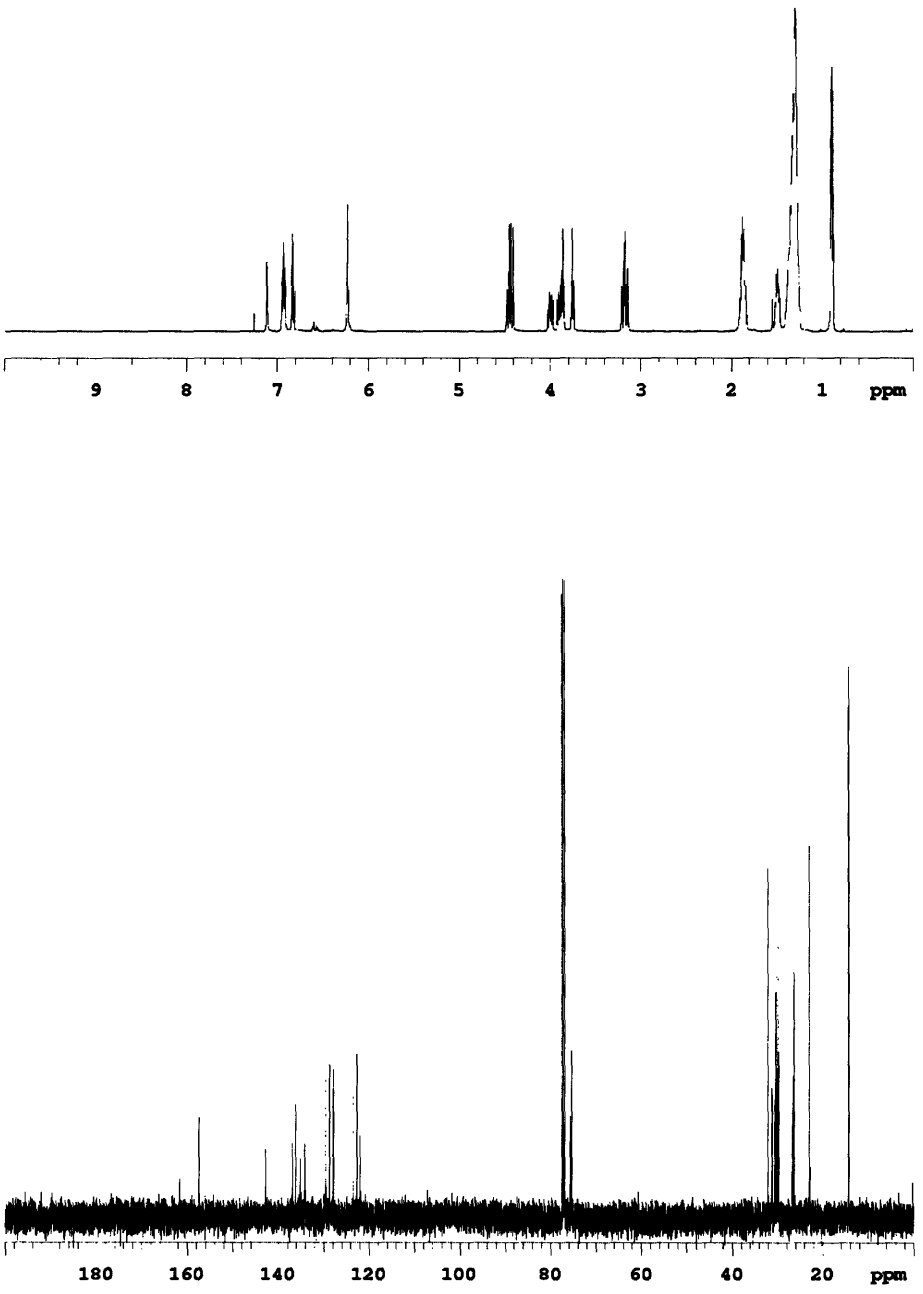

^{1}H (top) and ^{13}C (bottom) NMR spectra of **8** (Chapter 4).

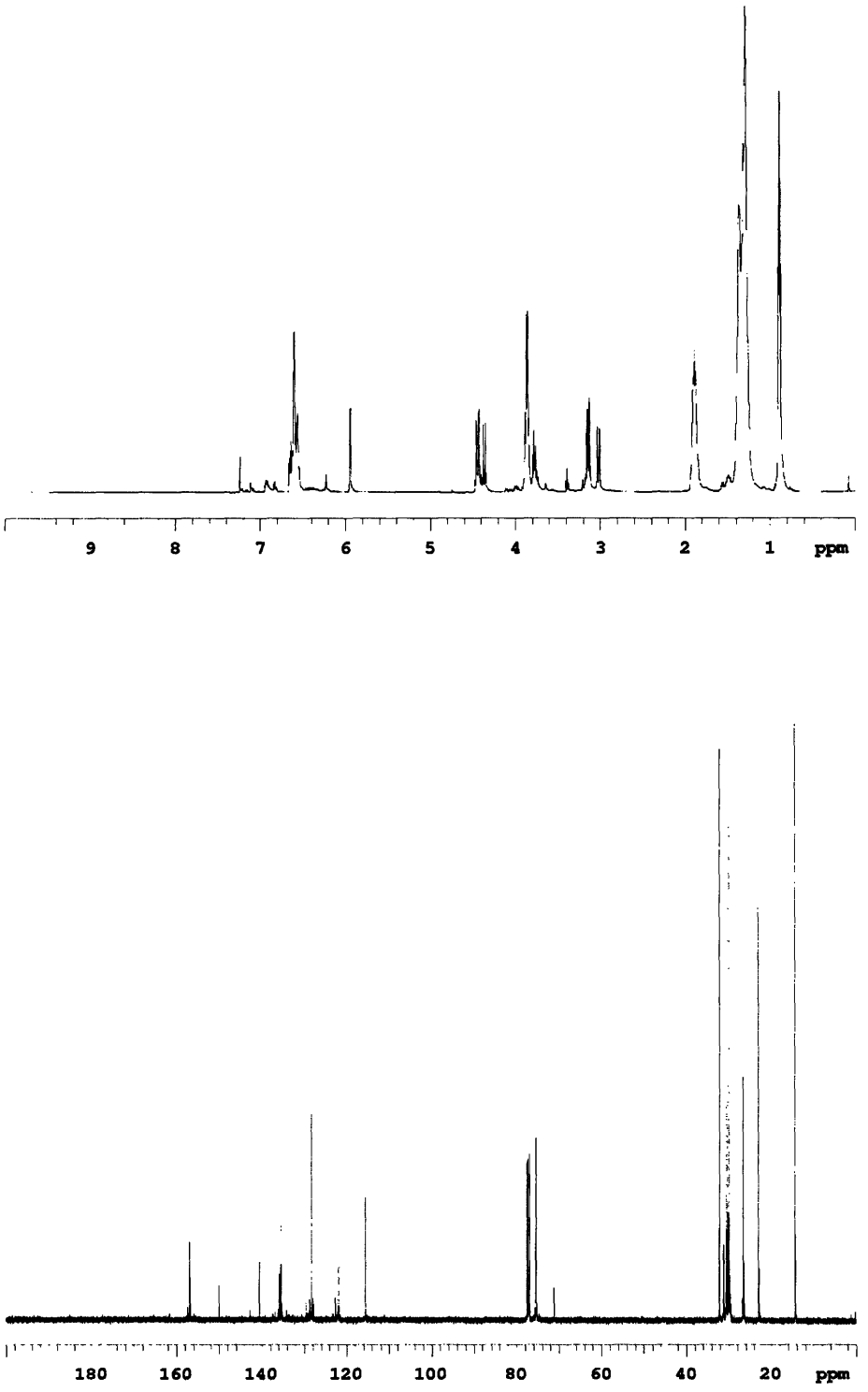

^{1}H (top) and ^{13}C (bottom) NMR spectra of **9** (Chapter 4).

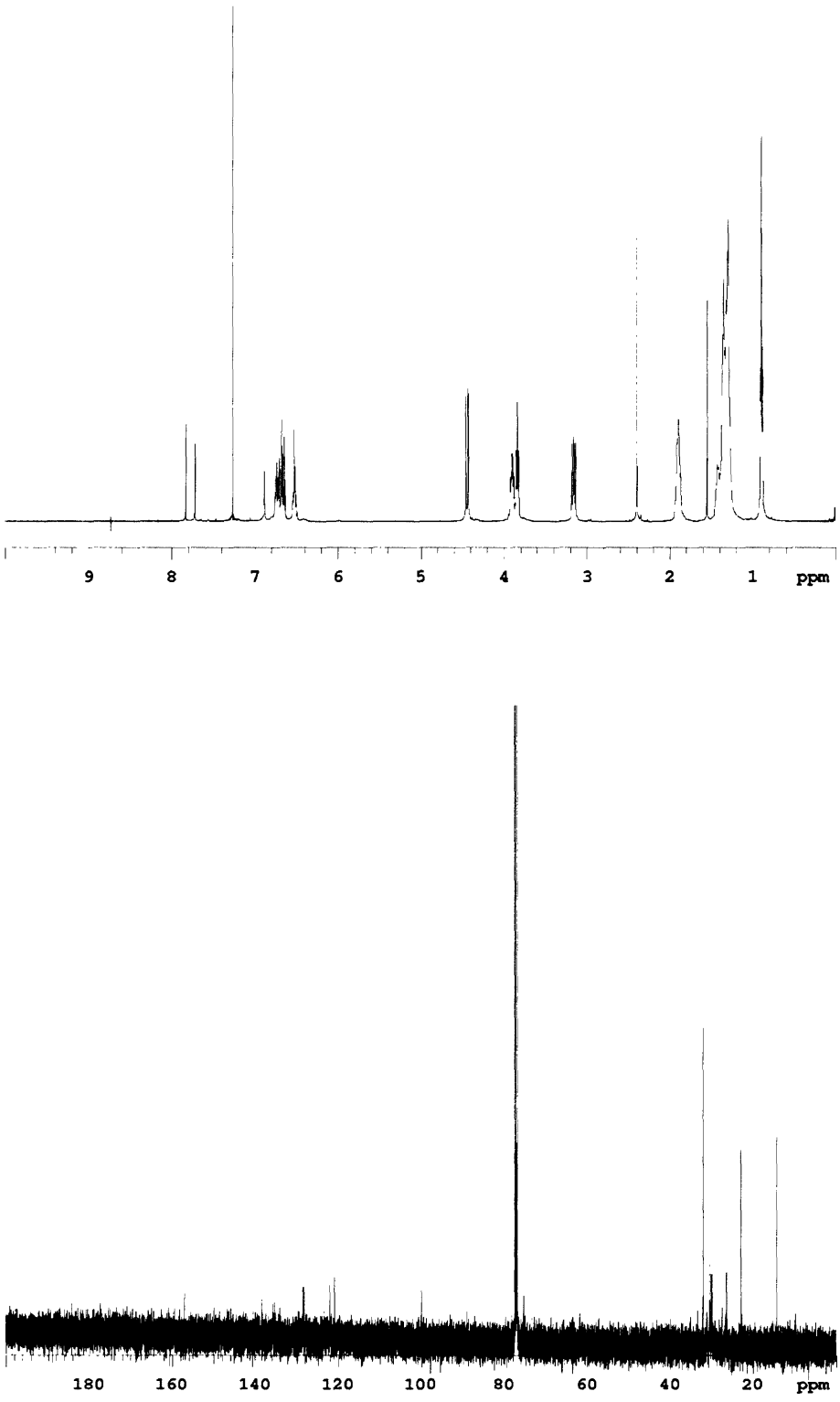

^{1}H (top) and ^{13}C (bottom) NMR spectra of **11** (Chapter 4).

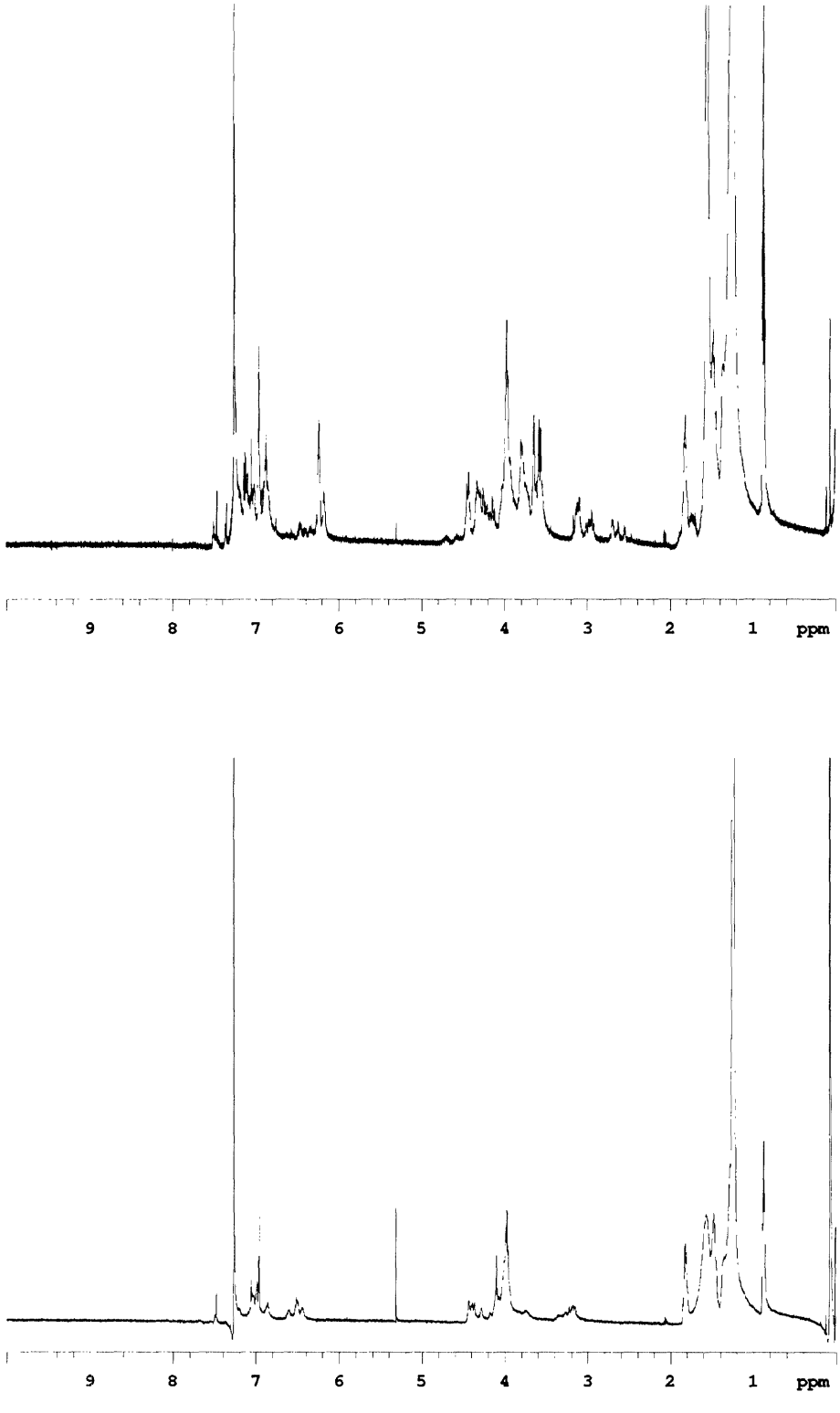

^{1}H NMR spectra of **12** (top) and **13** (bottom) (Chapter 4).

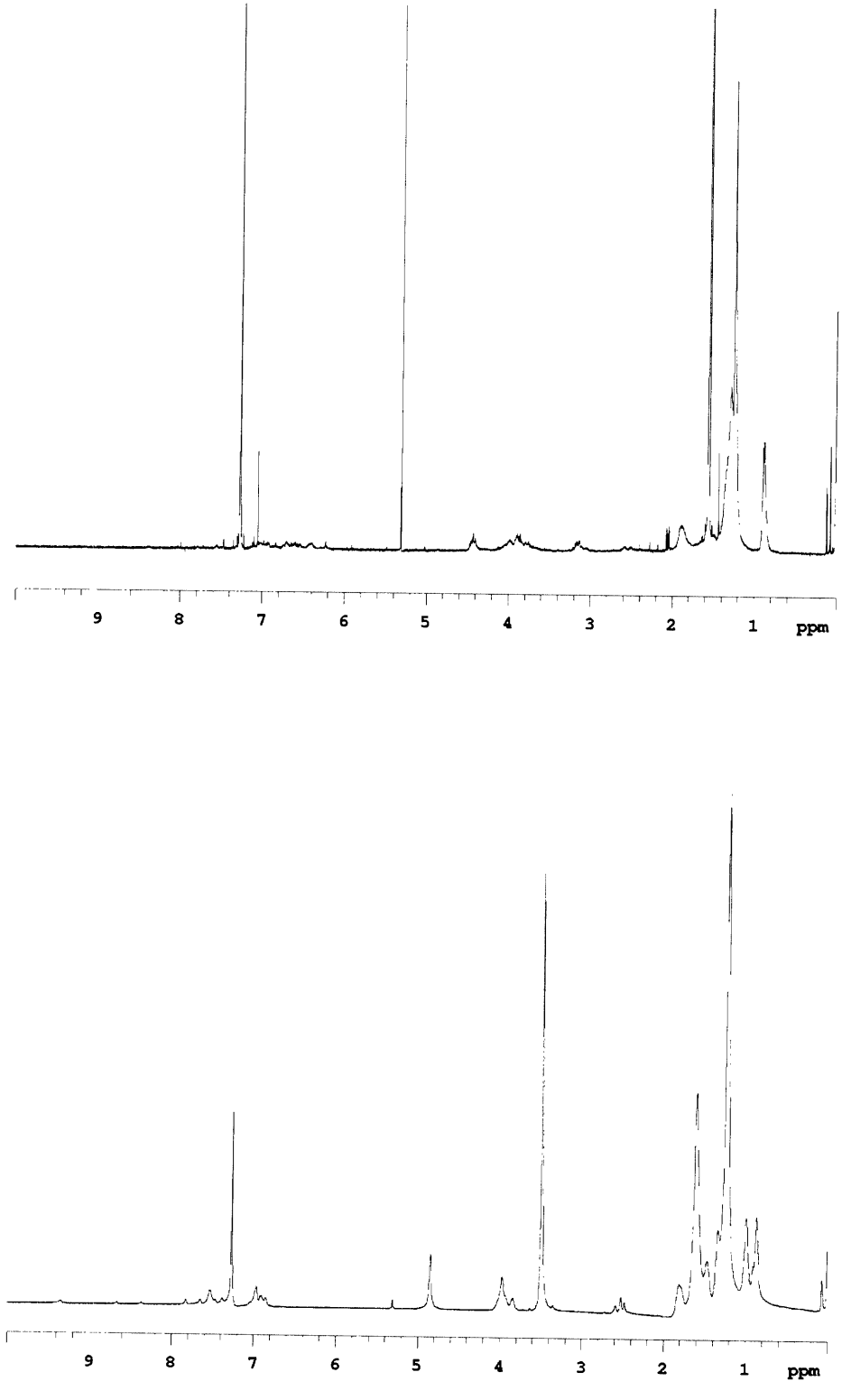

^{1}H NMR spectra of **14** (top) and **15** (bottom) (Chapter 4).

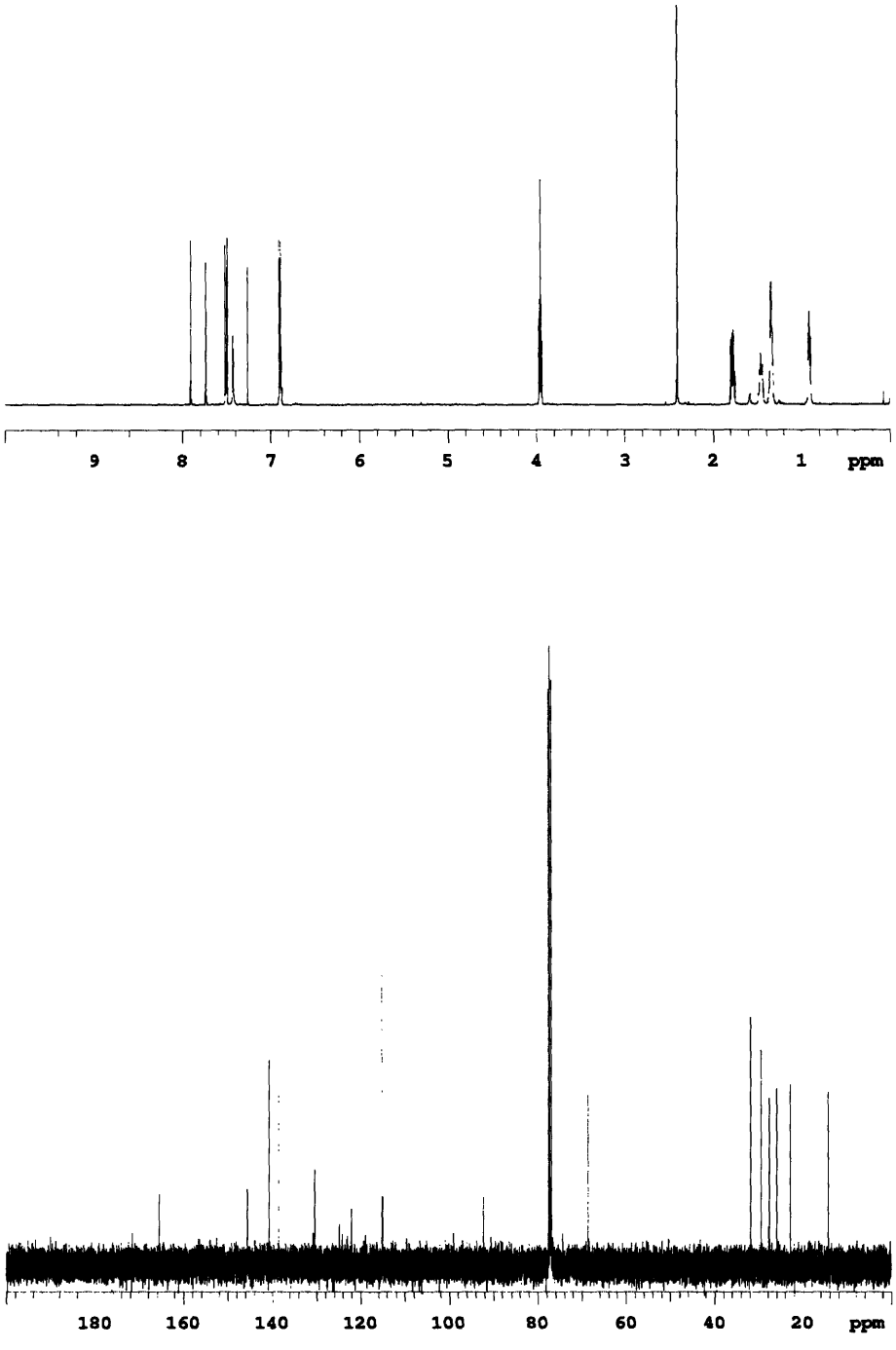

^{1}H (top) and ^{13}C (bottom) NMR spectra of **16** (Chapter 4).